SISSA
Scuola
Internazionale
Superiore di
Studi Avanzati

Physics Area - PhD course in
Statistical Physics

Entanglement and Asymmetry in Quantum Field Theory

Candidate:
Michele Fossati

Advisor:
Prof. Pasquale Calabrese

Academic Year 2024-2025

List of publications

1. M. Fossati, F. Ares, and P. Calabrese, *Symmetry-resolved entanglement in critical non-Hermitian systems*, *Phys. Rev. B* **107** (2023) 205153, arXiv:2303.05232.

2. F. Rottoli, M. Fossati, and P. Calabrese, *Entanglement Hamiltonian in the non-Hermitian SSH model*, *J. Stat. Mech.* (2024) 063102, arXiv:2402.04776.

3. M. Fossati, F. Ares, J. Dubail, and P. Calabrese, *Entanglement asymmetry in CFT and its relation to non-topological defects*, *JHEP* **05** (2024) 059, arXiv:2402.03446.

4. M. Fossati, C. Rylands, and P. Calabrese, *Entanglement asymmetry in CFT with boundary symmetry breaking*, *JHEP* **06** (2025) 089, arXiv:2411.10244.

5. F. Benini, P. Calabrese, M. Fossati, A. H. Singh, and M. Venuti, *Entanglement Asymmetry for Higher and Noninvertible Symmetries*, arXiv:2509.16311.

Contents

1 Introduction **1**
- 1.1 Entanglement entropy . . . 3
- 1.2 Entanglement asymmetry . . . 5
- 1.3 Symmetries as topological operators . . . 8
- 1.4 Outline of the thesis . . . 9

2 Bulk symmetry breaking **11**
- 2.1 Symmetries, topological defects, and entanglement asymmetry . . . 12
- 2.2 The XY spin chain and the massless Majorana fermion field theory 19
- 2.3 Calculation of the scaling dimension associated to n defects in the Majorana CFT . . . 22
- 2.4 Rényi entanglement asymmetry in the critical XY spin chain . . . 32
- 2.5 Concluding remarks . . . 39
- 2.A Fermionization and continuum limit of the XY spin chain . . . 40
- 2.B Defects in the Hamiltonian formalism . . . 42
- 2.C Numerical calculation of the charged moments . . . 43

3 Boundary symmetry breaking **44**
- 3.1 Asymmetry in the groundstate: analytical results . . . 45
- 3.2 Asymmetry in the groundstate: numerical results . . . 52
- 3.3 Boundary quenches: analytic results . . . 58
- 3.4 Boundary quenches: numerical results . . . 62

4 Generalized symmetries **69**
- 4.1 Introduction . . . 69
- 4.2 Entanglement asymmetry for generalized symmetries . . . 71
- 4.3 Asymmetry for the circle Hilbert space . . . 76
- 4.4 Asymmetry for the interval Hilbert space . . . 84
- 4.5 Spontaneous symmetry breaking . . . 96
- 4.6 Examples . . . 100
- 4.A Strongly separable algebras and the symmetrizer . . . 134
- 4.B Hopf algebras, modules, and tensor products . . . 140
- 4.C $\boldsymbol{F}$-symbols and the tube algebra . . . 144

4.D $\tilde{\boldsymbol{F}}$-symbols and the strip algebra 147
4.E Module categories over $\mathsf{Vec}_{\boldsymbol{G}}^{\omega}$ 148

5 Non-Hermitian systems **151**
5.1 *PT* symmetric non-Hermitian SSH model 153
5.2 Symmetry-resolved entanglement 157
5.3 Absolute charged moments in the *bc*-ghost CFT 160
5.4 Symmetry-resolved entanglement entropy of the *bc*-ghost CFT . . . 165
5.5 Charged moments and standard Rényi entropies 168
5.6 Entanglement spectrum 170
5.7 Entanglement Hamiltonians 174
5.8 Lattice entanglement Hamiltonians of the non-Hermitian SSH model 176
5.9 Concluding remarks 186
5.A Details of the computation of $P(\lambda)$ 188

Outlook **192**

This thesis is dedicated to the memory of Samuel Tamagnone, who left us suddenly, on an unfortunate day of April 2025. Whoever had met him cannot forget the energy and the joy that characterized him. We will forever cherish a spark of that in our hearts.

Acknowledgements

I would like to begin by thanking my supervisor, Pasquale Calabrese, for the trust he has shown in me from the very beginning, welcoming me to the Statistical Phisics group and accepting to be my supervisor even though I was coming from a different PhD program (and I still have to take his course!). I thank Jérôme Dubail for the warm welcome during my visits to Nancy and Strasbourg. I truly appreciated his openness, without ever placing hierarchy above anything else. I am also grateful for the picture he took of me with Cory Wong and for encouraging me to attend his concert during my visit in Nancy. I am deeply grateful for having had the opportunity to work with Francesco Benini. His attention to every detail and at the same time his synthetic view; his curiosity and his desire to to simply make the things clear have all been a great source of inspirationfor me.

Coming to the less senior people, I thank Filiberto for having guided me at the beginning of this journey, and for always being available when I needed support. I am thankful for the time spent with Federico: we managed to have fun, after all! I am also grateful to Colin, Eran and Eytan.

In the last year, I've had the big pleasure of spending most of my working time with Marco and Amartya, and to sign emails as MMA (which is not a reference to the gangster past of Amartya). I've learnt so many things from and with them. Aside from all the physics and math, I am particularly thankful to Amartya for having taken me out of a certain "loop", and to Marco for all the slackline sessions.

I have also learned a great deal of physics from other friends. I am particularly grateful to Luca Capizzi for several foundational (for me) discussions when I had just begun doing research, without any clue as to what a CFT was, and to Andrei for many exchanges on boundary conditions. I also thank Leonardo for some coffee chats that turned into several-hour-long blackboard discussions.

Un posto speciale è riservato alle persone con cui ho avuto la fortuna di condividere un tetto durante questi quattro anni. Ringrazio innanzitutto il Gaspa, con cui ne ho passate parecchie, incluso un tentativo (stranamente, fallito) di sciare la Gasparini-Florit al Nabois. Grazie Giulio, per un ottimo mese sulle note di Pippéro. Grazie Alex e Fra per un anno insieme che mi ha cambiato, e per *quel* momento sul balcone ascoltando i Vulfpeck. Grazie Alex, per la tua allegria spontanea che fa bene al cuore e per la voglia di nerdare ma sempre con tanto stile. Grazie

Franci, per essere sempre sul pezzo. A volte mi chiedo: cosa farebbe la Fra? Poi mi rispondo – e faccio la cosa giusta. Grazie Simo, per le Rotaboard sessions e per avermi sfamato nei momenti di vero bisogno (e anche tutti gli altri giorni). Grazie Vitto, per l'arte di sdrammatizzare e rendere tutto divertente. Grazie Salvo, miglior politico che conosca, Thom, per le cantate (anche quelle unofficial), ed Eli, con cui si sta sempre bene. Infine, grazie Marta, per aver portato il sole per tre anni filati.

Un grazie speciale va anche a Cri, Anna, Adrian, Masca, Santiago, Fabio Chiapolino, Marco Driusso, Jack B., Pietro C., Ele, Ben, Alfio, Laura, Gaso, Clem, Marina, Luca L., Anant, Pavi, Zeno, Lu, Davide e Meri, Samu G., il Matto, Fra G., Enri, Puurvash, Eli P., Kostas, Mica, Rick, Ludo tekno, Giulio B., Ila e Emma, Thomas B., e Claudio Caniglia.

Sono poi grato ad alcune realtà, più o meno organizzate, che tengono vivo il tessuto sociale triestino e che hanno reso molto più piacevole la mia permanenza in città: i regaz di Slackline Trieste, la ciclofficina Scontrosa Graziella e gli Swing Freaks.

Infine ringrazio la mia famiglia, che fa sempre il tifo per me.

Chapter 1

Introduction

In the last decades, quantum information has proved to be a fundamental tool for the study of quantum many-body systems. Let us start with a brief and very broad historical perspective.

Quantum information has its roots in classical computer science and information theory. Alan Turing is considered the father of the former, thanks to his work in the 1930s, where he introduced the concept of the Turing machine, providing a formal model for computation. On the other hand, Claude Shannon, in the 1940s, laid the foundations of information theory by providing a mathematical definition of information and introducing a formalism to quantify the transmission and processing of information.

The first encounter of computer science with quantum mechanics was led by Paul Benioff in the early 1980s, who formulated a quantum-mechanical model of a Turing machine. A few years later, David Deutsch extended this idea by introducing the concept of a universal quantum computer, capable of simulating the evolution of any finite quantum system. He also proposed the first quantum algorithm, laying the foundations of the field of quantum computation. Meanwhile, from the physics side, Richard Feynman suggested in 1982 that simulating quantum systems efficiently would itself require a quantum system.

In the 1990s, the power of quantum computation was demonstrated by two landmark results. Shor's algorithm (1994) showed that a quantum computer could factor large integers exponentially faster than any known classical algorithm. Soon after, Grover's algorithm (1996) provided a quadratic speedup for unstructured search problems. Progress continued in understanding how to deal with noise and decoherence. Major advances came in 1996 with the discovery of the CSS quantum error-correcting codes and later the stabilizer formalism. These discoveries established that quantum computers could outperform classical ones for certain tasks, transforming quantum computation from a theoretical possibility into a promising paradigm.

In the early decades of quantum information science, research focused not on

quantum many-body systems but rather on systems with only a few degrees of freedom, which could be used to store and manipulate information starting from individual qubits. Studies therefore centered on platforms such as single photons, trapped atoms or ions, and nuclear spins in NMR systems. The first works on the role of entanglement in many-body physics to the physics of extended systems arose in the study of black holes. The Bekenstein–Hawking formula [1, 2] states that the entropy of a black hole is proportional to its area — an unusual behavior, since typically entropy scales with the volume of a system. This inspired the search for other sources of entropy. It was then observed by Bombelli *et al.* [3] and by Srednicki [4] that the entanglement entropy of an extended quantum system scales as the area of the subsystem, resembling the black hole entropy. Subsequently, Holzhey, Larsen, and Wilczek [5] found that, in the ground state of a (1+1)-dimensional conformal field theory (CFT), the entanglement entropy scales as the logarithm of the subsystem size, with a prefactor proportional to the central charge. However, this result initially remained within the high-energy community, in studies related to black hole physics.

In the early 2000s, the study of entanglement began to spread to the condensed matter community. Among the early works, an important one was by Osborne and Nielsen [6], which studied entanglement in the ground state of a spin chain between a few sites and the rest of the chain, as a function of the Hamiltonian parameters, finding a peak in correspondence to quantum phase transitions. Similarly, in [7] the entanglement among two individual spins inside a spin chain was studied.

The first paper in the condensed matter community to study the entanglement entropy of a ground state as a function of subsystem size in certain critical lattice models was [8], by Vidal, Latorre, Rico, and Kitaev. As expected, the entanglement was found to scale logarithmically, with a prefactor proportional to the central charge of the CFT describing the low-energy physics. Entanglement was also shown to determine the efficiency of numerical techniques for classically simulating quantum systems [9, 10]. In 2004, Calabrese and Cardy [11] rederived the results of [5] for (1+1)d CFTs and generalized them to different geometries, also discussing massive QFTs and lattice models. At this point, the use of quantum information measures to study quantum many-body systems was definitively established.

A further milestone in the high-energy community was the Ryu–Takayanagi formula [12], within the context of AdS/CFT holography. It states that the entanglement entropy of a holographic CFT on a subsystem A can be obtained from the dual gravity theory in Anti–de Sitter spacetime. Specifically, it is proportional to the area of the minimal surface extending into the gravitational bulk and anchored on the boundary of A. This further consecrated the use of quantum information ideas and tools in high-energy physics and, more generally, in the study of extended quantum systems.

This thesis explores further uses of tools from quantum information theory in the study of extended quantum systems. We now introduce some quantities and

ideas that will be extensively used throughout the thesis.

1.1 Entanglement entropy

Let $|\psi\rangle$ be a pure state on a factorized Hilbert space $\mathcal{H} = \mathcal{H}_A \otimes \mathcal{H}_B$. $|\psi\rangle$ is said to be *separable* if it can be written as

$$|\psi\rangle = |\psi\rangle_A \otimes |\psi\rangle_B \tag{1.1.1}$$

otherwise it is said to be *entangled*. Entanglement can be quantified with the use of the *entanglement entropy*. This is defined as the Von Neumann entropy

$$S_A = -\operatorname{Tr}(\rho_A \log \rho_A) \tag{1.1.2}$$

of the *reduced density matrix* on $\mathcal{H}_A$

$$\rho_A = \operatorname{Tr}_{\mathcal{H}_B}(|\psi\rangle\langle\psi|). \tag{1.1.3}$$

The entanglement entropy is always non-negative and is equal to zero if and only if ρ_A is pure, i.e. if $|\psi\rangle$ is separable. Notice that even if we have defined it as the Von Neumann entropy of ρ_A, the entanglement entropy is a property of the bipartition, because $S_A = S_B$.

Sometimes it can be useful to access entanglement entropy via the Rényi entropies, defined as

$$S_A^{(n)} = \frac{1}{1-n} \log \operatorname{Tr}(\rho^n). \tag{1.1.4}$$

From those, it is possible to get the entanglement entropy from the limit

$$S_A = \lim_{n \to 1} S_A^{(n)}. \tag{1.1.5}$$

1.1.1 Entanglement entropy in QFT

In a $(d+1)$-dimensional QFT, given a d-dimensional spatial slice Σ, one can consider the Hilbert space $\mathcal{H}_\Sigma$ of states supported on Σ. In the wave-functional approach, states in $\mathcal{H}_\Sigma$ are constructed by path-integrals over a $(d+1)$ manifold whose boundary is Σ. Different states are constructed either varying the geometry of the $(d+1)$ manifold or inserting operators in the path integral. The groundstate of a theory is realized performing euclidean path integral over a manifold that extends infinitely in euclidean time. For instance, in a (1+1)d QFT: if $\Sigma = \mathbb{R}$, the path integral is done on a half-space; if $\Sigma = S^1$, the path integral is done on a half-infinite cylinder; if $\Sigma = [0, 1]$, the path integral is done on a half-infinite strip.

When studying the entanglement between two spatial regions, one considers a bipartition $\Sigma = A \cup B$ and would like to express the total Hilbert space as $\mathcal{H}_A \otimes \mathcal{H}_B$.

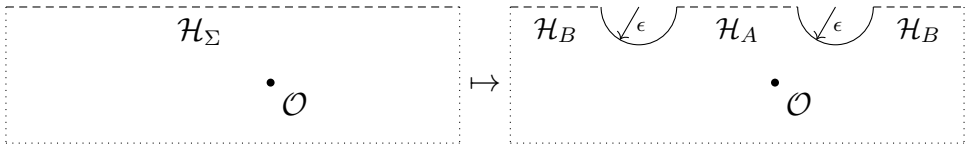


Figure 1.1: Insertion of the entangling surface between A and B. In this case we start from a state defined on the real line with a path integral over the lower half-plane, with the insertion of the operator $\mathcal{O}$ in a point. The entangling surface needs not to be circular, different shapes are equivalently good and correspond to different regularization schemes.

Unfortunately, if A and B are adjacent, this does not hold. However, if A and B are spatially separated by a finite region where the fields are not dynamical, such tensor product relation does hold. Such region at the interface between the two subsystems is called *entangling surface* [13]. Hence, in order to compute the entanglement entropy between two adjacent regions A and B, one first introduces by hand an entangling surface of typical length ϵ over which the fields are not dynamical, and then takes the limit $\epsilon \to 0$. We show an example of the insertion of the entangling surface in Fig. 1.1.

The entanglement entropy of a groundstates is said to obey an *area law*, it typically behaves like

$$S_A = \gamma \frac{|\partial A|}{\epsilon^{d-1}} + \text{subleading} \tag{1.1.6}$$

where γ is a non-universal coefficient that depends on the theory of study, on the shape of A, and on the regulation procedure—for what we described, it can depend on the shape of the entangling surface or also on the boundary condition set on it. Such behaviour was already observed in the first works [3, 4]. However, for a (1+1) CFT, the behaviour is different and when A is an interval of length ℓ it scales like [5, 11]

$$S_A \sim \frac{c}{3} \log(\ell/\epsilon) \tag{1.1.7}$$

where c is the central charge of the CFT.

A better sense of comprehension can be obtained looking at the expression for a generic (d+1) CFT, in the case in which A is a subsystem of typical length ℓ [14, 15]

$$S_A = p_1(\ell/\epsilon)^{d-1} + p_3(\ell/\epsilon)^{d-3} + \cdots + \begin{cases} p_{d-2}(\ell/\epsilon)^2 + \tilde{c}\log(\ell/\epsilon), & d \text{ odd} \\ p_{d-1}(\ell/\epsilon) + p_d, & d \text{ even} \end{cases} . \tag{1.1.8}$$

From this we can observe that the first term determines the area law (since $|\partial A| \sim \ell^{d-1}$), with subleading powers appearing one every two. For d odd there is a logarithmic term, whose coefficient $\tilde{c}$ is universal — for $d = 1$ it is equal to $c/3$, for $d = 3$ it is proportional to the central charge a [16] . While such results

were derived for a CFT, they are believed to hold for a generic QFT [15]. If the QFT flows to a CFT, then the central charges displayed would be the ones of the infra-red CFT. If the QFT flows to a gapped phase, and thus to a TQFT, the central charges would vanish. In $d = 2$, the constant term p_2 becomes topological and is called *topological entanglement entropy*[17, 18]

1.2 Entanglement asymmetry

Entanglement asymmetry quantifies how much a state breaks a given symmetry. It was first introduced under the name of "G-asymmetry" (where G is a group) in [19], within the context of resurce theory. It was later introduced independently in [20] under the name "entanglement asymmetry" in the context of quantum manybody systems. Similar quantities have been studied in the algebraic quantum field theory community under the name of "entropic order parameters" [21, 22]. In [23] we have extended it to generalized symmetries, as we will extensively discuss in chapter 4. Let us first define it for group-like symmetries.

Consider a density matrix $\rho \in \mathrm{End}(\mathcal{H})$ and a group G that acts unitarily on $\mathcal{H}$ with operators U_g where $g \in G$. We say that ρ is *symmetric* under G if

$$U_g \rho U_g^\dagger = \rho. \tag{1.2.1}$$

Then we define the *symmetrized density matrix* by acting with all the group elements on ρ and averaging over the group. For a finite group this reads

$$\rho_G = \frac{1}{|G|} \sum_{g \in G} U_g \rho U_g^\dagger \tag{1.2.2}$$

while for a compact Lie group this can be done integrating over G with the Haar measure

$$\rho_G = \frac{1}{\mathrm{vol}\, G} \int_G \mathrm{d}g\, U_g \rho U_g^\dagger. \tag{1.2.3}$$

The Haar measure is uniquely defined up to a positive multiplicative constant, often chosen such that $\int_G \mathrm{d}g = 1$. Here we don't stick to this choice, so we just write $\int_G \mathrm{d}g = \mathrm{vol}\, G$. The symmetrization map $\rho \mapsto \rho_G$ is sometimes called G-twirling operation [24]. Such map also corresponds to the projection over the subspace of operators that are symmetric under G, hence $\rho = \rho_G$ if and only if ρ is symmetric. The entanglement asymmetry, denoted by ΔS is then defined as the relative entropy between ρ and ρ_G

$$\Delta S(\rho) = S(\rho || \rho_G) = \mathrm{Tr}(\rho(\log \rho - \rho_G)). \tag{1.2.4}$$

Using the cyclicity of the trace, and the invariance of the Haar measure under left or right multiplication one can re-express it as

$$\Delta S(\rho) = S(\rho_G) - S(\rho). \tag{1.2.5}$$

Since it is a relative entropy, asymmetry enjoys a set of nice properties [25]

- It is non negative: $\Delta S(\rho) \geq 0$, $\forall \rho$
- Is equal to zero if and only if ρ is symmetric
- It is monotonic with the subsystem: $\Delta S(\rho_A) \geq \Delta S(\rho_{AB})$

For finite groups, it has an upper bound equal to $\log |G|$ [26]. For continuous groups, some bounds are discussed in [27].

As the entanglement entropy, entanglement asymmetry admits a "Rényi version", where Von Neumann entropies are replaced by Rényi entropies. The n-th Rényi asymmetry is defined as

$$\Delta S^{(n)}(\rho) = S^{(n)}(\rho_G) - S^{(n)}(\rho) = \frac{1}{1-n} \log \frac{\mathrm{Tr}\left((\rho_G)^n\right)}{\mathrm{Tr}\left(\rho^n\right)} \tag{1.2.6}$$

and gives the entanglement asymmetry in the limit $n \to 1$. For a finite group, substituting the definition of ρ_G and performing a change of variables on the sum, one obtains

$$\Delta S^{(n)}(\rho) = \frac{1}{1-n} \log \left[\frac{1}{|G|^{n-1}} \sum_{\substack{g_1,\dots,g_n \in G \\ \prod_j g_j = e}} \mathcal{Z}_n(g_1, \dots, g_n) \right], \tag{1.2.7}$$

where e is the identity element of the group and

$$\mathcal{Z}_n(g_1, \dots, g_n) = \mathcal{Z}_n(\mathbf{g}) = \frac{\mathrm{Tr}(\rho U_{g_1} \dots \rho U_{g_n})}{\mathrm{Tr}\left(\rho^n\right)}, \tag{1.2.8}$$

which we refer to as the *normalized charged moment*. Analogously, for a compact Lie group one obtains

$$\Delta S^{(n)}(\rho) = \frac{1}{1-n} \log \left[\frac{1}{(\mathrm{vol}\, G)^n} \int_{G^n} \mathrm{d}\mathbf{g} \frac{\mathrm{tr}(U_{g_1} \rho U_{g_1^{-1}} \dots U_{g_n} \rho U_{g_n^{-1}})}{\mathrm{tr}(\rho^n)} \right], \tag{1.2.9}$$

where $G^n = G \times \overset{n}{\cdots} \times G$ and $\mathbf{g} = (g_1, \dots, g_n) \in G^n$. This can be rewritten as

$$\Delta S^{(n)}(\rho) = \frac{1}{1-n} \log \left[\frac{1}{(\mathrm{vol}\, G)^{n-1}} \int_{G^n} \mathrm{d}\mathbf{g}\, \mathcal{Z}_n(\mathbf{g})\, \delta\left(\prod_{j=1}^{n} g_j - e \right) \right]. \tag{1.2.10}$$

1.2.1 Applications and a few relevant results

Entanglement asymmetry has been studied extensively in a variety of systems. The paper [20] directed the attention to the asymmetry of a subsystem (i.e. of a reduced density matrix), and studied its time evolution within a quench protocol where states that break a certain symmetry are evolved with a Hamiltonian that

has such symmetry. Over a subsystem, the reduced density matrix is expected to thermalize to a thermal ensemble, which should then be symmetric. Hence a *symmetry restoration* is expected, with the entanglement asymmetry going to zero as time passes. It was observed in [20] that the larger the asymmetry at initial time, the quicker it was going to zero in time. This has been called *quantum Mpemba effect*, and has been studied in a variety of setups, including integrable systems [28–31], CFTs [32], and quantum circuits [33, 34] (see [35] for a review).

Without considering time evolution, some classes of states have been studied. For instance, matrix product states [36], groundstates of spin chains [29, 37, 38], groundstates of field theories that display spontaneous symmetry breaking [39]. In [40] we have studied explicit symmetry breaking in groundstates of CFTs, and in [41] we have studied boundary symmetry breaking — i.e. the case in which a theory possess a symmetry, but the boundary conditions do not respect it. Another class of states are excited states in CFTs, and has been studied in [23, 32, 42]. We have extended the notion of entanglement asymmetry to generalized symmetries in [23]. In [43–46] the asymmetry with respect to $U(1)$ and $SU(N)$ symmetries was computed in the Page model of radiating black holes, yielding a cousin of the Page curve.

The most relevant result for the first two chapters of this thesis is that of Capizzi and Vitale on matrix product states (MPSs) [36]. They considered a translationally invariant MPS $|\psi\rangle$ with finite bond dimension, acted on onsite by a group G. Let H be the subgroup of G consisting of elements that commute with $\rho = |\psi\rangle\langle\psi|$. The asymmetry is computed on a subsystem A of ℓ sites. It is shown that for a finite group,

$$\lim_{\ell\to\infty} \Delta S(\rho_A) = \log \frac{|G|}{|H|}, \tag{1.2.11}$$

while for a compact Lie group,

$$\Delta S(\rho_A) = \frac{1}{2}(\dim \mathfrak{g} - \dim \mathfrak{h}) \log \ell + o(\log \ell). \tag{1.2.12}$$

In chapters 2 and 3 we will derive analogous formulas, together with results on the subleading terms for different classes of states. In chapter 2 we will consider ground states of CFTs — which cannot be described by MPSs with finite bond dimension — and in chapter 3 we also relax the assumption of translational invariance, adding the presence of boundaries.

1.2.2 Comparison with the use of order parameters

The traditional approach to study symmetry breaking is through order parameters. These are (local) operators that transform in an irreducible representation of the group, different from the trivial representation. Then one can show that if a state is symmetric, the expectation value of such operator has to vanish. Equivelently,

if the expectation value is not zero, one can conclude that the state breaks the symmetry.

However, the opposite implication (expectation value is zero $\implies$ symmetry is preserved) does not hold. Probably the simplest example is considering the state $|\psi\rangle = (|0\rangle + i\,|1\rangle)/\sqrt{2}$ on $\mathbb{C}^2$ with an action of $\mathbb{Z}_2$ implemented by $\{1, \sigma^x\}$. The Pauli matrix σ^z is odd under $\mathbb{Z}_2$ because $\sigma^x\sigma^z\sigma^x = -\sigma^z$, so σ^z is a good order parameter. One can see that even if the expectation value of the order parameter is zero, the state $|\psi\rangle$ is not symmetric. Indeed $\sigma^x\,|\psi\rangle = (|1\rangle + i\,|0\rangle)/\sqrt{2} = i\,(|0\rangle - i\,|1\rangle)/\sqrt{2}$ is different from $|\psi\rangle$, even in the projective space.

Entanglement asymmetry does not suffer from this problem, since a vanishing asymmetry does imply that the state is symmetric. Notice also that, in the previous example, choosing a different order parameter (e.g. σ^y) would have led to a nonzero expectation value, correctly detecting the symmetry breaking. In this sense, the asymmetry requires less information, as one does not need to find the appropriate order parameter.

The use of local order parameters often assumes some form of translational invariance, so that $\langle\psi|\,\mathcal{O}(x)\,|\psi\rangle$ does not depend on position. When translational invariance is absent—for instance, if the Hamiltonian is not translationally invariant, or if one studies a generic state not associated with a Hamiltonian—the order parameter becomes a function defined over the spatial manifold. In contrast, the asymmetry of the full system is a single number, providing a more compact characterization of the state. Local information can still be accessed by studying the asymmetry on subsystems.

The main down side of asymmetry is that it is difficult to compute. Analytic calculations have mostly used the replica-trick approach so far, computing the n-th Rényi asymmetry. Computing it for any n is a hard task, that typically involves computing correlation functions of a number of operators that scales linearly in n. Obtaining a closed form that allows to perform the limit $n \to 1$ is even harder. Numerically, Von Neumann asymmetry has been computed with exact diagonalization for instance in [20]. Numerics with free fermions and MPS allows for the calculation of Rényi asymmetry, but not for the Von Neumann asymmetry, so far.

1.3 Symmetries as topological operators

In the last decade, a new way of looking at symmetries in quantum field theory has been consolidated: the idea that the symmetries of a theory are identified with the presence of *topological operators*.

The fact that symmetries imply the presence of topological operators has been known for a long time. An elementary example is the case of a $U(1)$ symmetry, where Noether's theorem implies the existence of a conserved current j, whose

conservation law can be expressed as $d \star j = 0$. For a QFT in $(d+1)$ dimensions, the charge operator on a d-dimensional manifold Σ_d is obtained as the flux of the current

$$Q_{\Sigma_d} = \int_{\Sigma_d} \star j \tag{1.3.1}$$

and the $U(1)$ operator is obtained from its exponential

$$U_{\Sigma_d}(\alpha) = \exp\left(i\alpha Q_{\Sigma_d}\right) \qquad \alpha \in U(1). \tag{1.3.2}$$

Then, Stokes' theorem implies that the group operator depends on Σ_d only topologically, i.e. a continuous deformation of Σ_d does not change the operator. When the support manifolds of two topological operators coincide, the operators fuse according to the group-law multiplication

$$U_{\Sigma_d}(\alpha) U_{\Sigma_d}(\alpha') = U_{\Sigma_d}(\alpha + \alpha'). \tag{1.3.3}$$

Extended operators supported on submanifolds of spacetime are also called defects, since they correspond to modifications of the path integral localized on those submanifolds. If the submanifold has a time component, this can be viewed as a modification of the Hamiltonian — a defect that extends in time.

The new perspective, typically attributed to [47], is that the notion of symmetry itself can be redefined as the presence of topological operators. This naturally allows for generalizations: topological operators may be supported on submanifolds of higher codimension, giving rise to *higher-form symmetries*. These were introduced in [47] itself, which recast known results in a clear framework and showed that these new symmetries truly behave as symmetries, as they can lead to Ward identities, can be spontaneously broken, and can possess anomalies protected by the RG flow.

Another type of generalization is obtained by relaxing the requirement that topological operators or defects fuse according to a group multiplication law. These are referred to as *non-invertible symmetries*, or *categorical symmetries*. Examples of such topological defects were already known in two-dimensional rational CFTs [48–50], in integrable lattice models in two dimensions [51, 52], and in topologically ordered states [53]. In light of [47], these defects were recognized as proper symmetries, opening the door to connections with gauge theories, RG flows, and anomalies (see e.g. [54–56]).

1.4 Outline of the thesis

In chapter 2, we describe how to study entanglement asymmetry in quantum field theory using the replica trick. Specifically, we analyze (1+1)-dimensional CFTs with an explicitly broken symmetry, obtaining the asymptotic behaviour with the subsystem size, thereby extending (1.2.12). We also discuss the explicit example of the Majorana CFT.

In chapter 3, we consider instead the case where a symmetry is preserved in the bulk of the CFT but broken by a choice of boundary condition. We find that (1.2.11) still holds, with power-law subleading terms whose exponent is determined by the conformal dimension of certain boundary-changing operators. We then study quantum quenches, where a boundary condition is used to prepare the ground state of a CFT and is subsequently changed abruptly in time.

In chapter 4, we extend the notion of entanglement asymmetry to finite generalized symmetries. The crucial step is to define a symmetrizer, which can no longer be inherited from a group structure. We provide an explicit expression for the symmetrizer that applies both to higher-form and non-invertible symmetries in arbitrary dimensions. We then discuss several examples of non-invertible symmetries in (1+1)-dimensional CFTs and TQFTs.

The last chapter departs from the topic of entanglement asymmetry and explores some entanglement properties of non-Hermitian systems. In particular, we study the non-Hermitian SSH model and the non-unitary CFT describing one of its critical points, the *bc*-ghost CFT. For these systems, we investigate the *symmetry-resolved entanglement* and the entanglement Hamiltonian.

Lastly, in Appendix 5.A, we describe some future directions.

Chapter 2

Bulk explicit symmetry breaking

In this chapter, we examine the implications of quantum criticality for the entanglement asymmetry, using CFT methods. To this end, we develop a general scheme to compute the entanglement asymmetry in (1+1)-dimensional quantum field theories in terms of the charged moments of the subsystem's reduced density matrix. Employing the path integral formulation, the charged moments can be identified with the partition functions of the theory on Riemann surfaces with defect lines inserted along its branch cuts. These defect lines are associated with the elements of the symmetry group under analysis. A symmetry is explicitly broken when the associated defects are not topological, and any continuous deformation of these defects leads to a change in the partition function.

We apply this approach to determine the entanglement asymmetry in the ground state of the XY spin chain at the Ising critical line for the $U(1)$ group of spin rotations around the transverse direction. After fermionizing it through a Jordan-Wigner transformation, the scaling limit of this model is described by the massless Majorana fermion theory and the defect lines corresponding to this group are marginal. We then exploit conformal invariance to map the Riemann surfaces to a single cylinder with defect lines parallel to its axis. In this setup, the calculation of the partition functions for large subsystems boils down to computing the ground state energy of the massless Majorana fermion on a circle with equally-spaced marginal point defects. The spectrum of this theory has been studied on the lattice in Refs. [57, 58]. Here we revisit this problem and diagonalize systematically its Hamiltonian for an arbitrary number of equi-spaced point defects of different strengths.

The study of defects in the massless Majorana fermion and Ising CFTs has a long story, see e.g. [50–52, 59–67]. Partition functions on Riemann surfaces with (topological and non topological) defect lines also arise in the analysis of the entanglement across inhomogeneities, interfaces, or junctions and after measurements [68–81]; in particular, those with topological defect lines appear in the symmetry resolution of entanglement measures [82–87] (and many other papers)

which has recently been investigated in profusion.

The chapter is organized as follows. In Sec. 2.1 we show how to compute the entanglement asymmetry from the partition function on a Riemann surface with defect lines. We also derive the asymptotic behavior of the entanglement asymmetry for a generic compact Lie group in the ground state of a one dimensional critical system. In the rest of the sections, we focus on the critical XY spin chain/Kitaev chain, and the associated CFT, the massless Majorana fermion theory. In Sec. 2.2, we introduce these systems and we review the known previous results for the entanglement asymmetry. In Sec. 2.3, we calculate the partition function of the Majorana CFT on the Riemann surfaces that enter in the calculation of the entanglement asymmetry. In particular, by conformal invariance, these partition functions are given by the ground state energy of a massless Majorana fermion with evenly-spaced point defects. We diagonalize its Hamiltonian for an arbitrary number of defects with different strengths. In Sec. 2.4, we apply these results to obtain the entanglement asymmetry of the critical XY spin chain, checking them against exact numerical computations on the lattice. Finally, in Sec. 2.5, we draw our conclusions and consider future prospects. We also include several appendices where we discuss with more detail some technical points of the main text.

2.1 Symmetries, topological defects, and entanglement asymmetry

In this section, we briefly review the identification between symmetries and topological defects. Then we introduce the Rényi entanglement asymmetry as a quantifier of symmetry breaking and we interpret it in terms of defects. With simple scaling arguments, we derive some general results for the asymptotic behavior of the Rényi entanglement asymmetry in the ground state of a critical one dimensional quantum system in the thermodynamic limit.

2.1.1 Symmetries and topological defects

Global symmetries in spatially extended quantum systems are realized through extended operators that form a unitary representation of the symmetry group. In fact, if we consider a generic (1+1)-dimensional quantum field theory whose spacetime is a flat surface $\mathcal{M}$, then the action of an element g of the group G (either discrete or continuous) is implemented in its Hilbert space $\mathcal{H}$ by a unitary operator $U_{\Sigma_t,g}$ that has support on a spatial line $\Sigma_t \subset \mathcal{M}$ at a fixed time t.

The transformation of a field ϕ of the theory under the group G is described by a matrix R_g such that

$$U^\dagger_{\Sigma_t,g}\phi(x)U_{\Sigma_t,g} = R_g\phi(x), \quad x \in \Sigma_t. \tag{2.1.1}$$

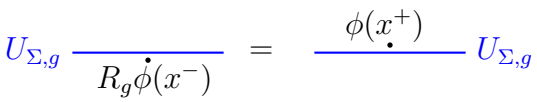


Figure 2.1: Graphical representation of (2.1.2). The insertion of an extended operator $U_{\Sigma,g}$ associated with the element g of a group G and with support on the line Σ corresponds, in the path integral approach, to a defect line along Σ with the gluing condition (2.1.2) for the field $\phi(x)$ at each side of the defect.

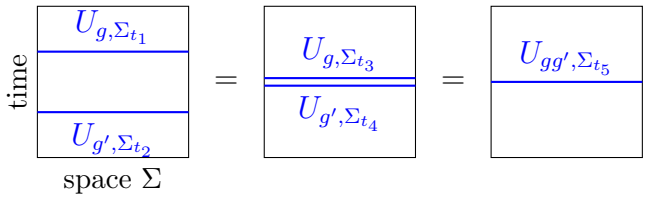


Figure 2.2: Each element g of a group G acts on the Hilbert space of an extended quantum system as a unitary operator $U_{\Sigma_t,g}$ defined along a line Σ_t at a fixed time t. If G is a symmetry of the theory, then any continuous transformation of Σ_t, as the ones performed in the figure, leaves invariant the partition function with insertions of these operators. We indicate this by the symbol = between the three diagrams. When two operators $U_{\Sigma_t,g}$ and $U_{\Sigma_t,g'}$ overlap, as in the right diagram, they can be fused according to the composition rule $U_{\Sigma_t,g}U_{\Sigma_t,g'} = U_{\Sigma_t,gg'}$.

Therefore, within the path integral formalism, the insertion of an operator $U_{\Sigma_t,g}$ in an expectation value is equivalent to performing a cut along the line Σ_t and imposing for the fields the following gluing conditions

$$\phi(x^+) = R_g\phi(x^-), \quad x \in \Sigma_t, \tag{2.1.2}$$

where $\phi(x^\pm)$ denote the field $\phi(x)$ at each side of the cut as we indicate in Fig. 2.1. The composition property $U_{\Sigma_t,g}U_{\Sigma_t,g'} = U_{\Sigma_t,gg'}$ can be then understood as the fusion of two cuts with gluing conditions R_g and $R_{g'}$ into a cut with gluing condition $R_gR_{g'} = R_{gg'}$ (see Fig. 2.2). In Euclidean spacetime, $U_{\Sigma,g}$ is not needed to be defined along a line Σ_t orthogonal to the time direction, but it can have support on any curve Σ on the surface $\mathcal{M}$. Due to the previous considerations, the extended operators $U_{\Sigma,g}$ are commonly referred to as *defects*, and when they enforce symmetries, they are *topological defects* [47]. A more detailed introduction to the role of topological operators in quantum systems can be found in, e.g., the recent review [88].

The question of whether a system is symmetric under a certain group can thus be reformulated as asking whether the defects associated to the symmetry are topological. In this chapter, we are interested in quantifying the extent to which a symmetry is broken or, in some sense, measuring how much the corresponding defects are not topological. This can be done with the entanglement asymmetry.

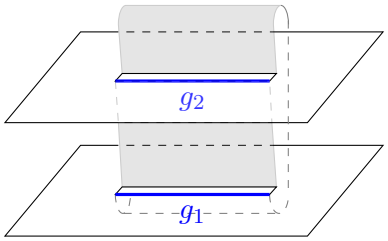


Figure 2.3: Riemann surface $\mathcal{M}_n$ for $n = 2$ (two sheets) with line defects (in blue) inserted along the branch cut of each sheet. The defects are associated respectively with the group elements g_1 and g_2. The quotient (2.1.5) of the partition functions on this surface with and without the line defects gives the normalized charged moment $\mathcal{Z}_2(\mathbf{g})$, defined in (1.2.8). The Dirac delta in (1.2.10) will set $g_2 = g_1^{-1}$.

2.1.2 Entanglement asymmetry from defects

In a (1+1) quantum field theory, using the path integral representation of the reduced density matrix ρ_A, the neutral moments $\mathrm{tr}(\rho_A^n)$ can be identified with the partition function on an n-sheet Riemann surface $\mathcal{M}_n$ [11]. If we consider the ground state $|0\rangle$ of the theory, i.e. $\rho = |0\rangle\langle 0|$, and a single interval of length ℓ as subsystem A, the surface $\mathcal{M}_n$ is constructed as follows. We take the spacetime $\mathcal{M}$ where the theory is defined, which is the complex plane when working in Euclidean time and in the thermodynamic limit (infinite spatial direction). To obtain $\mathcal{M}_n$, we perform a cut on $\mathcal{M}$ along the interval $A = [0, \ell]$, we replicate n times this cut plane, and we sew the copies together along the cuts in a cyclical way, as we show in Fig. 2.3 for $n = 2$. Denoting as $Z(\mathcal{M}_n)$ the partition function on this surface, the neutral moments of ρ_A are given by

$$\mathrm{tr}(\rho_A^n) = \frac{Z(\mathcal{M}_n)}{Z(\mathcal{M})^n}. \tag{2.1.3}$$

Following the discussion in Sec. 2.1.1, the insertion of the operators U_{A,g_j} in this trace, as in (1.2.8), corresponds to putting a defect line along the branch cut $[0, \ell]$ of each sheet of $\mathcal{M}_n$ with a gluing condition (2.1.2), being $g = g_j$, as depicted in Fig. 2.3. If $Z(\mathcal{M}_n^{\mathbf{g}})$ stands for the partition function on the surface $\mathcal{M}_n$ with these n defect lines, then we have that

$$\mathrm{tr}(\rho_A U_{A,g_1} \cdots \rho_A U_{A,g_n}) = \frac{Z(\mathcal{M}_n^{\mathbf{g}})}{Z(\mathcal{M})^n}. \tag{2.1.4}$$

Therefore, in the ground state, the normalized charged moments $\mathcal{Z}_n(\mathbf{g})$ introduced in (1.2.8) are the ratio of the partition functions on the surface $\mathcal{M}_n$ with and without n defect lines inserted at the branch cut of each sheet,

$$\mathcal{Z}_n(\mathbf{g}) = \frac{Z(\mathcal{M}_n^{\mathbf{g}})}{Z\left(\mathcal{M}_n\right)}. \tag{2.1.5}$$

If G is a symmetry of the theory, then $[\rho_A, U_{A,g}] = 0$ for all $g \in G$. As we have previously seen, this implies that the defect lines associated with the insertions U_{A,g_j} are topological and they can be moved between the sheets of $\mathcal{M}_n$ under continuous transformations leaving the partition function $Z(\mathcal{M}_n^{\mathbf{g}})$ invariant. In that case, it is possible to fuse them in the same sheet, which is equivalent to the equality $\mathrm{tr}(\rho_A U_{A,g_1} \dots \rho_A U_{A,g_n}) = \mathrm{tr}(\rho_A^n U_{A,g_1 \cdots g_n})$. Since the Dirac delta in (1.2.10) forces the product of all the group elements g_j to be the identity, the fusion yields $U_{A,g_1,\dots g_n} = \mathrm{id}_{\mathcal{H}}$. Consequently, $\mathcal{Z}_n(\mathbf{g}) = 1$ and, according to (1.2.10), the Rényi entanglement asymmetry vanishes. On the other hand, if G is not a symmetry, $[\rho_A, U_{A,g}] \neq 0$, then the defect lines associated to U_{A,g_j} are not topological. In that case, any continuous deformation of them does change the partition function $Z(\mathcal{M}_n^{\mathbf{g}})$ and, as a result, $\mathcal{Z}_n(\mathbf{g}) \neq 1$. In this sense, the entanglement asymmetry quantifies how much the defect lines associated with a group are non topological.

From generic scaling arguments, we can determine the asymptotic behavior of the partition functions $Z(\mathcal{M}_n)$ and $Z(\mathcal{M}_n^{\mathbf{g}})$. In two dimensions, the leading order contributions to the free energy $-\log Z$ are proportional to the area $|\mathcal{M}_n|$ of the surface $\mathcal{M}_n$, on which the partition function Z is defined. [Strictly speaking, the area $|\mathcal{M}_n|$ is infinity, but it can be regularized, for instance by imposing periodic boundary conditions both spatial and imaginary time directions for each sheet of $\mathcal{M}_n$, far away from the interval.] Therefore, in the absence of defects,

$$-\log Z(\mathcal{M}_n) = f_{\mathrm{bulk}}|\mathcal{M}_n| + O(1), \tag{2.1.6}$$

where f_{bulk} is the bulk free energy density. In the presence of defects, we expect that each of them contributes with an additional term proportional to the volume of the defect, which in this case is the length ℓ of the interval A. The free energy in that case is

$$-\log Z(\mathcal{M}_n^{\mathbf{g}}) = f_{\mathrm{bulk}}|\mathcal{M}_n| + T_n(\mathbf{g})\ell + O(1), \quad \text{with} \quad T_n(\mathbf{g}) \coloneqq \sum_{j=1}^{n} t(g_j), \tag{2.1.7}$$

and $t(g_j)$ can be interpreted as the line tension of the defect associated with the insertion U_{A,g_j}. All these terms are cut-off dependent and, therefore, non universal. Plugging (2.1.6) and (2.1.7) into (2.1.5), one sees that the bulk contribution in the free energy cancels, and the charged moments $\mathcal{Z}_n(\mathbf{g})$ decay exponentially with the subsystem length ℓ as

$$\mathcal{Z}_n(\mathbf{g}) = e^{-T_n(\mathbf{g})\ell + O(1)}. \tag{2.1.8}$$

If the theory is critical, the conical singularities at the branch points of the surface $\mathcal{M}_n$ give rise in (2.1.6) and (2.1.7) to an extra universal (cut-off independent) term,

$$-\log Z(\mathcal{M}_n^{\mathbf{g}}) = f_{\mathrm{bulk}}|\mathcal{M}_n| + T_n(\mathbf{g})\ell - \log Z_{\mathrm{CFT}}(\mathcal{M}_n^{\mathbf{g}}) + O(1), \tag{2.1.9}$$

which, as argued for instance in Ref. [89], behaves as $-\log Z_{\mathrm{CFT}}(\mathcal{M}_n^{\mathbf{g}}) \propto \log \ell$. The presence of defect lines may in general modify the coefficient of this term, so

$$\frac{Z_{\mathrm{CFT}}(\mathcal{M}_n^{\mathbf{g}})}{Z_{\mathrm{CFT}}(\mathcal{M}_n)} = \ell^{-\beta_n(\mathbf{g})} \tag{2.1.10}$$

and it does not cancel in the ratio (2.1.5) of partition functions that gives the normalized charge moments $\mathcal{Z}_n(\mathbf{g})$. Therefore, for a critical system, we expect

$$\mathcal{Z}_n(\mathbf{g}) = e^{-T_n(\mathbf{g})\ell + O(1)} \ell^{-\beta_n(\mathbf{g})}, \tag{2.1.11}$$

where the coefficient $\beta_n(\mathbf{g})$ is universal and can be computed in the infrared (IR) CFT that describes the critical system. It depends on the specific CFT and the nature of the defects corresponding to the group G under study, and we do not have a generic expression for it. Its computation has to be worked out case by case. In this chapter, we calculate it in the massless Majorana fermion field theory for a $U(1)$ group for which the defects are marginal.

Asymptotic behavior

Before delving into the study of the charged moments and entanglement asymmetry in a particular theory, it is insightful to explore the implications of the generic result of (2.1.11) for the asymptotic behavior of the entanglement asymmetry in the limit of large subsystem size ℓ.

When we plug (2.1.11) in (1.2.10), we have to perform an n-fold integral over the group G. Since the leading term in (2.1.11) decays exponentially with ℓ, the main contribution to this integral comes from the points $\mathbf{h} \in G^n$ where $\mathcal{Z}_n(\mathbf{h}) = 1$ (i.e. where both $T_n(\mathbf{h})$ and $\beta_n(\mathbf{h})$ vanish). These correspond to the elements of G that leave the reduced density matrix ρ_A invariant and form a symmetry subgroup H of G. i.e.

$$H = \left\{ h \in G \mid U_{A,h} \rho_A U_{A,h}^\dagger = \rho_A \right\}. \tag{2.1.12}$$

Therefore, the strategy is to perform a saddle point approximation of the integral (1.2.10) around the points $\mathbf{h} \in H^n$; see also Refs. [29, 31, 36, 90].

For simplicity, let us assume that H is a finite subgroup. In the integral (1.2.9) the numerator $\mathrm{tr}(U_{A,g_1} \rho_A U_{A,g_1^{-1}} \dots U_{A,g_n} \rho_A U_{A,g_n^{-1}})$ is invariant under a right multiplication $(g_1, \dots, g_n) \mapsto (g_1 h_1, \dots, g_n h_n)$. Consequently, all the saddle points $\mathbf{h} \in H^n$ contribute equally. Then, to calculate the integral (1.2.10) for $\ell \gg 1$, we can expand it around the identity point $(\mathrm{id}_G, \dots, \mathrm{id}_G) \in G^n$, where id_G is the identity in G, and multiply the result by the total number of saddle points, which is given in terms of the cardinality $|H|$ of H as $|H|^{n-1}$. We finally perform the integral by choosing some local coordinates on the group around the identity.

In a neighborhood $\mathcal{U}_{\mathrm{id}_G} \subset G$ of the identity, the group elements g can be written as $g = e^{iX}$, where X is an element of the Lie algebra $\mathfrak{g}$ associated with G, of

dimension $d = \dim G$. Let $\{J_a\}$, $a = 1, \dots, d$, be generators of $\mathfrak{g}$, if we take the local coordinate chart $\mathrm{x} = (x_1, \dots, x_d) \in \mathbb{R}^d \mapsto g(\mathrm{x}) = e^{i\sum_a x_a J_a}$, then, for an arbitrary function $f(g)$ on G, we have

$$\int_{\mathcal{U}_{\mathrm{id}_G}} \mathrm{d}g\, f(g) = \int_{g^{-1}(\mathcal{U}_{\mathrm{id}_G})} \mu(\mathrm{x})\mathrm{d}x\, f(g(\mathrm{x})), \tag{2.1.13}$$

where $\mu(\mathrm{x})\mathrm{d}x$ is the Haar measure of G in the local coordinates x. Since we have to perform an n-fold integral over G, we denote by $\mathbf{x}$ the coordinates for G^n, that is $\mathbf{x} = (\mathrm{x}_1, \dots, \mathrm{x}_n) \in \mathbb{R}^{dn}$. Now we can express the exponents $T_n(\mathbf{g})$ and $\beta_n(\mathbf{g})$ of the charged moments (2.1.11) in coordinates and expand them around the identity, which corresponds to $\mathbf{x} = \mathbf{0}$,

$$\begin{aligned} T_n(\mathbf{g}(\mathbf{x})) &= \frac{1}{2}\mathbf{x}^{\mathrm{t}}\mathsf{H}_{T_n}\mathbf{x} + O(\mathbf{x}^3), \\ \beta_n(\mathbf{g}(\mathbf{x})) &= \frac{1}{2}\mathbf{x}^{\mathrm{t}}\mathsf{H}_{\beta_n}\mathbf{x} + O(\mathbf{x}^3), \end{aligned} \tag{2.1.14}$$

where H_{T_n} and H_{β_n} are $dn \times dn$ Hessian matrices, made of $n \times n$ blocks of dimension $d \times d$. Therefore, in the local coordinate chart that we are considering, for large ℓ the n-fold integral (1.2.10) reads

$$\int_{G^n} \mathcal{Z}_n(\mathbf{g})\delta\Big(\prod_j g_j - \mathrm{id}_G\Big)\mathrm{d}\mathbf{g} \sim |H|^{n-1}\mu(0)^{n-1} \int_{\mathbb{R}^{dn}} \mathrm{d}\mathbf{x}\, e^{-\frac{1}{2}\mathbf{x}^{\mathrm{t}}(\mathsf{H}_{T_n}\ell + \mathsf{H}_{\beta_n}\log\ell)\mathbf{x}} \delta\left(\sum_{j=1}^{n} \mathrm{x}_j\right). \tag{2.1.15}$$

Here the factor $|H|^{n-1}$ counts the total number of saddle points. In coordinates, the Dirac delta $\delta\left(\prod_j g_j - \mathrm{id}_G\right)$ over the group G is replaced by $\delta\left(\sum_{j=1}^n \mathrm{x}_j\right)/\mu(0)$. Notice that we have also expanded the measure $\mu(\mathrm{x})$ around $\mathrm{x} = 0$ and restricted to the zeroth order term $\mu(0)$ since the next order terms yield subleading corrections in ℓ.

Since $T_n(\mathbf{g})$ is the sum of the contributions of each defect line according to (2.1.7), H_{T_n} is block diagonal, $\mathsf{H}_{T_n} = \mathrm{id}_n \otimes \mathsf{H}_t$, where H_t is the $d \times d$ dimensional Hessian of $t(g(x))$. Due to the cyclic property of the trace, the coefficient $\beta_n(\mathbf{g})$ is symmetric under cyclic permutations of the entries g_j of $\mathbf{g}$. Thus H_{β_n} is a block-circulant matrix; that is, it has the block structure

$$\mathsf{H}_{\beta_n} = \begin{pmatrix} \mathsf{C}_1 & \mathsf{C}_n & \cdots & \mathsf{C}_3 & \mathsf{C}_2 \\ \mathsf{C}_2 & \mathsf{C}_1 & \mathsf{C}_n & & \mathsf{C}_3 \\ \vdots & \mathsf{C}_2 & \mathsf{C}_1 & \ddots & \vdots \\ \mathsf{C}_{n-1} & & \ddots & \ddots & \mathsf{C}_n \\ \mathsf{C}_n & \mathsf{C}_{n-1} & \cdots & \mathsf{C}_2 & \mathsf{C}_1 \end{pmatrix}, \tag{2.1.16}$$

with blocks C_j of size $d \times d$. A block-circulant matrix can be diagonalized in blocks D_p, $p = 0, \dots, n-1$, with a Fourier transform of the blocks C_j,

$$\mathsf{D}_p = \sum_{j=1}^{n} \mathsf{C}_j e^{i\frac{2\pi}{n}jp}. \tag{2.1.17}$$

Therefore, if we apply the change of variables

$$\mathrm{x}_j = \frac{1}{\sqrt{n}} \sum_{p=0}^{n-1} \omega_p e^{-i\frac{2\pi}{n}jp}, \qquad j = 1, \dots, n, \tag{2.1.18}$$

then the integral (2.1.15) becomes

$$\int_{G^n} \mathcal{Z}_n(\mathbf{g}) \delta\Big(\prod_j g_j\Big) \mathrm{d}\mathbf{g} \sim \frac{|H|^{n-1}\mu(0)^{n-1}}{\sqrt{n}} \int_{\mathbb{R}^{dn}} \mathrm{d}\boldsymbol{\omega}\, e^{-\frac{1}{2}\sum_{p=0}^{n-1} \omega_p (\mathsf{H}_t \ell + \mathsf{D}_p \log \ell)\omega_p} \delta(\omega_0). \tag{2.1.19}$$

Integrating out the variable ω_0, we find

$$\int_{G^n} \mathcal{Z}_n(\mathbf{g}) \delta\Big(\prod_j g_j\Big) \mathrm{d}\mathbf{g} \sim \frac{|H|^{n-1}\mu(0)^{n-1}}{\sqrt{n}} \prod_{p=1}^{n-1} \int_{\mathbb{R}^d} \mathrm{d}\omega\, e^{-\frac{1}{2}\omega(\mathsf{H}_t \ell + \mathsf{D}_p \log \ell)\omega}. \tag{2.1.20}$$

The remaining integral is Gaussian and we can easily perform it, if we assume that $\mathsf{H}_t \ell + \mathsf{D}_p \log \ell$ is a symmetric definite-positive matrix,

$$\int_{\mathbb{R}^d} \mathrm{d}\omega e^{-\frac{1}{2}\omega(\mathsf{H}_t \ell + \mathsf{D}_p \log \ell)\omega} = \left(\det\left(2\pi(\mathsf{H}_t \ell + \mathsf{D}_p \log \ell)^{-1}\right)\right)^{1/2}. \tag{2.1.21}$$

Plugging it in (2.1.20), we obtain

$$\int_{G^n} \mathcal{Z}_n(\mathbf{g}) \delta\left(\prod_j g_j - \mathrm{id}_G\right) \mathrm{d}\mathbf{g} \sim \frac{(2\pi\ell)^{\frac{d(1-n)}{2}}}{\sqrt{n}} \left(\frac{|H|\mu(0)}{\sqrt{\det \mathsf{H}_t}}\right)^{n-1} \prod_{p=1}^{n-1} \left(\det\left(\mathbb{1}_{d\times d} + \mathsf{H}_t^{-1}\mathsf{D}_p \frac{\log \ell}{\ell}\right)\right)^{1/2}. \tag{2.1.22}$$

This result is independent of the local coordinate chart that we consider to perform the integration. In fact, under a change of local coordinates $\mathrm{x} \mapsto \mathrm{y}(\mathrm{x})$, the measure $\mu(\mathrm{x})$ transforms as $\mu(\mathrm{x}) = \left|\det(\partial y^\sigma/\partial x^b)\right| \mu'(\mathrm{y})$ and, because quadratic forms are $(0,2)$-tensor fields, the determinant of the Hessian H_t transforms as $\det \mathsf{H}_t(\mathrm{x}) = \left|\det(\partial y^\sigma/\partial x^b)\right|^2 \det \mathsf{H}'_t(\mathrm{y})$. Therefore, the quotient $\mu(0)/\sqrt{\det \mathsf{H}_t}$ is coordinate independent. The same applies for the terms $\det(\mathbb{1}_{d\times d} + \mathsf{H}_t^{-1}\mathsf{D}_p \log \ell/\ell)$.

Finally, applying (2.1.22) in (1.2.10) and using the identity $\log\det M = \mathrm{tr}\log M$ for a matrix M, we find that the Rényi entanglement asymmetry for a compact Lie group G in the ground state of a critical one dimensional quantum system behaves as

$$\Delta S_A^{(n)} = \frac{\dim G}{2} \log \ell + a_n + b_n \frac{\log \ell}{\ell} + \cdots, \tag{2.1.23}$$

where

$$a_n = \log \frac{\mathrm{vol}\, G}{|H|} + \frac{1}{2} \log \frac{n^{\frac{1}{n-1}} \det \mathsf{H}_t}{(2\pi)^{\dim G} \mu(0)^2}, \tag{2.1.24}$$

and

$$b_n = \frac{1}{2(n-1)} \sum_{p=1}^{n-1} \mathrm{tr}\left(\mathsf{D}_p \mathsf{H}_t^{-1}\right). \tag{2.1.25}$$

(2.1.23) is the first main result of this chapter. We stress that the first two terms in (2.1.23), of order $O(\log \ell)$ and $O(1)$ respectively, have already been observed in the XY spin chain when considering the particle number $U(1)$ (a)symmetry [29], and more generically for matrix product states in Ref. [91]. Crucially, what is new here is the last term in (2.1.23), of order $O(\log \ell/\ell)$. While the terms of order $O(\log \ell)$ and $O(1)$ are present in the ground state of critical and non-critical systems alike, the term of order $O(\log \ell/\ell)$ only appears when the system is at a critical point.

This $\log \ell/\ell$ term appears only when the exponent $\beta_n(\mathbf{g})$ in (2.1.11) is non-zero. Although this exponent is universal, the coefficient b_n is non-universal since it also depends on the defect tension $T_n(\mathbf{g})$ (via H_t), which is cut-off dependent. Semi-universal corrections of the form $\log \ell/\ell$ have been found in, e.g., the corner free energy in critical systems [92] and in the ground state full counting statistics of the critical XY spin chain [93].

We finally discuss the group structures that were not considered earlier. When both G and H are finite, it is straightforward to show that the logarithmic term is vanishing, the $O(1)$ term is just $\log(|G|/|H|)$ and there are no $\log \ell/\ell$ corrections (see also [91]). When both G and H are continuous, the leading $\log \ell$ term has a prefactor equal to $(\dim G - \dim H)/2$, but the explicit expressions for the subleading terms are more cumbersome and not very illuminating.

2.2 The XY spin chain and the massless Majorana fermion field theory

In the rest of the chapter, we focus on a particular gapless system: the XY spin chain at the Ising critical line. We consider its ground state, and compute the charged moments and the Rényi entanglement asymmetry associated with the rotations of the spin around the z-axis.

The Hamiltonian of the XY spin chain is

$$H_{\mathrm{XY}} = -\frac{1}{2} \sum_{j \in \mathbb{Z}} \left(\frac{1+\gamma}{2} \sigma_j^x \sigma_{j+1}^x + \frac{1-\gamma}{2} \sigma_j^y \sigma_{j+1}^y + h \sigma_j^z \right), \tag{2.2.1}$$

where σ_j^α are the Pauli matrices at the site j. The parameter γ tunes the anisotropy between the couplings in the x and y components of the spin and h is the strength of the transverse magnetic field. The XY spin chain is gapless along the lines $\gamma = 0$, $|h| < 1$ and $\gamma \neq 0$, $|h| = 1$ in parameter space, and the scaling limits along those lines are respectively the massless Dirac and Majorana fermion field theories.

For $\gamma \neq 0$, the Hamiltonian of (2.2.1) is not invariant under the rotations $U_\alpha = e^{i\alpha Q}$ around the z-axis, generated by the transverse magnetization

$$Q = \frac{1}{2}\sum_{j\in\mathbb{Z}}(\sigma_j^z - \mathbb{I}), \tag{2.2.2}$$

except for $\alpha = \pi$, which corresponds to the $\mathbb{Z}_2$ spin flip symmetry. The entanglement asymmetry associated with this $U(1)$ symmetry has been thoroughly studied in Ref. [29] for the ground state of (2.2.1) outside the critical lines $\gamma \neq 0$, $|h| = 1$ using exact methods on the lattice. In that case, the charged moments $\mathcal{Z}_n(\boldsymbol{\alpha})$ decay exponentially for large subsystem size ℓ as in (2.1.8), where the coefficient $T_n(\boldsymbol{\alpha}) = \sum_{j=1}^n t(\alpha_j)$ is the sum of the string tension $t(\alpha_j)$ of each defect, which here is given by [29]

$$t(\alpha) = -\int_{-\pi}^{\pi}\frac{\mathrm{d}k}{4\pi}\log(i\cos\xi_k\sin\alpha + \cos\alpha), \tag{2.2.3}$$

with

$$e^{i\xi_k} = \frac{h - \cos k + i\gamma\sin k}{\sqrt{(h-\cos k)^2 + \gamma^2\sin^2 k}}. \tag{2.2.4}$$

Note that the string tension $t(\alpha)$ is not real; as we will see in Sec. 2.3, this is related to the fact that the gluing conditions of the defects associated with this $U(1)$ group make the theory non-Hermitian.

To obtain the Rényi entanglement asymmetry, we can apply the general result of (2.1.23). In this case, since $G = U(1)$, we have that $\dim G = 1$, $\mathrm{vol}\, G = 2\pi$, $\mu(0) = 1$, and the symmetric subgroup is the $\mathbb{Z}_2$ spin-flip symmetry, $H = \mathbb{Z}_2$. Since $\dim G = 1$, the block H_t is a scalar and it is given by (2.2.3) such that $\mathsf{H}_t = t''(0) = \partial^2 t(\alpha)/\partial\alpha^2|_{\alpha=0}$.

In Ref. [29], the following result was derived for the XY chain out of the critical line $|h| = 1$:

$$\Delta S_A^{(n)} = \frac{1}{2}\log\ell + \frac{1}{2}\log\frac{\pi t''(0) n^{1/(n-1)}}{2} + O(\ell^{-1}), \tag{2.2.5}$$

with

$$t''(0) = \begin{cases} \frac{1}{2}\frac{\gamma}{\gamma+1}, & |h| < 1, \\ \frac{1}{2}\frac{\gamma^2}{1-\gamma^2}\left(\frac{|h|}{\sqrt{h^2+\gamma^2-1}} - 1\right), & |h| > 1. \end{cases} \tag{2.2.6}$$

Notice that $t''(0)$ is continuous at $|h| = 1$, reflecting the fact that this result also applies along the critical line. Indeed, in this case, the string tension $T_n(\boldsymbol{\alpha})$ is still given by (2.2.3), and following the same steps as in Ref. [29] one arrives at the same result.

However, crucially for this chapter, along the critical line $\gamma \neq 0$, $|h| = 1$, we also expect that the charged moments $\mathcal{Z}_n(\boldsymbol{\alpha})$ contain the algebraically decaying factor of (2.1.11), according to the general reasoning of Sec. 2.1.2. However, an

analytical expression for the coefficient $\beta_n(\boldsymbol{\alpha})$ is unknown. In what follows, we will obtain it by exploiting the conformal invariance of the underlying field theory.

As we have already mentioned, the scaling limit of the XY spin chain (2.2.1) along the critical lines $\gamma \neq 0$, $|h| = 1$ is the massless Majorana fermion field theory, whose Hamiltonian is

$$H = \frac{1}{2i} \int_{\mathbb{R}} \psi(x)\partial_x\psi(x) - \bar{\psi}(x)\partial_x\bar{\psi}(x)\mathrm{d}x, \tag{2.2.7}$$

where the Majorana fields $\psi(x)$ and $\bar{\psi}(x)$ satisfy the algebra

$$\{\psi(x), \psi(y)\} = \delta(x-y), \qquad \psi^\dagger(x) = \psi(x), \tag{2.2.8}$$
$$\{\bar{\psi}(x), \bar{\psi}(y)\} = \delta(x-y), \qquad \bar{\psi}^\dagger(x) = \bar{\psi}(x), \tag{2.2.9}$$

and $\{\psi(x), \bar{\psi}(y)\} = 0$. The $U(1)$ charge operator in (2.2.2) corresponds in this field theory to

$$Q = i \int_{\mathbb{R}} \psi(x)\bar{\psi}(x)\mathrm{d}x. \tag{2.2.10}$$

The details on the derivation of the Hamiltonian (2.2.1) and Q in the continuum limit are reported in Appendix 2.A.

The transformations

$$U_{A,\alpha} = e^{i\alpha Q_A} = \exp\left(-\alpha \int_A \psi(x)\bar{\psi}(x)\mathrm{d}x\right) \tag{2.2.11}$$

generated by the charge (2.2.10) in a subsystem A act on the fields $\psi(x)$, $\bar{\psi}(x)$ in the following way

$$U^\dagger_{A,\alpha}\Psi(x)U_{A,\alpha} = \tilde{R}_\alpha\Psi(x), \qquad \text{if } x \in A, \tag{2.2.12}$$

with

$$\Psi = \begin{pmatrix}\psi\\ \bar{\psi}\end{pmatrix}, \quad \tilde{R}_\alpha = \begin{pmatrix}\cos\alpha & -\sin\alpha\\ \sin\alpha & \cos\alpha\end{pmatrix} \in SO(2). \tag{2.2.13}$$

The group action consists of a rotation that mixes ψ and $\bar{\psi}$. In general, this is not a symmetry of the theory, unless $\alpha = \pi$, for which $\psi \mapsto -\psi$ and $\bar{\psi} \mapsto -\bar{\psi}$. For α purely imaginary, the defect can be realized in the classical 2d Ising model by rescaling the couplings on all the bonds that intersect the defect line. A dictionary between the two realizations is given, e.g., in [72].

Crucially for our analysis, the field $\psi(x)\bar{\psi}(x)$ has scaling dimension 1, therefore the line defect implemented by $U_{A,\alpha}$ corresponds to a marginal perturbation of the CFT action along the line. This is very important for the calculations reported in Section 2.3, as it it introduces a non-trivial dependence of the CFT partition function on the defect strength α. Indeed, if the perturbation were instead irrelevant, then the effects of the defect would be renormalized to zero in the IR limit. If the

perturbation were relevant, then the defect would flow to some fixed point in the IR, corresponding to some boundary condition along the line, and the CFT partition function would also be independent on the precise value of α. For instance, such a situation would occur if we looked at the asymmetry with respect to rotations around the x-axis, as opposed to the z-axis, corresponding to replacing σ_j^z with σ_j^x in (2.2.2). In the CFT, this would then correspond to a perturbation by the relevant operator $\sigma(x)$ with scaling dimension 1/8. The defect line would flow to a fixed boundary condition in the IR, and this would completely change the way we do the analysis, see in particular Ref. [94] for more details on that situation.

2.3 Calculation of the scaling dimension associated to n defects in the Majorana CFT

In Sec. 2.1.2, we have seen that the charged moments $\mathcal{Z}_n(\boldsymbol{\alpha})$ can be cast as the ratio $Z(\mathcal{M}_n^{\boldsymbol{\alpha}})/Z(\mathcal{M}_n)$ between the partition function $Z(\mathcal{M}_n^{\boldsymbol{\alpha}})$ of the model on the n-sheet Riemann surface $\mathcal{M}_n$ with n defect lines with strengths $\boldsymbol{\alpha} = (\alpha_1, \dots, \alpha_n)$ along its branch cuts and the one, $\mathcal{Z}(\mathcal{M}_n)$, without them. As we discussed, in critical systems, this ratio contains a universal term $Z_{\mathrm{CFT}}(\mathcal{M}_n^{\boldsymbol{\alpha}})/Z_{\mathrm{CFT}}(\mathcal{M}_n)$, fully determined by the CFT that describes the low-energy physics. In this section, we study it in the massless Majorana fermion theory (2.2.7) for the marginal defect lines (2.2.11).

When there are no defects, it is well-known [5, 11, 95] that, for a generic CFT,

$$\frac{Z_{\mathrm{CFT}}(\mathcal{M}_n)}{Z_{\mathrm{CFT}}(\mathcal{M})^n} \propto \ell^{-2\delta_n}, \qquad \delta_n = \frac{c}{12}\left(n - \frac{1}{n}\right), \tag{2.3.1}$$

where c is the central charge of the CFT, which for the massless Majorana fermion is $c = 1/2$.

In the massless Majorana fermion theory, when we insert the n marginal defect lines along each branch cut of the surface $\mathcal{M}_n$, the result (2.3.1) changes as

$$\frac{Z_{\mathrm{CFT}}(\mathcal{M}_n^{\boldsymbol{\alpha}})}{Z_{\mathrm{CFT}}(\mathcal{M})^n} \propto \ell^{-2\left(\delta_n + \frac{\tilde{\Delta}_n(\boldsymbol{\alpha})}{n}\right)}, \tag{2.3.2}$$

as we will show below. The contribution of the n marginal defects is encoded in the exponent $\tilde{\Delta}_n(\boldsymbol{\alpha})$. Then the ratio of the partition functions on the surface $\mathcal{M}_n$ with and without defects is

$$\frac{Z_{\mathrm{CFT}}(\mathcal{M}_n^{\boldsymbol{\alpha}})}{Z_{\mathrm{CFT}}(\mathcal{M}_n)} = \ell^{-\frac{2}{n}\tilde{\Delta}_n(\boldsymbol{\alpha})}, \tag{2.3.3}$$

and, comparing with (2.1.11), $\beta_n(\boldsymbol{\alpha}) = \frac{2}{n}\tilde{\Delta}_n(\boldsymbol{\alpha})$. The rest of the section will be devoted to deriving (2.3.2) and computing explicitly the coefficient $\tilde{\Delta}_n(\boldsymbol{\alpha})$.

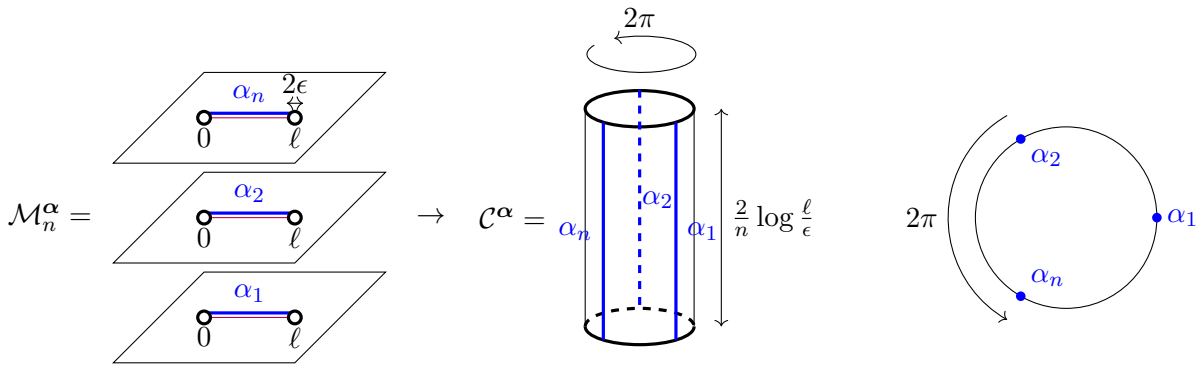


Figure 2.4: On the left, we represent the n-sheet Riemann surface $\mathcal{M}_n$ with n marginal defect lines inserted along the branch cut $[0, \ell]$ of each replica sheet, which arises in the calculation of the ground state charged moments $\mathcal{Z}_n(\boldsymbol{\alpha})$. At the branch points 0 and ℓ, two disks of radius ϵ have been removed as UV cut-off. Under the conformal transformation (2.3.4), $\mathcal{M}_n$ is mapped into the cylinder $\mathcal{C}$ on the middle, of circumference 2π and height $\frac{2}{n}\log\frac{\ell}{\epsilon}$. The defect lines in $\mathcal{M}_n$ are mapped into n evenly spaced vertical defects at the points $x_j = \frac{2\pi j}{n}, j = 1, \ldots, n$. The CFT partition functions on these two surfaces with the marginal defects are equal. On the right, top view of the cylinder $\mathcal{C}$ with the defects.

2.3.1 Conformal mapping to the cylinder with n defect lines

To determine the partition function $Z_{\text{CFT}}(\mathcal{M}_n^{\boldsymbol{\alpha}})$ with the n marginal defect lines, we perform the conformal transformation

$$z \mapsto w(z) = i \log\left[\left(\frac{z}{z-\ell}\right)^{1/n}\right]. \tag{2.3.4}$$

If at the branch points $z = 0$ and $z = \ell$ of the Riemann surface $\mathcal{M}_n$ we remove a disk of radius ϵ as a UV cut-off, then (2.3.4) maps $\mathcal{M}_n$ to a cylinder with circumference 2π and height $W = \frac{2}{n}\log(\ell/\epsilon)$, which we denote as $\mathcal{C}$, see Fig. 2.4. We choose as coordinates of the cylinder $w = x + i\tau$, with $x \sim x + 2\pi$ and $\tau \in [-\frac{1}{n}\log(\ell/\epsilon), \frac{1}{n}\log(\ell/\epsilon)]$.

Under (2.3.4), the n branch cuts $[0, \ell]$ of $\mathcal{M}_n$ are mapped to the equally-spaced lines $x_j = \frac{2\pi j}{n}$, $j = 1, \ldots, n$ ($x_n = 2\pi$ is identified with $x = 0$) on the cylinder, as we illustrate in Fig. 2.4. Thus, on the cylinder $\mathcal{C}$, the n marginal defects are inserted along these lines. We assume the Majorana fields $\psi, \bar{\psi}$ to have trivial monodromy on $\mathcal{M}_n$ along the cycle that connects all the replicas. Therefore, after the map (2.3.4), these fields satisfy anti-periodic boundary conditions on the cylinder since they have half-integer spin [96].

The next step is to carefully determine the gluing condition that is satisfied by the Majorana fields ψ and $\bar{\psi}$ across each defect after the conformal map (2.3.4) to the cylinder. In the previous section, we found that, on the Riemann surface $\mathcal{M}_n$,

the gluing condition across a defect with strength α_j is given by (2.2.12), i.e.

$$\Psi(z = x + i0^+) = \tilde{R}_{\alpha_j}\Psi(z = x + i0^-), \qquad \text{for} \quad x \in [0, \ell], \tag{2.3.5}$$

where the 2×2 matrix $\tilde{R}_{\alpha_j}$ is defined in (2.2.13). Crucially, this gluing condition changes under the conformal transformation (2.3.4). Indeed, since the Majorana fields ψ and $\bar{\psi}$ are primaries with conformal dimension $1/2$, they transform as

$$\psi(w) = \left(\frac{dw}{dz}\right)^{-1/2}\psi(z), \qquad \bar{\psi}(\bar{w}) = \left(\frac{d\bar{w}}{d\bar{z}}\right)^{-1/2}\bar{\psi}(\bar{z}). \tag{2.3.6}$$

Combining this with (2.3.5) and noting that a point slightly above the defect on $\mathcal{M}_n$ (i.e. at $z = x + i0^+$) is mapped to a point slightly to the left of the defect on the cylinder (i.e. at $w = x_j + i\tau + 0^-$), we find that the condition that ψ and $\bar{\psi}$ must satisfy across the defect at the line $x_j = \frac{2\pi j}{n}$ on the cylinder $\mathcal{C}$ is

$$\Psi(w = x_j + i\tau + 0^-) = R_{i\alpha_j}\Psi(w = x_j + i\tau + 0^+), \tag{2.3.7}$$

where we define

$$R_{i\alpha_j} = \begin{pmatrix} \left(\frac{dw}{dz}\right)^{-1/2} & 0 \\ 0 & \left(\frac{d\bar{w}}{d\bar{z}}\right)^{-1/2} \end{pmatrix} \tilde{R}_{\alpha_j} \begin{pmatrix} \left(\frac{dw}{dz}\right)^{1/2} & 0 \\ 0 & \left(\frac{d\bar{w}}{d\bar{z}}\right)^{1/2} \end{pmatrix} = \begin{pmatrix} \cos\alpha_j & i\sin\alpha_j \\ i\sin\alpha_j & \cos\alpha_j \end{pmatrix}. \tag{2.3.8}$$

Observe that, in the first equality, we can take out a factor $\left|\frac{dw}{dz}\right|^{-1/2}$ from the first matrix and a factor $\left|\frac{dw}{dz}\right|^{1/2}$ from the third one. Taking into account that $\frac{dw}{dz}/\left|\frac{dw}{dz}\right| = i$ for $z = x + i0^+$, we find the second equality.

In summary, using the conformal transformation (2.3.4), the partition function $Z_{\text{CFT}}(\mathcal{M}_n^{\boldsymbol{\alpha}})$ of the massless Majorana fermion with n marginal defect lines at the branch cuts of the surface $\mathcal{M}_n$ is equal to the partition function $Z_{\text{CFT}}(\mathcal{C}^{\boldsymbol{\alpha}})$ of the theory on the cylinder $\mathcal{C}$ with n equally-spaced defect lines along its longitudinal direction and described by the gluing conditions (2.3.7). If we impose conformal boundary conditions $|a\rangle$ and $|b\rangle$ at the extremes of the cylinder $\mathcal{C}$, the partition function $Z_{\text{CFT}}(\mathcal{C}^{\boldsymbol{\alpha}})$ can be written as

$$Z_{\text{CFT}}(\mathcal{C}^{\boldsymbol{\alpha}}) = \langle a|\, e^{-WH}\, |b\rangle\,, \tag{2.3.9}$$

where H is the Hamiltonian of the free Majorana fermion (2.2.7) defined on a circle of length 2π with the fields ψ and $\bar{\psi}$ satisfying the gluing conditions (2.3.8) at the points $x_j = \frac{2\pi j}{n}$, $j = 1, \ldots, n$ with strengths $\alpha = \alpha_1, \alpha_2, \ldots, \alpha_n$ respectively. Alternatively, as we show in detail in Appendix 2.B, these conditions can be explicitly implemented in the Hamiltonian (2.2.7) by including in it n point defects of the form $\psi(x_j)\bar{\psi}(x_j)$,

$$H = \frac{1}{2i}\int_0^{2\pi}(\psi\partial_x\psi - \bar{\psi}\partial_x\bar{\psi})\mathrm{d}x + \sum_{j=1}^{n} i\mu_j\psi(x_j)\bar{\psi}(x_j), \tag{2.3.10}$$

where the parameters μ_j are related to the strength of the defects by $\mu_j/2 = i \arctan(\alpha_j/2)$.

For $W \gg 2\pi$, i.e. for large subsystem length ℓ, the dominant term in the partition function (2.3.9) is given by the ground state energy $E(\boldsymbol{\alpha})$ of the Hamiltonian with defects (2.3.10),

$$Z_{\mathrm{CFT}}(\mathcal{C}^{\boldsymbol{\alpha}}) \propto e^{-WE(\boldsymbol{\alpha})}. \tag{2.3.11}$$

The ground state energy should satisfy the usual CFT formula

$$E(\boldsymbol{\alpha}) = \tilde{\Delta}_n(\boldsymbol{\alpha}) - \frac{c}{12}, \tag{2.3.12}$$

where $\tilde{\Delta}_n(\boldsymbol{\alpha})$ takes into account the contribution of the defects and, consequently, it vanishes, $\tilde{\Delta}_n(\mathbf{0}) = 0$, in their absence. It may be interpreted as the scaling dimension of a n-defect insertion operator. Combining the two previous equations, and taking into account that $W = \frac{2}{n}\log(\ell/\epsilon)$, we arrive at (2.3.2). Therefore, since $\tilde{\Delta}_n(\boldsymbol{\alpha}) = E(\boldsymbol{\alpha}) - E(\mathbf{0})$, the problem of computing the scaling dimension $\tilde{\Delta}_n(\boldsymbol{\alpha})$ boils down to determining the ground state energy of the Hamiltonian (2.3.10) with n point defects. We will devote the rest of this section to calculating it.

However, before proceeding, it is important to note that the gluing condition (2.3.8) on the cylinder presents an issue: if $\alpha \in \mathbb{R}$, it does not respect the self-adjointness of the Majorana fields $\psi(w)$ and $\bar{\psi}(\bar{w})$. The same problem arises in the Hamiltonian with defects (2.3.10), which is not Hermitian for $\alpha \in \mathbb{R}$. To calculate $\tilde{\Delta}_n(\boldsymbol{\alpha})$, it is important that the Hamiltonian is Hermitian to ensure that its spectrum is real and, therefore, the energy of its ground state is well-defined. In order to cure this problem, we can analytically continue the defect strength $\alpha \to -i\lambda$ with $\lambda \in \mathbb{R}$. This changes the 2×2 gluing matrix (2.3.8)

$$R_{i\alpha} \to R_\lambda = \begin{pmatrix} \cosh\lambda & \sinh\lambda \\ \sinh\lambda & \cosh\lambda \end{pmatrix}. \tag{2.3.13}$$

Since all its entries are real, it is now compatible with the self-adjointness of the Majorana fields. This analytic continuation also makes the Hamiltonian with defects (2.3.10) Hermitian. In the following, we carry out the calculation of the ground state energy assuming that the gluing matrix is (2.3.13) with $\lambda \in \mathbb{R}$. We will eventually take $\lambda \to i\alpha$ in the final result, which we check against exact numerical calculations in the XY spin chain.

2.3.2 Ground state energy for a single defect ($n = 1$)

We start by solving the case of a single marginal defect. We take the spatial coordinate x defined on the interval $x \in [-\pi, \pi]$ with the points $x = -\pi$ and π identified and, for simplicity, we put the defect at $x = 0$. We impose the following boundary conditions for the fields $\psi(x)$, $\bar{\psi}(x)$ at $x = 0$ and $x = \pi$:

$$\Psi(0^-) = R_\lambda \Psi(0^+), \qquad \Psi(-\pi) = -\Psi(\pi). \tag{2.3.14}$$

The first one is the gluing condition for the defect, while the second one is the anti-periodic boundary condition. With these boundary conditions imposed on the fields, the Hamiltonian is

$$H = \frac{1}{2i}\int_{-\pi}^{0} \mathrm{d}x\, \Psi^\dagger D\Psi + \frac{1}{2i}\int_{0}^{\pi} \mathrm{d}x\, \Psi^\dagger D\Psi, \qquad D = \begin{pmatrix} \partial_x & 0 \\ 0 & -\partial_x \end{pmatrix}. \tag{2.3.15}$$

Diagonalization of the Hamiltonian

The goal now is to diagonalize the Hamiltonian (2.3.15). To do this, we look for pairs of functions $(u(x), v(x))$ that satisfy the same gluing and anti-periodic boundary conditions as $\Psi(x)$,

$$\begin{pmatrix} u(0^-) \\ v(0^-) \end{pmatrix} = R_\lambda \begin{pmatrix} u(0^+) \\ v(0^+) \end{pmatrix}, \quad \begin{pmatrix} u(-\pi) \\ v(-\pi) \end{pmatrix} = -\begin{pmatrix} u(\pi) \\ v(\pi) \end{pmatrix}, \tag{2.3.16}$$

and are eigenstates of the differential operator $\frac{1}{i}D$. These are piecewise plane waves,

$$u_k(x) = \begin{cases} A_0 e^{ikx}, & x \in (-\pi, 0), \\ A_1 e^{ikx}, & x \in (0, \pi), \end{cases} \qquad v_k(x) = \begin{cases} B_0 e^{-ikx}, & x \in (-\pi, 0), \\ B_1 e^{-ikx}, & x \in (0, \pi). \end{cases} \tag{2.3.17}$$

If they satisfy the boundary conditions, then such wavefunctions are automatically eigenfunctions of $\frac{1}{i}D$ with eigenvalue k.

The conditions (2.3.16) impose the following constraints on the amplitudes:

$$\begin{pmatrix} A_0 \\ B_0 \end{pmatrix} = R_\lambda \begin{pmatrix} A_1 \\ B_1 \end{pmatrix}, \qquad \begin{pmatrix} A_0 e^{-ik\pi} \\ B_0 e^{ik\pi} \end{pmatrix} = -\begin{pmatrix} A_1 e^{ik\pi} \\ B_1 e^{-ik\pi} \end{pmatrix}. \tag{2.3.18}$$

This linear system of equations admits a non-zero solution if and only if

$$\det\left[\mathbb{I} + R_\lambda \begin{pmatrix} e^{-ik2\pi} & 0 \\ 0 & e^{ik2\pi} \end{pmatrix}\right] = 0. \tag{2.3.19}$$

Let us introduce the polynomial

$$P_\lambda(z) = z \det\left[\mathbb{I} + R_\lambda \begin{pmatrix} 1/z & 0 \\ 0 & z \end{pmatrix}\right] \tag{2.3.20}$$

of degree 2. (2.3.19) is equivalent to the polynomial equation

$$P_\lambda(z) = 0 \tag{2.3.21}$$

for the variable $z = e^{i2\pi k}$. From the explicit form of R_λ, we find that $P_\lambda(z)$ is

$$P_\lambda(z) = \text{const.} \times (z - e^{i\theta})(z - e^{-i\theta}), \tag{2.3.22}$$

with

$$\theta = 2\arctan\left(\tanh\frac{\lambda}{2}\right) + \pi \ \in [0, 2\pi). \tag{2.3.23}$$

Then the full set of solutions k of (2.3.19) is

$$k \in \mathcal{S}_\lambda = \left(\mathbb{Z} + \frac{\theta}{2\pi}\right) \cup \left(\mathbb{Z} - \frac{\theta}{2\pi}\right). \tag{2.3.24}$$

For each solution $k \in \mathcal{S}_\lambda$, the pair (u_k, v_k) can be used to construct a Bogoliubov mode for the Hamiltonian (2.3.15), taking the scalar product with the two-component field $(\psi, \bar{\psi})$

$$\eta_k = \int_{-\pi}^{\pi} \mathrm{d}x\, [u_k^*(x)\psi(x) + v_k^*(x)\bar{\psi}(x)], \tag{2.3.25}$$

which automatically satisfies $[H, \eta_k] = k\,\eta_k$. Then, using the orthonormality of the set of functions $(u_k(x), v_k(x))$ we get

$$H = \frac{1}{2}\sum_{k\in\mathcal{S}_\lambda} k\eta_k^\dagger\eta_k, \tag{2.3.26}$$

where the sum in k runs over all the solutions in (2.3.24) and the modes satisfy the anticommutation relations $\{\eta_k^\dagger, \eta_q\} = \delta_{k,q}$.

Notice that, taking the complex conjugate of the eigenvalue equation for $\frac{1}{i}D$, we get that (u_k^*, v_k^*) is an eigenvector with eigenvalue $-k$,

$$D\begin{pmatrix} u_k \\ v_k \end{pmatrix} = ik\begin{pmatrix} u_k \\ v_k \end{pmatrix} \implies D\begin{pmatrix} u_k^* \\ v_k^* \end{pmatrix} = -ik\begin{pmatrix} u_k^* \\ v_k^* \end{pmatrix}. \tag{2.3.27}$$

Thus we can set $u_{-k}(x) = u_k^*(x)$ and $v_{-k}(x) = v_k^*(x)$. This implies that $\eta_{-k} = \eta_k^\dagger$, and (2.3.26) can be rewritten in the form

$$H = \frac{1}{2}\sum_{k\in\mathcal{S}_\lambda} k\,\eta_k\eta_{-k}. \tag{2.3.28}$$

Alternatively, we can express it as a sum restricted to the set of positive solutions k, $\mathcal{S}_\lambda^+ = \{k \in \mathcal{S}_\lambda \mid k > 0\}$,

$$H = \sum_{k\in\mathcal{S}_\lambda^+} k\,(\eta_k\eta_{-k} - 1/2). \tag{2.3.29}$$

Ground state energy

From (2.3.29), it is clear that the ground state of the single-defect Hamiltonian (2.3.15) is the state annihilated by all the modes η_{-k} for $k \in \mathcal{S}_\lambda^+$. The ground state energy is

$$E(\lambda) = -\frac{1}{2}\sum_{k\in\mathcal{S}^+} k = -\frac{1}{2}\left[\sum_{m=0}^{\infty}\left(m + \frac{\theta}{2\pi}\right) + \sum_{m=1}^{\infty}\left(m - \frac{\theta}{2\pi}\right)\right]. \tag{2.3.30}$$

These infinite sums can be evaluated by zeta-regularization. Taking into account that

$$\lim_{s\to -1}\sum_{m=0}^{\infty}(m+a)^{-s}=\zeta(-1,a), \tag{2.3.31}$$

where $\zeta(s,a)=\sum_{m=0}^{\infty}(m+a)^{-s}$ is the Hurtwitz zeta function, the ground state energy can be written as

$$E(\lambda)=-\frac{1}{2}\left[\zeta\left(-1,\frac{\theta}{2\pi}\right)+\zeta\left(-1,1-\frac{\theta}{2\pi}\right)\right]. \tag{2.3.32}$$

Using the identity $\zeta(-1,a)=-\frac{1}{12}+\frac{a}{2}-\frac{a^2}{2}=\zeta(-1,1-a)$, we arrive at

$$E(\lambda)=\frac{1}{2}\left(\frac{1}{\pi}\arctan\left(\tanh\frac{\lambda}{2}\right)\right)^2-\frac{1}{24}. \tag{2.3.33}$$

Identifying this expression with the standard formula for the ground state energy in a CFT,

$$E(\lambda)=\Delta_1(\lambda)-\frac{c}{12}, \tag{2.3.34}$$

with $c=1/2$ for the massless Majorana fermion, we find that the scaling dimension associated with the insertion of a single marginal defect of strength λ is

$$\Delta_1(\lambda)=\frac{1}{2\pi^2}\arctan^2\left(\tanh\frac{\lambda}{2}\right). \tag{2.3.35}$$

Connection with previous works

The scaling dimension associated with a single defect was computed in Ref. [58] applying lattice methods in the quantum Ising chain and in Ref. [62] using a boundary CFT approach. In the latter, the Ising CFT with a defect is folded along the defect, obtaining a $\mathbb{Z}_2$ orbifold of the compact boson in which the defect is encoded in the boundary condition. The relation between such bosonic boundary condition and our gluing parameter λ can be found in Ref. [72].

In the case $n=1$, the charged moments (1.2.8) specialize to $\mathcal{Z}_1(\alpha)=\mathrm{Tr}(\rho_A e^{i\alpha Q_A})$. This is the full counting statistics, i.e. the cumulant generating function, of the charge Q_A in the subsystem A. In our setup, it corresponds to the expectation value of a single defect line on the single replica surface $\mathcal{M}$. In the ground state of the critical XY spin chain, this quantity was calculated in Refs. [97, 98] employing lattice methods, see also [93, 99, 100], and obtaining that $\mathcal{Z}_1(\alpha)=e^{-t(\alpha)\ell}\ell^{-2\tilde{\Delta}_1(\alpha)}$, with $t(\alpha)$ given by (2.2.3), and the exponent $\tilde{\Delta}_1(\alpha)=\Delta_1(-i\alpha)$ that we have found in (2.3.35) using CFT.

Notice that the case $\lambda=i\pi$ corresponds to the $\mathbb{Z}_2$ spin-flip symmetry of the spin chain and the associated defect is topological — the ε Verlinde line [48, 50, 63]. When this line is open, as in our case, two disorder operators $\mu(z)$ are inserted

at its end-points [50]. Therefore, by the Kramers-Wannier duality, $\mathcal{Z}_1(\pi)$ should be proportional to the two-point function of the spin fields $\sigma(z)$ at its end-points, $\mathcal{Z}_1(\pi) \propto \langle\sigma(0)\sigma(\ell)\rangle = \ell^{-2\Delta_\sigma}$, which have scaling dimension $\Delta_\sigma = 1/8$, that is precisely $\Delta_1(i\pi)$.

2.3.3 Ground state energy for n equally-spaced defects

We now extend the calculation of the previous section to the case of multiple defects. In this section we take the spatial coordinate x in the interval $[0, 2\pi]$, and we put the defects at positions $x_j = \frac{2\pi j}{n}$ with $j = 1, \ldots, n$. We also define $x_0 = 0$. The Hamiltonian is

$$H = \sum_{j=1}^{n} \frac{1}{2i} \int_{x_{j-1}}^{x_j} \mathrm{d}x\, \Psi^\dagger D \Psi, \qquad D = \begin{pmatrix} \partial_x & 0 \\ 0 & -\partial_x \end{pmatrix}, \tag{2.3.36}$$

with the following gluing conditions corresponding to n equally-spaced defects of strengths λ_1, λ_2, …, λ_n,

$$\Psi(x_j + 0^-) = R_{\lambda_j} \Psi(x_j + 0^+), \tag{2.3.37}$$

where the matrix R_λ was defined in (2.3.13), and the anti-periodic boundary condition $\Psi(0) = -\Psi(2\pi)$.

Diagonalization of the Hamiltonian

To diagonalize that Hamiltonian, we proceed as in the $n = 1$ case. We look for pairs of functions $(u_k(x), v_k(x))$ that satisfy the same gluing conditions as $\Psi(x)$ and are eigenstates of $\frac{1}{i}D$. We look for solutions in the form of piecewise plane waves,

$$u_k(x) = \begin{cases} A_0 e^{ikx}, & x \in (0, x_1), \\ A_1 e^{ikx}, & x \in (x_1, x_2), \\ \vdots & \\ A_n e^{ikx}, & x \in (x_{n-1}, x_n), \end{cases} \qquad v_k(x) = \begin{cases} B_0 e^{-ikx}, & x \in (0, x_1), \\ B_1 e^{-ikx}, & x \in (x_1, x_2), \\ \vdots & \\ B_n e^{-ikx}, & x \in (x_{n-1}, x_n). \end{cases} \tag{2.3.38}$$

The gluing conditions (2.3.37) imply the following relations between consecutive amplitudes

$$\begin{pmatrix} A_{j-1} \\ B_{j-1} \end{pmatrix} = \begin{pmatrix} e^{-ikx_j} & 0 \\ 0 & e^{ikx_j} \end{pmatrix} R_{\lambda_j} \begin{pmatrix} e^{ikx_j} & 0 \\ 0 & e^{-ikx_j} \end{pmatrix} \begin{pmatrix} A_j \\ B_j \end{pmatrix}, \tag{2.3.39}$$

while the anti-periodicity condition implies

$$\begin{pmatrix} A_0 \\ B_0 \end{pmatrix} = - \begin{pmatrix} e^{ik2\pi} & 0 \\ 0 & e^{-ik2\pi} \end{pmatrix} \begin{pmatrix} A_n \\ B_n \end{pmatrix}. \tag{2.3.40}$$

This system of equations admits a non-zero solution if and only if k is such that

$$\det\left(\mathbb{I}+R_{\lambda_1}\begin{pmatrix}e^{-i\frac{k2\pi}{n}} & 0\\ 0 & e^{i\frac{k2\pi}{n}}\end{pmatrix}R_{\lambda_2}\begin{pmatrix}e^{-i\frac{k2\pi}{n}} & 0\\ 0 & e^{i\frac{k2\pi}{n}}\end{pmatrix}\dots R_{\lambda_n}\begin{pmatrix}e^{-i\frac{k2\pi}{n}} & 0\\ 0 & e^{i\frac{k2\pi}{n}}\end{pmatrix}\right)=0. \tag{2.3.41}$$

It is convenient to define the polynomial

$$P_{\boldsymbol{\lambda}}(z)=z^n\det\left(\mathbb{I}+R_{\lambda_1}\begin{pmatrix}1/z & 0\\ 0 & z\end{pmatrix}R_{\lambda_2}\begin{pmatrix}1/z & 0\\ 0 & -z\end{pmatrix}\dots R_{\lambda_n}\begin{pmatrix}1/z & 0\\ 0 & z\end{pmatrix}\right), \tag{2.3.42}$$

of degree $2n$. This polynomial is palindromic, i.e. it satisfies $P_{\boldsymbol{\lambda}}(z)=z^{2n}P_{\boldsymbol{\lambda}}(1/z)$, and it has real coefficients. Let us call z_j, $j=1,\dots,2n$, the roots of that polynomial. When $\boldsymbol{\lambda}\in\mathbb{R}^n$, the roots lie on the unit circle $|z_j|=1$. This corresponds to having real solutions for k in (2.3.41). Therefore, in this case, we can write $z_j=e^{i\theta_j}$ with $\theta_j\in[0,2\pi)$. Later, when we will analytically continue our result, the relation between z_j and θ_j will just be $\theta_j=-i\operatorname{Log} z_j$, without the property $\theta_j\in\mathbb{R}$.

The polynomial (2.3.42) can be rewritten in terms of its roots

$$P_{\boldsymbol{\lambda}}(z)=\text{const.}\times\prod_{j=1}^{2n}(z-e^{i\theta_j(\boldsymbol{\lambda})}),\qquad \theta_j(\boldsymbol{\lambda})\in[0,2\pi), \tag{2.3.43}$$

and each root determines a family of solutions to the quantization condition (2.3.41) for k via $z_j=e^{ik2\pi/n}$. The set of all such solutions is then

$$\mathcal{S}_{\boldsymbol{\lambda}}=\bigcup_{j=1}^{2n}n\left(\mathbb{Z}+\frac{\theta_j(\boldsymbol{\lambda})}{2\pi}\right). \tag{2.3.44}$$

Each $k\in\mathcal{S}_{\boldsymbol{\lambda}}$ defines a Bogoliubov mode

$$\eta_k=\int_0^{2\pi}\mathrm{d}x\,[u_k^*(x)\psi(x)+v_k^*(x)\bar{\psi}(x)], \tag{2.3.45}$$

which automatically satisfies $[H,\eta_k]=k\,\eta_k$ along with $(\eta_k)^\dagger=\eta_{-k}$, and the canonical anticommutation relations $\{\eta_k^\dagger,\eta_q\}=\delta_{k,q}$. Then the n-defect Hamiltonian (2.3.36) is diagonal in terms of them,

$$H=\frac{1}{2}\sum_{k\in\mathcal{S}_\lambda}k\eta_k^\dagger\eta_k, \tag{2.3.46}$$

where the sum runs over all the solutions k of (2.3.41). Alternatively, one can write it as

$$H=\sum_{k\in\mathcal{S}_{\boldsymbol{\lambda}}^+}k(\eta_k\eta_{-k}-1/2), \tag{2.3.47}$$

where the sum is now restricted to the set of positive solutions, $\mathcal{S}_{\boldsymbol{\lambda}}^+=\{k\in\mathcal{S}_{\boldsymbol{\lambda}}|k>0\}$. This expression is particularly convenient to compute the ground state energy.

Ground state energy

According to (2.3.47), the ground state of the n-defect Hamiltonian (2.3.36) corresponds to the configuration with all the positive modes k occupied. Its energy is

$$E(\boldsymbol{\lambda}) = -\frac{1}{2}\sum_{k\in\mathcal{S}^+_{\boldsymbol{\lambda}}} k = -\frac{1}{2}\sum_{j=1}^{2n}\sum_{m=0}^{\infty} n\left(m+\frac{\theta_j}{2\pi}\right). \tag{2.3.48}$$

As in the $n = 1$ case above, these divergent series can be evaluated by zeta-regularization, using (2.3.31),

$$E(\boldsymbol{\lambda}) = -\frac{n}{2}\sum_{j=1}^{2n}\zeta\left(-1,\frac{\theta_j}{2\pi}\right). \tag{2.3.49}$$

If we apply the identity $\zeta(-1,a) = \frac{1}{24} - \frac{(a-1/2)^2}{2}$ for the Hurwitz zeta function, then we obtain

$$E(\boldsymbol{\lambda}) = \frac{n}{2}\sum_{j=1}^{2n}\left(\frac{1}{2}\left(\frac{\theta_j}{2\pi}-\frac{1}{2}\right)^2 - \frac{1}{24}\right). \tag{2.3.50}$$

This expression should be identified with the usual CFT formula for the ground state energy, $E = \Delta_n(\boldsymbol{\lambda}) - c/12$, with $c = 1/2$. Therefore, we find that for n equally-spaced defects the scaling dimension $\Delta_n(\boldsymbol{\lambda})$ is

$$\Delta_n(\boldsymbol{\lambda}) = -\frac{n^2-1}{24} + \frac{n}{4}\sum_{j=1}^{2n}\left(\frac{\theta_j}{2\pi}-\frac{1}{2}\right)^2. \tag{2.3.51}$$

This is the second main result of this chapter section, which we will use to derive the Rényi entanglement asymmetry of the critical XY spin chain in the next section, where we also report the explicit expression of $\Delta_n(\boldsymbol{\lambda})$ for $n = 2$ and 3. As a first check of (2.3.51), note that, when $\lambda_1 = \lambda_2 = \cdots = \lambda_n = 0$, we must obtain $\Delta_n(\mathbf{0}) = 0$. In fact, in that case, the polynomial (2.3.42) is $P_{\boldsymbol{\lambda}}(z) = (z^n+1)^2$ and its roots are $z_j = e^{i2\pi\frac{j-1/2}{n}}$, $j = 1,\dots,n$, all with multiplicity 2. Therefore, we have $\theta_j = \theta_{j+n} = 2\pi(j-1/2)/n$ for $1 \le j \le n$. Inserting these roots in (2.3.51) and performing the sum, we find $\Delta_n(\mathbf{0}) = 0$ as it should be.

2.3.4 Summary

For the convenience of the reader, let us briefly summarize the main result of this section. It is the second important result of this chapter. It gives the exact scaling dimension $\Delta_n(\boldsymbol{\lambda})$ associated with the insertion of n-equally-spaced marginal defects in the massless Majorana fermion on a circle, with strengths $\lambda_1,\dots,\lambda_n$. The result is given by (2.3.51), which can also be rewritten in the form

$$\Delta_n(\boldsymbol{\lambda}) = -\frac{n^2-1}{24} + \frac{n}{4}\sum_{j=1}^{2n}\left(\frac{\mathrm{Log}(-z_j)}{2\pi i}\right)^2, \tag{2.3.52}$$

where Log(.) is the principal value of the logarithm, whose imaginary part takes values in $(-\pi, \pi]$ and its branch cut is taken along the negative real axis, and the z_j's ($j = 1, \dots, 2n$) are the $2n$ roots of the following polynomial of degree $2n$:

$$P_{\boldsymbol{\lambda}}(z) = z^n \det\left(\mathbb{I} + R_{\lambda_1}\begin{pmatrix} 1/z & 0 \\ 0 & z \end{pmatrix} R_{\lambda_2}\begin{pmatrix} 1/z & 0 \\ 0 & z \end{pmatrix} \dots R_{\lambda_n}\begin{pmatrix} 1/z & 0 \\ 0 & z \end{pmatrix}\right), \quad (2.3.53)$$

with

$$R_\lambda = \begin{pmatrix} \cosh\lambda & \sinh\lambda \\ \sinh\lambda & \cosh\lambda \end{pmatrix}. \quad (2.3.54)$$

We have derived this result for defect strengths $\lambda_j \in \mathbb{R}$, but it can be analytically continued to $\lambda_j \in \mathbb{C}$. In particular, in what follows, we will take $\lambda_j \to i\alpha_j$ to derive the Rényi entanglement asymmetry in the critical XY spin chain.

2.4 Rényi entanglement asymmetry in the critical XY spin chain

In this section, we derive the asymptotic behavior of the Rényi entanglement asymmetry in the ground state of the critical XY spin chain using the results obtained above. At the critical lines $\gamma \neq 0$, $|h| = 1$, the charged moments $\mathcal{Z}_n(\boldsymbol{\alpha})$ behave as in (2.1.11) for large subsystem length ℓ. While the string tension $T_n(\boldsymbol{\alpha})$ is given by (2.2.3), we have found in Sec. 2.3.3 that the scaling dimension $\tilde{\Delta}_n(\boldsymbol{\alpha})$ can be obtained, upon the analytic continuation $\boldsymbol{\lambda} = i\boldsymbol{\alpha}$, from (2.3.52), which further requires to determine the roots of the polynomial (2.3.53). Unfortunately, we are not able to find a general expression for these roots. Here we first consider the cases $n = 2$ and 3, and we check our analytic prediction for $\mathcal{Z}_n(\boldsymbol{\alpha})$ against exact numerical results in the ground state of the XY spin chain. We then derive by applying the saddle point approximation discussed in Sec. 2.1.2 the asymptotic behavior of the Rényi entanglement asymmetry for any integer index n, and by analytically continuing it, the replica limit $n \to 1$.

2.4.1 Numerical checks

$n = 2$ charged moments

In the case of two defects located at the points indicated in the left panel of Fig. 2.5, the polynomial of (2.3.42) reads

$$P_{\boldsymbol{\lambda}}(z) = \cosh\lambda_1 \cosh\lambda_2 (1 + z^4) + 2(1 + \sinh\lambda_1 \sinh\lambda_2) z^2. \quad (2.4.1)$$

It is a bit cumbersome to write the roots explicitly, but using them in (2.3.52) we arrive at the formula for the scaling dimension associated with the insertion of two

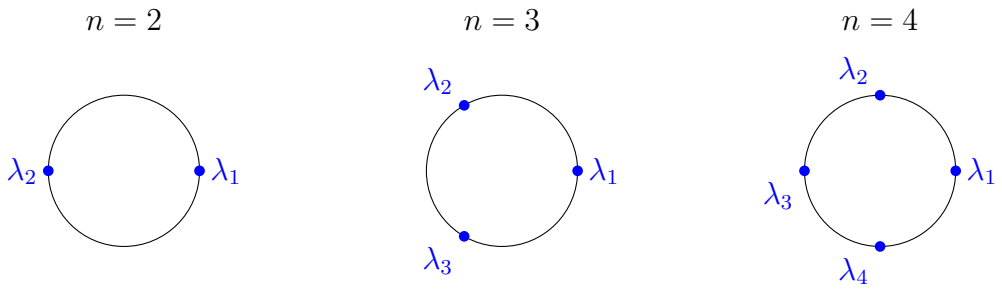


Figure 2.5: Disposition of the point defects on the circle in the calculation of the charged moments $\mathcal{Z}_n(\boldsymbol{\alpha})$ for $n = 2$, 3 and 4. If the circle has length 2π, then the defect of strength λ_j is located at the point $x_j = \frac{2\pi j}{n}$.

defects

$$\Delta_2(\lambda_1, \lambda_2) = \frac{1}{2\pi^2}\left[\arctan\left(\tanh\frac{\lambda_1}{2}\right) - \arctan\left(\tanh\frac{\lambda_2}{2}\right)\right]^2. \tag{2.4.2}$$

To keep formulas compact, here we write the roots only in the special case $\lambda_2 = -\lambda_1 = \lambda$, which is the case that we use below in our analysis of the asymmetry. In that case the four roots are:

$$z = \pm\frac{i \pm \sinh\lambda}{\cosh\lambda}, \tag{2.4.3}$$

and, taking $\theta = -i\log z$, their arguments are

$$\theta_1 = \pi - \theta_2 = 2\arctan\tanh(\lambda/2) + \frac{\pi}{2}, \tag{2.4.4}$$

$$\theta_3 = 3\pi - \theta_4 = 2\arctan\tanh(\lambda/2) + \frac{3\pi}{2}. \tag{2.4.5}$$

Plugging them in (2.3.52), we obtain

$$\Delta_2(\lambda, -\lambda) = \frac{2}{\pi^2}\arctan^2\left(\tanh\frac{\lambda}{2}\right) \tag{2.4.6}$$

and, taking the analytic continuation $\lambda = i\alpha$,

$$\tilde{\Delta}_2(\alpha, -\alpha) = -\frac{2}{\pi^2}\operatorname{arctanh}^2\left(\tan\frac{\alpha}{2}\right). \tag{2.4.7}$$

Note that, in (2.4.7), $\tilde{\Delta}_2(\alpha, -\alpha)$ is only well-defined in the interval $\alpha \in (-\pi/2, \pi/2)$ since the domain of definition of $\operatorname{arctanh}(x)$ is $x \in (-1, 1)$. On the other hand, the ground state of the critical XY spin chain is invariant under the subgroup $\mathbb{Z}_2 \subset U(1)$ of spin flips, which implies that the charged moments $\mathcal{Z}_2(\boldsymbol{\alpha})$

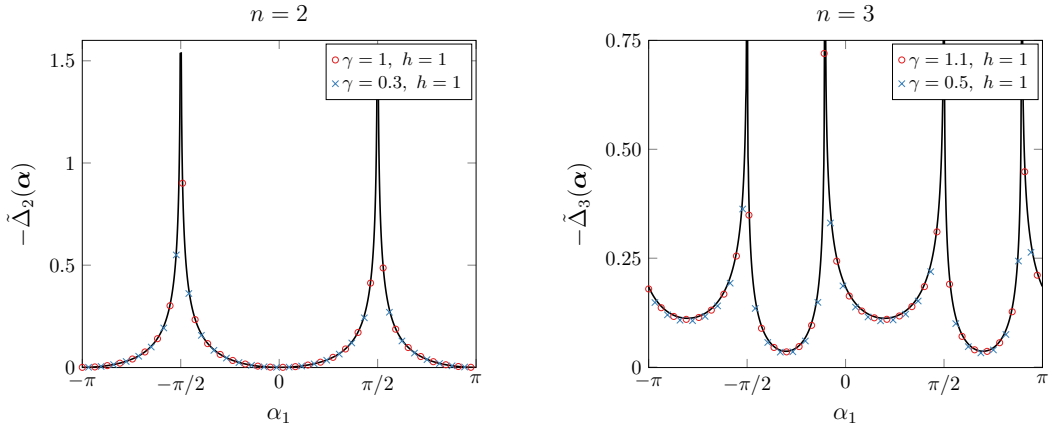


Figure 2.6: Scaling dimension $\tilde{\Delta}_n(\boldsymbol{\alpha})$ for two (left panel) and three (right panel) defects, which appears in the asymptotic behavior of the charged moments $\mathcal{Z}_n(\boldsymbol{\alpha})$. For $n = 2$, we take $\alpha_2 = -\alpha_1$ and we vary α_1. For $n = 3$, we set $\alpha_1 + \alpha_2 + \alpha_3 = 0$ and change α_1 with $\alpha_2 = 1.9$. The symbols have been obtained numerically as detailed in the main text for the ground state of the XY spin chain along the critical line $\gamma > 0$ and $h = 1$. The curves are the CFT prediction (2.3.52), that for $n = 2$ simplifies to (2.4.8).

are periodic $\mathcal{Z}_2(\boldsymbol{\alpha} + \boldsymbol{\pi}) = \mathcal{Z}_2(\boldsymbol{\alpha})$. Therefore, (2.4.7) must be extended outside the interval $\alpha \in (-\pi/2, \pi/2)$ such that this periodicity is satisfied,

$$\tilde{\Delta}_2(\alpha, -\alpha) = \begin{cases} -\frac{2}{\pi^2} \operatorname{arctanh}^2 \left(\tan \frac{\alpha}{2}\right), & \alpha \in (-\pi/2, \pi/2), \\ -\frac{2}{\pi^2} \operatorname{arctanh}^2 \left(\tan \frac{\pi-\alpha}{2}\right), & \alpha \in (-\pi, -\pi/2) \cup (\pi/2, \pi). \end{cases} \tag{2.4.8}$$

In the left panel of Fig. 2.6, we numerically check this result. As we explain in Appendix 2.C, the charged moments $\mathcal{Z}_n(\boldsymbol{\alpha})$ can be exactly calculated numerically in the ground state of the critical XY spin chain with (2.C.4). Using this expression together with (2.2.3), we compute $\log(\mathcal{Z}_2(\boldsymbol{\alpha}) e^{T_2(\boldsymbol{\alpha})\ell})$ with $\boldsymbol{\alpha} = (\alpha, -\alpha)$ for a fixed α and $\ell = 50, 60, \ldots, 100$ and we fit the curve $-\tilde{\Delta}_2(\boldsymbol{\alpha}) \log \ell + \text{const.}$ to this set of points. In the plot on the left side of Fig. 2.6, the symbols correspond to the values of $\tilde{\Delta}_2(\boldsymbol{\alpha})$ obtained in the fit for different angles α and couplings $(h = 1, \gamma)$, while the solid curve is the prediction of (2.4.8). We obtain a very good agreement between them.

The divergence of $\tilde{\Delta}_2(\boldsymbol{\alpha})$ in $\boldsymbol{\alpha} = (\pm\pi/2, \mp\pi/2)$ does not mean that the charged moment is divergent itself but that the charged moment has a different scaling in ℓ. We numerically observe that in this case the scaling is $\log \mathcal{Z}_2(\boldsymbol{\alpha}) = -T(\boldsymbol{\alpha})\ell + O\left((\log \ell)^2\right)$. In general, we observe this anomalous scaling with a $(\log \ell)^2$ term in the charged moment $\mathcal{Z}_n(\boldsymbol{\alpha})$ for every n when at least one α_j is equal to $\pi/2$. Being these points a measure zero set in the integral for the asymmetry, the analysis performed in Sec. 2.1.2 does not change.

$n = 3$ charged moments

For three defects at the positions of the middle panel of Fig. 2.5 on a circle, the polynomial (2.3.42) is

$$P_{\boldsymbol{\lambda}}(z) = C_{\boldsymbol{\lambda}} + S_{\boldsymbol{\lambda}} z^2 + 2z^3 + S_{\boldsymbol{\lambda}} z^4 + C_{\boldsymbol{\lambda}} z^6, \tag{2.4.9}$$

with

$$C_{\boldsymbol{\lambda}} = \cosh\lambda_1 \cosh\lambda_2 \cosh\lambda_3, \quad S_{\boldsymbol{\lambda}} = \sinh\lambda_1 \sinh\lambda_2 \cosh\lambda_3 + \text{cycl. perm.} \tag{2.4.10}$$

To compute the coefficient $\tilde{\Delta}_3(\boldsymbol{\alpha})$ that enters in the asymptotic behavior of the charged moment $\mathcal{Z}_3(\boldsymbol{\alpha})$, we have to impose $\lambda_1 + \lambda_2 + \lambda_3 = 0$ due to the Dirac delta in (1.2.10). In that case, $S_{\boldsymbol{\lambda}} = 1 - C_{\boldsymbol{\lambda}}$ and the polynomial has two equal roots $z_1 = z_2 = -1$. The other four roots are

$$\begin{aligned} z_3 = z_4^* &= \frac{\sqrt{C_{\boldsymbol{\lambda}}} + \sqrt{C_{\boldsymbol{\lambda}} - 1} \pm i\sqrt{1 + 2C_{\boldsymbol{\lambda}} - 2\sqrt{C_{\boldsymbol{\lambda}}(C_{\boldsymbol{\lambda}} - 1)}}}{2\sqrt{C_{\boldsymbol{\lambda}}}}, \\ z_5 = z_6^* &= \frac{\sqrt{C_{\boldsymbol{\lambda}}} - \sqrt{C_{\boldsymbol{\lambda}} - 1} \pm i\sqrt{1 + 2C_{\boldsymbol{\lambda}} + 2\sqrt{C_{\boldsymbol{\lambda}}(C_{\boldsymbol{\lambda}} - 1)}}}{2\sqrt{C_{\boldsymbol{\lambda}}}}. \end{aligned} \tag{2.4.11}$$

Plugging them in (2.3.52) and performing the analytic continuation $\boldsymbol{\lambda} = i\boldsymbol{\alpha}$, we obtain the analytic expression for $\tilde{\Delta}_3(\boldsymbol{\alpha})$. We numerically check it in the right panel of Fig. 2.6 as we have done for the case $n = 2$. We can calculate the exact value of the charged moment $\mathcal{Z}_3(\boldsymbol{\alpha})$ in the critical XY spin chain employing (2.C.4) in the appendix. Combining it with (2.2.3), we compute $\log(\mathcal{Z}_3(\boldsymbol{\alpha}) e^{\ell T_3(\boldsymbol{\alpha})})$ for a given $\boldsymbol{\alpha} = (\alpha_1, \alpha_2, -\alpha_1 - \alpha_2)$ and $\ell = 50, 60, \ldots, 100$. With the resulting set of points, we fit the function $-2\tilde{\Delta}_3(\boldsymbol{\alpha})/3 \log \ell + \text{const}$. In the plot on the right side of Fig. 2.6, the symbols represent the coefficient $\tilde{\Delta}_3(\boldsymbol{\alpha})$ that we get in the fit in terms of α for different couplings $(h = 1, \gamma)$ and the curve is the CFT prediction of (2.3.52) using the roots (2.4.11). The agreement is excellent.

2.4.2 Asymptotic behavior of the entanglement asymmetry

We now compute the asymptotic behavior of the entanglement asymmetry for large subsystem size ℓ applying the general result (2.1.23). As we have seen in Sec. 2.2, for the $U(1)$ group that we are considering we have $\operatorname{vol} G = 2\pi$, $\dim G = 1$, $\mu(0) = 1$, and the symmetric subgroup H is the $\mathbb{Z}_2$ spin-flip symmetry. The string tension $T_n(\boldsymbol{\alpha})$ is given by (2.2.3), $\mathsf{H}_t = t''(0)$, and, according to (2.2.6), $t''(0) = \gamma/(2(1+\gamma))$ at the critical lines $|h| = 1$. Since $\dim G = 1$, the matrices D_p, defined in (2.1.17), that enter in the calculation of the coefficient b_n of the $\log \ell/\ell$ term are scalars and correspond to the eigenvalues ν_p of the Hessian matrix of the scaling dimension $\Delta_n(\boldsymbol{\lambda})$,

$$(\mathsf{H}_{\Delta_n})_{ab} = \left(\frac{\partial^2 \Delta_n(\boldsymbol{\lambda})}{\partial\lambda_a \partial\lambda_b} \right)_{\boldsymbol{\lambda}=\mathbf{0}}, \quad a, b = 1, \ldots, n, \tag{2.4.12}$$

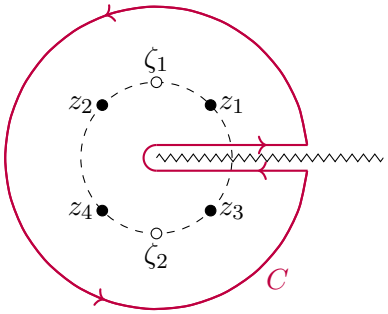


Figure 2.7: Schematic representation of the contour integral that gives the scaling dimension $\Delta_n(\boldsymbol{\lambda})$ for the case $n = 2$. The zig-zag line is the branch cut $[0, \infty)$ of the function $\mathrm{Log}(z)$. The filled black dots are the roots z_j of the polynomial $P_{\boldsymbol{\lambda}}(z)$ and the white ones represent the poles of the integrand in (2.4.16), after expanding quadratically $P_{\boldsymbol{\lambda}}(z)$ in $\boldsymbol{\lambda}$.

such that $\mathsf{D}_p = -2\nu_p/n$ (recall that in our case $\beta_n(\boldsymbol{\alpha}) = \frac{2}{n}\Delta_n(i\boldsymbol{\alpha})$). Therefore, (2.1.23) reads in this case as

$$\Delta S_A^{(n)} = \frac{1}{2}\log \ell + a_n + b_n \frac{\log \ell}{\ell} + \cdots \tag{2.4.13}$$

with

$$a_n = \frac{1}{2}\log \frac{\pi t''(0) n^{\frac{1}{n-1}}}{2} \tag{2.4.14}$$

and

$$b_n = \frac{1}{n(1-n)t''(0)} \sum_{p=1}^{n-1} \nu_p. \tag{2.4.15}$$

The Hessian of $\Delta_n(\boldsymbol{\lambda})$

The only missing ingredient are the eigenvalues ν_p of the Hessian (2.4.12) of the scaling dimension $\tilde{\Delta}_n(\boldsymbol{\alpha})$. To calculate the latter, it is convenient to rewrite (2.3.52) as a contour integral using the residue theorem,

$$\Delta_n(\boldsymbol{\lambda}) = \frac{1}{2\pi i} \oint_C \mathrm{d}z f_n(z) \frac{\mathrm{d}}{\mathrm{d}z} \mathrm{Log}\, P_{\boldsymbol{\lambda}}(z), \tag{2.4.16}$$

with

$$f_n(z) = -\frac{n^2-1}{48\, n} + \frac{n}{4}\left(\frac{i\,\mathrm{Log}(-z)}{2\pi}\right)^2. \tag{2.4.17}$$

The polynomial $P_{\boldsymbol{\lambda}}(z)$ is defined in (2.3.53). The contour C encircles all the roots of $P_{\boldsymbol{\lambda}}(z)$ as we depict in Fig. 2.7, leaving the branch cut of $\mathrm{Log}(z)$ outside of the region that it delimits. The advantage of this approach is that we can easily calculate the second derivatives of $\Delta_n(\boldsymbol{\lambda})$ at $\boldsymbol{\lambda} = \mathbf{0}$ by expanding quadratically the polynomial

$P_{\boldsymbol{\lambda}}(z)$ around this point. If we rewrite (2.3.53) in the form

$$P_{\boldsymbol{\lambda}}(z) = z^n \left\{ 2 + \mathrm{tr}\left[R_{\lambda_1} \begin{pmatrix} 1/z & 0 \\ 0 & z \end{pmatrix} \dots R_{\lambda_n} \begin{pmatrix} 1/z & 0 \\ 0 & z \end{pmatrix} \right] \right\}, \tag{2.4.18}$$

then it is easy perform the expansion,

$$P_{\boldsymbol{\lambda}}(z) = P_0(z) \left[1 + \frac{1}{2} \sum_{a,b=1}^{n} \lambda_a \lambda_b \frac{z^{2n-2|b-a|} + z^{2|b-a|}}{(z^n+1)^2} \right] + O(\lambda^3), \tag{2.4.19}$$

where $P_0(z) = (z^n+1)^2$. If we plug it in the contour integral (2.4.16) and we integrate by parts, we find

$$\Delta_n(\boldsymbol{\lambda}) = -\frac{1}{2} \sum_{a,b=1}^{n} \lambda_a \lambda_b \oint_C \frac{\mathrm{d}z}{2\pi i} \frac{\mathrm{d}f_n(z)}{\mathrm{d}z} \frac{z^{2(n-|b-a|)} + z^{2|b-a|}}{(z^n+1)^2} + O(\lambda^3), \tag{2.4.20}$$

and

$$\frac{\mathrm{d}f_n(z)}{\mathrm{d}z} = -\frac{n}{8\pi^2} \frac{\mathrm{Log}(-z)}{z}. \tag{2.4.21}$$

Observe that, according to this result, $\Delta_n(\boldsymbol{\lambda}) = 0$, as expected. Therefore, the components of the Hessian of $\Delta_n(\boldsymbol{\lambda})$ can be identified with

$$(\mathsf{H}_{\Delta_n})_{ab} = -\oint_C \frac{\mathrm{d}z}{2\pi i} \frac{\mathrm{d}f_n(z)}{\mathrm{d}z} \frac{z^{2(n-|b-a|)} + z^{2|b-a|}}{(z^n+1)^2}. \tag{2.4.22}$$

Given that $0 \leq |b-a| \leq n-1$, the numerator of the integrand above is, up to the $\mathrm{Log}(z)$ factor, a polynomial. Since the cut of the logarithm lies outside the region enclosed by C, then the only singularities the contribute to the integral are the zeros of z^n+1 in the denominator, $\zeta_j = e^{i\frac{2\pi}{n}(j-\frac{1}{2})}$, $j = 1, \dots, n$. Applying the residue theorem, we have

$$(\mathsf{H}_{\Delta_n})_{ab} = \frac{n}{8\pi^2} \sum_{j=1}^{n} \mathrm{res}\left[\frac{\mathrm{Log}(-z)}{z} \frac{z^{2(n-|b-a|)} + z^{2|b-a|}}{(z^n+1)^2},\ \zeta_j \right]. \tag{2.4.23}$$

These residues can be evaluated explicitly,

$$\mathrm{res}\left[\frac{z^{p-1}\,\mathrm{Log}(-z)}{(z^n+1)^2},\ \zeta_j \right] = \frac{\zeta_j^p}{n^2} \left(1 + (p-n) \frac{i\pi(2j-n-1)}{n} \right).$$

After summing them in (2.4.23), we eventually find that the Hessian of $\Delta_n(\boldsymbol{\alpha})$ is a circulant matrix,

$$(\mathsf{H}_{\Delta_n})_{ab} = c_{a-b}, \quad \text{with} \quad c_l = \frac{1}{4\pi^2} \times \begin{cases} 1, & \text{if} \quad l = 0, \\ \frac{2\pi}{n} \frac{l-n/2}{\sin(\frac{2\pi}{n} l)}, & \text{if} \quad l = 1, \dots, n-1, \end{cases} \tag{2.4.24}$$

as a consequence of the symmetry under the cyclic exchange of the replicas.

Application to the asymmetry

According to (2.4.15), the coefficient of the $\log \ell/\ell$ term in the asymmetry is given by the eigenvalues ν_p of the Hessian H_{Δ_n}. In our case, since the it is a circulant matrix, the eigenvalues are given by the Fourier transform of its entries,

$$\nu_p = \sum_{l=0}^{n-1} c_l e^{i\frac{2\pi p l}{n}}. \tag{2.4.25}$$

Combining (2.4.15) and (2.4.25), and doing carefully the sums, we find that

$$b_n = \frac{\gamma+1}{2\gamma} \times \begin{cases} \dfrac{1}{(1-n)\pi^2} + \dfrac{1}{n(n-1)\pi} \displaystyle\sum_{l=1}^{n/2-1} \csc\left(\frac{2\pi l}{n}\right), & n \text{ even}, \\ -\dfrac{1}{n\pi^2} - \dfrac{1}{n^2(n-1)\pi} \displaystyle\sum_{l=1}^{n-1} (n-2l)\csc\left(\frac{2\pi l}{n}\right), & n \text{ odd}, \end{cases} \tag{2.4.26}$$

where we have taken into account that $t''(0) = \gamma/(2(\gamma+1))$. This result can be analytically continued to non integer values of n by using the integral representation of the cosecant function

$$\csc(\pi z) = \frac{1}{\pi}\int_0^\infty \mathrm{d}x \frac{x^z}{x^2+x}. \tag{2.4.27}$$

Applying it in (2.4.26) for n even, we find

$$b_n = -\frac{\gamma+1}{2\gamma}\left[\frac{1}{(n-1)\pi^2} + \frac{1}{n(n-1)\pi^2}\int_0^\infty \frac{\mathrm{d}x}{x(x+1)}\frac{x^{2/n}-x}{1-x^{2/n}}\right]. \tag{2.4.28}$$

It turns out this expression reproduces the exact values of the coefficient b_n for n odd as well, so (2.4.26) and (2.4.28) are equivalent expressions for all integer n.

Eqns. (2.4.26)-(2.4.28) are the third main result of this chapter: we have arrived at the exact expression for the coefficient b_n of the $\log \ell/\ell$ term in the Rényi entanglement asymmetry of the XY spin chain at criticality.

Finally, taking the replica limit $n \to 1$ in (2.4.28), we find that the coefficient for the (von Neumann) entanglement asymmetry is

$$\lim_{n\to 1} b_n = -\frac{4+\pi^2}{16\pi^2}\frac{\gamma+1}{\gamma}. \tag{2.4.29}$$

Thus, our final result is that the entanglement asymmetry at criticality in the XY spin chain is

$$\Delta S_A = \frac{1}{2}\log \ell + \frac{1}{2}\log\frac{\pi\gamma}{4(1+\gamma)} + \frac{1}{2} - \frac{4+\pi^2}{16\pi^2}\frac{\gamma+1}{\gamma}\frac{\log \ell}{\ell} + \cdots \tag{2.4.30}$$

We stress once again that what is remarkable here is the $\log \ell/\ell$ term, which only appears in critical systems. We also stress that the 'semi-universality' of b_n (in the sense of Ref. [92]) is manifest here, because it depends on the parameter γ of the XY Hamiltonian. A truly universal quantity —such as, for instance, the scaling dimension $\Delta_n(\boldsymbol{\lambda})$— would depend only on the CFT data and not on the details of the underlying microscopic model, so it would not depend on γ.

2.5 Concluding remarks

In this chapter, we have analyzed the entanglement asymmetry in one dimensional critical extended quantum systems using CFT methods. This observable measures how much a symmetry is broken in a part of the system. Applying the replica trick, it can be obtained from the charged moments of the subsystem's reduced density matrix. We have seen that, in the ground state of a 1+1 dimensional quantum field theory, using the correspondence between the unitary operators that represent the symmetry group in the Hilbert space and defect lines in the path integral approach, the charged moments can be identified with a quotient of the partition functions of the theory on a Riemann surface with and without defect lines inserted along each branch cut. When the state respects the symmetry, the defects are topological and any deformation leaves the partition function invariant, yielding a zero asymmetry. In this formulation, the entanglement asymmetry can be interpreted as a measure of how much the defects are non topological. Utilizing well-known scaling arguments for the partition function in two dimensions, we have deduced the asymptotic behavior of the charged moments that provide the entanglement asymmetry. While for non critical systems the moments decay exponentially with the subsystem size, see Refs. [28, 29, 36], in the critical case we have found that they contain an extra algebraic factor. The coefficient of the exponential decaying term can be interpreted as the line tension of the defects and is non-universal; that is, it depends on the specific lattice realization of the field theory. The exponent of the algebraic factor is universal and, therefore, it is fully determined by the CFT that describes the critical point and depends on the properties of the defects associated with the symmetry group. From this result, we have derived the asymptotic behavior of the ground state entanglement asymmetry for a generic compact Lie group. Both for non-critical and critical systems, it grows at leading order logarithmically with the subsystem size ℓ and a coefficient proportional to the dimension of the Lie group. Criticality yields a $\log \ell/\ell$ correction, which is semi-universal as its coefficient depends not only on the universal exponent of the charged moments but also on the defect tension.

In the rest of the chapter, we have specialized to the ground state of the XY spin chain, which explicitly breaks the $U(1)$ symmetry of spin rotations around the transverse axis. The charged moments and the entanglement asymmetry of this model have been investigated outside the critical lines in Ref. [29] employing lattice methods. Here we have considered the critical lines described by the massless Majorana fermion theory in the scaling limit, after fermionizing it with a Jordan-Wigner transformation. In this case, the defect lines correspond to a marginal deformation of this CFT. Exploiting conformal invariance, the universal exponent that appears in the charged moments can be identified with the ground state energy of the massless Majorana fermion theory on a circle with equi-spaced marginal point defects of different strength. To obtain it, we have carefully diagonalized its

Hamiltonian for an arbitrary number of defects. Combining this result with those found in Ref. [29] for the non-universal exponential term, we have obtained an analytic expression for the entanglement asymmetry.

A crucial point in our problem is that the defects we are considering are marginal, which makes non-trivial the dependence of the CFT partition function on them. As we have already emphasized, the partition function hinges on the specific CFT and symmetry group under study. Therefore, it would be desirable to consider other models and symmetries; for example, the $SU(2)$ group of spin rotations in the critical XXZ spin chain, whose continuum limit is the massless compact boson.

2.A Fermionization and continuum limit of the XY spin chain

The fermionization of the XY spin chain is performed with the Jordan-Wigner transformation [101]. For completeness, we present it it in multiple steps. First we map the spin chain to a model with complex lattice fermions, the Kitaev chain. Then we further map the system to lattice Majorana fermions. Finally, we take the continuum limit and get the Majorana CFT.

We consider the XY spin chain, writing explicitely the ferromagnetic coupling J. While in the main text this is set to $J = 1$, here is important to have it in order to perform the continuum limit carefully. The Hamiltonian then is

$$H_{\mathrm{XY}} = -\frac{J}{2}\sum_{j\in\mathbb{Z}}\left(\frac{1+\gamma}{2}\sigma_j^x\sigma_{j+1}^x + \frac{1-\gamma}{2}\sigma_j^y\sigma_{j+1}^y + h\sigma_j^z\right). \tag{2.A.1}$$

Kitaev chain. The Jordan-Wigner transformation is

$$\sigma_j^x = e^{i\pi\sum_{l<j}c_l^\dagger c_l}\left(c_j^\dagger + c_j\right), \quad \sigma_j^y = e^{i\pi\sum_{l<j}c_l^\dagger c_l} i\left(c_j^\dagger - c_j\right), \quad \sigma_j^z = 1 - 2c_j^\dagger c_j, \tag{2.A.2}$$

and the operators c_j, $c_j^\dagger$ satisfy the anticommutation relations $\{c_j, c_l\} = 0$ and $\{c_j, c_l^\dagger\} = \delta_{jl}$. Then the Hamiltonian (2.2.1) of the XY model is mapped to the Hamiltonian of the Kitaev chain

$$H_{\mathrm{Kit}} = -\frac{J}{2}\sum_{j\in\mathbb{Z}}\left[c_j^\dagger c_{j+1} + c_{j+1}^\dagger c_j + \gamma\left(c_j^\dagger c_{j+1}^\dagger + c_{j+1}c_j\right) + h\left(1 - 2c_j^\dagger c_j\right)\right] \tag{2.A.3}$$

and the charge Q_A for $A = \{1, \dots, \ell\}$ becomes $Q_A = \sum_{j\in A} c_j^\dagger c_j$.

It is well known that the XY model flows in the infra-red to the Ising CFT for $h = 1$, $\gamma \in \mathbb{R}$. Thus all these points in the parameter space belong to the same universality class. For simplicity, we consider the case $h = \gamma = 1$.

Majorana Chain. Each pair of complex fermion operators $c_j, c_j^\dagger$ can be split in the following pair of Majorana operators

$$c_j^\dagger = \frac{1}{2}\left(a_{2j} + i a_{2j+1}\right), \qquad c_j = \frac{1}{2}\left(a_{2j} - i a_{2j+1}\right), \tag{2.A.4}$$

which satisfy the algebra $a_j^\dagger = a_j$ and $\{a_j, a_j\} = 2\delta_{jl}$. Then the Hamiltonian becomes

$$H_{\text{Maj}} = \frac{iJ}{2}\sum_{j\in\mathbb{Z}} a_{j+1}a_j \tag{2.A.5}$$

and the charge

$$Q_A = \frac{1}{2}\sum_{j\in A}\left(1 + i a_{2j+1}a_{2j}\right). \tag{2.A.6}$$

Continuum limit. The continuum limit is performed by first defining the following new Majorana lattice operators ψ_j, $\bar\psi_j$

$$a_{2j} = \psi_j + \bar\psi_j, \qquad a_{2j+1} = \psi_j - \bar\psi_j, \tag{2.A.7}$$

which form two anticommuting families of Majorana fermions, with algebra

$$\{\psi_j, \psi_l\} = \delta_{jl}, \qquad \{\bar\psi_j, \bar\psi_l\} = \delta_{jl}, \qquad \{\psi_j, \bar\psi_l\} = 0. \tag{2.A.8}$$

The Hamiltonian in these variables reads

$$H_{\text{Maj}'} = \frac{iJ}{2}\sum_{j\in\mathbb{Z}}\left(2\psi_j\bar\psi_j + \psi_j\psi_{j-1} + \bar\psi_j\psi_{j-1} - \psi_j\bar\psi_{j-1} - \bar\psi_j\bar\psi_{j-1}\right) \tag{2.A.9}$$

and the charge

$$Q_A = \frac{1}{2}\sum_{j\in A}\left(1 + i2\psi_j\bar\psi_j\right). \tag{2.A.10}$$

Finally, we perform the continuum limit. We call the continuum variable $x \in \mathbb{R}$ and introduce a lattice spacing s so that

$$\psi_j \simeq \frac{\psi(x)}{\sqrt{s}}, \qquad \psi_{j-1} \simeq \frac{\psi(x-s)}{\sqrt{s}} \simeq \frac{1}{\sqrt{s}}(\psi(x) - s\partial_x\psi(x)). \tag{2.A.11}$$

The continuum fields satisfy the algebra $\{\psi(x), \psi(y)\} = \delta(x-y)$, $\{\bar\psi(x), \bar\psi(y)\} = \delta(x-y)$, $\{\psi(x), \bar\psi(y)\} = 0$. The Hamiltonian becomes

$$H = \frac{J'}{2i}\int_{\mathbb{R}} \mathrm{d}x\left[\psi(x)\partial_x\psi(x) - \bar\psi(x)\partial_x\bar\psi(x)\right], \tag{2.A.12}$$

where J' is the continuum version of J, given by $J' = Js$ in the limit $s \to 0$ and $J \to \infty$. Deriving the equations of motion for ψ and $\bar\psi$, J' can be recognized to be the sound velocity, which we set to 1. Finally, the charge operator, discarding the constant term in (2.A.10) that acts trivially on the Hilbert space, becomes

$$Q_A = i\int_A \psi(x)\bar\psi(x)\mathrm{d}x. \tag{2.A.13}$$

2.B Defects in the Hamiltonian formalism

In this Appendix, we consider a massless Majorana fermion on a line, with a defect implemented as a localized mass term

$$H_\mu = \frac{1}{2i}\int_{\mathbb{R}} (\psi\partial_x\psi - \bar\psi\partial_x\bar\psi)\mathrm{d}x - i\mu\,\psi(0)\bar\psi(0), \qquad \mu\in\mathbb{R}. \tag{2.B.1}$$

We show that this formulation is equivalent to the one given in the main text, where the defect is only encoded in the gluing conditions. We provide the explicit relation between the defect strength μ and the gluing parameter λ. We find that if the defect term in the Hamiltonian is Hermitian, then λ has to be real. This is a further justification of the analytic continuation $\alpha\mapsto -i\lambda$ that is performed in the main text.

We have the following commutators

$$[H_\mu,\psi(x)] = i\partial_x\psi(x) + i\mu\delta(x)\bar\psi(0), \tag{2.B.2}$$
$$\big[H_\mu,\bar\psi(x)\big] = -i\partial_x\bar\psi(x) - i\mu\delta(x)\psi(0). \tag{2.B.3}$$

To relate this to gluing conditions at the origin, we can look for eigenmodes of that Hamiltonian of the form

$$\eta_k = \int_{\mathbb{R}} \big[u_k^*(x)\psi(x) + v_k^*(x)\bar\psi(x)\big]\,\mathrm{d}x, \tag{2.B.4}$$

with

$$u_k(x) = \begin{cases} A_0 e^{ikx}, & x<0,\\ A_1 e^{ikx}, & x>0,\end{cases} \qquad v_k(x) = \begin{cases} B_0 e^{-ikx}, & x<0,\\ B_1 e^{-ikx}, & x>0,\end{cases} \tag{2.B.5}$$

for some constants A_0, A_1, B_0, B_1. This Ansatz gives the following commutator with the Hamiltonian,

$$[H_\mu,\eta_k] = k\eta_k - i\left(A_0^* - A_1^* - \frac{\mu}{2}(B_0^*+B_1^*)\right)\psi(0) + i\left(B_0^* - B_1^* - \frac{\mu}{2}(A_0^*+A_1^*)\right)\bar\psi(0). \tag{2.B.6}$$

We see that η_k is a Bogoliubov mode with energy k if the last two terms vanish. This gives the constraint

$$\begin{pmatrix} A_0\\ B_0\end{pmatrix} = \begin{pmatrix} \frac{1+\mu^2/4}{1-\mu^2/4} & \frac{\mu}{1-\mu^2/4}\\ \frac{\mu}{1-\mu^2/4} & \frac{1+\mu^2/4}{1-\mu^2/4}\end{pmatrix}\begin{pmatrix} A_1\\ B_1\end{pmatrix}. \tag{2.B.7}$$

Thus, we recover the gluing condition (2.3.7) with the matrix (2.3.13) obtained after the analytic continuation of the gluing parameter, provided that

$$\frac{\mu}{2} = \tanh\left(\frac{\lambda}{2}\right). \tag{2.B.8}$$

2.C Numerical calculation of the charged moments

In this Appendix, we report the formulae that we employ to compute numerically the charged moments (1.2.8) for the $U(1)$ group of spin rotations around the z axis in the ground state of the XY spin chain (2.2.1). As we show in Appendix 2.A, this model maps into a quadratic fermionic chain after the Jordan-Wigner transformation (2.A.2). Therefore, its ground state satisfies Wick theorem. This implies that the reduced density matrix ρ_A of a single interval A of length ℓ is Gaussian and it is fully determined by the $2\ell \times 2\ell$ two-point fermionic correlation matrix [102]

$$\Gamma_{jj'} = 2\mathrm{tr}\left[\rho_A \begin{pmatrix} c_j \\ c_j^\dagger \end{pmatrix} (c_{j'}^\dagger, c_{j'})\right] - \delta_{jj'}, \tag{2.C.1}$$

with $j, j' = 1, \dots, \ell$. For the ground state of the XY spin chain, its entries are

$$\Gamma_{jj'} = \int_0^{2\pi} \frac{\mathrm{d}k}{2\pi} \mathcal{G}(k) e^{-ik(j-j')}, \tag{2.C.2}$$

where $\mathcal{G}(k)$ is the 2×2 matrix

$$\mathcal{G}(k) = \begin{pmatrix} \cos\xi_k & -i\sin\xi_k \\ i\sin\xi_k & -\cos\xi_k \end{pmatrix} \tag{2.C.3}$$

and $\cos\xi_k$, $\sin\xi_k$ are given in (2.2.4).

After the Jordan-Wigner transformation, the transverse magnetization (2.2.2) that generates the $U(1)$ symmetry is also quadratic and, consequently, Gaussian. Therefore, the charged moments $\mathcal{Z}_n(\boldsymbol{\alpha})$ are the trace of a product of Gaussian operators. Using the well-known properties of this kind of operators, the charged moments can be calculated in terms of the two-point correlataion matrix Γ as

$$\mathcal{Z}_n(\boldsymbol{\alpha}) = \sqrt{\det\left[\left(\frac{I-\Gamma}{2}\right)^n \left(I + \prod_{j=1}^{n} W_j\right)\right]}, \tag{2.C.4}$$

where $W_j = (I+\Gamma)(I-\Gamma)^{-1} e^{i\alpha_{j,j+1} n_A}$ and n_A is a diagonal matrix with $(n_A)_{2j,2j} = 1$, $(n_A)_{2j-1,2j-1} = -1$, $j = 1, \cdots, \ell$. The detailed derivation of this expression can be found in Ref. [31]. We use it to obtain the exact numerical values of the charged moments in the plots of Fig. 2.6.

Chapter 3

Boundary explicit symmetry breaking

In this chapter, we employ the entanglement asymmetry to study the ground state properties of (1+1)-dimensional conformal field theories in the presence of symmetry breaking boundary conditions, as well as quantum quenches in which the boundary condition is changed.

In Sec. 3.1, we first consider the ground state of a conformal field theory, T on the half-infinite line $x \in [0, \infty)$, with a boundary condition, a, at $x = 0$. Our subsystem of interest $A = [0, \ell]$ extends from the boundary see Fig. 3.1. The CFT is assumed to possess a global symmetry, G, which is broken by the choice of a non-symmetric boundary condition a. We use the methods of boundary conformal field theory to derive analytic expressions for the entanglement asymmetry. As a warm up, we study the first normalized charged moment $\mathcal{Z}_1(g)$ (1.2.8), also called string order parameter [103–105]. This can be considered a probe of symmetry breaking itself, since having $\mathcal{Z}_1(g) = 1 \, \forall g \in G$ implies that ρ_A is symmetric. We find that the charged moments decay with a power law in ℓ, with an exponent that depends on the scaling dimension of a certain boundary condition changing operator, and that the entanglement asymmetry saturates to $\log |G|$, with specific power-law corrections. In Sec. 3.2, we then benchmark these against numerical results obtained using tensor network methods on lattice systems, specifically the Ising spin chain and the 3-state Potts model.

Secondly, in Secs. 3.3 and 3.4, we study quantum quenches in which the initial state is given by the groundstate of the CFT with a certain boundary condition. Then the boundary condition is changed abruptly. We monitor the time evolution of the local magnetization, the entanglement entropy, and, numerically, the entanglement asymmetry.

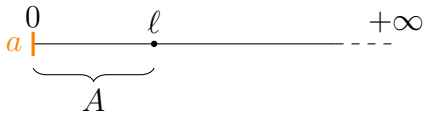


Figure 3.1: We consider a one dimensional, G symmetric CFT on the half line subject to a conformal boundary condition, a on the left edge which breaks the G symmetry. We invetigate properties of the subsystem A which extend from the boundary a distance ℓ into the bulk.

3.1 Asymmetry in the groundstate: analytical results

Main results

Let us briefly present our main results of this with their derivation following in the next subsection. We consider a boundary condition a at $x = 0$ and the subsystem $A = [0, \ell]$. We find that the string order parameter admits the scaling form

$$\mathcal{Z}_1(g) \propto \ell^{-2h_{\mu_g} - h_{\Psi_{(ga,a)}}} \tag{3.1.1}$$

where h_{μ_g} is the scaling dimension of the (diagonal) disorder operator associated to the group element $g \in G$ and $h_{\Psi_{(ga,a)}}$ the conformal dimension of the boundary-condition-changing operator $\Psi_{(ga,a)}$ that changes the boundary condition from a to ga.

For a finite group G of cardinality $|G|$, we find that, when the boundary condition a fully breaks the symmetry, i.e. when $ga \neq a$, $\forall g \in G$, the entanglement asymmetry scales as

$$\Delta S_A^{(n)} = \log |G| - c_n \ell^{-2h^{\min}} + o(\ell^{-2h^{\min}}) \tag{3.1.2}$$

with $h^{\min}$ being the minimal dimension of the boundary-condition-changing operators within the group G, i.e.,

$$h^{\min} = \min_{g \in G, g \neq e} h_{\Psi_{(ga,a)}}. \tag{3.1.3}$$

The constant c_n is just a non-universal amplitude. On the other hand, when the boundary condition is G-symmetric, the asymmetry vanishes. For the intermediate case of a boundary condition that is symmetric under a subgroup H of G, the asymmetry is

$$\Delta S_A^{(n)} = \log \frac{|G|}{|H|} - c_n \ell^{-2h^{\min}} + o(\ell^{-2h^{\min}}) \tag{3.1.4}$$

with

$$h^{\min} = \min_{g \in G, g \notin H} h_{\Psi_{(ga,a)}}. \tag{3.1.5}$$

Note that, as the string order parameter approaches zero for large subsystems, cf. (3.1.1), one might be tempted to infer that the subsystem becomes increasingly symmetric as its size grows. However, the result for the entanglement asymmetry in (3.1.2) demonstrates otherwise, highlighting the greater effectiveness of entanglement asymmetry in detecting symmetry breaking at the subsystem level. Moreover, the string order parameter on the subsystem remains nonzero even in the presence of a symmetry preserving boundary, where $ga = a$ and $h_{\Psi_{(ga,a)}} = 0$.

We emphasize also that, while the traditional order parameter approach may yield a nonzero value in certain cases, its value decays algebraically away from the symmetry breaking boundary. Moreover, its value provides no direct information on the symmetry being broken. In contrast, the asymmetry does not decay as the subsystem increases correctly reflecting the fact that the symmetry is not restored and its value indeed provides information on the broken symmetry group.

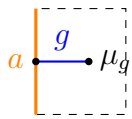
3.1.1 String order parameter

We begin by considering the string order parameter in the ground state of our chosen CFT, T. This can be expressed as

$$\mathcal{Z}_1(g) = \lim_{\beta\to\infty} \frac{\mathrm{tr}[U_{A,g} e^{-\beta H_a}]}{\mathrm{tr}[e^{-\beta H_a}]} \tag{3.1.6}$$

where H_a is the Hamiltonian of the theory on the half line subject to boundary condition a at $x = 0$. As is standard, our theory, T, then lives on the right half complex plane, coordinated by z, with a certain line operator, corresponding to g, inserted along $\mathrm{Re}(z) = (0, \ell]$. In addition, the points $z \to \pm i\infty$ should be identified. Recall that, in order to have a well defined insertion of a line operator, some conditions at its endpoints need to be specified. These consist of declaring on which defect operator (also called the *disorder operator* or *twist field*) the line ends in the bulk, and with which junction the line is connected to the boundary. We call the defect operator μ_g and assume that it is a diagonal primary operator, that is $h_{\mu_g} = \bar{h}_{\mu_g}$.

It is useful at this point, to introduce a diagrammatic representation of our quantities of interest. In particular, we express the expectation value of g in the groundstate in the following way

$$\mathcal{Z}_1(g) = \Big\langle$$ 

$$\Big\rangle, \tag{3.1.7}$$

where on the right hand side, the orange line indicates the boundary condition a, at $\mathrm{Re}(z) = 0$, the dashed lines imply that the theory lives on the full right half plane, the blue line denotes the line operator and the black dots denote local defect operators or junctions which are inserted where the line operators terminates.

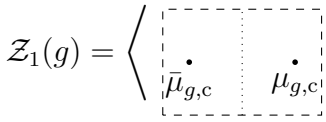
Throughout this work we are considering the case where the bulk theory is G-symmetric, meaning that the line operator is topological. In the diagrammatic notation, this means that the blue line can be completely deformed to any shape provided its endpoints remain fixed and no other operators or boundaries are encountered.

We first consider the case in which the boundary condition is G-invariant, and we denote it with i. In that case, the junction between the boundary and the line operator is also topological[106]. This is because the line can be deformed in the bulk and made to act on the boundary. If the boundary is G-symmetric, then the line can disappear on the boundary. Therefore, the position of the junction can be moved without changing the expectation value. This is represented diagrammatically as,



(3.1.8)

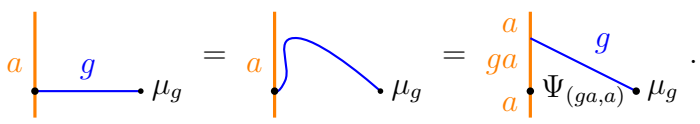
Accordingly, the position of the junction cannot enter in any expectation value. Note however, that the position of the defect operator in the bulk, is not topological and so cannot be moved without changing $\mathcal{Z}_1(g)$. We can then use the doubling trick [107] to evaluate the expectation value. In particular, we map T to a chiral theory T_{c} which lives on the full complex plane. Under this mapping anti holomorphic fields on the right half plane get mapped to the left half plane $\bar{\mu}_g(z) \to \bar{\mu}_{g,\mathrm{c}}(-\bar{z})$ while the holomorphic parts remain in the right half plane $\mu_g(z) \to \mu_{g,\mathrm{c}}(z)$. We assume that $\mu_{g,\mathrm{c}}$ and $\bar{\mu}_{g,\mathrm{c}}$ have the same conformal dimension, denoted by h_{μ_g}. This then maps the expectation value in the boundary CFT into a chiral expectation value on the complex plane. Following this we obtain



$$\propto \ell^{-2h_{\mu_g}}. \tag{3.1.9}$$

where $\langle\cdot\rangle_{\mathrm{c}}$ refers to the expectation value in the chiral theory T_{c}. Here we see that the scaling behaviour depends explicitly on the dimension of the defect operator which terminates the line operator. If we were to consider instead a finite system such that the line operator ended on another G-symmetric boundary then we would obtain that $\mathcal{Z}_1(g) = 1$, in line with the fact that the ground state would be symmetric.

If the boundary condition is not G-invariant, then the junction cannot be topological. This is because moving the line in the bulk and making it act on the boundary will change the boundary, and thus produce a boundary changing operator which we denote by $\Psi_{(ga,a)}$. This is depicted in terms of diagrams as



(3.1.10)

In this sense the junction "hides a boundary changing operator" with a positive conformal dimension. This was pointed out in the case of the Ising CFT in [108]. Notice that the topmost junction appearing in the RHS of (3.1.10) is instead topological, as it can be further moved away. The position of this latter junction, as in the case discussed above, will then not enter in any expectation value. We once again apply the doubling trick, taking into account the boundary changing operator that is contained in the junction and is not doubled. We obtain

$$\mathcal{Z}_1(g) = \Big\langle \mu_{g,\mathrm{c}}\, \Psi_{(ga,a)}\, \mu_{g,\mathrm{c}} \Big\rangle_{\mathrm{c}} \propto \ell^{-2h_{\mu_g} - h_{\Psi_{(ga,a)}}} \tag{3.1.11}$$

where in the last step we used the expression for three point functions of primary fields in CFT and we have denoted by $h_{\Psi_{(ga,a)}}$ the scaling dimension of $\Psi_{(ga,a)}$. Therefore, the symmetry breaking boundary condition results in a stronger decay of the string order parameter away from the boundary. As a consequence, for Lie groups this leads to larger fluctuations of the group generators in the subsystem, as one might expect.

3.1.2 Entanglement asymmetry

We now turn to the calculation of the higher order normalized charged moments $\mathcal{Z}_n(\mathbf{g})$ with a view to obtaining the entanglement asymmetry. In this section we restrict to the case where G is a discrete group and has cardinality $|G|$. We now consider the case in which the boundary condition a breaks G fully, although the case where a subgroup is preserved can be studied using the same techniques. In the language of [106], a is a simple boundary condition, that belongs to the regular module category of Vec_G, i.e. a multiplet of $|G|$ boundary conditions.

We can express $\mathcal{Z}_n(\mathbf{g})$ in terms of expectation values in the n-replicated theory of the group operator $U_{A,g_1} \otimes \cdots \otimes U_{A,g_n}$ and the replica-change operator R, which we now introduce. Letting $T^{\otimes n}$ denote the n-replicated theory, we take R be the line operator in $T^{\otimes n}$ that implements the $\mathbb{Z}_n$ cyclic permutation which shifts the replica labels by 1. In other words, R transforms a local operator, $\mathcal{O} = O_1 \otimes \cdots \otimes O_n$ into $\mathcal{O}' = O_n \otimes O_1 \otimes \cdots \otimes O_{n-1}$. This can be depicted graphically in the following way

$$\underset{\mathcal{O}\,\bullet}{\overset{}{\longrightarrow}} R \;=\; \underset{}{\overset{\mathcal{O}'\,\bullet}{\longrightarrow}} R\,. \tag{3.1.12}$$

An analogous action on line operators that cross R also exists as does the natural graphical representation. We will call R the *replica change operator*. R is the analogue of the branch cut of the Riemann surface when one replicates the space-time manifold instead of replicating the theory [11]. The line R can end on a *branch-point twist-field* $\mathcal{T}$ [109, 110], and when combined with a line operator that

implements the element $\mathbf{g}$ can end on a *composite twist field* $\mathcal{T}^{\mathbf{g}}$, which is the one routinely used to compute symmetry resolved entanglement [82, 111].

The normalized partition function, $\mathcal{Z}_n(\mathbf{g})$, can then be written as the ratio of two expectation values in the replicated theory. Namely, it is the ratio of the expectation value of the replicated line operator $U_{A,g_1} \otimes \cdots \otimes U_{A,g_n}$ with that of the R_A, the replica line operator restricted to the subsystem. In diagrams we express this as

$$\mathcal{Z}_n(\mathbf{g}) = \Big\langle \; a^{\otimes n} \;\; \mathbf{g} \;\; \mathcal{T}^{\mathbf{g}} \;\; R \; \Big\rangle \Big/ \Big\langle \; a^{\otimes n} \;\; \mathcal{T} \;\; R \; \Big\rangle \,. \tag{3.1.13}$$

To understand how we can evaluate this ratio we consider first, the simplest case of $n = 2$ and recall that in order to calculate ΔS_A we only require the neutral charged moments, i.e. $\mathcal{Z}_2(g, g^{-1})$. In terms of these

$$\Delta S_A^{(2)} = \log|G| - \log\left(1 + \sum_{g\in G, g\neq e} \mathcal{Z}_2(g, g^{-1})\right), \tag{3.1.14}$$

where we have used that $\mathcal{Z}_2(e, e) = 1$. To evaluate the elements of the sum, $\mathcal{Z}_2(g, g^{-1})$, $g \neq e$ we make use of the fact that the line operator is topological in the bulk and also that we can move the lines in each replica independently. This means we can move the g line in the first replica as in (3.1.10) which leaves behind the boundary changing operator $\Psi_{(ga,a)}$ and creates a topological junction which can be moved at will. Since the points $\pm\infty$ in the temporal direction are identified, we can move the line g along the whole first replica until it crosses the replica-change line R from below. After crossing R, the line then switches to the second replica and the boundary condition on the first replica has changed to ga. The line g then fuses with g^{-1} in the second replica, producing the identity line but leaving behind its hidden boundary changing operator. The result is that the lines g and g^{-1} have disappeared, the boundary condition on the first replica is ga, and that there are two boundary changing operators $\Psi_{(ga,a)}$, one for each replica. Pictorially, the result is

$$\begin{aligned}\mathcal{Z}_2(g, g^{-1}) &= \Big\langle \; ga \otimes a \;\; \Psi^{\otimes 2}_{(ga,a)} \;\; \mathcal{T} \;\; R \; \Big\rangle \Big/ \Big\langle \; a^{\otimes 2} \;\; \mathcal{T} \;\; R \; \Big\rangle \\ &= \frac{\langle \Psi^{\otimes 2}_{(ga,a)}(0)\mathcal{T}(\ell)\rangle}{\langle \mathcal{T}(\ell)\rangle}.\end{aligned} \tag{3.1.15}$$

where in the second line we re-express the result in the more standard non-graphical manner. Then, using once again the doubling trick [107], this time for the replicated theory, we have that $\langle \Psi^{\otimes 2}_{(ga,a)}(0)\mathcal{T}(\ell)\rangle / \langle \mathcal{T}(\ell)\rangle$ is proportional to a ratio of chiral

correlators in the replicated chiral theory $T_c^{\otimes n}$, i.e

$$\mathcal{Z}_2(g,g^{-1}) = \left\langle \bar{\mathcal{T}}_{\rm c}\, \Psi^{\otimes 2}_{(ga,a)}\, \mathcal{T}_{\rm c} \right\rangle_{\rm c} \Big/ \left\langle \bar{\mathcal{T}}_{\rm c} \qquad \mathcal{T}_{\rm c} \right\rangle_{\rm c} \tag{3.1.16}$$
$$= \frac{\langle \bar{\mathcal{T}}_{\rm c}(-\ell)\Psi^{\otimes 2}_{(ga,a)}(0)\mathcal{T}_{\rm c}(\ell)\rangle_{\rm c}}{\langle \bar{\mathcal{T}}_{\rm c}(-\ell)\mathcal{T}_{\rm c}(\ell)\rangle_{\rm c}}.$$

Since the structure of 3-point functions and 2-point functions of primary fields in the chiral theory are known we arrive at

$$\mathcal{Z}_2(g,g^{-1}) \propto \ell^{-2h_{\Psi_{(ga,a)}}}. \tag{3.1.17}$$

Hence, we find that the normalized charged moment decays algebraically in ℓ with a power that is two times the conformal weight of the boundary changing operator $\Psi_{(ga,a)}$. In contrast to the $n = 1$ charged moment discussed in the previous subsection, the dimension of the defect operator μ_g does not appear, which results from the neutrality of the charged moment. Moreover, the dimension of the branch-point twist field operator is absent which originates from the normalization.

Plugging (3.1.17) into (3.1.14), we can expand the log for large ℓ. Retaining only the leading term in this expansion we get

$$\Delta S_A^{(2)} = \log|G| - c_2 \ell^{-2h^{\min}} + o(\ell^{-2h^{\min}}) \tag{3.1.18}$$

with

$$h^{\min} = \min_{g\in G, g\neq e} h_{\Psi_{(ga,a)}} \tag{3.1.19}$$

and c_2 is a proportionality constant that incorporates various non-universal terms and the dependence on the short-distance regulator. $h^{\min}$ is guaranteed to be positive because $ga \neq a$, and both a and ga are simple boundaries. Therefore there cannot be a topological boundary changing operator that connects the two [106].

The preceding analysis can be straightforwardly generalized to a higher number of replicas. Consider the normalized charged moment $\mathcal{Z}_n(\mathbf{g})$ with $\mathbf{g} = (g_1, \ldots, g_n)$, subject to the neutrality condition $\prod_{j=1}^n g_j = e$. We can repeat the topological manipulation we carried out above: The g_1 line is moved from the first replica to the second replica, leaving in its wake $\Psi_{(g_1 a,a)}$. Then the boundary in the first replica becomes $g_1 a$ and the line in the second replica becomes $g_1 g_2$. The fused $g_1 g_2$ line is then moved to the third replica, leaving behind this time $\Psi_{(g_1 g_2 a, g_1 a)}$. Continuing in this fashion we fuse all the lines to the identity. In the end, we will get the following boundary condition of the replicated theory

$$g_1 a \otimes g_1 g_2 a \cdots \otimes \left(\prod_{j=1}^{n-1} g_j\right) a \otimes a \tag{3.1.20}$$

and the insertion of following boundary changing operator

$$\Phi = \Psi_{(g_1 a, a)} \otimes \Psi_{(g_1 g_2 a, g_1 a)} \otimes \cdots \otimes \Psi_{(a, (\prod_{j=1}^{n-1} g_j) a)} \tag{3.1.21}$$

at the origin. The dimension h_Φ of Φ is just the sum of the dimensions of the boundary condition changing operators that comprise it. After this, the doubling trick can be applied as in (3.1.16), producing

$$\mathcal{Z}_n(\mathbf{g}) \propto \ell^{-h_\Phi}. \tag{3.1.22}$$

provided $\mathbf{g} \neq \boldsymbol{e}$ where $\boldsymbol{e} = (e, \dots, e)$ in which case $\mathcal{Z}_n(\boldsymbol{e}) = 1$. The leading behaviour in $\sum_{\mathbf{g} \neq \boldsymbol{e}} \mathcal{Z}_n(\mathbf{g})$ for large ℓ is given by the values of $\mathbf{g}$ for which h_Φ is minimum. The minimum value of h_Φ is realized only if $\mathbf{g}$ contains only two non-trivial group elements, and the other entries are identities, i.e. only if $\mathbf{g}$ is of the form $\mathbf{g} = (\dots, g, \dots, g^{-1}, \dots)$ where the dots are identities. Notice that this structure resembles the one for the OPE of two twist fields where it enters the bulk operator with the minimal dimension [112].

Consequently, the leading term in $\sum_{\mathbf{g} \neq \boldsymbol{e}} \mathcal{Z}_n(\mathbf{g})$ goes like $\ell^{-2h^{\min}}$ and in particular is independent of the replica index. From this we get that the leading asymptotic behavior of the Rényi entanglement asymmetry *for every* n is

$$\Delta S_A^{(n)} = \log |G| - c_n \ell^{-2h^{\min}} + o\left(\ell^{-2h^{\min}}\right). \tag{3.1.23}$$

where c_n is again a non-universal constant. Finally, to get the entanglement asymmetry, one should analytically continue the result in the variable n and take the limit $n \to 1$. Since the power-law exponent is independent of n, we get

$$\Delta S_A = \log |G| - c_1 \ell^{-2h^{\min}} + o\left(\ell^{-2h^{\min}}\right), \tag{3.1.24}$$

where we have assumed that the analytic continuation of the amplitude, c_1, does not vanish. Thus, the entanglement asymmetry in a critical system with boundary symmetry breaking approaches a universal value, dependent only on the cardinality of the broken symmetry group, for large subsystem sizes. The corrections to this are algebraic with a universal exponent whose value is given by the smallest scaling dimension of the boundary changing operators which are not invariant under the symmetry.

If the group G is not fully broken by the boundary condition, leaving a residual symmetry subgroup H of cardinality $|H|$, the asymmetry is given by (3.1.24) with $|G|$ replaced by $|G|/|H|$ and now

$$h^{\min} = \min_{g \in G, g \notin H} h_{\Psi_{(ga,a)}}. \tag{3.1.25}$$

Also here $h^{\min} > 0$, for the same reason explained earlier.

Finally, if the boundary condition a preserves the symmetry, then the topological manipulation discussed before implies $\mathcal{Z}_n(g_1, \dots, g_n) = 1$, $\forall g_1, \dots, g_n \in G$ and hence the asymmetry vanishes.

3.2 Asymmetry in the groundstate: numerical results

In this section we examine our results on the entanglement asymmetry and the string order parameter $\mathcal{Z}_1(g)$ in two specific examples, the critical Ising model and the critical 3-state Potts model. We then check these predictions against numerical simulations on lattice systems which are described by these CFTs at low energy. All numerical simulations were conducted by constructing an MPS approximation of the ground state for a finite chain of total length L using DMRG, implemented with the TeNPy library [113].

3.2.1 Critical Ising model

We start with the Ising CFT which notoriously has an internal $\mathbb{Z}_2$ spin-flip symmetry. This is implemented by the Verlinde line associated to the ϵ primary field, that we denote by η. The conformal boundary conditions are denoted by $f, +, -$. Here, f is the free boundary condition, where no constraint is set at the boundary spins, and $+, -$ are the fixed boundary conditions [114]. When fused with the boundary as in (3.1.10), the η line acts on the boundary conditions as

$$\eta \triangleright f = f \qquad \eta \triangleright + = - \qquad \eta \triangleright - = +. \tag{3.2.1}$$

For this reason, when the η line hits perpendicularly the boundary, it forms a topological junction with the f boundary condition. In contrast, the junction with a fixed boundary condition is necessarily non-topological. Moving the η line when attached to the $+$ boundary as in (3.1.10) produces a boundary changing operator $\Psi_{(+,-)}$, which has conformal dimension $h_{\Psi_{(+,-)}} = 1/2$ [115]. In the bulk, the η line can end on the primaries $\mu, \psi, \bar{\psi}$ [63, 116].

The Ising CFT is realized as the low energy effective field theory of the critical transverse field Ising chain. The Hamiltonian of the semi-infinite chain with free boundary condition at its left edge is given by

$$H_f = -\sum_{j=1}^{\infty}(X_j X_{j+1} + Z_j), \tag{3.2.2}$$

where X_j, Z_j are the Pauli matrices for the spins at site j and the free boundary is simply implemented by truncating the chain at site $j = 1$. We denote the ground state of this system by $|\text{gs}, f\rangle$. To implement the fixed boundary conditions, however we should include an extra site at $j = 0$ on which an additional longitudinal field acts. The Hamiltonian is

$$H_{\pm} = -\sum_{j=0}^{\infty}(X_j X_{j+1} + Z_j) - hX_0. \tag{3.2.3}$$

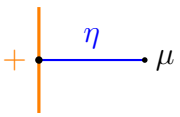
where the $\pm$ boundary conditions arise in the limit $h \to \pm\infty$. In this limit, the $j = 0$ spin becomes completely magnetized, and any finite energy state is of the form $|\psi\rangle = |\pm\rangle \otimes |\text{bulk}\rangle$, where $|\pm\rangle$ denote the eigenstates of X_0 and $|\text{bulk}\rangle$ denotes the state of the system for $j \geq 1$. It is important to note that the site at $j = 0$ is an auxiliary spin which is included so as to implement the fixed boundary condition. At low energy it is the properties of the $|\text{bulk}\rangle$ part of the states which will be described by the Ising CFT. We denote the ground state of this Hamiltonian, including the auxiliary spin, by $|\text{gs}, \pm\rangle$.

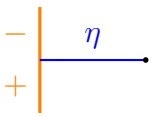
The string order parameter. The string order parameter is given by the expectation value of the lattice spin flip operator on the subsystem A which is $\eta_A = \prod_{j\in A} Z_j$. Under the renormalization group, the bulk endpoint becomes the disorder operator μ with conformal dimension $(1/16, 1/16)$. The primaries ψ and $\bar{\psi}$ can be ruled out as they are $\mathbb{Z}_2$-odd. If the lattice boundary condition is free, the operator $\prod_{j=1}^{\ell} Z_j$ flows to the η line, with the topological junction with the free boundary. The analytical prediction in (3.1.9) gives

$$\langle \text{gs}, f | \, \eta_A \, | \text{gs}, f \rangle \propto \ell^{-1/8}. \tag{3.2.4}$$

To check this prediction we perform numerical simulations using tensor networks on the Hamiltonian (3.2.2). To implement this we use a finite but large chain of $L = 500$ sites and impose either free or $+$ boundary conditions at the site $j = L$. The results are shown in the left panel of Fig. 3.2 where the symbols indicate numerical data and the dashed line depicts the prediction of (3.2.4). We see excellent agreement up to subsystem sizes approaching half the chain length when finite size effects become important.

We now examine the case of fixed boundary condition, focusing on the $+$ case. In this instance, the operator $\prod_{j=1}^{\ell} Z_j$ flows to the η line connected with the non-topological junction to the $+$ boundary. We stress that here we did not include the site 0 in the spin flip operator. Indeed $\prod_{j=0}^{\ell} Z_j$ flips the site 0 and therefore is a map from the Hilbert space with $+$ bc to the Hilbert space with $-$ bc. Therefore, $\prod_{j=0}^{\ell} Z_j$ flows to the η line attached to the boundaries $+$ and $-$ with a topological junction. This can be summarized graphically as

$$\prod_{j=1}^{\ell} Z_j \rightsquigarrow$$ 

$$\qquad \prod_{j=0}^{\ell} Z_j \rightsquigarrow$$ 

. (3.2.5)

As a result one can immediately determine that

$$\langle \text{gs}, + | \prod_{j=0}^{\ell} Z_j \, | \text{gs}, + \rangle = 0. \tag{3.2.6}$$

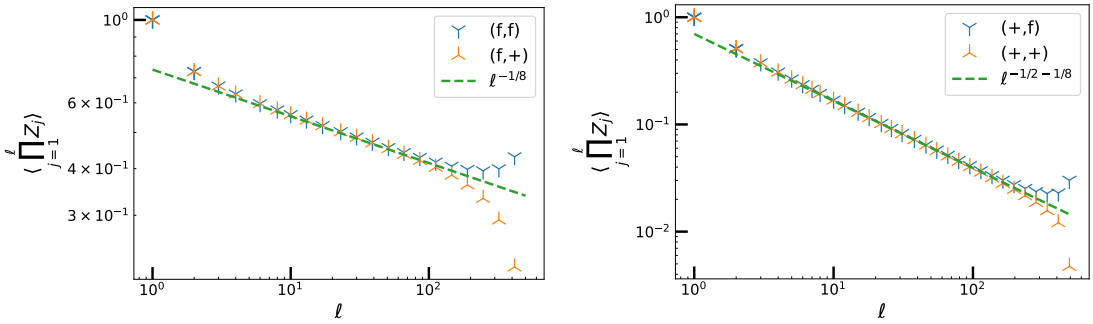


Figure 3.2: Expectation value of the string order parameter $\eta_A = \prod_{j\in A} Z_j$ in the Ising chain with different BCs. On the left we set the BC in 0 to be f, and consider the combinations $(f,+)$ and (f,f). We observe excellent agreement with the predicted decay, which scales as $\ell^{-1/8}$ (3.2.4). On the right, we set the BC in 0 to be $+$, and we consider the combinations $(+,f)$ and $(+,+)$. We observe good agreement with the prediction of a decay proportional to $\ell^{-5/8}$, cf. (3.2.7). The spin chain has $L = 500$ sites, and the $+$ BC is implemented with a boundary field $h = 500$.

On the other hand, a sensible choice is to restrict the flip operator to the bulk sites, excluding the frozen spin at $j = 0$. In that case, our prediction (3.1.11) reads,

$$\langle \mathrm{gs}, + | \prod_{j=1}^{\ell} Z_j \, | \mathrm{gs}, + \rangle \propto \ell^{-1/8-1/2} = \ell^{-5/8}. \tag{3.2.7}$$

We check this numerically, as before and plot the result in the right panel of Fig. 3.2. Once again we see excellent agreement between numerics and the CFT prediction.

Entanglement asymmetry. We now determine the $\mathbb{Z}_2$ entanglement asymmetry for the Ising model with $+$ boundary condition. We specifically investigate the $n = 2$ case, which is in fact the most experimentally relevant instance [117]. In this case, the asymmetry is given exactly by

$$\Delta S_A^{(2)} = \log 2 - \log\left(1 + \mathcal{Z}_2(\eta,\eta)\right), \tag{3.2.8}$$

where the CFT predicts that charged moment behaves as

$$\mathcal{Z}_2(\eta,\eta) \propto \ell^{-1} \tag{3.2.9}$$

and we used that $h_{\Psi_{(+,-)}} = 1/2$ in (3.1.18). In the left panel of Fig. 3.3, we compare our prediction for the charged moment with numerical data, which confirms the accuracy of the theoretical result: the correct power law scaling is reproduced before finite size effects kick in. In the right panel we plot the entanglement asymmetry which exhibits the anticipated behaviour: ΔS_A approaches $\log 2$ with corrections going as $1/\ell$ for large subsystem size.

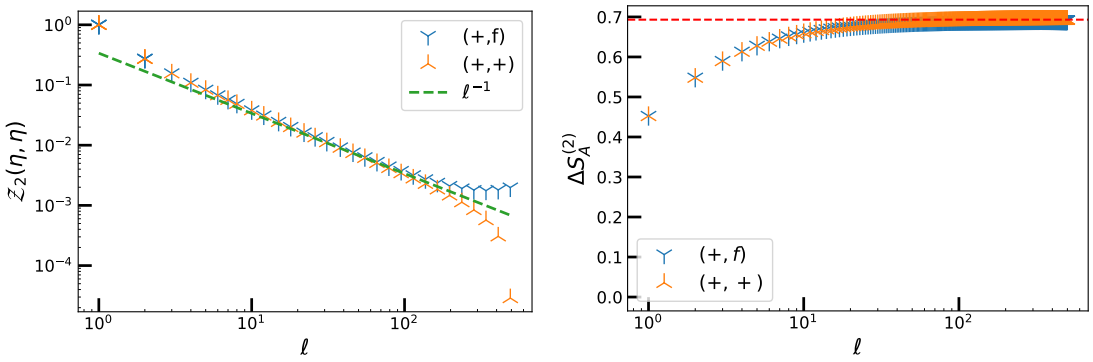


Figure 3.3: Normalized charged moment $\mathcal{Z}_2(\eta,\eta)$ (left) and second Rényi entanglement asymmetry $\Delta S_A^{(2)}$ (right) for the critical Ising model with + boundary condition imposed at $j = 1$. The parameters are the same as in Fig. 3.2. On the left, we display $\mathcal{Z}_2(\eta,\eta)$ and the dashed line is the prediction (3.2.9). On the right, we plot the entanglement asymmetry which approaches $\log 2$, independently of the boundary condition imposed at the right boundary.

3.2.2 Critical 3-state Potts model

Having examined the simplest case of a CFT with a discrete symmetry in the previous section, we now move on to a more intricate example and study the $n = 2$ entanglement asymmetry for the $\mathbb{Z}_3$ symmetry of the critical three-state Potts model, in the case of fixed boundary conditions.

The three state Potts model is a generalization of the Ising model with an enlarged global symmetry [96]. A possible lattice realization is made in terms of a spin chain chain with a three-dimensional local Hilbert space $\mathbb{C}^3$. The critical Hamiltonian on a semi infinite chain with a free boundary condition on the left edge is given by

$$H_f = -\sum_{j=1}^{\infty}(X_j X_{j+1}^\dagger + X_{j+1}X_j^\dagger + Z_j + Z_j^\dagger) \tag{3.2.10}$$

where we have introduced the clock operator X and the shift operator Z, defined by

$$X = \begin{pmatrix} 0 & 1 & 0 \\ 0 & 0 & 1 \\ 1 & 0 & 0 \end{pmatrix} \qquad Z = \begin{pmatrix} 1 & 0 & 0 \\ 0 & e^{i2\pi/3} & 0 \\ 0 & 0 & e^{-i2\pi/3} \end{pmatrix}. \tag{3.2.11}$$

This lattice model flows to the three-state Potts CFT which admits eight conformal boundary conditions [118, 119]. The simplest ones to implement on the lattice are the free and the three fixed ones. The free is implemented by simply truncating the chain as is done in (3.2.10). The fixed boundary conditions can be implemented in the lattice using a similar procedure to the Ising model. We add an auxiliary

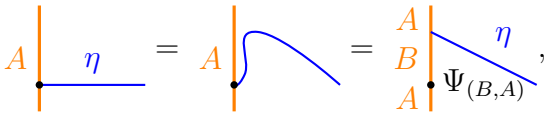
spin to the chain and fix it to be in one of the states $|A\rangle = (1,1,1)^T, |B\rangle = (1, e^{i2\pi/3}, e^{-i2\pi/3})^T$ or $|C\rangle = (1, e^{-i2\pi/3}, e^{i2\pi/3})^T$ with an energetic constraint which is imposed by an external field. For instance, the fixed A-type boundary condition can be obtained with the Hamiltonian

$$H_A = -\sum_{j=0}^{\infty}(X_j X_{j+1}^\dagger + X_{j+1}X_j^\dagger + Z_j + Z_j^\dagger) - h(X_0 + X_0^\dagger) \tag{3.2.12}$$

in the limit $h \to +\infty$. As before, we should consider only the sites $j \geq 1$ to be the region described by the CFT. The three-state Potts model has an internal S_3 symmetry and we focus on the breaking of its $\mathbb{Z}_3$ Abelian subgroup by the inclusion of the A-type boundary condition. This $\mathbb{Z}_3$ symmetry is generated by

$$\eta_A = \prod_{j=1}^{\ell} Z_j \tag{3.2.13}$$

which acts by permuting cyclically A, B and C. In the bulk, this operator flows to the topological line η (notation from [55]). The junction with the A-type boundary "contains" a boundary-changing operator $\Psi_{(B,A)}$, as one can see from



(3.2.14)

and $\Psi_{(B,A)}$ has conformal dimension 2/3 [114].

From the definition (1.2.7), the second Rényi asymmetry for the $\mathbb{Z}_3$ group is

$$\Delta S_A^{(2)} = \log 3 - \log\left(1 + \mathcal{Z}_2(\eta, \eta^{-1}) + \mathcal{Z}_2(\eta^{-1}, \eta)\right), \tag{3.2.15}$$

and from the cyclicity of the trace in (1.2.8), it follows that $\mathcal{Z}_2(\eta, \eta^{-1}) = \mathcal{Z}_2(\eta^{-1}, \eta)$. In the large ℓ limit, the lattice model is described by the CFT, where, according to (3.1.17), we have

$$\mathcal{Z}_2(\eta, \eta^{-1}) \propto \ell^{-4/3}. \tag{3.2.16}$$

This result is numerically validated in Fig. 3.4. In the left panel, we display data obtained for a chain of size $L = 100$. The numerical results align closely with the theoretical prediction given by (3.2.16), demonstrating both the accuracy of our analytical approach and the robustness of the numerical methods employed.

Finally, using (3.2.15) we have that the asymmetry approaches $\log 3$ with a power law correction given by

$$\Delta S_A^{(2)} = \log 3 - c_2 \ell^{-4/3} + o\left(\ell^{-4/3}\right). \tag{3.2.17}$$

On the right of Fig. 3.4 we plot the entanglement asymmetry obtained numerically and see that it behaves as predicted by (3.2.17).

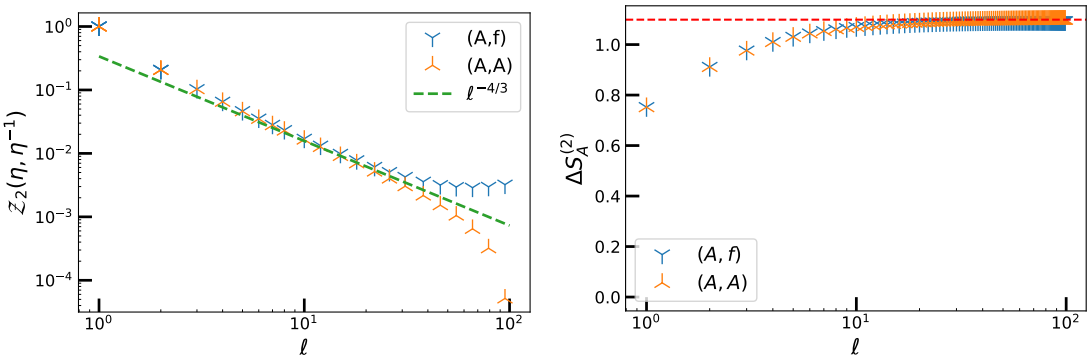


Figure 3.4: Normalized charged moment $\mathcal{Z}_2(\eta,\eta^{-1})$ (left) and second Rényi entanglement asymmetry $\Delta S_A^{(2)}$ (right) for the critical 3-state Potts model with the A-type boundary condition imposed at $j = 1$. The data corresponds to chain of total size $L = 100$. On the left, we display $\mathcal{Z}_2(\eta,\eta^{-1})$ and the dashed line is the prediction (3.2.16). On the right, we plot the entanglement asymmetry which approaches $\log 3$, independently of the boundary condition imposed at the right boundary.

3.2.3 Interval starting at the right boundary

In the preceding sections, we examined symmetry breaking in a subsystem that starts at the symmetry-breaking boundary condition. However, it is also insightful to explore the case where the subsystem does not include this boundary. Unlike entanglement entropy, entanglement asymmetry is not symmetric with respect to exchanging the subsystem with its complement, i.e. $\Delta S_A \neq \Delta S_{\bar{A}}$ where $\bar{A}$ is the set $x \notin A$. This is natural since there is no reason to expect, e.g., the level of symmetry breaking in a small subsystem, A be related to the that of the much bigger $\bar{A}$. To explore this further we consider numerical simulations in both the critical Ising and three-state Potts chains of the normalized charged moments and entanglement asymmetry for $\bar{A}$. For this geometry we have no CFT prediction.

Let us start with a finite critical Ising chain with + and free boundary conditions at either end. We first examine the normalized charged moment $\mathcal{Z}_2(\eta,\eta)$ which is reported in the inset of the left panel of Fig. 3.5. It turns out that this is well described by the curve ℓ/L without any adjustable parameter. Then we move to the entanglement asymmetry $\Delta S_{\bar{A}}$ reported in the main panel. We observe an almost linear behavior; however, upon closer inspection, a slight bending becomes apparent. Notice that for $\ell = 0$, we recover $\log 2$, as it should, since there we probe the symmetry breaking of the full system. The behavior of both the charged moment and the entanglement asymmetry is markedly different from the behavior seen above in Fig. 3.3.

We now move to the critical 3-state Potts chain with the A-type and free boundary conditions at either end. We first examine the normalized charged moment $\mathcal{Z}_2(\eta,\eta^{-1})$ which is reported in the inset of the right panel of Fig. 3.5. It

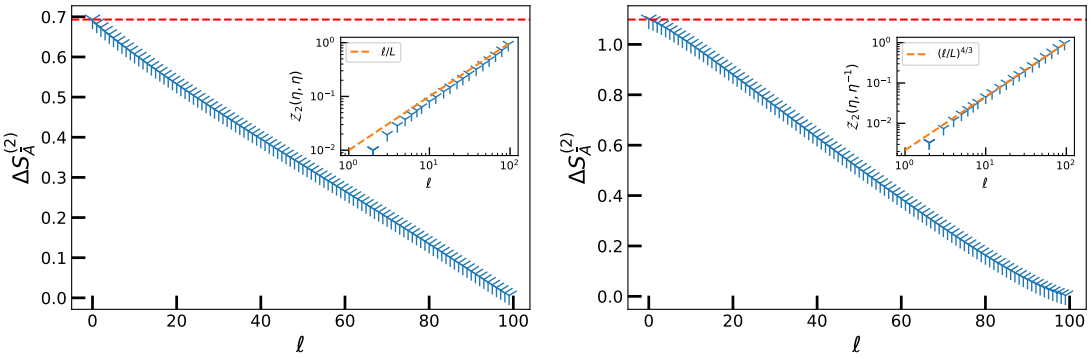


Figure 3.5: The entanglement asymmetry $\Delta S_{\bar{A}}$ for the subsystem $\bar{A} = (\ell, L]$. The insets show the normalized charged moments, $\mathcal{Z}_2$. Left: The ground state of the Ising model with + boundary condition at $j = 1$ and free boundary condition at $j = L$. The parameters are $L = 100$, $h = 500$. The red dashed line indicates the maximum value of $\log 2$. In the inset the dashed line is the power law behavior ℓ/L without any fitting parameter. Right: The ground state of the 3-state Potts model with A boundary condition at $j = 1$ and free boundary condition at $j = L$. The parameters are $L = 100$, $h = 500$. The red dashed line indicates the maximum value of $\log 3$. In the inset the dashed line is the power law behavior $(\ell/L)^{4/3}$ without any fitting parameter.

turns out that this is well described by the curve $(\ell/L)^{4/3}$ without any adjustable parameter. The entanglement asymmetry $\Delta S_{\bar{A}}$ is reported in the main panel. Again we have an almost linear behavior, but this time the bending is much more pronounced compared to the Ising model on the left. For $\ell = 0$, we recover $\log 3$, as expected.

Overall, these numerical results indicate that the normalized charged moments exhibit algebraic scaling, with an exponent that may be connected to the dimension of the boundary condition changing operator. However, we currently lack a concrete CFT prediction for this specific geometry. Nonetheless, the simplicity of the observed behavior suggests that deriving a corresponding CFT prediction for this scenario should be feasible, but it is beyond the scope of this work.

3.3 Boundary quenches: analytic results

We study the time evolution of a $(1+1)$d CFT on the positive half-line $[0, +\infty)$. We consider the groundstate with a certain boundary condition a in $x = 0$ and evolve it with a different boundary condition b—i.e. we perform a local quench on the boundary condition. We assume the boundary conditions to be *simple* in the sense of [106].

The groundstate with boundary condition a is denoted as $|\mathrm{gs}, a\rangle$ and is prepared by a euclidean path integral from time $\tau = -\infty$ to $\tau = 0$, and spatially extended on $[0, +\infty)$, see the left panel of Fig. 3.6. It belongs to the Hilbert space $\mathcal{H}_{(a,\cdot)}$ of

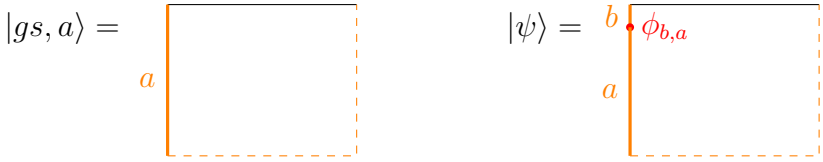


Figure 3.6: Euclidean path-integral preparation of the groundstate with boundary condition a (on the left), and path integral preparation of the state $|\psi\rangle$ of (3.3.1) (on the right).

states on the positive half-line with boundary condition a.

In order to evolve the state using a boundary condition b, one has to embed it into the Hilbert space with boundary condition b. This can be done with the use of a boundary-changing operator $\hat{\phi}_{b,a} : \mathcal{H}_a \to \mathcal{H}_b$. The state at time $t = 0$ is then

$$|\psi\rangle = \mathcal{N} e^{-\epsilon H_b} \hat{\phi}_{b,a} |gs, a\rangle \tag{3.3.1}$$

where $e^{-\epsilon H_b}$ is added to make the state normalizable [120] and $\mathcal{N}$ is a normalization is such that $|| \, |\psi(0)\rangle \, || = 1$. The limit $\epsilon \to 0$ will be performed at the end of the calculation. A pictorial description is in the right panel of Fig. 3.6.

We consider the expectation value of a local spinless primary operator $\hat{\mathcal{O}}(x) \in \mathrm{End}(\mathcal{H}_b)$ on the state $|\psi\rangle$ at time t. Analytically continuing time to euclidean signature we obtain a one point function $\langle \mathcal{O}(z) \rangle_{\mathsf{M}}$, where $z = x + i\tau$ and M is the right-half plane. On M, the boundary condition on the imaginary axis is a on $(-i\infty, -i\epsilon) \cup (i\epsilon, i\infty)$ and is b on $(-i\epsilon, i\epsilon)$. The boundary changing field $\phi_{b,a}$ is inserted at $-i\epsilon$ and its adjoint is inserted in $i\epsilon$. We also have assumed here that the velocity of the CFT is 1. In formulas, this is

$$\langle \hat{\mathcal{O}}(x) \rangle_t = \langle \psi | \, e^{itH} \hat{\mathcal{O}}(x) e^{-itH} \, |\psi\rangle \tag{3.3.2}$$

$$\stackrel{\tau = it}{=} \langle \psi | \, e^{\tau H} \hat{\mathcal{O}}(x) e^{-\tau H} \, |\psi\rangle \tag{3.3.3}$$

$$= \langle \mathcal{O}(z) \rangle_{\mathsf{M}}. \tag{3.3.4}$$

A pictorial representation of $\langle \mathcal{O}(z) \rangle_{\mathsf{M}}$ is given in Fig. 3.7. Notice that the euclidean time difference between the insertion of $\mathcal{O}$ and $\phi_{b,a}$ is $\epsilon + \tau$, while the euclidean time difference between the insertion of $\phi^\dagger_{b,a}$ and $\mathcal{O}$ is $\epsilon - \tau$, as expected from (3.3.3).

With the global conformal map

$$\begin{aligned} f &: \mathsf{M} \to \mathbb{H} \\ f(z) &= \frac{z + i\epsilon}{z - i\epsilon} =: w \end{aligned} \tag{3.3.5}$$

the geometry M can be mapped to the upper-half plane $\mathbb{H}$ where the boundary condition b is set on $(-\infty, 0)$ and the boundary condition a is set on $(0, +\infty)$. Here

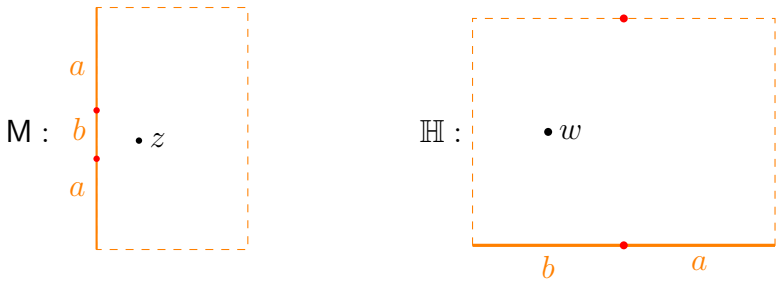


Figure 3.7: Left: geometry M, $z = x + i\tau$

the boundary changing operators are inserted at $w = 0$ and $w = \infty$. Then the one-point function of the scalar primary can be expressed as

$$\langle \mathcal{O}(z) \rangle_{\mathsf{M}} = |f'(z)|^{\Delta_\mathcal{O}} \, \langle \mathcal{O}(f(z)) \rangle_{\mathbb{H}}. \tag{3.3.6}$$

The one-point function on of a bulk spinless field on $\mathbb{H}$ has a generic form

$$\langle \mathcal{O}(w) \rangle_{\mathbb{H}} = \mathcal{F}(\cos\theta)(2\,\mathrm{Im}(w))^{-2\Delta_\mathcal{O}} \tag{3.3.7}$$

where $\theta = \arg w$ [121]. When w is close to the real axis the one-point function feels only the presence of the boundary condition a or b respectively. Hence it holds $\mathcal{F}(1) = \mathcal{A}^a_{\mathcal{O},\mathbb{I}}$ and $\mathcal{F}(-1) = \mathcal{A}^a_{\mathcal{O},\mathbb{I}}$, where $\mathcal{A}^a_{\mathcal{O},\phi}$ is the bulk-boundary structure constant between the bulk field $\mathcal{O}$ and the boundary field ϕ on the boundary a, and $\mathbb{I}$ is the identity (such structure constants are known for a wide class of CFTs [122, 123]).

For the conformal transformation considered, we have

$$\mathrm{Im}(w) = \frac{2x\epsilon}{x^2 + (\tau - \epsilon)^2} \qquad\qquad |f'(z)| = \frac{2\epsilon}{x^2 + (\tau - \epsilon)^2} \tag{3.3.8}$$

so that

$$\langle \mathcal{O}(z) \rangle_{\mathsf{M}} = \mathcal{F}_{ab}(\cos\theta)(2x)^{-\Delta_\mathcal{O}}. \tag{3.3.9}$$

Then we have

$$\cos\theta = \frac{\mathrm{Re}(w)}{|w|} = \frac{x^2 + \tau^2 - \epsilon^2}{\sqrt{(x^2 + (\epsilon - \tau)^2)(x^2 + (\epsilon + \tau)^2)}} \tag{3.3.10}$$

which, after setting $\tau = it$ and sending $\epsilon \to 0$, becomes

$$\lim_{\epsilon \to 0} \cos\theta \big|_{\tau = it} = \mathrm{sgn}(x - t). \tag{3.3.11}$$

so that, in the limit, the analytic continuation of $\mathcal{F}_{ab}(\cos\theta)$ is equal to $\mathcal{A}^a_{\mathcal{O},\mathbb{I}}$ for $t < x$, and equal to $\mathcal{A}^b_{\mathcal{O},\mathbb{I}}$ for $t > x$. Now recall that the expectation value of $\hat{\mathcal{O}}(x)$ on the groundstate with boundary condition a is

$$\langle \mathrm{gs}, a | \, \hat{\mathcal{O}}(x) \, | \mathrm{gs}, a \rangle = \mathcal{A}^a_{\mathcal{O},\mathbb{I}}(2x)^{-2\Delta_\mathcal{O}}. \tag{3.3.12}$$

Therefore, we get that for $t < x$ the expectation value of $\hat{\mathcal{O}}(x)$ at time t is the same as the one in the groundstate with boundary condition a, while for $t > x$ it becomes equal to the one in the groundstate with boundary condition b.

$$\langle \hat{O}(x) \rangle_t = \begin{cases} \langle \mathrm{gs}, a | \, \hat{\mathcal{O}}(x) \, | \mathrm{gs}, a \rangle & \text{if } t < x \\ \langle \mathrm{gs}, b | \, \hat{\mathcal{O}}(x) \, | \mathrm{gs}, b \rangle & \text{if } t > x. \end{cases} \tag{3.3.13}$$

3.3.1 Time evolution of the entanglement entropy

The same construction can be used to study the entanglement entropy at time t, on a bipartition in two intervals, one of which is attached to the boundary.

We recall the basic definitions. On a spatial bipartition $A \cup B$, given a pure state ρ, the reduced density matrix ρ_A is obtained performing the partial trace of ρ over the Hilbert space supported on B. The n-th Rényi entropy is $S^{(n)} = (1-n)^{-1} \log \mathrm{tr}\, [\rho_A^n]$, and in the limit $n \to 1$ gives the entanglement entropy $S = -\,\mathrm{tr}\, \rho_A \log \rho_A$.

The Rényi entropy at time t is then computed from the identity

$$\mathrm{tr}\, [\rho(t)_A^n] = {}^{\otimes n}\langle \psi(t) | \, R_A \, | \psi(t) \rangle^{\otimes n}, \tag{3.3.14}$$

where R_A is the linear map that permutes cyclically the replicas in A and acts as the identity on B To make the procedure well defined we follow the construction of [13], and add entangling surface centered in x, so that the subsystems are $A = [0, x - \delta]$ and $B = [x + \delta, \infty)$, and the boundary condition c is set at the entangling surface.

Let $\mathrm{tr}\, [\rho(i\tau)_A^n]$ be the analytic continuation in euclidean time of $\mathrm{tr}\, [\rho(t)_A^n]$. This can be expressed as a ratio of partition functions, depicted in Fig. 3.8. At the numerator one has the partition function of n copies of the CFT on the right-halfplane, with boundary condition on the imaginary axis set to be $a^{\otimes n}$ on $(-i\infty, -i\epsilon) \cup (i\epsilon, i\infty)$ and $b^{\otimes n}$ on $(-i\epsilon, i\epsilon)$; a disk of radius δ centered in $z = x + i\tau$ is removed, and the boundary condition $d^{\otimes n}$ is set; the line operator R which implements the permutation of the replicas connects the entangling surface with the boundary on the imaginary axis. Since the boundary condition is invariant under permutations, the junction betweent the line R and the boundary is topological, as the line itself. At the denominator, there is the same partition function, with the exception that the line operator R is omitted. The denominator comes from the normalization of the reduced density matrix $\rho(t)_A$.

In the limit $\delta \to 0$ each circle with boundary condition d appearing in the denominator becomes equal to the identity field times the g-factor g_d. The n circles displayed in the numerator, with the line R attached become the replica twist field $\mathcal{T}_n$ times $\delta^{\Delta_{\mathcal{T}_n}} g_c$ (where $\Delta_{\mathcal{T}_n} = \frac{c}{12}(n - 1/n)$ is the scaling dimension of $\mathcal{T}_n$ [95]). This is analogous to the procedure explained in [13] — in that case, a replicated manifold (n-sheeted Riemann surface) was considered, instead of a replicated theory. We then get

$$\mathrm{tr}\, [\rho(\tau)_A^n] = g_d^{1-n} \, \delta^{\Delta_{\mathcal{T}_n}} \, \langle \mathcal{T}_n(z) \rangle_{\mathsf{M}} \tag{3.3.15}$$

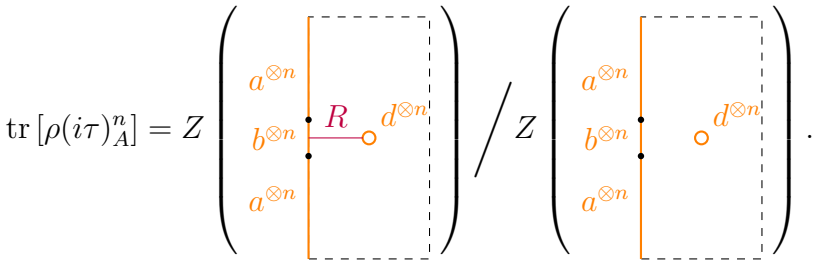


Figure 3.8: The analytic continuation to euclidean time of (3.3.14), expressed in terms of partition functions of the n-replicated CFT.

where it is understood that the theory that lives on M is now the n-replicated theory.

From this point, one can follow exactly the procedure done for one-point functions explained previously, obtaining that

$$\mathrm{tr}\,[\rho(t)_A^n] = \begin{cases} g_a^{1-n} g_d^{1-n} (2x/\epsilon')^{-\Delta_{\mathcal{T}_n}} & t < x \\ g_b^{1-n} g_d^{1-n} (2x/\epsilon')^{-\Delta_{\mathcal{T}_n}} & t > x. \end{cases} \tag{3.3.16}$$

Finally, we recall that the Rényi entropies in the ground state of a CFT on a half-line, where one subsystem is attached to the boundary with boundary conditions (b.c.) a and d at the entangling surface, follow the scaling [124]

$$S^{(n)}_{A,\text{ground state}} = \frac{c}{12}\frac{n+1}{n}\log\left(\frac{2x}{\epsilon'}\right) + \log(g_a) + \log(g_d). \tag{3.3.17}$$

From this expression, we see that the Rényi entropies, like all one-point functions of scalar primaries, exhibit a light-cone behavior: the entropies transition from those of the initial ground state (with b.c. a) to those of the final ground state (with b.c. b) when the subsystem $A = [0, x]$ enters the light cone. The jump is given by

$$S_A^{(n)}(t) - S_A^{(n)}(0) = \begin{cases} 0 & \text{if } t < x \\ \log\left(\frac{g_b}{g_a}\right) & \text{if } t > x. \end{cases} \tag{3.3.18}$$

Since this relation holds for all Rényi entropies, it also holds for the entanglement entropy.

3.4 Boundary quenches: numerical results

We specify the general results to the Ising CFT, which admits a simple lattice realization, where we can perform numerics. In the Ising CFT there are three conformal boundary conditions : two "fixed" boundary conditions , + and −, and a "free" boundary condition f [125]. We study the time evolution of the magnetization

(or spin) operator σ, and of the entanglement entropy for a subsystem A attached to the left boundary. We also study the time evolution of the $\mathbb{Z}_2$ entanglement asymmetry on ρ_A.

Quantum Ising model on an open chain We consider the critical quantum Ising model on an open chain of L sites. The Hamiltonian with "free" boundary conditions on both endpoints

$$H_{(f,f)} = -\sum_{j=1}^{L-1} X_j X_{j+1} - \sum_{j=1}^{L} Z_j. \tag{3.4.1}$$

Fixed boundary conditions are set adding an extra spin to the chain, which is polarized with infinite longitudinal field. For instance, the Hamiltonian for fixed boundary conditions on both endpoints is

$$H^{\text{extra}}_{(\pm,\pm)} = -\sum_{j=0}^{L} X_j X_{j+1} - \sum_{j=1}^{L} Z_j - h_L X_1 - h_R X_L, \tag{3.4.2}$$

and the boundary condition $+$ is obtained setting h_L, h_R to $+\infty$, while $h_L, h_R = -\infty$ realizes the boundary condition $-$. The Hilbert space of finite energy states is then $|\pm\rangle \otimes (\mathbb{C}^2)^{\otimes L} \otimes |\pm\rangle$. Since $X_0, X_{L+1} = \pm 1$, the Hamiltonian that acts on $(\mathcal{H})^{\otimes L}$ is

$$H_{(\pm,\pm)} = -\sum_{j=1}^{L-1} X_j X_{j+1} - \sum_{j=1}^{L} Z_j \pm X_1 \pm X_L, \tag{3.4.3}$$

thus effectively setting a boundary field with absolute value 1 on a chain of length L.

Finally, we recall that the lattice magnetization operator X_j flows to the CFT operator σ. We also recall that with the current normalization of the Hamiltonian, the velocity is $v = 2$. Hence, in order to match with the previous sections, we will replace t with t/v.

Conformal data The bulk-boundary structure constants are [122]

$$\mathcal{A}^{+}_{\sigma,\mathbb{I}} = -\mathcal{A}^{-}_{\sigma,\mathbb{I}} = \sqrt{2} \qquad\qquad \mathcal{A}^{f}_{\sigma,\mathbb{I}} = 0 \tag{3.4.4}$$

and the values of the g-factors of the conformal boundary conditions are [126]

$$g_+ = g_- = 1/\sqrt{2} \qquad\qquad g_f = 1. \tag{3.4.5}$$

Periodicities and change of sign in the magnetization As we already said, numerical simulations are necessarily performed on a chain of finite length. We do not provide complete analytic result for the time evolution of observables on

such geometry, but with a simple algebraic argument we predict the occurrence (or absence) of a change of sign in the magnetization at time $t = 2L/v$.

The Ising CFT is a diagonal rational CFT (RCFT). In a diagonal RCFT, there exist a conformal boundary condition associated to each conformal primary. The interval Hilbert space $\mathcal{H}_{a,b}$ can be decomposed in irreducible modules of its chiral algebra, denoted by $\mathcal{V}_c$. The multiplicities with which they appear are given by the fusion rules of the primaries [114]

$$\mathcal{H}_{a,b} = \bigoplus_c N_{\bar{a},b}^c \mathcal{V}_c. \tag{3.4.6}$$

Here it is assumed the right boundary to be oriented upwards and the left boundary to be oriented downwards. The Hamiltonian on the interval Hilbert space is

$$H_{a,b} = \frac{\pi}{L}\left(L_0 - \frac{c}{24}\right) \tag{3.4.7}$$

and the time evolution operator is $U(t) = \exp(-itH)$. Since the eigenvalues of L_0 on the irreducible module $\mathcal{V}_c$ take values in $h_c + \mathbb{N}$, at time $t = 2L$ all the states in a given module are evolved by the same phase, we thus get

$$U(2L) = e^{i\pi c/12} \times \bigoplus_a e^{i2\pi h_a} \mathbb{1}_{\mathcal{V}_a}. \tag{3.4.8}$$

We can now specialize the Ising CFT, showing that this explains why the sign of the magnetization changes for some boundary conditions. In the Ising CFT, $\bar{a} = a$ and the relation between the boundary conditions and primaries is $(\mathbb{I}, \varepsilon, \sigma) \leftrightarrow (+, -, f)$. We also denote them with their conformal dimensions, which are $(0, 1/2, 1/16)$. Hence we get

$$\mathcal{H}_{f,f} = \mathcal{V}_0 \oplus \mathcal{V}_{1/2} \qquad \mathcal{H}_{f,+} = \mathcal{H}_{f,-} = \mathcal{V}_{1/16}. \tag{3.4.9}$$

At time $t = 2L$, with boundary conditions (f, f) one obtains

$$U(2L) = e^{i\pi c/12} \begin{pmatrix} \mathbb{1}_{\mathcal{V}_0} & 0 \\ 0 & -\mathbb{1}_{\mathcal{V}_{1/2}} \end{pmatrix} \tag{3.4.10}$$

Now recall that the states in $\mathcal{V}_0$ are $\mathbb{Z}_2$-even, while the states in $\mathcal{V}_{1/2}$ are $\mathbb{Z}_2$-odd. Then, up to a global phase, $U(2L)$ is equal to the $\mathbb{Z}_2$ spin-flip operator, hence

$$U(2L)\,\hat{\sigma}(x)\,U(2L)^\dagger = -\hat{\sigma}(x) \tag{3.4.11}$$

i.e. the magnetization profile changes sign at time $t = 2L$. At time $t = 4L$, one has $U(4L) = e^{i\pi c/6}\mathbb{1}_{\mathcal{H}_{f,f}}$, so the time evolution is periodic with period $4L$.

When other choices of boundary conditions are taken, the Hilbert space is made of a single Virasoro module. Then the magnetization does not change sign, as $U(2L) \propto \mathbb{1}_{\mathcal{H}_{a,b}}$ and $U(2L)\,\hat{\sigma}(x)U(2L)^\dagger = \hat{\sigma}(x)$.

3.4.1 Numerical simulations

We perform matrix product states (MPSs) simulations to confirm the analytical results of Sec. 3.3. Simulations are done with the Tenpy library [127] on a chain of 150 sites. Lattice spacing is assumed to be the unit length, so $L = 150$. The groundstate is obtained with the DMRG algorithm, and then evolved in time with the TEBD algorithm, with a time step $dt = 0.05$.

We also study the second Rényi asymmetry for $\mathbb{Z}_2 \simeq \{\mathrm{id}, \prod_{j=1}^{L} Z_j\}$ describing the spin-flip action.

Quench $+ \to f$ The quench $+ \to f$ is performed preparing the groundstate with boundary condition $+$ on the left edge, then turning off the boundary field and evolving in time with the boundary condition "free". We choose a boundary condition $b \in \{+, -, f\}$ on the right boundary and leave it unchanged during the quench. We repeat the simulation for the three possible values of b. For times and positions much smaller than L, the system behaves as if it was semi-infinite, so the results of Sec. 3.3 apply. From (3.4.4), we expect the magnetization to vanish inside the light-cone, and from (3.3.18) we expect the entropy to have a positive jump of $\log(\sqrt{2})$. These are observed and reported in Fig. 3.9. The change of sign of the magnetization at time $t = 2L$ predicted by (3.4.11) is observed when the time evolution is with boundary conditions (f, f), while it is absent for other choices of boundary conditions .

The $\mathbb{Z}_2$-asymmetry on $A = [0, x]$ also displays a lightcone behaviour. At $t = 0$ it starts from a positive value — approximately $\log 2$, with with power-law corrections, as explained in [41]. It then becomes zero when $[0, x]$ enters the lightcone, thus showing that the symmetry is restored.

Quench $f \to +$ We then study the opposite quench, in which the left boundary condition is changed from "free" to $+$. We keep the right boundary condition b fixed, for the three possible values of b. We report the results in Fig. 3.10.

As expected, for small values of x, the magnetization becomes positive in in the light-cone. Its value at initial time would be zero on an infinite chain, but is affected by the boundary condition b on the right at finite size. The entropy is expected to have a negative jump of $-\log\sqrt{2}$, which is clearly observed when the right boundary condition is f. When the right boundary condition is $+$ or $-$ the jump is not uniform: it is negative for $x/L \sim 0$ and positive for $x/L \sim 1$. The jumps are smaller than $\log\sqrt{2}$ in absolute value, and we believe that they converge to such values for large enough L.

The $\mathbb{Z}_2$ asymmetry is here reported on the right subsystem B. When the right boundary condition is f, it is zero at initial time, since the state is symmetric at initial time. Then, as time passes, the symmetry remains broken on $[x, L]$ if $x > t/v$, hence the light-cone behaviour. When the right boundary condition is fixed, the

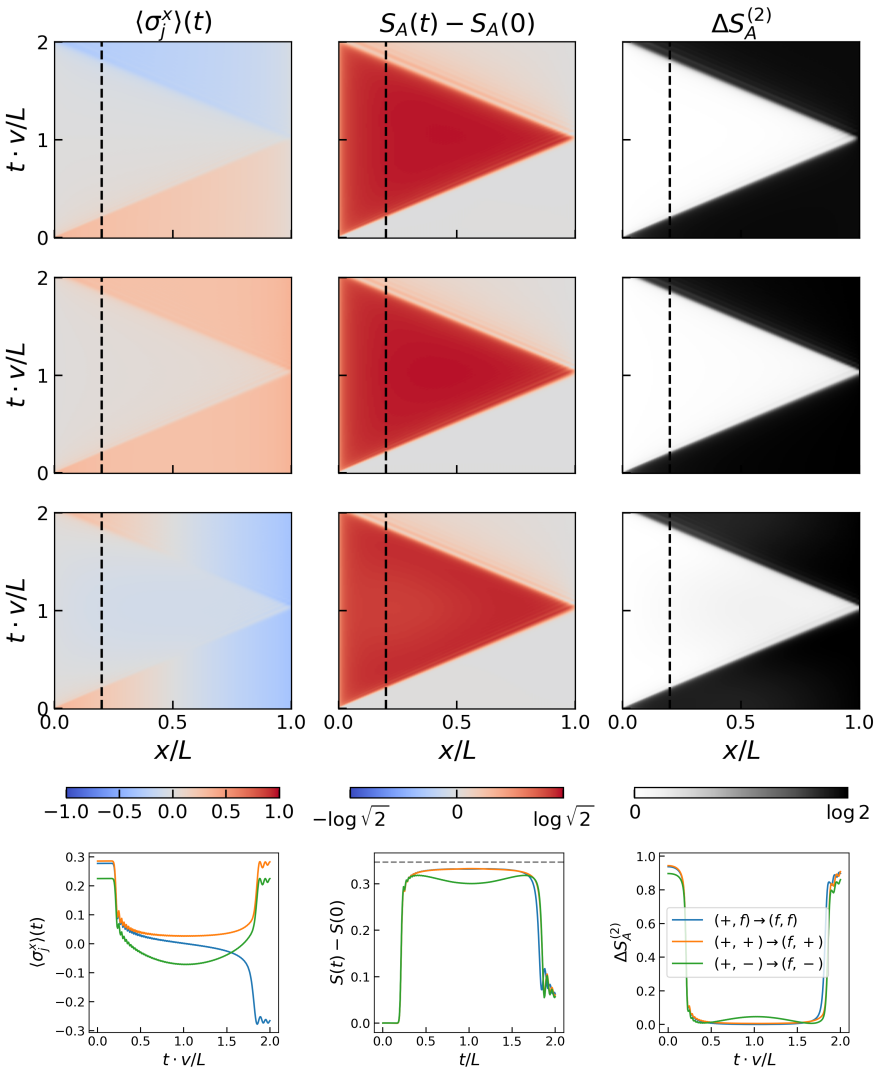


Figure 3.9: **Top**: Space-time plot of the quench $(+, b) \to (f, b)$. Every row is a different quench, where b is fixed respectively to $f, +, m$. Columns are respectively: magnetization, jump in the entanglement entropy, second Rényi asymmetry on A. The predicted light-cone behaviour is observed in the magnetization and in the entanglement entropy. **Bottom**: The same observables, on a fixed site at $x/L = 1/5$, as a function of time.

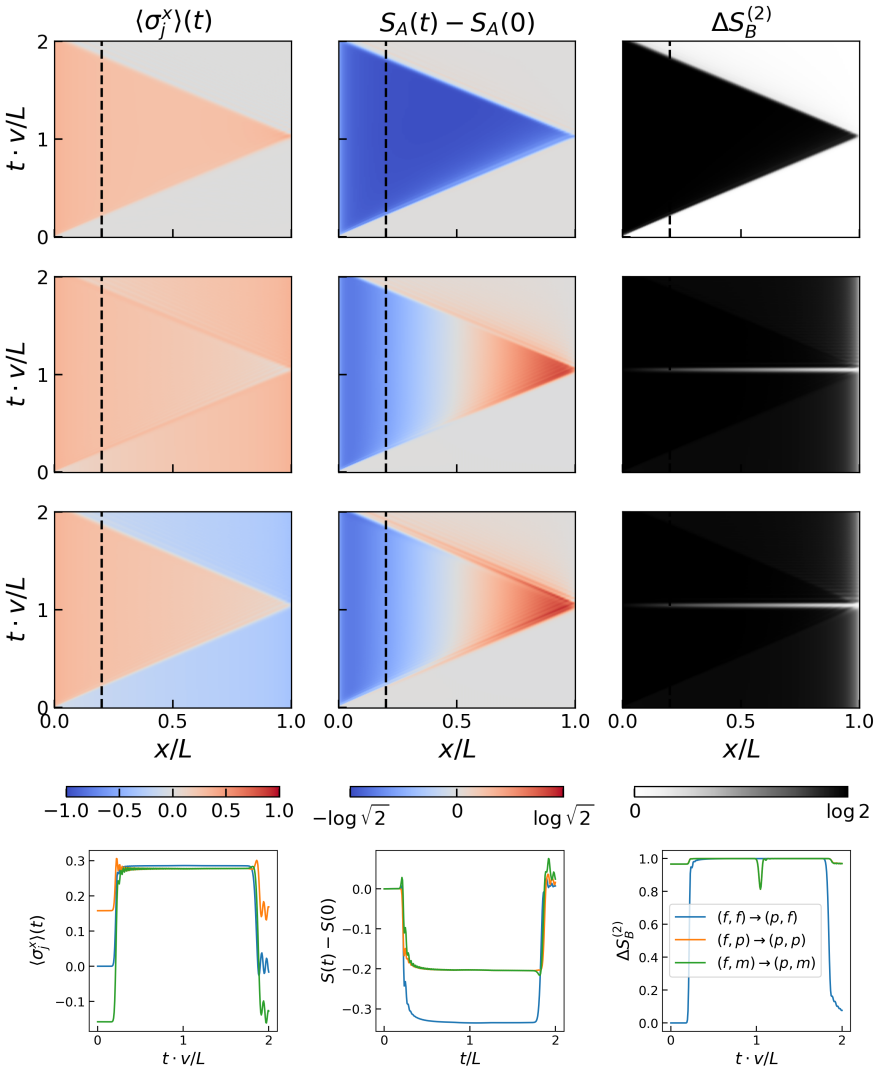


Figure 3.10: **Top**: Space-time plot of the quench $(f, b) \to (+, b)$. Every row is a different quench, where b is fixed respectively to $f, +, m$. Columns are respectively: magnetization, jump in the entanglement entropy, second Rényi asymmetry on the right subsystem B. **Bottom**: The same observables, on a fixed site at $x/L = 1/5$, as a function of time.

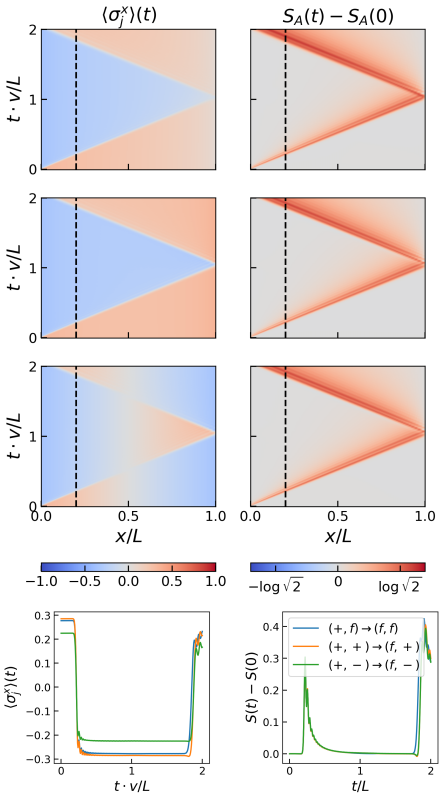


Figure 3.11: Quench $(+, b) \to (-, b)$, spacetime plot. Every row is a different quench, where b is fixed respectively to $f, +, m$. Columns display magnetization and variation in the entanglement entropy.

asymmetry is non-zero even at initial time. At time $t = L/v$ the asymmetry is approximately linear in x – behaviour typical of the groundstate $(+, f)$. This matches with the spatial profile of the magnetization at $t = L/v$, as well as the entanglement entropy.

Quench $+ \to -$ Lastly, we consider the boundary quench in which the boundary field is initially non-zero and undergoes a change of sign at $t = 0$. Here the magnetization close to the left edge is expected to change sign, while from (3.3.18) and (3.4.5) the entropy should not display any jump. Results are shown in Fig. 3.11. Magnetization does indeed change sign when crossing the lightcone. The entanglement entropy has a spike in the correspondence of the lightcone, restoring to its initial value after that, as expected.

Chapter 4

Entanglement asymmetry for generalized symmetries

4.1 Introduction

In this chapter we aim to define asymmetry for *generalized symmetries*, which include the cases of both higher-form [47] and noninvertible [54] symmetries.[1] In the modern formulation, the (finite internal) symmetries of a local quantum field theory are described by topological defects of various dimensions [47]. These objects fit naturally into mathematical structures known as (higher) fusion categories [54, 55, 130–133]. The latter not only encode which defects are present in a given theory, but also how they can fuse and join together, as well as various manifestations of anomalies (*e.g.*, braiding phases and transformations produced by manipulations of the topological defects). Such a generalized definition of "symmetry" goes well beyond ordinary symmetry groups. For the finite internal symmetries of unitary QFTs, we propose to define asymmetry through the following construction.

A QFT associates a Hilbert space of states to each possible spatial manifold. Consider thus a (possibly mixed) state, whose asymmetry one wishes to compute, described by a density matrix. One might be interested in studying the asymmetry of the full system, or of a subsystem. In the latter case, to each spatial subregion A and choice of boundary conditions, one can associate another Hilbert space and a reduced density matrix [13]. Moreover, one may choose whether or not to include the twisted sectors in these Hilbert spaces. In any case, one ends up with a (sub)system Hilbert space $\mathcal{H}$ and a (reduced) density matrix ρ. The symmetry defects, when laid parallel to the spatial manifold, give rise to an action on the (sub)system Hilbert space through a finite-dimensional C^*-algebra $\mathcal{A}$. We then propose to construct a "symmetrizer" S, that produces a symmetrized density

[1] The asymmetry for higher-form symmetries is studied in greater detail, from a different perspective, in [128]. On the other hand, a generalized Landau paradigm for noninvertible symmetries was advocated in [129].

matrix ρ_{S} from ρ. Concisely, S is the projector to the space of operators on $\mathcal{H}$ that commute with the symmetry algebra $\mathcal{A}$. Lastly, one quantifies how much ρ_{S} differs from ρ. Following [20], we use relative entropy or its Rényi version.[2] This defines, respectively, entanglement and Rényi asymmetries with respect to generalized symmetries.

In fact, this definition applies even beyond local quantum field theories — for instance, to lattice models. Once the relevant Hilbert space and finite-dimensional C^*-algebra of symmetry operators have been identified, our definition of asymmetry can be used.

To be concrete, we analyze in detail the case of two-dimensional unitary quantum field theories, where symmetries are implemented by the topological lines of a unitary fusion category $\mathscr{C}$. First, we consider QFTs placed on a spatial circle S^1 and study the asymmetry of the full system. The simplest setup is to restrict to the untwisted Hilbert space, on which the symmetry acts through a fusion algebra. On the other hand, one can encompass the total Hilbert space of untwisted and twisted sectors, on which a noninvertible symmetry has a more sophisticated action that mixes the untwisted sector with the twisted ones, and that is described by the so-called tube algebra $\mathsf{Tube}(\mathscr{C})$ [134]. We compare the asymmetries computed with respect to the fusion and tube algebras, finding that the latter is a more refined detector of symmetry breaking, especially in the case of noninvertible symmetries. We investigate this issue in the context of a class of excited states in CFTs, created by the insertion of local operators.

Moreover, we compute entanglement asymmetry in two-dimensional gapped phases with spontaneous symmetry breaking (SSB), employing a topological quantum field theory (TQFT) description. We find that vacua related by noninvertible symmetries need not have the same asymmetry, whereas for group-like symmetries they always do. This is another manifestation of the fact that vacua arising from the spontaneous breaking of a noninvertible symmetry can exhibit different physics [135, 136].

Next, we study the asymmetry of subsystems when the subregion A is an interval. In order to properly define a subsystem Hilbert space and a symmetry action on it, one needs to specify boundary conditions, mathematically described by a $\mathscr{C}$-module category $\mathscr{M}$. The noninvertible symmetry then acts through the so-called strip algebra $\mathsf{Strip}_{\mathscr{C}}(\mathscr{M})$ [137, 138]. When the theory admits (strongly or weakly [106]) symmetric boundary conditions, the definition of asymmetry is straightforward — otherwise,[3] we implement an averaging protocol over the boundary conditions related by symmetry. For excited states in CFTs (*e.g.*, in the Ising CFT), we investigate how the asymmetry varies with the subsystem size, and compare it

[2] Other functions that quantify the difference could be used as well; see, for instance, [35] for a discussion.

[3] For instance, the presence of 't Hooft anomalies in the theory prevents the existence of symmetric boundary conditions [106, 139], in a sense that we spell out more precisely in Sec. 4.4.

with the asymmetry of the full system. For group-like symmetries, we find that the choice of boundary conditions eventually does not affect the asymmetry, thus validating previous, less rigorous approaches in the literature in which the boundary conditions (and the possible influence of 't Hooft anomalies) were not taken into account. For noninvertible symmetries, instead, a proper account of the boundary conditions seems inevitable in order to compute the asymmetry explicitly.

Finally, we note that when the symmetry algebra $\mathcal{A}$ has special properties or additional structure, there might exist other equivalent presentations of the symmetrizer S (and hence of the asymmetries). For instance, strip algebras are always (weak) Hopf algebras [138], leading us to an alternative formula for S.

The chapter is organized as follows. In Sec. 4.2 we put forward our definition of asymmetry for generalized symmetries, whose core is the symmetrizer S with respect to a finite-dimensional semisimple algebra. In Sec. 4.3, focusing on two-dimensional theories, we study the asymmetry of states on a spatial circle, with respect to both the fusion and tube algebras. In Sec. 4.4, instead, we study the asymmetry of states on an interval with respect to the strip algebra. The possible definitions of the symmetrizer depend strongly on the available types of boundary conditions. We also present an alternative formula valid in the case of (weak) Hopf algebras. The asymmetry on the circle is applied in Sec. 4.5 to the detection of spontaneous symmetry breaking in 2d gapped phases. Finally, Sec. 4.6 is devoted to concrete examples that we work out in detail: group-like symmetries, as well as a collection of fusion categories including the Ising, $\mathsf{Rep}(H_8)$, Fibonacci, and Haagerup ones. More technical aspects are collected in appendices.

4.2 Entanglement asymmetry for generalized symmetries

In the modern formulation, the finite internal symmetries of a quantum field theory are described by a (higher) fusion category. Its objects, the morphisms between objects, the morphisms between morphisms, and so on, describe the topological operators of various codimensions in the quantum field theory and their intersections, and correspond to the symmetry elements. The full structure of the fusion category encodes phase factors (such as braiding phases and 't Hooft anomalies) as well as more general transformations produced by moves of the topological operators, which constitute the symmetry structure.

Depending on the physical setup, the symmetry category gives rise to different algebras of symmetry operators, as we now describe. A quantum field theory associates a Hilbert space of states to each spatial manifold. If we are interested in a subsystem (*i.e.*, a subregion) A, we can use the procedure of [13] (that we review in Sec. 4.4) to produce the Hilbert space of the QFT on a spatial manifold A with boundaries. Besides, we may want to include or not to include twisted sectors, *i.e.*,

to allow the insertion of topological operators along the time direction so that they pierce the spatial manifold. In all cases, we end up with a Hilbert space $\mathcal{H}$. We can construct symmetry operators acting on this space by taking topological defects laid along the spatial slice. Under the multiplication given by fusing the defects, they give rise to an algebra $\mathcal{A}$. We call $\{\mathcal{X}_a\}$ a basis of the algebra.

For technical reasons, in this chapter we focus on unitary quantum field theories with finite internal symmetries. These are described by a unitary (higher) fusion category, which contains a finite number of simple objects. As a result, the algebra $\mathcal{A}$ is a finite-dimensional C^*-algebra, which in particular is semisimple.

Let us re-introduce entanglement asymmetry from scratch, independently from groups, as was done in Sec. 1.2. Entanglement asymmetry is a quantum-information-based measure of symmetry breaking in pure or mixed states. Given a density matrix ρ, in order to quantify how much this breaks the symmetry, we compare it with a symmetrized version of itself, that we call ρ_{S}. Entanglement asymmetry is then defined as the relative entropy

$$\Delta S[\rho] \equiv S[\rho\|\rho_{\mathsf{S}}] \equiv \operatorname{Tr}\big(\rho\,(\log\rho - \log\rho_{\mathsf{S}})\big)\ . \tag{4.2.1}$$

Because of the properties of ρ_{S}, entanglement asymmetry can also be written, as we show below around (4.2.13), as a difference

$$\Delta S[\rho] = S[\rho_{\mathsf{S}}] - S[\rho]\ , \tag{4.2.2}$$

where $S[\rho] \equiv -\operatorname{Tr}(\rho\log\rho)$ is the von Neumann entropy. From standard properties of relative entropy, it follows that entanglement asymmetry is nonnegative, $\Delta S[\rho] \geq 0$, and that it vanishes if and only if $\rho = \rho_{\mathsf{S}}$. One can also define Rényi asymmetries, characterized by an index n:[4]

$$\Delta S^{(n)}[\rho] = \frac{1}{1-n}\log\frac{\operatorname{Tr}(\rho_{\mathsf{S}}^n)}{\operatorname{Tr}(\rho^n)}\ . \tag{4.2.3}$$

The entanglement asymmetry is reproduced in the limit $n \to 1$.

Given a Hilbert space $\mathcal{H}$ and a density matrix $\rho \in \operatorname{End}(\mathcal{H})$, in order to obtain the symmetrized version of ρ we need to construct a *symmetrizer* map $\mathsf{S} \in \operatorname{End}\big(\operatorname{End}(\mathcal{H})\big)$ such that

$$\mathsf{S}\colon\ \rho \mapsto \rho_{\mathsf{S}}\ . \tag{4.2.4}$$

The symmetrizer is characterized by the following properties:

1. It is a linear projector, in particular $(\rho_{\mathsf{S}})_{\mathsf{S}} = \rho_{\mathsf{S}}$.

[4] If ρ is a pure state, this reduces to the Rényi entropy, which is nonnegative (independently of the details of the symmetrization procedure). For a generic state, it has been proven in [140, 141] that the Rényi asymmetries are nonnegative for every n for the case of a $U(1)$ symmetry. The proof therein generalizes to any Abelian algebra, because the symmetrizer still takes the form (4.3.4). To the best of our knowledge, we are not aware of a proof of nonnegativity for a non-Abelian algebra or for a non-Abelian group.

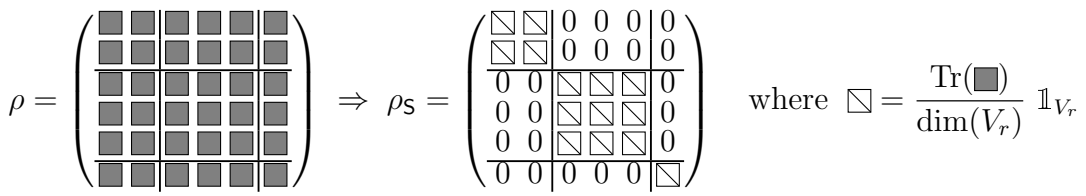


Figure 4.1: The Hilbert space splits as $\mathcal{H} = \bigoplus_r n_r V_r$ where V_r is the r-th irreducible representation of $\mathcal{A}$, while n_r is its degeneracy. A similar block decomposition applies to density matrices. The symmetrizer acts by setting to zero the off-diagonal blocks, and keeping sub-blocks proportional to the identity on the diagonal.

2. Its image is symmetry-invariant, namely $\mathcal{X}_a \, \rho_{\mathsf{S}} = \rho_{\mathsf{S}} \, \mathcal{X}_a$ for all $\mathcal{X}_a \in \mathcal{A}$.

3. If ρ is already symmetry-invariant, then $\rho_{\mathsf{S}} = \rho$.

4. It is trace-preserving, namely $\mathrm{Tr}(\rho_{\mathsf{S}}) = \mathrm{Tr}(\rho)$.

5. It maps density matrices to density matrices: $\rho_{\mathsf{S}}^\dagger = \rho_{\mathsf{S}}$ and $\rho_{\mathsf{S}} \geq 0$.

Notice that while properties 1. – 4. only depend on the product structure on $\mathcal{A}$, property 5. also depends on its $*$-structure.

Properties 1. – 3. can be more compactly stated as follows: S is a linear projector to the vector space of operators that commute with the algebra $\mathcal{A}$. Indeed, property 2. states that the image of S is contained in the space of commuting operators, while property 3. states that commuting operators are contained in the image of S. Properties 4. and 5., on the other hand, guarantee that ρ_{S} is a normalized density matrix (as long as ρ is) so that it makes sense to compute its von Neumann or Rényi entropies.

An intuitive picture for the action of the symmetrizer is the following. Decomposing the Hilbert space $\mathcal{H}$ into a direct sum of irreducible representations of $\mathcal{A}$ (with multiplicities), we can decompose both ρ and ρ_{S} into blocks that map irreducible representations to irreducible representations. Property 2. states that ρ_{S} commutes with every element of the algebra $\mathcal{A}$. Then, Schur's lemma (see, *e.g.*, [142]) implies that every block of ρ_{S} that connects two different irreducible representations must be the zero map, and that every block of ρ_{S} that connects two equal irreducible representations must be proportional to the identity. In Appendix 4.A.2 we show that the action of the symmetrizer S on ρ is precisely that of setting to zero the blocks that connect different irreducible representations, and to replace the blocks that connect equal irreducible representations with blocks proportional to the identity matrix, with a prefactor such that the trace of each block is preserved. See Fig. 4.1 for a graphical representation.

It turns out that such a symmetrizer has a simple and universal construction[5]

[5]What we mean by "universal" is that the symmetrizer can be constructed using just elements of the symmetry algebra under consideration, without other specific knowledge of the particular theory.

when the symmetry action on the Hilbert space gives rise to a *strongly-separable algebra*. Consider a unital associative algebra $\mathcal{A}$ over the complex field $\mathbb{C}$ defined by the product

$$\mathcal{X}_a \times \mathcal{X}_b = \sum\nolimits_c T^c_{ab}\, \mathcal{X}_c \,, \tag{4.2.5}$$

where $\{\mathcal{X}_a\}$ is a basis while $T^c_{ab} \in \mathbb{C}$ are the structure coefficients. We will often omit the product sign $\times$. Associativity corresponds to the identity $\sum_m T^m_{ab}\, T^d_{mc} = \sum_m T^d_{am}\, T^m_{bc}$. We indicate the unit element, which in general is a linear combination of the basis elements, as $\mathcal{X}_{\mathbb{1}}$. The regular representation is defined by the left action of the algebra on itself, and is explicitly given by the matrices $(T_a)^c{}_b = T^c_{ab}$. Define a trace $\mathrm{Tr}\colon \mathcal{A} \to \mathbb{C}$ for every element $X = \sum_a x^a \mathcal{X}_a \in \mathcal{A}$ as

$$\mathrm{Tr}(X) = \mathrm{Tr}\Big(\sum\nolimits_a x^a \mathcal{X}_a\Big) \equiv \sum\nolimits_a x^a\, \mathrm{Tr}(T_a) = \sum\nolimits_{am} x^a\, T^m_{am} \,. \tag{4.2.6}$$

Then consider the symmetric bilinear form

$$K_{ab} = \mathrm{Tr}(\mathcal{X}_a \mathcal{X}_b) = \mathrm{Tr}(T_a T_b) = \sum\nolimits_{mn} T^m_{an}\, T^n_{bm} \,. \tag{4.2.7}$$

As explained above, in this chapter we will be dealing with finite-dimensional unital semisimple algebras over the complex field $\mathbb{C}$. For such algebras, using the Wedderburn–Artin theorem (see Appendix 4.A), one can verify that the bilinear form (4.2.7) is non-degenerate. The inverse matrix $K^{-1} \equiv \tilde{K}$ allows one to construct a special element $e \in \mathcal{A} \otimes \mathcal{A}$ called the *symmetric separability idempotent* (SSI):

$$e = \sum\nolimits_{ab} \tilde{K}^{ab}\, \mathcal{X}_a \otimes \mathcal{X}_b \,, \tag{4.2.8}$$

whose defining properties will be discussed shortly. An algebra for which such an object exists is called strongly separable. One can also prove (we give some details in Appendix 4.A) that the structure coefficients satisfy the pivotal relation

$$T^b_{ca} = \sum\nolimits_{b'c'} \tilde{K}^{bb'}\, K_{cc'}\, T^{c'}_{ab'} \,. \tag{4.2.9}$$

Besides, one can explicitly construct the identity (or unit) element

$$\mathcal{X}_{\mathbb{1}} = \sum\nolimits_{abc} T^b_{ab}\, \tilde{K}^{ac} \mathcal{X}_c = \sum\nolimits_{abc} \tilde{K}^{ab}\, T^c_{ab}\, \mathcal{X}_c \tag{4.2.10}$$

and verify that $\mathcal{X}_{\mathbb{1}} \mathcal{X}_a = \mathcal{X}_a \mathcal{X}_{\mathbb{1}} = \mathcal{X}_a$ for all $\mathcal{X}_a \in \mathcal{A}$, as well as $\mathrm{Tr}(\mathcal{X}_{\mathbb{1}}) = \dim \mathcal{A}$. The SSI has the following properties. First, it is symmetric under the exchange of the two factors in the tensor product. Second, denoting the product as $XY = \mu(X \otimes Y)$ in terms of $\mu\colon \mathcal{A} \otimes \mathcal{A} \to \mathcal{A}$, the contraction of the SSI gives the unit element: $\mu(e) = \mathcal{X}_{\mathbb{1}}$. Third, the SSI commutes with every element of the algebra, $\mathcal{X}_a\, e = e\, \mathcal{X}_a$, where multiplication from the left/right acts on the first/second factor. Fourth, the SSI is idempotent as an element of $\mathcal{A} \otimes \mathcal{A}^{\mathrm{op}}$ (where $\mathcal{A}^{\mathrm{op}}$ is the same as $\mathcal{A}$ but elements are multiplied in the opposite order): $e^2 = e$. The one in (4.2.8) is the unique element with these properties.

The algebras we are interested in are also C^*-algebras and in particular have a $*$-structure, namely an anti-linear involution $\dagger\colon \mathcal{A} \to \mathcal{A}$ such that $(XY)^\dagger = Y^\dagger X^\dagger$. By a version of the Wedderburn–Artin theorem [143], one can show that the SSI is Hermitian, $e^\dagger = e$, and that there exists a special basis $\{\mathcal{X}_{\underline{a}}\}$ in which it takes the simple form $e = \sum_{\underline{a}} \mathcal{X}_{\underline{a}}^\dagger \otimes \mathcal{X}_{\underline{a}}$. See Appendix 4.A for more details.

The SSI provides then the general formula for the symmetrizer $\mathsf{S}\colon \rho_{\mathsf{S}} = e(\rho)$, where the first factor of e acts on ρ from the left while the second factor from the right. More explicitly:

$$\boxed{\rho_{\mathsf{S}} = \sum\nolimits_{ab} \tilde{K}^{ab}\, \mathcal{X}_a\, \rho\, \mathcal{X}_b} \,. \tag{4.2.11}$$

One can easily verify that the properties of the SSI guarantee the properties 1. – 4. of the symmetrizer. Besides, assuming that $\rho^\dagger = \rho$ and $\rho \geq 0$, one verifies that $\rho_{\mathsf{S}}^\dagger = \rho_{\mathsf{S}}$ (using that $e^\dagger = e$) and that $\rho_{\mathsf{S}} \geq 0$ (using the simple form of e in the special basis). As we will show, one can also find equivalent alternative expressions for the SSI when the algebra $\mathcal{A}$ has extra properties or extra structure. For instance, for commutative algebras one can rewrite (4.2.11) as a sum over projectors on one-dimensional representations, while for (weak) Hopf algebras one can rewrite (4.2.11) in terms of the coproduct and antipode operations.

In the special case that the symmetry is a standard 0-form invertible symmetry given by a group G,[6] previous literature has studied the simplest algebra $\mathcal{A}$ that can describe the symmetry action, namely the group algebra $\mathbb{C}[G]$, which is the fusion algebra associated to this symmetry. Its basis elements (and generators) $\mathcal{X}_g$ correspond to the group elements $g \in G$ and to the simple objects $\mathcal{L}_g$ of the fusion category Vec_G. The structure coefficients are $T_{gh}^k = \delta^k_{(gh)}$, where (gh) is the group multiplication. The bilinear form is then $K_{gh} = |G|\, \delta_{g,h^{-1}}$ and its inverse is $\tilde{K}^{gh} = |G|^{-1}\, \delta^{g,h^{-1}}$. The symmetrizer reads:

$$\rho_{\mathsf{S}} = \frac{1}{|G|} \sum\nolimits_{g\in G} \mathcal{L}_g\, \rho\, \mathcal{L}_{g^{-1}} \,. \tag{4.2.12}$$

This expression agrees with what already used in previous literature (*e.g.*[19, 20, 37, 39]).

For the symmetrizer (4.2.11) it is easy to prove that the two definitions (4.2.1) and (4.2.2) coincide. It is enough to notice that

$$\begin{aligned} \mathrm{Tr}\big(\rho_{\mathsf{S}} \log \rho_{\mathsf{S}}\big) &= \sum\nolimits_{ab} \tilde{K}_{ab}\, \mathrm{Tr}\big(\mathcal{X}_a\, \rho\, \mathcal{X}_b \log \rho_{\mathsf{S}}\big) \\ &= \sum\nolimits_{ab} \tilde{K}_{ab}\, \mathrm{Tr}\big(\rho\, \mathcal{X}_b \log(\rho_{\mathsf{S}})\, \mathcal{X}_a\big) = \mathrm{Tr}\big(\rho\, (\log \rho_{\mathsf{S}})_{\mathsf{S}}\big) \,, \end{aligned} \tag{4.2.13}$$

but $(\log \rho_{\mathsf{S}})_{\mathsf{S}} = \log \rho_{\mathsf{S}}$ because $\log \rho_{\mathsf{S}}$ commutes with the algebra, as does ρ_{S}.

Finally, given the algebra $\mathcal{A}$ corresponding to a chosen symmetry action, to what extent is the symmetrizer (4.2.11) unique? If we require that the symmetrizer be

[6] In the modern language of [47], a 0-form symmetry is a standard symmetry that acts on local operators and is implemented by spacetime-codimension-1 topological operators.

expressible solely in terms of the symmetry operators $\mathcal{X}_a$ — *i.e.*, that it be universal — then the uniqueness of the SSI e implies the uniqueness of S. Equivalently, as we show in Appendix 4.A.2, the form of the symmetrized density matrix is fixed as in Fig. 4.1, and this completely specifies the action of the symmetrizer. One could relax the requirement of universality and look for more general maps (which would require theory-specific operators). Yet one can argue that S, being a self-adjoint projector onto the space of operators that commute with $\mathcal{A}$, is completely determined.

4.3 Asymmetry for the circle Hilbert space

The construction in the previous section is general and it allows one to define the asymmetry for any type of finite internal symmetry, including higher-form [47] and noninvertible [54] generalized symmetries. In the following, however, we will present concrete constructions focusing on the case of two-dimensional unitary theories. In two dimensions, one can reduce to the case that only 0-form symmetries are present [144, 145]. Hence, the internal symmetries of a 2d unitary theory are described by a unitary fusion category $\mathscr{C}$ whose objects are the symmetry elements, namely the topological lines that implement the action of the symmetry in the theory. We call $\{\mathcal{L}_a\}$ the simple lines, that are finite in number.

In this work we study two natural Hilbert spaces: the circle Hilbert space and the interval Hilbert space for a choice of boundary conditions. Three algebras will play a central role: the fusion algebra of $\mathscr{C}$, the tube algebra $\mathsf{Tube}(\mathscr{C})$, and the strip algebra $\mathsf{Strip}_{\mathscr{C}}(\mathscr{M})$ for a chosen $\mathscr{C}$-module category $\mathscr{M}$. The first two act on the circle Hilbert space, while the latter acts on the interval Hilbert space. We first consider the case that the two-dimensional theory is on a spatial circle S^1 and we are interested in the asymmetry of a (possibly mixed) state ρ of the full system. We study the richer case of the interval Hilbert space (relevant for studying the asymmetry of subsystems, or the asymmetry of a theory on the interval) in Sec. 4.4. In the limit that the radius of S^1 goes to infinity, one can study the asymmetry of states at infinite volume. In particular, for CFTs or gapped systems (TQFTs) one can use conformal transformations or diffeomorphisms, respectively, to obtain the asymmetry of states on the infinite real line $\mathbb{R}$.[7]

The simplest algebra $\mathcal{A}$ to study is the one obtained by laying the topological lines on a spatial slice and letting them act on the untwisted Hilbert space $\mathcal{H}_1$: this is the standard fusion algebra associated to the fusion category $\mathscr{C}$ (Sec. 4.3.1). A more sophisticated algebra, that allows for a more accurate detection of symmetry breaking, is obtained by acting on the total Hilbert space $\mathcal{H}_{\text{Tube}}$ of all untwisted

[7] For generic QFTs, on $\mathbb{R}$ one usually chooses boundary conditions at infinity that fix a particular vacuum state that satisfies cluster decomposition. The infinite-volume limit of S^1, in contrast, keeps the Hilbert space constructed over the whole vector space of degenerate vacua.



Figure 4.2: Left: action of the fusion algebra (4.3.1) of the symmetry category $\mathscr{C}$ on the untwisted Hilbert space on S^1. The product of two elements of the algebra is realized by stacking the corresponding lines on the cylinder and fusing them. Right: the corresponding action of the fusion algebra on local operators.

and twisted sectors: this is the tube algebra of $\mathscr{C}$ (Sec. 4.3.2).

4.3.1 Fusion algebra

Associated to every fusion category $\mathscr{C}$ is a fusion algebra $\mathcal{A}$ spanned by the objects $\mathcal{L}_a$. Such an algebra is unital and associative and takes the general form (4.2.5), however in the basis in which $\mathcal{X}_a$ are the simple lines $\mathcal{L}_a$, the coefficients T_{ab}^c are constrained to be nonnegative integer numbers $N_{ab}^c \in \mathbb{N}$. We thus write the fusion algebra as

$$\mathcal{L}_a \times \mathcal{L}_b = \sum\nolimits_c N_{ab}^c \, \mathcal{L}_c \ . \tag{4.3.1}$$

Besides, associated to the rigid structure of $\mathscr{C}$ is a conjugation operation on $\mathcal{A}$: there exists an element of the chosen basis, that we call $\mathcal{L}_1$, such that the matrix $C_{ab} \equiv N_{ab}^1$ is involutive, namely $C^2 = \mathbb{1}$. Since the coefficients are natural numbers, this implies that for every a there exists a unique $\bar{a}$ such that $N_{ab}^1 = \delta_{b\bar{a}}$ and $\bar{\bar{a}} = a$. Conjugation is then the map

$$\mathcal{L}_a \ \mapsto \ \mathcal{L}_a^\dagger \equiv \mathcal{L}_{\bar{a}} = \sum\nolimits_b C_{ab} \, \mathcal{L}_b = \sum\nolimits_b N_{ab}^1 \, \mathcal{L}_b \ . \tag{4.3.2}$$

This is also called duality. Conjugation is required to be an algebra anti-automorphism: $N_{\bar{a}\bar{b}}^{\bar{c}} = N_{ba}^c$. This is then extended to the whole fusion algebra by anti-linearity. Conjugation and associativity allow one to derive that $N_{ab}^c = N_{b\bar{c}}^{\bar{a}}$, hence one obtains the pivotal relations

$$N_{ab}^c = N_{\bar{a}c}^b = N_{c\bar{b}}^a = N_{b\bar{c}}^{\bar{a}} = N_{\bar{c}a}^{\bar{b}} = N_{\bar{b}\bar{a}}^{\bar{c}} \ . \tag{4.3.3}$$

When applied to the conjugation matrix, they imply that $N_{1a}^b = N_{a1}^b = \delta_a^b$ so that $\mathcal{L}_1$ is in fact the unit element for the fusion algebra, it is unique and self-dual, and indeed it corresponds to the transparent identity line of $\mathscr{C}$.

The fusion algebra describes the action of the symmetry on the untwisted Hilbert space $\mathcal{H}_1$ on S^1, as depicted in Fig. 4.2 on the left. It also describes the action of the symmetry on untwisted local operators, as depicted in Fig. 4.2 on the

right.[8] One can prove (as we review in Appendix 4.A.1) that finite-dimensional fusion algebras are automatically C^*-algebras and thus semisimple and strongly separable. Therefore, if we are interested in defining and computing the asymmetry of (possibly mixed) states on $\mathcal{H}_1$ with respect to the fusion algebra, we can define the symmetrizer S — and hence entanglement and Rényi asymmetries — using the universal formula (4.2.11). We will describe some concrete results in Secs. 4.3.3 and 4.5, and present detailed computations in various examples in Sec. 4.6.

Commutative case. In the case of an Abelian algebra, the symmetrizer S can be described in an alternative but equivalent way, that we now present. The irreducible representations of a commutative algebra are one-dimensional. Therefore, the blocks shown in Fig. 4.1 are one-dimensional and the symmetrizer simply acts by setting to zero all blocks that connect different irreducible representations. Let $P_r : \mathcal{H} \to \mathcal{H}$ denote the projector onto the r-th irreducible representation. The symmetrizer then reads[9]

$$\rho_{\mathsf{S}} = \sum\nolimits_r P_r \, \rho \, P_r \ . \tag{4.3.4}$$

If we further assume that the algebra is a commutative *fusion algebra*, an explicit formula for P_r in terms of simple lines is available. This was discussed in [146] in the context of fusion algebras of modular fusion categories, but in fact it holds more generally for arbitrary fusion algebras. In the following we review the construction, partially based on [147].

The matrices $(N_a)^b{}_c \equiv N_{ac}^b$ give the regular representation of the algebra. They satisfy $N_{\bar{a}} = N_a^{\mathsf{T}} = N_a^\dagger$ and in the Abelian case they all commute. It follows that they are normal matrices and can be simultaneously diagonalized with a unitary transformation. Let us call $w^{(r)}$ the common eigenvectors, that are orthogonal with respect to the standard Hermitian product, and $\nu_{a(r)}$ the eigenvalues:

$$N_a \, w^{(r)} = \nu_{a(r)} \, w^{(r)} \ . \tag{4.3.5}$$

Note that $r = 1, \dots, \dim \mathcal{A}$. For each r, the eigenvalues provide a one-dimensional representation of the fusion algebra, namely

$$\nu_{a(r)} \, \nu_{b(r)} = \sum\nolimits_c N_{ab}^c \, \nu_{c(r)} \ . \tag{4.3.6}$$

This also shows that the eigenvectors can be taken to be equal to the eigenvalues: $w_a^{(r)} = \nu_{\bar{a}(r)}$, as one can check. Orthogonality of the vectors implies that $\sum_a \nu^*_{a(r)} \, \nu_{a(m)} = |s_r|^{-2} \, \delta_{rm}$ for some numbers s_r that we can take in $\mathbb{R}_{>0}$. One defines the matrix

$$S_{ar} = \nu_{a(r)} \, s_r \ . \tag{4.3.7}$$

[8] In CFTs there is a one-to-one correspondence between untwisted states on S^1 and untwisted local operators. In generic QFTs there is no such a correspondence, but it is still true that both states and local operators transform in representations of the fusion algebra.

[9] The expression (4.3.4) agrees with the formula originally proposed in [20] for invertible Abelian symmetries.

Note that $\nu_{1(r)} = 1$ in all representations r since $\mathcal{L}_1$ is the identity, thus $s_r = S_{1r}$. The action of the fusion algebra on its representations is usually written as

$$N_a\, w^{(r)} = \frac{S_{ar}}{S_{1r}}\, w^{(r)} \ , \tag{4.3.8}$$

and the matrix S_{ar} is called the S-matrix. One checks that it is unitary, $S^\dagger S = \mathbb{1}$, and therefore also $SS^\dagger = \mathbb{1}$. Such identities correspond to the orthogonality and completeness of characters. The relations (4.3.6) can then be written as

$$N_{ab}^c = \sum\nolimits_r \frac{S_{ar}\, S_{br}\, S_{cr}^*}{S_{1r}} \ , \tag{4.3.9}$$

which is the Verlinde formula. It also shows that S^T diagonalizes the matrices N_a, and that $\nu_{\bar{a}(r)} = \nu_{a(r)}^*$. Notice that when $\mathscr{C}$ is a modular fusion category, the S-matrix is also symmetric, but in general it is not.

The projector onto the r-th irreducible representation is then given by

$$P_r = S_{1r} \sum\nolimits_a S_{ar}^*\, \mathcal{L}_a \ . \tag{4.3.10}$$

One can verify, using the Verlinde formula and unitarity of the S-matrix, that the set $\{P_r\}$ forms a family of orthogonal projectors, *i.e.* they satisfy $P_r P_s = \delta_{rs} P_r$, and that if $|\psi\rangle$ belongs to the r-th irreducible representation then $P_{r'}|\psi\rangle = \delta_{rr'}|\psi\rangle$. Finally, one can verify that the expression (4.3.4) with P_r given by (4.3.10) agrees with (4.2.11).[10]

Note that for a noncommutative algebra the formula (4.3.4) would fail. From Fig. 4.1 it is clear that this would only put the density matrix in a block-diagonal form, without further projection to the identity matrix inside each sub-block. In Sec. 4.6.6 we study the simplest noninvertible and non-Abelian example: the Haagerup fusion algebra $H_{(3)}$.

4.3.2 Tube algebra

On a spatial S^1, a noninvertible symmetry can map (un)twisted sectors to other (un)twisted sectors. One can thus construct a more sophisticated and complete action of the symmetry on the total Hilbert space

$$\mathcal{H}_{\text{Tube}} = \bigoplus\nolimits_{a\,\in\,\text{Irr}(\mathscr{C})} \mathcal{H}_a \ , \tag{4.3.11}$$

where $\mathcal{H}_a$ are the Hilbert spaces on S^1 twisted by the lines $\mathcal{L}_a$ (and thus $\mathcal{H}_1$ is the untwisted sector), and $\text{Irr}(\mathscr{C})$ is the set of simple objects in $\mathscr{C}$. The finite-dimensional C^*-algebra $\mathcal{A}$ that is obtained in this way is called the *tube algebra*

[10] The expression in (4.3.4) is $\rho_\mathsf{S} = \sum_{ab}\Big(\sum_r S_{1r}^2 S_{ar}^* S_{br}^*\Big)\, \mathcal{L}_a \rho \mathcal{L}_b$. We need to show that $\sum_r S_{1r}^2 S_{ar}^* S_{br}^* = \tilde{K}^{ab}$. This is easily verified by multiplying both sides by the matrix K_{bc}, using its definition (4.2.7) and the Verlinde formula (4.3.9) twice.

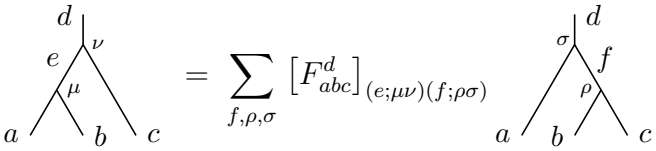
$\mathsf{Tube}(\mathscr{C})$ [134]. This algebra does not only depend on the fusion rules of $\mathscr{C}$, but rather also on its F-symbols (which are the components of the associator).

In order to describe the algebra, let us first fix our notation (that follows [148]). The nonnegative integers N_{ab}^c represent the dimensions of the vector spaces of morphisms between lines: $N_{ab}^c = \dim\big(\mathrm{Hom}(\mathcal{L}_a \otimes \mathcal{L}_b, \mathcal{L}_c)\big) = \dim\big(\mathrm{Hom}(\mathcal{L}_{\bar{c}}, \mathcal{L}_{\bar{b}} \otimes \mathcal{L}_{\bar{a}})\big)$. The second equality is because conjugation corresponds to inverting the direction of a line:



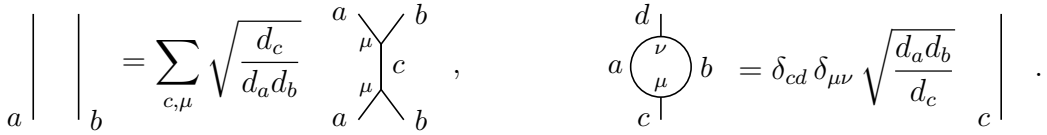
(4.3.12)

which physically is realized by a 180-degree rotation. The tensor product is associative, however it involves a change of basis in the vector spaces of morphisms described by the F-symbols:



(4.3.13)

Here and in the following, unless stated otherwise, all lines have implicit arrows oriented from bottom to top. Roman letters label the lines, while Greek letters label the basis of morphisms. The F-symbol F^d_{abc} is an element of $\mathrm{End}\big(\mathrm{Hom}(\mathcal{L}_a \otimes \mathcal{L}_b \otimes \mathcal{L}_c, \mathcal{L}_d)\big)$ represented by an invertible square matrix of size $N^d_{abc} = \sum_e N^e_{ab} N^d_{ec}$. As in [148], we choose the bases of morphisms in such a way that the F-symbols are *unitary* matrices[11] and $[F^d_{abc}] = \mathbb{1}$ whenever a, b, or c is 1 (and fusion is possible). The F-symbols satisfy the pentagon equation. We spell it out, together with other details, in Appendix 4.C. The bases are normalized so that the following hold:



(4.3.14)

The positive real numbers d_a are the quantum dimensions, which are associated to each line $\mathcal{L}_a$ and furnish a 1d representation of the fusion algebra: $d_a d_b = \sum_c N^c_{ab}\, d_c$.

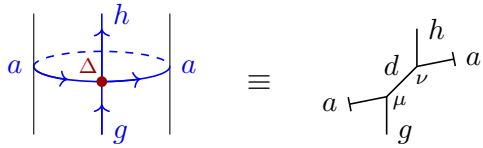
The tube algebra is generated by topological configurations in which a simple line $\mathcal{L}_a$ — stretched horizontally — can interpolate between two (un)twisted sectors $\mathcal{H}_g$ and $\mathcal{H}_h$, as in Fig. 4.3 left. Equivalently, the generators map (un)twisted local operators $\mathcal{O}_g$ (that live at the end of a line $\mathcal{L}_g$) to (un)twisted operators $\mathcal{O}_h$ via the so-called lasso action, as in Fig. 4.3 right. The configuration is described by a "cross",

[11] The existence of such bases is guaranteed by the fact that the fusion category is unitary. Without such an assumption, our formulas below would still be correct but in terms of inverse matrices, as opposed to Hermitian conjugate matrices.



Figure 4.3: Left: action of the tube algebra $\mathsf{Tube}(\mathscr{C})$ on the total Hilbert space on S^1 (left) and on (un)twisted point operators (right). The product of two elements of the algebra is realized by stacking the corresponding elements on the cylinder and then resolving the configuration.

where the horizontal line $\mathcal{L}_a$ is closed in a circle, while the vertical line $\mathcal{L}_g$ lies below and $\mathcal{L}_h$ lies above. The intersection Δ is an element of $\mathrm{Hom}(\mathcal{L}_a \otimes \mathcal{L}_g, \mathcal{L}_h \otimes \mathcal{L}_a)$, which has dimension $\sum_d N_{ag}^d N_{ha}^d$ (note that $N_{ha}^d = N_{\bar{h}d}^a$). It is convenient to decompose the intersection into trivalent junctions:

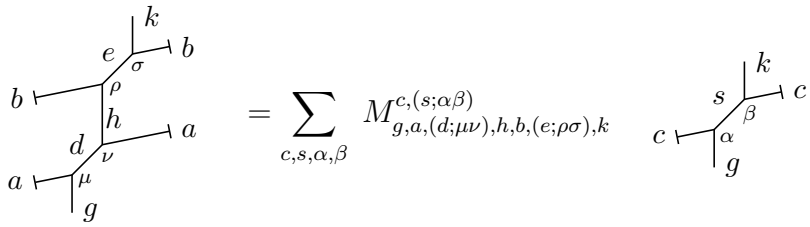


(4.3.15)

We will use the graphical notation on the r.h.s., and use the indicated basis for the tube algebra. All lines have an implicit arrow from bottom to top, and the tick at the beginning or end of a line indicates the "trace" described in [148]. The dimension of the tube algebra is

$$\dim\big(\mathsf{Tube}(\mathscr{C})\big) = \sum\nolimits_{g,a,d,h} N_{ag}^d N_{ha}^d \,. \tag{4.3.16}$$

In the tube algebra we multiply elements by placing one cylinder on top of the other (the product is such that bottom acts first, top acts second). The product is zero if there is no possible junction between adjacent vertical lines. In the case of the basis elements (4.3.15), because only simple lines are involved, this forces the vertical lines to be the same. We define a product matrix:



(4.3.17)

The computation of M is performed in Appendix 4.C, and the result is:

$$M^{c,(s;\alpha\beta)}_{g,a,(d;\mu\nu),h,b,(e;\rho\sigma),k} = \sqrt{\frac{d_a d_b d_h d_s}{d_d d_e d_c}} \sum_{\gamma,\eta,\lambda} \big[F^s_{kba}\big]^*_{(e;\sigma\eta)(c;\gamma\beta)} \big[F^s_{bha}\big]_{(e;\rho\eta)(d;\nu\lambda)} \big[F^s_{bag}\big]^*_{(c;\gamma\alpha)(d;\mu\lambda)} \,. \tag{4.3.18}$$

The sums are over a basis of morphisms $\mathcal{L}_b \otimes \mathcal{L}_a \xrightarrow{\gamma} \mathcal{L}_c$, $\mathcal{L}_e \otimes \mathcal{L}_a \xrightarrow{\eta} \mathcal{L}_s$, and $\mathcal{L}_b \otimes \mathcal{L}_d \xrightarrow{\lambda} \mathcal{L}_s$. In the special case that all $N_{ab}^c \in \{0,1\}$ and thus junctions are multiplicity free, we have:

$$M^{c,s}_{g,a,d,h,b,e,k} = \sqrt{\frac{d_a d_b d_h d_s}{d_d d_e d_c}} \left[F^s_{kba}\right]^*_{ec} \left[F^s_{bha}\right]_{ed} \left[F^s_{bag}\right]^*_{cd} . \tag{4.3.19}$$

In Appendix 4.C we verify that the product is associative. One can also check that the generators of the tube algebra that map the untwisted sector to itself, *i.e.*, the elements with $g = h = 1$ in (4.3.15), form a subalgebra[12] that is identical to the fusion algebra.

Tube algebras are finite-dimensional C^*-algebras (see, *e.g.*, [149] for a proof) and so in particular they are semisimple. Given the product in (4.3.17), one constructs the bilinear form K and then the symmetrizer S with respect to the tube algebra using the universal formula (4.2.11). Since the fusion algebra is a subspace of the tube algebra closed under multiplication, we expect the asymmetry with respect to the tube algebra to be bigger or equal to the asymmetry with respect to the fusion algebra.[13] In other words, we expect $\mathsf{Tube}(\mathscr{C})$ to be a more accurate detector of symmetry breaking. We discuss explicit examples of this fact in the next section.

4.3.3 Excited states in CFTs

An interesting class of theories where certain asymmetries can be computed analytically is given by two-dimensional CFTs. The vacuum $|0\rangle$ of a 2d unitary CFT does not break any internal symmetry, therefore its asymmetries vanish. What is more interesting is to compute the asymmetry of *excited states*. An accessible class of states is obtained by performing the Euclidean path-integral on a half-space with the insertion of local operators:[14]

$$|\psi\rangle = \left(\sum_i \mathcal{O}_i(z_i)\right)|0\rangle . \tag{4.3.20}$$

Here $\mathcal{O}_i$ are local operators, while $z_i \in \mathbb{C}$ denote points in the Euclidean lower half-plane.

In the case of invertible symmetries, the asymmetries of such states have been computed, *e.g.*, in [32, 42, 150]. Here we compare the asymmetries (of the whole system on $\mathbb{R}$ or S^1) with respect to the fusion algebras of invertible and noninvertible symmetries, and with respect to the tube algebra. We show, in a specific example, that the larger the algebra is, the more powerful the asymmetry is in detecting symmetry breaking.

[12] In this chapter, by subalgebra we simply mean a subspace of the algebra that is closed under product. We do not require that the identity of the subalgebra be equal to that of the original algebra, which indeed does not happen in this case.

[13] It would be interesting to prove this expectation, or to find a counterexample.

[14] We can think of these states as arising from a local quench at Lorentzian time $t = 0$.

Consider the example of the Ising CFT, which has three untwisted primary scalar local operators: the identity 1, the energy operator ε, and the spin operator σ. We study this example in Sec. 4.6.2. First, consider the $\mathbb{Z}_2$ spin-flip symmetry that maps $\sigma \mapsto -\sigma$. Since 1 and ε are neutral, any state constructed using them has vanishing asymmetry. The spin operator is odd, but the states $\sigma(z)|0\rangle$ have vanishing asymmetry because, as rays in the Hilbert space, they are mapped to themselves (equivalently, the density matrices $\rho \propto \sigma(z)|0\rangle\langle 0|\sigma(\bar{z})$ commute with the fusion or group algebra). Therefore, in order to detect any asymmetry, one should consider states such as $\big(1+\sigma(z)\big)|0\rangle$.

Next, consider the full noninvertible symmetry, namely the Ising fusion category $\mathscr{C}$ (see Sec. 4.6.2), which includes Kramers–Wannier self-duality. This symmetry is more powerful because ε is not invariant. We can thus detect symmetry breaking in states such as $\big(1+\sigma(z)\big)|0\rangle$ but also $\big(1+\varepsilon(z)\big)|0\rangle$. We compute the asymmetries of the latter on $\mathbb{R}$ with respect to the fusion algebra of Ising in (4.6.37), and plot the second Rényi asymmetry in Fig. 4.9.

Finally, consider the tube algebra of $\mathscr{C}$. Since Kramers–Wannier duality maps the spin operator σ to the disorder (or twist) operator μ, under the action of the tube algebra the operators (σ, μ) form a two-dimensional representation. This time even the states $\sigma(z)|0\rangle$ exhibit nonvanishing asymmetry, that we compute around (4.6.51), because they are mapped to different states in $\mathcal{H}_{\text{Tube}}$ (even when considered as rays).

Commutative algebras. For CFTs, whenever the symmetry algebra $\mathcal{A}$ is commutative, the asymmetries of the full system in the excited states (4.3.20) can be easily computed in terms of two-point functions.

Consider a pure state prepared by a Euclidean path-integral with the insertion of a sum of local operators in the Euclidean past. The Hilbert space could be the one on the circle or on the real line. The operators transform in irreducible representations of the symmetry algebra $\mathcal{A}$, which in the Abelian case are all one-dimensional. The state is

$$|\psi\rangle = \sum\nolimits_a |\psi_a\rangle = Z^{-\frac{1}{2}} \sum\nolimits_a$$  . (4.3.21)

The sum is over irreducible representations of $\mathcal{A}$, and each component is the Euclidean path-integral on a half-plane or a half-cylinder (in order to prepare a state on $\mathbb{R}$ or S^1, respectively) with the insertion of $\phi_a(z)$, as depicted, while Z is the path-integral on the plane or the cylinder with no insertions. The normalization of the states is provided by the 2-point functions:

$$\langle \psi_a | \psi_a \rangle = \big\langle \phi_a^\dagger(\bar{z})\, \phi_a(z) \big\rangle \,, \tag{4.3.22}$$

where $\bar{z}$ is the point specular to z with respect to the spatial cut. The density

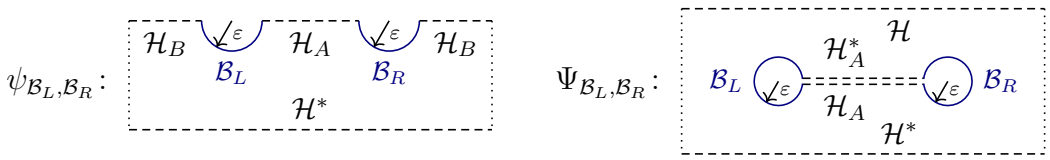


Figure 4.4: Left: the map $\psi_{\mathcal{B}_L,\mathcal{B}_R}\colon \mathcal{H} \to \mathcal{H}_A \otimes \mathcal{H}_B$ constructed with the path-integral on a strip, where $\mathcal{B}_{L,R}$ are boundary conditions at two removed half-discs of radius ε. Right: the map $\Psi_{\mathcal{B}_L,\mathcal{B}_R}\colon \mathrm{End}(\mathcal{H}) \to \mathrm{End}(\mathcal{H}_A)$ constructed via the path-integral on a strip with a finite-size cut, with the same boundary conditions imposed.

matrix for $|\psi\rangle$ is

$$\rho = \frac{1}{R}\,|\psi\rangle\langle\psi| = \frac{1}{R}\sum\nolimits_{ab} |\psi_a\rangle\langle\psi_b| \qquad \text{with} \qquad R = \sum\nolimits_a \langle\psi_a|\psi_a\rangle\ . \tag{4.3.23}$$

When the algebra is commutative we can use (4.3.4), hence the symmetrized matrix is

$$\rho_{\mathsf{S}} = \frac{1}{R}\sum\nolimits_a |\psi_a\rangle\langle\psi_a| \tag{4.3.24}$$

and the asymmetries are

$$\Delta S^{(n)} = \frac{1}{1-n}\log\left[\sum\nolimits_a \frac{\langle\psi_a|\psi_a\rangle^n}{R^n}\right], \qquad \Delta S = -\sum\nolimits_a \frac{\langle\psi_a|\psi_a\rangle}{R}\log\frac{\langle\psi_a|\psi_a\rangle}{R}\ , \tag{4.3.25}$$

where we used orthogonality between the states $|\psi_a\rangle$. Because of (4.3.22), the asymmetries are expressed in terms of two-point functions.

4.4 Asymmetry for the interval Hilbert space

The entanglement entropy, and likewise the entanglement asymmetry, of a subsystem is normally defined assuming that the Hilbert space factorizes: $\mathcal{H} = \mathcal{H}_A \otimes \mathcal{H}_B$. Here A is the subsystem of interest, while B is its complement. This allows one to define the reduced density matrix $\rho_A = \mathrm{Tr}_B(\rho)$ from the complete density matrix ρ (that could be pure or mixed), and then compute the entropy or the asymmetry of ρ_A. In quantum field theory one usually takes A to be a spatial subregion, and here we will consider the case that A is an interval. However, in quantum field theory the Hilbert space does not actually factorize. A consequence is that entanglement entropy is divergent and it requires a regularization.

A convenient regularization was proposed in [13]. One constructs a linear map

$$\psi_{\mathcal{B}}\colon \mathcal{H} \to \mathcal{H}_A \otimes \mathcal{H}_B \tag{4.4.1}$$

and computes the entanglement entropy in the image of $\psi_{\mathcal{B}}$. Such a map can be constructed as the path-integral on a strip, in which the lower (or incoming) boundary has the geometry underlying $\mathcal{H}$, while the upper (or outgoing) boundary is

the union of two disjoint parts with geometries underlying $\mathcal{H}_A$ and $\mathcal{H}_B$, respectively. In the case that $\mathcal{H}_A$ is an interval, one removes two small half-discs of radius ε at the two entangling points that bound A, and specifies some boundary conditions $\mathcal{B}_{L,R}$ there.[15] Eventually, the limit $\varepsilon \to 0$ is taken. We depict the setup in Fig. 4.4 left. Given the map $\psi_{\mathcal{B}}$ between Hilbert spaces, one also constructs the linear map

$$\Psi_{\mathcal{B}} \colon \mathrm{End}(\mathcal{H}) \to \mathrm{End}(\mathcal{H}_A) \tag{4.4.2}$$

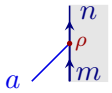
that acts on density matrices and already includes the partial trace on $\mathcal{H}_B$. It can be constructed as the path-integral on a strip obtained from a copy of $\psi_{\mathcal{B}}$ and a copy of its dual, glued along B. We depict the setup in Fig. 4.4 right. The path-integral constructions of those maps are particularly useful when also the states we want to analyze have a path-integral preparation, as we will see.

Once we have a (generically mixed) state in $\mathcal{H}_A$, we can define asymmetry in the general way described in Sec. 4.2. We need to identify how the symmetry acts on $\mathcal{H}_A$, which is the Hilbert space on an interval with boundary conditions $\mathcal{B}_{L,R}$. Such an action is given by the strip algebra, that we describe next. Note that $\mathcal{H}_A$ could also describe the asymmetry of the full system on an interval with boundary conditions; in this case one would not take the limit $\varepsilon \to 0$. For invertible symmetries, asymmetry with boundaries have been studied in [41, 151].

4.4.1 Strip algebra

The action of the symmetry on the interval Hilbert space is described by the strip algebra $\mathsf{Strip}_{\mathscr{C}}(\mathscr{M})$ [137, 138]. Let us first recall how the symmetry properties of boundary conditions are described in terms of *module categories*. In a left-module category $\mathscr{M}$ the simple objects $\mathcal{B}_m$ correspond to right boundary conditions. The fusion of simple bulk lines $\mathcal{L}_a$ (from the left) with simple boundaries $\mathcal{B}_m$ is described by a fusion algebra:

$$\mathcal{L}_a \times \mathcal{B}_m = \sum\nolimits_n \tilde{N}_{am}^n \, \mathcal{B}_n \ , \qquad \text{depicted as} \qquad \tag{4.4.3}$$



and where the fusion coefficients $\tilde{N}_{am}^n \in \mathbb{N}$. The number $\tilde{N}_{am}^n$ measures the dimension of the vector space of morphisms $\mathrm{Hom}(\mathcal{L}_a \otimes \mathcal{B}_m, \mathcal{B}_n)$, and the index ρ labels a basis of vectors when such a dimension is larger than 1. Simplicity of the objects $\mathcal{B}_m$ and the pivotal relation state that

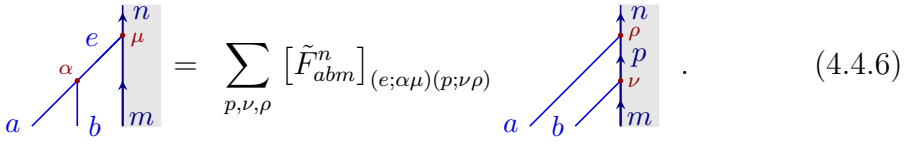
$$\tilde{N}_{1m}^n = \delta_m^n \ , \qquad \tilde{N}_{am}^n = \tilde{N}_{\bar{a}n}^m \ . \tag{4.4.4}$$

Associativity of the product $\mathcal{L}_a \times \mathcal{L}_b \times \mathcal{B}_m$ requires

$$\sum\nolimits_p \tilde{N}_{ap}^n \, \tilde{N}_{bm}^p = \sum\nolimits_c N_{ab}^c \, \tilde{N}_{cm}^n \ \equiv \ \tilde{N}_{abm}^n \ . \tag{4.4.5}$$

[15] In (4.4.1) we used the compact notation $\mathcal{B}$ to indicate the collection of boundary conditions used.

This means that the matrices $(\tilde{N}_a)^n{}_m$ furnish a nonnegative-integer-valued matrix representation (NIM-rep) of the bulk fusion algebra. There is a change of basis involved in the associativity of the tensor product, described by the $\tilde{F}$-symbols:



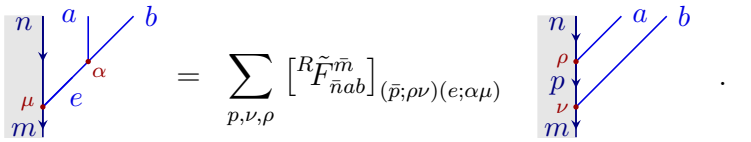
$$= \sum_{p,\nu,\rho} \left[\tilde{F}^n_{abm}\right]_{(e;\alpha\mu)(p;\nu\rho)} \quad . \tag{4.4.6}$$

We indicate right boundaries with upward arrows, while all bulk lines run from bottom to top. The $\tilde{F}$-symbols are unitary square matrices of size $\tilde{N}^n_{abm}$ and hence relations similar to (4.4.6) can be obtained using unitarity or the associator diagram. We work in a basis in which $\tilde{F}^n_{abm} = \mathbb{1}$ whenever a or b are equal to 1. The $\tilde{F}$-symbols satisfy a left-module pentagon equation, that also involves the F-symbols, reported in (4.D.1). One can define the quantum dimension $\tilde{d}_m$ of a boundary condition as the disc partition function with that boundary condition. Those quantum dimensions satisfy the relations:

$$d_a\, \tilde{d}_m = \sum\nolimits_n \tilde{N}^n_{am}\, \tilde{d}_n \ . \tag{4.4.7}$$

Thus the boundary quantum dimensions are the components of a common eigenvector of the matrices $\tilde{N}_a$ (with eigenvalues d_a).[16] In a unitary theory $\tilde{d}_m > 0$. Notice that the quantum dimensions $\tilde{d}_m$ are ambiguous by a common rescaling: this is because the disc partition functions can be rescaled by adding an Euler counterterm to the action.

A right-module category is defined in a similar way, but the objects correspond to left boundary conditions and bulk lines act on them from the right. We describe the associativity of the tensor product with symbols ${}^R\tilde{F}$:



$$= \sum_{p,\nu,\rho} \left[{}^R\tilde{F}^{\bar{m}}_{\bar{n}ab}\right]_{(\bar{p};\rho\nu)(e;\alpha\mu)} \quad . \tag{4.4.8}$$

We use downward arrows to indicate left boundary conditions. The symbols ${}^R\tilde{F}$ satisfy their own right-module pentagon equation, that we report in (4.D.2). For simplicity, we will restrict to the case that the same module is used on the right and on the left. If $[\tilde{F}]$ solves the left-module pentagon equation (4.D.1), then $[{}^R\tilde{F}]$ defined as

$$\left[{}^R\tilde{F}^{\bar{m}}_{\bar{n}ab}\right]_{(\bar{p};\rho\nu)(e;\alpha\mu)} \equiv \left[\tilde{F}^n_{abm}\right]^*_{(e;\alpha\mu)(p;\nu\rho)} \qquad \text{or simply} \qquad \left[{}^R\tilde{F}^{\bar{m}}_{\bar{n}ab}\right]_{\bar{p}e} \equiv \left[\tilde{F}^n_{abm}\right]^*_{ep} \tag{4.4.9}$$

[16] Indeed, using that $d_a = d_{\bar{a}}$ and the pivotal relation, (4.4.7) can be rewritten as $d_{\bar{a}}\, \tilde{d}_m = \sum_n \tilde{N}^m_{\bar{a}n}\, \tilde{d}_n$.

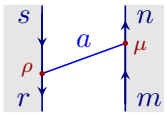
solves the right-module pentagon equation (4.D.2). Besides, this identification guarantees that if right boundary conditions are bent into left boundary conditions, their junctions with bulk lines can be moved from right to left. We thus regard this $[{}^R\tilde{F}]$ symbols as the right-module version of the left-module $[\tilde{F}]$.

A module category that always exists is the *regular module*, in which we identify the boundary conditions with the bulk lines, $\mathcal{B}_m = \mathcal{L}_m$, and thus also the boundary and bulk fusion algebras are identified: $\tilde{N} = N$. This is the module in which the fusion category $\mathscr{C}$ acts on itself. The $\tilde{F}$-symbols are simply identified with the F-symbols:

$$\text{regular module:} \qquad \tilde{F} = F \ . \tag{4.4.10}$$

For the right module, one could either use the gauge (4.4.9) as we will do, or use a different gauge in which $\tilde{F} = {}^R\tilde{F} = F$. Both solve the right-module pentagon equation (4.D.2).

The strip algebra is generated by the following basis elements:

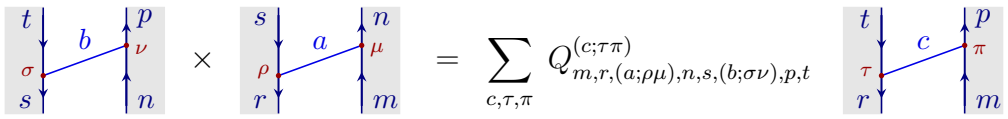


(4.4.11)

where the line $\mathcal{L}_a$ acts both on the bulk as well as on the boundary by changing the boundary conditions. We will always make the same choice of module category for the left and right boundary condition. It is however easy to extend all formulas to the general case. The dimension of the algebra is

$$\dim\big(\mathsf{Strip}_{\mathscr{C}}(\mathscr{M})\big) = \sum\nolimits_{m,r,a,n,s} \tilde{N}^n_{am}\, \tilde{N}^s_{ar} \ . \tag{4.4.12}$$

The product in the algebra is easily computed using the two moves above and (4.3.14):



$$= \sum_{c,\tau,\pi} Q^{(c;\tau\pi)}_{m,r,(a;\rho\mu),n,s,(b;\sigma\nu),p,t} \ , \tag{4.4.13}$$

where

$$Q^{(c;\tau\pi)}_{m,r,(a;\rho\mu),n,s,(b;\sigma\nu),p,t} = \sum\nolimits_{\alpha} \sqrt{\frac{d_a d_b}{d_c}}\, \big[\tilde{F}^t_{bar}\big]_{(c;\alpha\tau)(s;\rho\sigma)} \big[\tilde{F}^p_{bam}\big]^*_{(c;\alpha\pi)(n;\mu\nu)} \ . \tag{4.4.14}$$

The sum is over a basis of morphisms $\mathcal{L}_b \otimes \mathcal{L}_a \xrightarrow{\alpha} \mathcal{L}_c$. With no multiplicities this simplifies to

$$Q^{c}_{m,r,a,n,s,b,p,t} = \sqrt{\frac{d_a d_b}{d_c}}\, \big[\tilde{F}^t_{bar}\big]_{cs} \big[\tilde{F}^p_{bam}\big]^*_{cn} \ . \tag{4.4.15}$$

We verify in Appendix 4.D that such a product is associative.

Since, in our context, the boundary conditions are introduced as a tool to regularize the entanglement entropy, it is desirable to use symmetry-invariant

boundary conditions, in order not to contaminate the measurement of symmetry breaking coming from the state with an effect due to the boundaries.[17] The type of symmetry-invariant boundary conditions available in a given theory depends on the structure of the symmetry, and in particular on the presence of 't Hooft anomalies [139]. For noninvertible symmetries, one can distinguish three situations [106]: theories with strongly-symmetric simple boundaries, theories with only weakly-symmetric simple boundaries, and theories with no symmetric simple boundaries. We will discuss these three cases in turn.

4.4.2 Strongly-symmetric boundary conditions

The most favorable case is when there exists a module category made of a single simple boundary. Such a boundary condition is automatically symmetry-invariant, meaning that it is invariant (up to rescaling) under parallel fusion with the lines $\mathcal{L}_a \in \mathscr{C}$. Yet, there might be multiple junctions between a given bulk line $\mathcal{L}_a$ and the boundary. Such a boundary condition was called "strongly-symmetric" in [106]. It makes the definition and computation of entanglement asymmetry particularly simple. Such a boundary condition exists if and only if the symmetry is free from 't Hooft anomalies.[18]

A strongly-symmetric boundary condition is described by a module category in which there is a single simple object: $\mathcal{B}$. Since the boundary index takes a single value, we henceforth indicate it with a dot. The fusion coefficients and the $\tilde{F}$-symbols simplify:

$$\tilde{N}_1^{\cdot}{}_{\cdot} = 1 \ , \qquad \tilde{N}_a^{\cdot}{}_{\cdot} = \tilde{N}_{\bar{a}}^{\cdot}{}_{\cdot} = d_a \geq 1 \ , \qquad \left[\tilde{F}_{ab\cdot}^{\cdot}\right]^*_{(c;\delta\rho)(\cdot\,;\nu\mu)} \equiv m_{a\mu,b\nu}^{c\rho;\delta} \ . \tag{4.4.16}$$

The fact that the boundary fusion coefficients are equal to the quantum dimensions immediately follows from (4.4.7). Thus a necessary condition for the existence of strongly-symmetric boundary conditions in $\mathscr{C}$ is that all quantum dimensions are integer. Notice that when $\tilde{N}_a^{\cdot}{}_{\cdot} > 1$ there are multiple junctions between the line $\mathcal{L}_a$ and the boundary. It turns out that there is a one-to-one correspondence between:

- left-module categories over $\mathscr{C}$ with only one simple object;
- fiber functors of the fusion category $\mathscr{C}$;

[17] On the other hand, as previously mentioned, it is an interesting question to study the asymmetry of boundary conditions. This has been analyzed in [41, 151].

[18] More precisely, when the 't Hooft anomaly vanishes there always exists a module category with a single simple object, that can describe a strongly-symmetric boundary condition. Whether such a boundary condition actually exists in a given theory depends on the theory itself and on extra properties we might require to the boundary condition, for instance conformality. A similar comment applies to the regular module category that always exists, irrespective of 't Hooft anomalies.

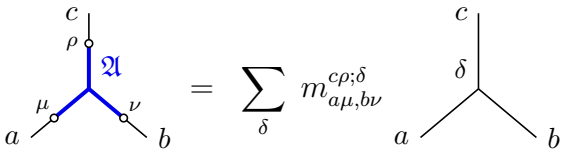
- maximal haploid algebra objects $\mathfrak{A}$ in $\mathscr{C}$.[19]

The first entry corresponds to a strongly-symmetric boundary condition. The second entry corresponds to a trivially-gapped phase (*a.k.a.* SPT phase, or invertible TQFT) for the symmetry, and thus the symmetry is non-anomalous. We see that strongly-symmetric boundary conditions exist if and only if the symmetry is non-anomalous. The third entry corresponds to a maximal gauging of the whole symmetry (possible only in the absence of anomalies).

The redefinitions in (4.4.16) make the correspondence with the maximal algebra object $\mathfrak{A}$ explicit. This is

$$\mathfrak{A} = \bigoplus_a d_a \, \mathcal{L}_a \ , \tag{4.4.17}$$

where $d_a \in \mathbb{N}$ counts the dimension of $\mathrm{Hom}(\mathcal{L}_a, \mathfrak{A})$.[20] The symbols m are the components of the multiplication morphism $m\colon \mathfrak{A} \otimes \mathfrak{A} \to \mathfrak{A}$:



$$= \sum_\delta m_{a\mu,b\nu}^{c\rho;\delta} \quad . \tag{4.4.18}$$

The requirement that m be associative, namely that $m\big(m(x \otimes y) \otimes z\big) = m\big(x \otimes m(y \otimes z)\big)$ for all $x, y, z \in \mathfrak{A}$, when written in components, boils down to the constraint [49]:

$$\sum\nolimits_{e,\epsilon,\alpha,\beta} m_{a\mu,b\nu}^{e\epsilon;\alpha} \, m_{e\epsilon,c\rho}^{d\sigma;\beta} \, \big[F_{abc}^d\big]_{(e;\alpha\beta)(f;\gamma\delta)} = \sum\nolimits_\phi m_{a\mu,f\phi}^{d\sigma;\delta} \, m_{b\nu,c\rho}^{f\phi;\gamma} \ . \tag{4.4.19}$$

Using the correspondence in (4.4.16) and unitarity, this equation is equivalent to the left-module pentagon equation (4.D.1) (for module categories with one simple object). Notice that a fusion category $\mathscr{C}$ can admit multiple inequivalent maximal algebra objects $\mathfrak{A}$: they will have the same decomposition (4.4.17), but would differ in the product m.[21]

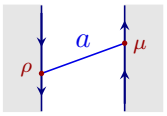
[19] More precisely, one is typically interested in equivalence classes of the objects listed above. The relevant equivalence relations are, respectively: equivalence of $\mathscr{C}$-module categories; equivalence of tensor functors; Morita equivalence of algebras. In particular, the last one turns out to be the correct equivalence that corresponds to equivalent module categories, as opposed to the stronger isomorphism of algebras [152, 153].

[20] Haploid means that $\dim\big(\mathrm{Hom}(\mathcal{L}_1, \mathfrak{A})\big) = 1$.

[21] The construction is more general, see App. A of [106] as well as [54, 152, 154]. For any module, choose a simple object (a boundary), then the so-called internal Hom construction produces a (in general not maximal) haploid algebra object in $\mathscr{C}$. The algebra objects one obtains from the various simple objects (boundaries) of a given module can be different, but are all Morita equivalent. All haploid, semisimple, indecomposable algebra objects are obtained in this way, by considering all possible indecomposable module categories. Indeed, from the algebra object one can construct a module category such that the internal Hom construction gives back that algebra.

The corresponding strip algebra is generated by the basis elements

$$H_{(a;\rho\mu)} \equiv \tag{4.4.20}$$



and the product is given by

$$\begin{aligned} Q^{(c;\tau\pi)}_{(a;\rho\mu)(b;\sigma\nu)} &= \sum\nolimits_{\alpha} \sqrt{\frac{d_a d_b}{d_c}}\, \big[\tilde{F}^{\cdot}_{ba\,\cdot}\big]_{(c;\alpha\tau)(\cdot\,;\rho\sigma)} \big[\tilde{F}^{\cdot}_{ba\,\cdot}\big]^{*}_{(c;\alpha\pi)(\cdot\,;\mu\nu)} \\ &= \sum\nolimits_{\alpha} \sqrt{\frac{d_a d_b}{d_c}}\, \big(m^{c\tau;\alpha}_{b\sigma,a\rho}\big)^{*} \big(m^{c\pi;\alpha}_{b\nu,a\mu}\big)\ . \end{aligned} \tag{4.4.21}$$

The sum is over a basis of morphisms $\mathcal{L}_b \otimes \mathcal{L}_a \xrightarrow{\alpha} \mathcal{L}_c$. This defines a finite-dimensional semisimple algebra $\mathcal{A}$, whose symmetrizer can be constructed using the universal formula (4.2.11).

4.4.3 Weakly-symmetric boundary conditions

When strongly-symmetric boundary conditions do not exist, we are forced to consider modules with multiple simple objects. This means that we have to deal with a set of boundary conditions that form a "multiplet" under fusion with the bulk symmetry lines. It might happen, however, that the module contains one particular simple boundary $\hat{\mathcal{B}}$ (equal to $\mathcal{B}_m$ for a particular value $m = \hat{m}$) such that the fusion of any bulk line $\mathcal{L}_a$ with $\hat{\mathcal{B}}$ contains $\hat{\mathcal{B}}$ itself: $\mathcal{L}_a \otimes \hat{\mathcal{B}} \supseteq \hat{\mathcal{B}}$. This happens when

$$\tilde{N}^{\hat{m}}_{a\hat{m}} \geq 1 \qquad \text{for all } a\ . \tag{4.4.22}$$

This means that every bulk like $\mathcal{L}_a$ has at least one topological junction with the boundary $\hat{\mathcal{B}}$. Such a boundary condition was called "weakly-symmetric" in [106]. It allows us to restrict to a subspace of the strip algebra in which we have all bulk lines but only the boundary $\hat{\mathcal{B}}$, and that is closed under strip-algebra product. When multiple junctions exist, $N^{\hat{m}}_{a\hat{m}} > 1$, in general one has to keep all of them in order to obtain a closed algebra.[22] We call the resulting algebra a *reduced strip algebra*.

Note that the reduced strip algebra always admits a symmetrizer. Indeed, its C^*-structure is simply the restriction of the C^*-structure of the full strip algebra. In particular, the C^* condition (4.A.23) is still satisfied and the reduced strip algebra is thus semisimple and strongly separable. The symmetrizer can be constructed using the universal formula (4.2.11).

It turns out [106] that a fusion category $\mathscr{C}$ admits a weakly-symmetric boundary condition if and only if there exists a (not necessarily maximal) haploid algebra object

$$\mathfrak{A} = \bigoplus\nolimits_{a} N_a^{(\mathfrak{A})}\, \mathcal{L}_a \qquad \text{such that } N_a^{(\mathfrak{A})} \geq 1 \text{ for all } a\,. \tag{4.4.23}$$

[22] In some cases it might be possible to restrict to a subspace of the junction space.

We introduced the nonnegative integer numbers $N_a^{(\mathfrak{A})} \equiv \dim\big(\mathrm{Hom}(\mathcal{L}_a, \mathfrak{A})\big)$, that for haploid algebra objects always satisfy $N_a^{(\mathfrak{A})} \leq d_a$ [155]. The connection between boundaries and algebra objects goes through the internal Hom construction (see footnote 21). Haploid algebra objects are the noninvertible generalization of anomaly-free subgroups of an invertible symmetry group with a choice of discrete torsion. Thus, a weakly-symmetric boundary condition exists if and only if there exists a gauging of $\mathscr{C}$ that involves all simple lines in $\mathscr{C}$. When the gauging is maximal, $N_a^{(\mathfrak{A})} = d_a$, which is possible only in the absence of 't Hooft anomalies, the boundary condition is actually strongly symmetric.

4.4.4 Non-symmetric boundary conditions

It might happen that a given theory does not admit neither strongly- nor weakly-symmetric boundary conditions, either because the symmetry has a severe enough 't Hooft anomaly to prevent them, or because we insist on some extra property, for instance conformality, of the boundary conditions. In such cases, the boundary condition at the entangling surface necessarily breaks the symmetry, implying a nonzero asymmetry on subsystems even when the original state is invariant. To overcome this, and to detect symmetry breaking of states independently of the boundary conditions at the entangling surface, we consider a map $\Psi_{\mathcal{B}}$ (see (4.4.2)) that produces a statistical mixture of density matrices with different boundary conditions. We show that there exists a choice of coefficients such that the invariant state prepared by the empty path-integral exhibits indeed vanishing asymmetry. The procedure can be carried out for any choice of module category $\mathscr{M}$, as we show here. However, in the examples in Sec. 4.6 we specialize to the regular module category.

At a formal level, we could define a symmetric "composite" boundary condition $|\mathcal{B}_{\mathsf{S}}\rangle$ if we allow for arbitrary linear combinations of boundaries (which we denote here as kets because we regard them as element of a vector space):

$$|\mathcal{B}_{\mathsf{S}}\rangle = \sum\nolimits_m \tilde{d}_m \, |\mathcal{B}_m\rangle \qquad \text{so that} \qquad \mathcal{L}_a \, |\mathcal{B}_{\mathsf{S}}\rangle = d_a \, |\mathcal{B}_{\mathsf{S}}\rangle \ . \tag{4.4.24}$$

Here d_a and $\tilde{d}_m$ are the bulk and boundary quantum dimensions, and we used (4.4.7) to prove the second equality.[23]

We exploit this idea — in the case of unitary and normalizable CFTs and insisting on conformal boundary conditions — to construct a symmetric density matrix ρ on the interval Hilbert space starting from an invariant state, even in the absence of invariant simple boundary conditions. Consider a module category $\mathscr{M}$, and let ρ_{mn} be the reduced density matrix of the vacuum (or of another

[23] One also uses the pivotal relation: $\mathcal{L}_a \, |\mathcal{B}_{\mathsf{S}}\rangle = \sum_{mn} \tilde{d}_m \tilde{N}_{am}^n \, |\mathcal{B}_n\rangle = \sum_{mn} \tilde{N}_{\bar{a}n}^m \tilde{d}_m \, |\mathcal{B}_n\rangle$, as well as $d_a = d_{\bar{a}}$.

state invariant under the symmetry) constructed with simple boundary conditions $\mathcal{B}_m, \mathcal{B}_n \in \mathscr{M}$. We construct an "average" over boundary conditions as follows:

$$\rho = \frac{1}{D} \sum_{m,n \in \mathrm{Irr}(\mathscr{M})} \tilde{d}_m \, \tilde{d}_n \, \rho_{mn} = \frac{1}{D} \sum_{m,n \in \mathrm{Irr}(\mathscr{M})} \frac{\tilde{d}_m \, \tilde{d}_n}{Z_{mn}} \, \tilde{\rho}_{mn} \ , \quad D = \Big(\textstyle\sum_{m \in \mathrm{Irr}(\mathscr{M})} \tilde{d}_m \Big)^2 . \tag{4.4.25}$$

Here $\tilde{\rho}_{mn}$ is the unnormalized density matrix produced by the path-integral realization of $\Psi_{\mathcal{B}}$ in (4.4.2) with boundary conditions $\mathcal{B}_m$ and $\mathcal{B}_n$, as depicted in Fig. 4.13, while $Z_{mn} = \mathrm{Tr}(\tilde{\rho}_{mn})$. We show that in the limit $\varepsilon \to 0$, ρ commutes with the strip algebra and thus it has vanishing asymmetry. The interval Hilbert space $\mathcal{H}$ decomposes in the various sectors with simple boundary conditions as $\mathcal{H} = \bigoplus_{m,n} \mathcal{H}_{m,n}$. We want to show that, for every $O \in \mathrm{End}(\mathcal{H})$:

$$\lim_{\varepsilon \to 0} \mathrm{Tr}\big(\rho \, H^{r,s}_{m,n} \, O \big) = \lim_{\varepsilon \to 0} \mathrm{Tr}\big(H^{r,s}_{m,n} \, \rho \, O \big) \ . \tag{4.4.26}$$

Here $H^{r,s}_{m,n}$ is a basis element of the strip algebra in $\mathrm{Hom}(\mathcal{H}_{m,n}, \mathcal{H}_{r,s})$. By matching boundary conditions and using (4.4.25), the previous equation is equivalent to

$$\lim_{\varepsilon \to 0} \frac{\tilde{d}_r \, \tilde{d}_s}{Z_{rs}} \, \mathrm{Tr}\big(\tilde{\rho}_{rs} \, H^{r,s}_{m,n} \, O^{m,n}_{r,s} \big) = \lim_{\varepsilon \to 0} \frac{\tilde{d}_m \, \tilde{d}_n}{Z_{mn}} \, \mathrm{Tr}\big(H^{r,s}_{m,n} \, \tilde{\rho}_{mn} \, O^{m,n}_{r,s} \big) \ , \tag{4.4.27}$$

where $O^{m,n}_{r,s}$ is the component of O in $\mathrm{Hom}(\mathcal{H}_{r,s}, \mathcal{H}_{m,n})$. Notice that $\tilde{\rho}_{rs} \, H^{r,s}_{m,n} = H^{r,s}_{m,n} \, \tilde{\rho}_{mn}$ since, by assumption, lines can be slid past the matrices $\tilde{\rho}_{mn}$ (even for finite ε). Thus, because the operators $O^{m,n}_{r,s}$ are completely arbitrary, we only need to check that

$$\lim_{\varepsilon \to 0} \frac{\tilde{d}_r \, \tilde{d}_s}{Z_{rs}} = \lim_{\varepsilon \to 0} \frac{\tilde{d}_m \, \tilde{d}_n}{Z_{mn}} \ . \tag{4.4.28}$$

This equation is indeed satisfied because

$$\lim_{\varepsilon \to 0} Z_{rs} = \tilde{d}_r \, \tilde{d}_s \, Z(\mathbb{C}) \ , \tag{4.4.29}$$

where $Z(\mathbb{C})$ is the Euclidean partition function on the plane. This can be argued as follows. Recall that Z_{rs} is the partition function on the plane with two discs of radius ε removed (see Fig. 4.13). The discs are centered, say, at $z = 0$ and $z = \ell$. Following [13], this geometry can be mapped to a cylinder of length $2\log(\ell/\varepsilon)$ with the transformation $w = \log\big(z/(\ell - z)\big)$. The partition function can then be rewritten as a closed-channel amplitude:

$$Z_{rs} = W \, \big\langle s \big| \, (\varepsilon/\ell)^{L_0 + \bar{L}_0 - c/12)} \, \big| r \big\rangle \ , \tag{4.4.30}$$

where W is a Weyl factor, while $|r\rangle, |s\rangle$ are Cardy states. Inserting a resolution of the identity with eigenstates of the cylinder Hamiltonian, in the limit $\varepsilon \to 0$ (which

corresponds to a cylinder of infinite length) only the ground state $|0\rangle$ remains.[24] Thus one gets

$$\lim_{\varepsilon\to 0} Z_{rs} = \lim_{\varepsilon\to 0} g_r\, g_s\, W \left\langle 0\right| (\varepsilon/\ell)^{L_0+\bar{L}_0-c/12} \left|0\right\rangle , \tag{4.4.31}$$

where $g_r \equiv \langle r|0\rangle$ is the g-factor [126]. Because of the state/operator correspondence, the term $\lim_{\varepsilon\to 0}\langle 0| (\varepsilon/\ell)^{L_0+\bar{L}_0-c/12} |0\rangle$ becomes the partition function of an infinite cylinder, with no insertions at infinity. We can then undo the Weyl transformation, reabsorbing the factor W, to obtain $\lim_{\varepsilon\to 0} Z_{rs} = g_r\, g_s\, Z(\mathbb{C})$. The g-factors can be interpreted as disc partition functions [156] for a specific choice of Euler counterterm, and thus they satisfy the equation of boundary quantum dimensions (4.4.7) (see also [157]). Hence we can choose a normalization such that $\tilde{d}_r = g_r$, and obtain (4.4.29).[25]

Large subsystem limits. Given the asymmetry of some state, computed on the interval subsystem using one of the types of boundary conditions discussed above, what is the relation between its large subsystem limit and the asymmetry of the full system, computed using the fusion or tube algebras?

In Sec. 4.6.1 we analyze invertible group-like symmetries. In particular we consider excited CFT states created by the insertion of local operators in Euclidean time. We find that the entanglement and Rényi asymmetries on an interval, as long as our "averaging" protocol is used, are independent of the choice of boundary conditions. Moreover, for untwisted states, the large subsystem limits of the asymmetries coincide with the asymmetries of the full system, computed with respect to either the fusion or the tube algebra (since they coincide for untwisted states).

In Sec. 4.6.3 we study certain excited states in two copies of the Ising CFT, utilizing the $\mathsf{Rep}(H_8)$ (*a.k.a.* $\mathbb{Z}_2\times\mathbb{Z}_2$ Tambara–Yamagami) noninvertible symmetry that admits a strongly-symmetric boundary condition. The result is similar: the second Rényi entropy on the interval subsystem asymptotes in the large subsystem limit to the second Rényi entropy of the full system, computed with respect to the tube algebra (not the fusion algebra, which in general is different).

On the other hand, in Secs. 4.6.2 and 4.6.4 we study certain excited states in the Ising CFT, utilizing its Ising fusion category (*a.k.a.* $\mathbb{Z}_2$ Tambara–Yamagami) symmetry, which does not admit symmetric boundary conditions and which then forces us to resort to the averaging protocol. This time we find that the large subsystem limit of the second Rényi asymmetry on an interval is qualitatively

[24] For unitary CFTs with discrete spectrum, $|0\rangle$ is the ground state. More generally, $|0\rangle$ is the lowest-dimension state that overlaps with the Cardy states $|r\rangle, |s\rangle$. See the discussion in [13].

[25] With a generic normalization (*i.e.*, choice of Euler counterterm), the g-factors g_m are proportional to the boundary quantum dimensions $\tilde{d}_m$ and thus they satisfy (4.4.7). This implies that $\lim_{\varepsilon\to 0} \tilde{d}_m\tilde{d}_n/Z_{mn}$ is independent from m, n. This is enough to prove (4.4.28), even with generic normalization.

similar to, but slightly smaller than, the asymmetry of the full system with respect to the tube algebra. A similar behavior is found in Sec. 4.6.5 when studying the Fibonacci fusion category symmetry with its weakly-symmetric boundary condition. It would be interesting to understand these results more systematically.

4.4.5 Symmetrizer from (weak) Hopf algebra structure

We can find an alternative, but equivalent, formula for the symmetrizer by leveraging the following reasoning that holds in the invertible case for a symmetry group G (or equivalently, for the group algebra $\mathbb{C}[G]$). Consider a Hilbert space $\mathcal{H}$ that carries a representation of G. A density matrix $\rho \in \mathrm{End}(\mathcal{H})$ is an element of $\mathcal{H} \otimes \mathcal{H}^\vee$ (the second factor being the dual space). This tensor product itself carries a representation of G, which decomposes into a sum of irreducible representations. Then, the symmetrization operation is reproduced by applying to this space the projector onto the trivial representation. The obstacle in generalizing this reasoning to the noninvertible case is that for a generic algebra $\mathcal{A}$ the concepts of tensor product of representations, of dual (or conjugate) representation, and of trivial representation, are not defined. In the special case that the algebra is *Hopf*, however, these concepts are available and the symmetrizer can be written as the projector onto the trivial representation. Moreover, we will see that if the algebra is only *weak Hopf*, a formula similar to that of the Hopf case applies, even though it lacks that interpretation. It was shown in [137, 138] that the strip algebras are always weak Hopf, therefore we can apply the strategy above to the case of the interval Hilbert space.[26]

Let us first consider the case that a strip algebra $\mathcal{A}$ is constructed using a strongly-symmetric boundary condition. We can show that such a strip algebra is a Hopf algebra. We provide definitions and basic properties in Appendix 4.B and prove the claim in Appendix 4.B.1.

Concisely, a Hopf algebra comes equipped with (besides its unit and its associative product) the following algebra homomorphisms: a coassociative coproduct $\Delta\colon \mathcal{A} \to \mathcal{A} \otimes \mathcal{A}$ such that $\Delta(\mathbb{1}) = \mathbb{1} \otimes \mathbb{1}$ and a counit $\epsilon\colon \mathcal{A} \to \mathbb{C}$. In addition, it comes with an antipode $S\colon \mathcal{A} \to \mathcal{A}$, which is a linear algebra anti-homomorphism, *i.e.*, $S(xy) = S(y)\,S(x)$. In finite-dimensional semisimple Hopf algebras one proves that $S \circ S = \mathrm{id}$. The one-dimensional "trivial" representation $r_\epsilon\colon \mathcal{A} \to \mathrm{End}(\mathbb{C}) \cong \mathbb{C}$, which behaves as the identity under the tensor product of representations, is provided by the counit:

$$r_\epsilon(x) = \epsilon(x) \qquad \forall\, x \in \mathcal{A}\,. \tag{4.4.32}$$

The tensor product of representations is constructed using the coproduct Δ. Given two representations $r_1\colon \mathcal{A} \to \mathrm{End}(V_1)$ and $r_2\colon \mathcal{A} \to \mathrm{End}(V_2)$ on vector spaces $V_{1,2}$,

[26] On the contrary, the tube algebra is in general not a weak Hopf algebra. One can still define a tensor product of representations using the so-called Day convolution product [158]. We do not explore such a possibility here.

their tensor product representation $r_{12}\colon \mathcal{A} \to \mathrm{End}(V_1 \otimes V_2)$ is defined as

$$r_{12} = (r_1 \otimes r_2) \circ \Delta \quad i.e. \quad r_{12}(x)\; v_1 \otimes v_2 = \sum\nolimits_i \Big[r_1\big(x^i_{(1)}\big)\, v_1 \Big] \otimes \Big[r_2\big(x^i_{(2)}\big)\, v_2 \Big]\,, \tag{4.4.33}$$

where $v_{1,2} \in V_{1,2}$ and we used Sweedler's notation to write $\Delta(x) = \sum_i x^i_{(1)} \otimes x^i_{(2)}$. Using (4.B.2), one sees that the representation r_ϵ multiplies trivially with any other representation. Finally, given a representation $r\colon \mathcal{A} \to \mathrm{End}(V)$, its conjugate representation $r^*\colon \mathcal{A} \to \mathrm{End}(V^\vee)$ is constructed using the antipode:

$$\big\langle r^*(x)\, f,\, v \big\rangle \equiv \big\langle f,\, r\big(S(x)\big)\, v \big\rangle \qquad\qquad \forall\, x \in \mathcal{A},\;\; v \in V,\;\; f \in V^\vee, \tag{4.4.34}$$

where the angular brackets denote the evaluation of a functional on a vector. More compactly, this can be written as $r^* = (r \circ S)^{\mathsf{T}}$. Using (4.B.6) one sees that the trivial representation is self-conjugate.

Associated to r_ϵ there is a minimal central idempotent (MCI) $P_\epsilon \in \mathcal{A}$, *i.e.*, the projector to the trivial representation. It satisfies[27]

$$P_\epsilon\, x = x\, P_\epsilon = \epsilon(x)\, P_\epsilon \qquad\qquad \forall\, x \in \mathcal{A}\,. \tag{4.4.35}$$

Taking x equal to one of the MCIs P_i (*i.e.*, a projector to an irreducible representation of $\mathcal{A}$), one obtains $\epsilon(P_i) = \delta_{i\epsilon}$, confirming that P_ϵ projects to the trivial representation.

We claim that the symmetrizer can be written as

$$\mathsf{S} = (\mathrm{id} \otimes S) \circ \Delta(P_\epsilon) \tag{4.4.36}$$

which was proven to be a separability idempotent for a Hopf algebra in [159]. When acting on the space $\mathcal{H} \otimes \mathcal{H}^\vee \cong \mathrm{End}(\mathcal{H})$, this operator is precisely the action of the projector to the trivial representation P_ϵ on density matrices. More explicitly:

$$\rho_{\mathsf{S}} = \sum\nolimits_i (P_\epsilon)^i_{(1)}\; \rho\; S\big((P_\epsilon)^i_{(2)}\big) \tag{4.4.37}$$

where $\Delta(P_\epsilon) = \sum_i (P_\epsilon)^i_{(1)} \otimes (P_\epsilon)^i_{(2)}$. The disadvantage of this formula is that one needs to explicitly construct the projector P_ϵ to the trivial representation. In Appendix 4.B.2 we prove that (4.4.37) satisfies properties 1. – 4. listed in Sec. 4.2. The expression in (4.4.37) is also universal, in the sense that it is written solely in terms of the elements of $\mathcal{A}$. As we commented at the end of Sec. 4.2, this completely fixes the symmetrizer and thus (4.4.37) agrees with (4.2.11). Notice that the universal formula (4.2.11) only depends on the product structure on $\mathcal{A}$,

[27] The first equality is the centrality of projectors. For the second equality, since $P_\epsilon^2 = P_\epsilon$ and the trivial representation is one-dimensional, then P_ϵ is a basis for the image of the projector in the regular representation (recall that a 1d representation occurs only once inside the regular representation), and thus $P_\epsilon\, x = \alpha(x)\, P_\epsilon$ for some $\alpha \in \mathbb{C}$. Applying ϵ to both sides we find $\alpha(x) = \epsilon(x)$.

therefore different Hopf algebras that share the same product structure will give rise, through (4.4.37), to the same symmetrizer.

For weak Hopf algebras (and in particular for generic strip algebras) a similar recipe exists to compute the separability idempotent. Referring to [160], one introduces the left and right projectors $\Pi^{\mathrm{L}}, \Pi^{\mathrm{R}} \colon \mathcal{A} \to \mathcal{A}$ as

$$\Pi^{\mathrm{L}}(x) = \sum\nolimits_i \epsilon\big(\mathbb{1}^i_{(1)}\, x\big)\, \mathbb{1}^i_{(2)} \ , \qquad \Pi^{\mathrm{R}}(x) = \sum\nolimits_i \mathbb{1}^i_{(1)}\, \epsilon\big(x\, \mathbb{1}^i_{(2)}\big) \ , \tag{4.4.38}$$

acting on $x \in \mathcal{A}$. Then one defines the left and right normalized integrals as those elements $\ell, r \in \mathcal{A}$ such that

$$x\,\ell = \Pi^{\mathrm{L}}(x)\,\ell \ , \qquad \Pi^{\mathrm{L}}(\ell) = \mathbb{1} \ , \qquad \text{or} \qquad r\,x = r\,\Pi^{\mathrm{R}}(x) \ , \qquad \Pi^{\mathrm{R}}(r) = \mathbb{1} \ , \tag{4.4.39}$$

for all $x \in \mathcal{A}$. In general, being a left integral does not imply being a right integral. When this happens, one talks about *Haar integrals*. That is, a Haar integral h is defined as a simultaneous left and right normalized integral. When it exists, it is unique. The necessary and sufficient conditions for its existence are spelled out in Th. 3.27 of [160]. Strip algebras satisfy those conditions, thanks to the fact that $S^2 = \mathrm{id}$ [138].[28] The symmetrizer is then given by

$$\mathsf{S} = (\mathrm{id} \otimes S) \circ \Delta(h) \ , \tag{4.4.40}$$

where $h \in \mathcal{A}$ is the Haar integral. In Appendix 4.B.2 we verify that such an expression satisfies the properties 1. – 4. and thus, being also universal, it agrees with (4.2.11).

Note that in the case of a Hopf algebra, both the left and right projectors reduce to

$$\Pi^{\mathrm{L}}(x) = \Pi^{\mathrm{R}}(x) = \epsilon(x)\, \mathbb{1} \tag{4.4.41}$$

because $\Delta(\mathbb{1}) = \mathbb{1} \otimes \mathbb{1}$. Then the Haar integral h is equal to the projector P_ϵ.

4.5 Spontaneous symmetry breaking

A natural application of entanglement asymmetry is to detect spontaneous symmetry breaking in gapped phases. In the far IR, a gapped phase is described by a topological field theory on which the symmetry acts. Therefore, for a given fusion category $\mathscr{C}$, the possible indecomposable and inequivalent (from the symmetry point of view) two-dimensional gapped phases are in one-to-one correspondence with indecomposable two-dimensional $\mathscr{C}$-symmetric TQFTs, which in turn are in

[28] In the notation of Th. 3.27 in [160], $g = \mathbb{1}$. Then, the second condition therein is satisfied because the trace of $\mathbb{1}$ in any representation is the dimension of that representation. Alternatively, the existence of the Haar integral is guaranteed by the existence of a C^*-structure, by Th. 4.5 of [160]. In the case of strip algebras, such a structure indeed exists [137, 138].

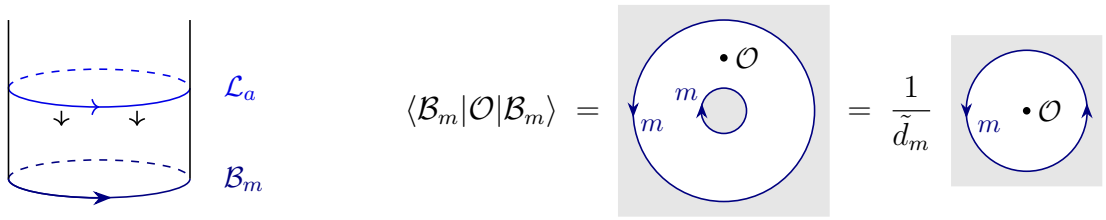
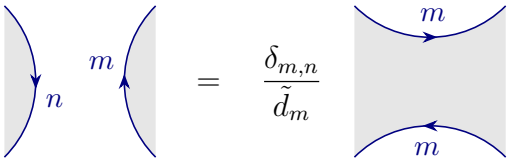


Figure 4.5: Left: the clustering states, or vacua, $|\mathcal{B}_m\rangle$ on the circle are created by the simple boundaries. Right: Correlation functions in those states are computed by disc partition functions.

one-to-one correspondence with indecomposable module categories for $\mathscr{C}$ [56]. We can then use entanglement asymmetry to try to distinguish the various phases.

Consider a 2d gapped phase described by a certain 2d $\mathscr{C}$-symmetric TQFT in the IR, and let $\mathscr{M}$ be the corresponding left-module category. On the circle S^1 the TQFT has a finite number of states. If the symmetry is unbroken, the circle Hilbert space is one-dimensional and the entanglement asymmetry with respect to the fusion algebra vanishes.[29] On the other hand, when a finite symmetry is spontaneously broken we expect a higher-dimensional circle Hilbert space on which the symmetry acts. We are not interested in computing the asymmetry of generic vectors in that Hilbert space, but only of very special vectors that we call "vacua": these are the states that satisfy the cluster decomposition property. Such states form a preferred basis of the Hilbert space. It turns out that they are in correspondence with the simple boundaries $\mathcal{B}_m$ of the corresponding module category $\mathscr{M}$, and can be constructed using open/closed duality [154]: one simply considers the cylinder with the boundary condition $\mathcal{B}_m$ in the past, as in Fig. 4.5 left.

To prove that the states created by simple boundaries satisfy cluster decomposition one uses a boundary crossing relation proven in [154]:



. (4.5.1)

A correlator $\langle \mathcal{B}_m | \mathcal{O} | \mathcal{B}_m \rangle$ is the annulus partition function with boundaries $\mathcal{B}_m$ and with the insertion of a local operator $\mathcal{O}$, as in Fig. 4.5 right. Using the crossing relation, such a correlator is equal to $1/\tilde{d}_m$ times the disc one-point function of $\mathcal{O}$ with boundary $\mathcal{B}_m$, that we call $Z_{D_2}[\mathcal{O}]$. If $\mathcal{O}$ is the identity operator, the latter is equal to $\tilde{d}_m$ and thus the correlator is normalized. The crossing relation can then

[29] Here we only consider indecomposable gapped phases.

be used to break a disc into two discs, hence one obtains:

$$\langle \mathcal{B}_m|\mathcal{O}_1\mathcal{O}_2|\mathcal{B}_m\rangle = \frac{1}{\tilde{d}_m} Z_{D_2}[\mathcal{O}_1\mathcal{O}_2] = \frac{1}{\tilde{d}_m^2} Z_{D_2}[\mathcal{O}_1]\, Z_{D_2}[\mathcal{O}_2] = \langle \mathcal{B}_m|\mathcal{O}_1|\mathcal{B}_m\rangle \langle \mathcal{B}_m|\mathcal{O}_2|\mathcal{B}_m\rangle \ . \tag{4.5.2}$$

This shows that in the states $|\mathcal{B}_m\rangle$ all correlation functions are equal to products of one-point functions, which is cluster decomposition for topological theories.

The fusion category $\mathscr{C}$ acts on the untwisted circle Hilbert space according to its fusion algebra, as described in Sec. 4.3.1. As is clear from Fig. 4.5 left, the action of the lines on the states is dictated by the fusion coefficients $\tilde{N}_{am}^n$ (4.4.3) of the corresponding module category $\mathscr{M}$:

$$\mathcal{L}_a\,|\mathcal{B}_m\rangle = \sum\nolimits_n \tilde{N}_{am}^n\,|\mathcal{B}_n\rangle \ . \tag{4.5.3}$$

Thus the clustering states of a gapped phase furnish a NIM-rep of the fusion algebra. This allows one to easily compute the entanglement asymmetry of the various vacua.

In Sec. 4.6 we analyze various examples of spontaneous symmetry breaking and compute the asymmetry of the different vacua. In Sec. 4.6.1 we consider an invertible finite symmetry group G spontaneously broken to a subgroup H, and reproduce the result of [36] that the entanglement and Rényi asymmetries are equal to $\Delta S = \log(N_{\text{vac}})$, where $N_{\text{vac}} = |G|/|H|$ is the number of vacua.[30] In the rest of Sec. 4.6 we study broken noninvertible symmetries. One of the outcomes is that the asymmetries can take more general values, and are not directly related to the number of vacua. Another outcome is that, as opposed to the invertible case, different vacua can exhibit inequivalent physical properties (as already anticipated in [135, 136]), and in particular can have different asymmetries. For instance, in a theory that spontaneously breaks the Ising symmetry, one vacuum has $\Delta S = \log 2$ while two other vacua (which are related by the invertible part of the symmetry) have $\Delta S = \frac{3}{2}\log 2$ (see Sec. 4.6.2).

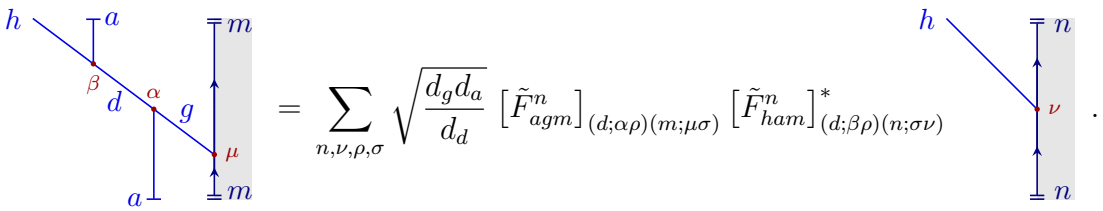
4.5.1 Detecting SPT phases

In the case of an invertible anomaly-free finite symmetry G, two-dimensional gapped phases are classified by the conjugacy class of an unbroken subgroup $H \subseteq G$ as well as an SPT phase for H (see Appendix 4.E for the precise classification and construction). In particular, even when the full group G is unbroken, one could have inequivalent trivially-gapped phases with a single vacuum but distinguished by the SPT phase. Since they have a single vacuum, ordinary order parameters cannot detect the different SPT phases, and the asymmetries necessarily vanish. Interestingly, it was noted in [161] that in some examples twisted order parameters can distinguish different SPT phases. Can, likewise, one of the symmetry algebras

[30] The result of [36] used matrix product states. Our derivation, that uses the low-energy TQFT description, is valid in two or more spacetime dimensions.

$\mathcal{A}$ introduced so far be used to distinguish those phases? This question clearly generalizes to anomalous as well as noninvertible symmetries.

Below we show in one example that, indeed, the action of the tube algebra can often distinguish different gapped phases. For that, we need the tube algebra action on TQFT states, including the twisted states. By open/closed duality, this is computed from the data of the corresponding module category $\mathscr{M}$. Using the various moves already discussed in the case of fusion categories, in particular those in (4.3.14) and in Figs. 4.17 and 4.18, adapted to module categories, we find the following relation:



(4.5.4)

The sum is over a basis of morphisms $\mathcal{L}_h \otimes \mathcal{B}_n \xrightarrow{\nu} \mathcal{B}_n$, $\mathcal{L}_d \otimes \mathcal{B}_m \xrightarrow{\rho} \mathcal{B}_n$, $\mathcal{L}_a \otimes \mathcal{B}_m \xrightarrow{\sigma} \mathcal{B}_n$, while the ticks indicate the "trace" of [148], *i.e.*, that the lines are attached. The configuration on the r.h.s., if rotated clockwise by 90 degrees, represents a twisted state $\left|\mathcal{B}^{(h)}_{n,\nu}\right\rangle \in \mathcal{H}_h$, where $\mathcal{H}_h$ is an h-twisted sector of dimension

$$\dim(\mathcal{H}_h) = \sum\nolimits_n \tilde{N}^n_{hn} \,. \tag{4.5.5}$$

The configuration on the l.h.s. of (4.5.4), on the other hand, represents the action of the tube algebra basis element (4.3.15) on a twisted state $\left|\mathcal{B}^{(g)}_{m,\mu}\right\rangle$. In the special case that $g = h = 1$ and $d = a$, (4.5.4) reproduces the fusion algebra action on the untwisted circle Hilbert space $\mathcal{H}_1$.

Example: SPT phases. In order to exhibit how the tube algebra action distinguishes different phases, consider the example, proposed in [161], of an invertible symmetry group $G = \mathbb{Z}_2 \times \mathbb{Z}_2$ with no anomaly, $\omega = 1$. The indecomposable gapped phases are labeled by conjugation classes of subgroups $H \subseteq G$ and cocycles $\psi \in H^2\big(H, U(1)\big)$. In this case the possibilities are: for $H = \{1\}$ the completely broken phase; for the three inequivalent subgroups $H = \mathbb{Z}_2$ a broken phase with unbroken $\mathbb{Z}_2$; for $H = G$ two unbroken phases distinguished by the cocycle $\psi \in H^2\big(\mathbb{Z}_2 \times \mathbb{Z}_2, U(1)\big) = \mathbb{Z}_2$.

Let us focus on the two unbroken phases, which are SPT phases. The corresponding module categories have a single simple object that we indicate with a dot, the modules are multiplicity-free since $N^{\cdot}_{g\cdot} = 1$ for all $g \in G$, and the $\tilde{F}$-symbols are

$$\left[\tilde{F}^{\cdot}_{ab\cdot}\right] = \psi(a,b) \tag{4.5.6}$$

where $a, b \in G$ and the missing indices are fixed. The trivial cocycle, corresponding to the trivial SPT phase, is $\psi = 1$. The non-trivial cocycle, instead, corresponding

to the nontrivial SPT phase, has a representative

$$\psi\big((a_1,a_2)\,,\,(b_1,b_2)\big) = (-1)^{a_1 b_2} \tag{4.5.7}$$

where $a_i, b_j \in \{0,1\}$. Both phases have four (un)twisted sectors, each with a single state. Since the symmetry is invertible and Abelian, the tube algebra basis elements (4.3.15) have $g = h$: we label them by $g, a \in G$. They do not change the sector of the state, but, in the nontrivial SPT phase, they act according to the following table:

$g\backslash a$	$(0,0)$	$(1,0)$	$(0,1)$	$(1,1)$
$(0,0)$	1	1	1	1
$(1,0)$	1	1	-1	-1
$(0,1)$	1	-1	1	-1
$(1,1)$	1	-1	-1	1

(4.5.8)

This reproduces the results in Sec. 4.5.4 of [161]. In the untwisted sector $g = (0,0)$, all elements a of G act trivially. On the other hand, in each nontrivial twisted sector $\mathcal{H}_g$, the element with $a = g$ acts trivially but the other two flip the sign of the state.

Extrapolating to the general case, one can often distinguish different SPT phases by the tube algebra representations under which their untwisted and twisted states transform. Unfortunately it may happen that two inequivalent SPT phases realize exactly the same tube algebra representations.[31]

4.6 Examples

In this section we collect a number of examples in two-dimensional theories with details about the computation of entanglement and Rényi asymmetries, in order to exhibit general features.

4.6.1 Group-like symmetries

Consider an invertible symmetry given by a finite group G. The corresponding fusion category is $\mathsf{Vec}^{\omega}_{G}$, whose simple lines $\mathcal{L}_g$ are in correspondence with the elements $g \in G$ and they all have dimension $d_g = 1$. The fusion coefficients are $N_{gh}^{k} = \delta^{k}_{(gh)}$ where (gh) denotes the group multiplication of g with h. In particular, there are no multiplicities at the junctions. The symmetrizer with respect to the fusion algebra is

$$\rho_{\mathsf{S}} = \frac{1}{|G|} \sum\nolimits_{g\in G} \mathcal{L}_g\, \rho\, \mathcal{L}_{g^{-1}} \ . \tag{4.6.1}$$

[31] This happens if the Lagrangian algebras in the Drinfeld center of $\mathscr{C}$ that determine the gapped phases have exactly the same decomposition in simple lines, and only differ by the product morphism.

A possible 't Hooft anomaly is described by a class $\omega \in H^3\big(G, U(1)\big)$, which fixes the nonvanishing F-symbols to be

$$\big[F^{ghk}_{g,h,k}\big]_{gh,hk} = \omega(g,h,k)\ . \tag{4.6.2}$$

We use normalized representatives ω, meaning that $\omega(g,h,k) = 1$ whenever one or more of g, h, k are equal to the identity $1 \in G$. Different representatives of the same class produce the F-symbols in different gauges.

Spontaneous symmetry breaking. The possible indecomposable G-symmetric TQFTs, in correspondence with the possible indecomposable $\mathscr{C}$-module categories, are characterized by the conjugation class of a subgroup $H \subseteq G$ (besides a cochain ψ, which however will not play a role here), as reviewed in Appendix 4.E. They describe the SSB pattern $G \to H$ at very low energies. The clustering vacua $|m\rangle$, in correspondence with the simple boundaries $\mathcal{B}_m$, are labeled by the cosets $m \in G/H$. The vacua furnish a simple NIM-rep of the fusion algebra:

$$\mathcal{L}_g\,|m\rangle = |gm\rangle\ . \tag{4.6.3}$$

Here gm is the coset with representative ga, if $a \in G$ is a representative of m.

Consider the pure state $\rho = |m\rangle\langle m|$ of a vacuum on the circle. Using (4.6.1), the corresponding symmetrized density matrix with respect to the fusion algebra is

$$\rho_{\mathsf{S}} = \frac{1}{|G|}\sum\nolimits_{g\in G} \mathcal{L}_g\,\rho\,\mathcal{L}_{g^{-1}} = \frac{1}{|G|}\sum\nolimits_{g\in G} |gm\rangle\langle gm| = \frac{1}{|G/H|}\sum\nolimits_{p\in G/H} |p\rangle\langle p|\ . \tag{4.6.4}$$

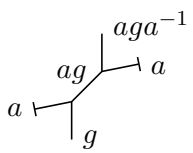
In the second equality we used that $\mathcal{L}_{g^{-1}} = \mathcal{L}_g^\dagger$. Because of the crossing relation (4.5.1), the vacua are orthonormal and thus $\mathrm{Tr}(\rho_{\mathsf{S}}^n) = \big|G/H\big|^{1-n}$. The asymmetries easily follow:

$$\Delta S[\rho] = \Delta S^{(n)}[\rho] = \log\big|G/H\big|\ . \tag{4.6.5}$$

This computation reproduces the result of [36], obtained using matrix product states. Notice that the derivation here applies verbatim to spacetime dimensions higher than two as well.

Tube algebra

The tube algebra of Vec^ω_G (which is given by the twisted quantum double of G) is generated by the basis elements:

$\tau_{g,a} \equiv$ 

. (4.6.6)

The product is given by:

$$\tau_{h,b} \times \tau_{g,a} = \delta_{h,aga^{-1}} \frac{\omega(b, aga^{-1}, a)}{\omega(baga^{-1}b^{-1}, b, a)\,\omega(b, a, g)} \tau_{g,ba} \,. \tag{4.6.7}$$

From here the structure constants $T^{k,c}_{h,b;\,g,a}$ are immediately read off. The phase factor appearing in the product can be interpreted as a twisted 2-cocycle. Indeed, define

$$\beta_g(x, y) = \frac{\omega(g, x, y)\,\omega(x, y, y^{-1}x^{-1}gxy)}{\omega(x, x^{-1}gx, y)} \,. \tag{4.6.8}$$

One verifies that this is a normalized twisted 2-cocycle, where x has an adjoint action on $g \in G$ (this also appeared in [162] Sec. 4.B).[32] We can write the tube algebra product as

$$\tau_{h,b} \times \tau_{g,a} = \frac{\delta_{h,aga^{-1}}}{\beta_{baga^{-1}b^{-1}}(b, a)} \tau_{g,ba} \,. \tag{4.6.9}$$

The identity element is $\mathcal{X}_{\mathbb{1}} = \sum_g \tau_{g,1}$. Associativity of the product coincides with the twisted cocycle condition for β. The non-degenerate bilinear form can be written as

$$K_{h,b;\,g,a} = \frac{|G|\;\delta_{h,aga^{-1}}\,\delta_{b,a^{-1}}}{\beta_g(a^{-1}, a)} \,. \tag{4.6.10}$$

From its inverse matrix $\tilde{K}^{g,a;\,h,b}$ one obtains the symmetrizer:

$$\rho_{\mathsf{S}} = \frac{1}{|G|} \sum\nolimits_{g,a} \beta_g(a^{-1}, a)\; \tau_{g,a}\, \rho\, \tau_{aga^{-1},a^{-1}} \,. \tag{4.6.11}$$

Using the twisted cocycle condition one proves the relation $\beta_{aga^{-1}}(a, a^{-1}) = \beta_g(a^{-1}, a)$ which is useful to check directly some properties of the symmetrizer.

Strip algebras

Let us now study the case of the interval Hilbert space using the strip algebras. The possible boundary conditions are given in terms of module categories, whose classification in the case of invertible finite symmetries is reviewed in Appendix 4.E.

In the non-anomalous case, one can always choose strongly-symmetric boundary conditions (but see footnote 18). From Appendix 4.E, those are classified by $\psi \in H^2\big(G, U(1)\big)$. Explicitly, one has

$$\tilde{N}^{\cdot}_{a\,\cdot} = 1 \,, \qquad \big[\tilde{F}^{\cdot}_{a,b,\cdot}\big]_{c,\cdot} = \big(m^c_{a,b}\big)^* = \delta^c_{ab}\;\psi(a, b) \,. \tag{4.6.12}$$

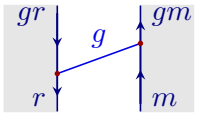
Note that there are no multiplicities at the boundary junctions. In terms of the basis elements H_g defined in (4.4.20), we see that the cocycle cancels out from the product (4.4.21) so that $H_g \times H_h = H_{gh}$. The strip algebra $\mathsf{Strip}_{\mathsf{Vec}_G}(\mathsf{Vec})$ is thus

[32] The twisted cocycle condition is $d\beta_g(x, y, z) = \beta_{x^{-1}gx}(y, z)\,\beta_g(x, yz)/\beta_g(xy, z)\beta_g(x, y) = 1$. See also App. A of [163] for a review on twisted cocycles.

isomorphic to the group algebra $\mathbb{C}[G]$ (which is also the fusion algebra) regardless of the class of ψ.[33] One finds the symmetrizer

$$\rho_{\mathsf{S}} = \frac{1}{|G|} \sum\nolimits_{g\in G} H_g \, \rho \, H_{g^{-1}} \ . \tag{4.6.13}$$

On the other hand, a boundary condition that can always be chosen regardless of the value of the anomaly cocycle $\omega \in H^3\big(G, U(1)\big)$ is the regular module (but see footnote 18). In this case we obtain the algebra $\mathsf{Strip}_{\mathsf{Vec}_G^\omega}(\mathsf{Vec}_G^\omega)$, generated by the basis elements:

$H^g_{r,m} \ \equiv$ 

(4.6.14)

with $g, m, r \in G$ and $\tilde{N}^n_{gm} = \delta^n_{(gm)}$. The product is given by:

$$H^b_{s,n} \ \times \ H^a_{r,m} = \delta_{s,ar} \, \delta_{n,am} \, \frac{\omega(b,a,r)}{\omega(b,a,m)} \, H^{ba}_{r,m} \ . \tag{4.6.15}$$

Also in this case the phase can be interpreted as a twisted cocycle (in which the action on r, m is in the regular representation) and associativity as its closure. In this case, however, there exists an isomorphism with $\mathsf{Strip}_{\mathsf{Vec}_G}(\mathsf{Vec}_G)$, namely, with the strip algebra of the symmetry without anomaly [138]. The isomorphism is given by[34]

$$\begin{aligned} \varphi \colon \mathsf{Strip}_{\mathsf{Vec}_G}(\mathsf{Vec}_G) &\to \mathsf{Strip}_{\mathsf{Vec}_G^\omega}(\mathsf{Vec}_G^\omega) \ , \\ \varphi\big(H^a_{r,m}\big) &= \omega(a, r, r^{-1}m) \, H^a_{r,m} \ , \end{aligned} \tag{4.6.16}$$

then extended by linearity. Indeed one verifies that

$$\varphi\big(H^b_{ar,am}\big) \times_\omega \varphi\big(H^a_{r,m}\big) = \varphi\big(H^b_{ar,am} \times_{\omega=1} H^a_{r,m}\big) \tag{4.6.17}$$

using that $d\omega(b, a, r, r^{-1}m) = 1$. Here we made explicit where we used the anomalous product (4.6.15) or the non-anomalous one. The non-degenerate bilinear form can be written as

$$K_{s,n,b;\,r,m,a} = |G| \, \frac{\omega(a^{-1}, a, r)}{\omega(a^{-1}, a, m)} \, \delta_{s,ar} \, \delta_{n,am} \, \delta_{b,a^{-1}} \ . \tag{4.6.18}$$

From its inverse one obtains the symmetrizer

$$\rho_{\mathsf{S}} = \frac{1}{|G|} \sum_{r,m,a} \frac{\omega(a^{-1}, a, m)}{\omega(a^{-1}, a, r)} \, H^a_{r,m} \, \rho \, H^{a^{-1}}_{ar,am} = \frac{1}{|G|} \sum_{r,m,a} \varphi(H^a_{r,m}) \, \rho \, \varphi(H^{a^{-1}}_{ar,am}) \ . \tag{4.6.19}$$

The rewriting in terms of φ makes it manifest that the symmetrizers for the two strip algebras are the same up to a phase redefinition of the basis elements.

[33] Alternatively, the cocycle can be reabsorbed with a change of basis of the junction vector spaces [138].

[34] The two algebras share the same underlying vector space, hence we denote a basis of both with the same notation $H^a_{r,m}$.

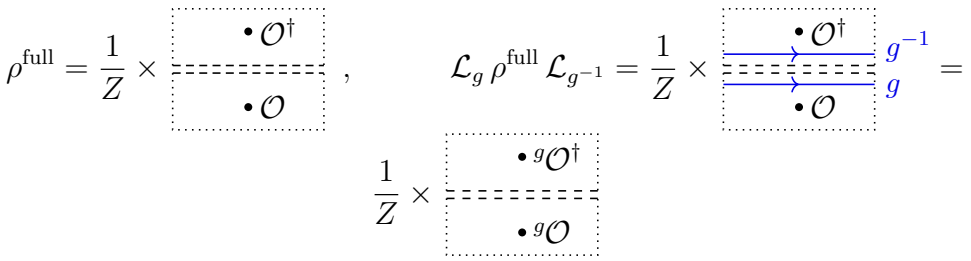


Figure 4.6: Left: path-integral representation of the state on the real line. The operator $\mathcal{O}$ is inserted at $z = x - i\tau$, while the operator $\mathcal{O}^\dagger$ is inserted at the specular image $\bar{z} = x + i\tau$. The normalization by the partition function Z ensures that $\mathrm{Tr}\big(\rho^{\text{full}}\big) = 1$. Right: path-integral representation of $\mathcal{L}_g\,\rho^{\text{full}}\,\mathcal{L}_{g^{-1}}$.

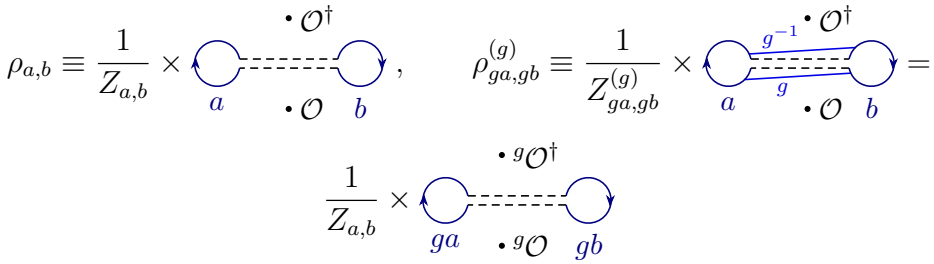


Figure 4.7: Left: path-integral construction of the reduced density matrix $\rho_{a,b}$. The dashed lines are the two open boundaries (cuts). The constant $Z_{a,b}$ is the partition function obtained by gluing the two cuts, so as to ensure that $\mathrm{Tr}(\rho_{a,b}) = 1$. Right: path-integral construction of the rotated density matrix $\rho^{(g)}_{ga,gb}$ where $Z^{(g)}_{ga,gb} \equiv Z_{a,b}\,\omega(g^{-1}, g, a)/\omega(g^{-1}, g, b)$.

Asymmetries in CFTs. Consider a CFT and a state on the real line $\mathbb{R}$ created by the Euclidean path-integral on a half space with the insertion of local operators. The corresponding density matrix ρ^{full} is prepared by a Euclidean path-integral in which the future half-space is the specular image of the past half-space, and there is a cut along the real line. This is depicted in Fig. 4.6 left. There, Z is the partition function on the plane obtained by closing the cut, so as to ensure that $\mathrm{Tr}\big(\rho^{\text{full}}\big) = 1$.

To construct the reduced density matrix for a single interval along the real line, we apply the procedure of Sec. 4.4. Consider first the case that we use boundary conditions a, b chosen from the regular module. We depict the path-integral construction of $\rho_{a,b}$ in Fig. 4.7 left, where $Z_{a,b}$ is the partition function obtained by closing the cut so as to ensure that $\mathrm{Tr}(\rho_{a,b}) = 1$. For simplicity, in the figures we indicate only one operator insertion $\mathcal{O}$ and its specular image $\mathcal{O}^\dagger$, but the argument applies to any number of insertions. To obtain the symmetrized density matrix we apply (4.6.19). Since the symmetry elements $H^g_{r,m}$ project to zero when their boundary conditions do not match those of the state, we remain

with a single sum:

$$\rho_{\mathsf{S}} = \frac{1}{|G|}\sum_g \frac{\omega(g^{-1},g,b)}{\omega(g^{-1},g,a)}\, H^g_{a,b}\,\rho_{a,b}\,H^{g^{-1}}_{ga,gb} \equiv \frac{1}{|G|}\sum_g \rho^{(g)}_{ga,gb}\,. \tag{4.6.20}$$

In the last equality we introduced the rotated density matrices $\rho^{(g)}_{ga,gb}$ whose path-integral construction is depicted in Fig. 4.7 right. They belong to $\mathrm{End}(\mathcal{H}_{ga,gb})$. The constant prefactor is $Z^{(g)}_{ga,gb} = Z_{a,b}\,\omega(g^{-1},g,a)/\omega(g^{-1},g,b)$. To obtain the second presentation one moves the line of $H^g_{a,b}$ through infinity and then annihilates it with $H^{g^{-1}}_{ga,gb}$. When the line crosses an operator $\mathcal{O}$, the latter gets transformed to ${}^g\mathcal{O}$. Since Hilbert spaces constructed with different simple boundary conditions are orthogonal, the moments of ρ_{S} simplify:

$$\mathrm{Tr}\big(\rho^n_{\mathsf{S}}\big) = \frac{1}{|G|^n}\sum_g \mathrm{Tr}\big[(\rho^{(g)}_{ga,gb})^n\big] = \frac{1}{|G|^{n-1}}\,\mathrm{Tr}\big(\rho^n_{a,b}\big)\,. \tag{4.6.21}$$

The Rényi and entanglement asymmetries are then

$$\Delta S^{(n)}[\rho_{a,b}] = \Delta S[\rho_{a,b}] = \log|G| \qquad \text{for all } n\,. \tag{4.6.22}$$

This result does not depend on the state, and in particular it applies to the vacuum as well. Its interpretation is that the boundary conditions completely break the symmetry, therefore $\Delta S^{(n)}$ and ΔS reach their maximal value irrespective of the state. This observable is clearly not very interesting. To make it interesting, we should rather use a symmetric combination of boundary conditions, as described in Sec. 4.4.4.

Consider then the "averaged" reduced density matrix

$$\rho = \frac{1}{|G|^2}\sum_{a,b}\rho_{a,b}\,. \tag{4.6.23}$$

The symmetrized matrix this time can be written as

$$\rho_{\mathsf{S}} = \frac{1}{|G|^3}\sum_{a,b,g}\rho^{(g)}_{a,b}\,, \tag{4.6.24}$$

where $\rho^{(g)}_{a,b}$ is defined in Fig. 4.7 right. One computes

$$\mathrm{Tr}\big(\rho^n\big) = \frac{1}{|G|^{2n}}\sum_{a,b}\mathrm{Tr}\big(\rho^n_{a,b}\big)\,, \qquad \mathrm{Tr}\big(\rho^n_{\mathsf{S}}\big) = \frac{1}{|G|^{3n}}\sum_{a,b}\sum_{g_1,\dots,g_n}\mathrm{Tr}\Big(\rho^{(g_1)}_{a,b}\cdots\rho^{(g_n)}_{a,b}\Big)\,. \tag{4.6.25}$$

From the path-integral representation of $\rho_{a,b}$ (see Fig. 4.7), $\mathrm{Tr}\big(\rho^n_{a,b}\big)$ is equal to $Z^{-n}_{a,b}$ times the partition function on an n-sheeted Riemann surface with operators $\mathcal{O}$ and $\mathcal{O}^\dagger$ inserted in each replica. In this manifold, the n copies of the boundary with boundary condition a are glued together to form a single boundary that spans all replicas, and the same holds for the boundaries with boundary condition b.

$$\left\langle {}^{g_1}\mathcal{O}^\dagger\, {}^{g_1}\mathcal{O}\ \dots\ {}^{g_n}\mathcal{O}^\dagger\, {}^{g_n}\mathcal{O} \right\rangle_{\mathcal{M}_n} \equiv$$

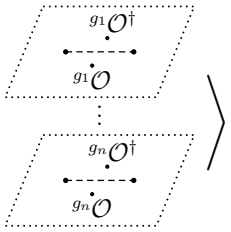


Figure 4.8: Correlator on the n-sheeted Riemann surface $\mathcal{M}_n$. It is understood that the lower rim of each cut (denoted by a dashed segment) is glued to the upper rim of the cut of the sheet above it (and the uppermost sheet is connected to the lowermost sheet). Two branch points sit at the ends of the branch cut. In the j-th replica the operator ${}^{g_j}\mathcal{O}$ is inserted at $z = x - i\tau$ while the operator ${}^{g_j}\mathcal{O}^\dagger$ is inserted at $\bar{z} = x + i\tau$.

Similarly, $\mathrm{Tr}\big(\rho_{a,b}^{(g_1)} \cdots \rho_{a,b}^{(g_n)}\big)$ is equal to $\prod_i 1/Z_{g_i^{-1}a,g_i^{-1}b}$ times the partition function on an n-sheeted Riemann surface with operators ${}^{g_j}\mathcal{O}$ and ${}^{g_j}\mathcal{O}^\dagger$ inserted in the j-th replica and with one a and one b boundary.

In the limit $\varepsilon \to 0$, the dependence of the traces on the boundary conditions becomes very simple. As described in (4.4.29), in the limit each partition function produces a factor of the boundary quantum dimension from each shrinking disc. Thus, the partition function on the n-sheeted Riemann surface becomes $\tilde{d}_a \tilde{d}_b$ times the partition function on a similar Riemann surface, where the boundary discs are shrunk to a branch point and all insertions of fields remain at the same position. For a group-like symmetry all boundary quantum dimensions $\tilde{d}$ are equal. We thus obtain the same factor $\tilde{d}^{2(1-n)}$ from both $\lim_{\varepsilon\to 0} \mathrm{Tr}(\rho^n)$ and $\lim_{\varepsilon\to 0} \mathrm{Tr}(\rho_{\mathsf{S}}^n)$, which simplifies in the ratio. Besides, once the $\varepsilon \to 0$ limit is taken, there is no dependence on a and b left and we can easily sum over them. The result can be expressed in terms of correlation functions on a Riemann surface with branch points:

$$\lim_{\varepsilon\to 0} \Delta S^{(n)}[\rho] = \frac{1}{1-n} \log\left[\frac{1}{|G|^n} \sum_{g_1,\dots,g_n} \frac{\left\langle {}^{g_1}\mathcal{O}^\dagger\, {}^{g_1}\mathcal{O}\ \dots\ {}^{g_n}\mathcal{O}^\dagger\, {}^{g_n}\mathcal{O} \right\rangle_{\mathcal{M}_n}}{\left\langle \mathcal{O}^\dagger\, \mathcal{O} \cdots \mathcal{O}^\dagger\, \mathcal{O} \right\rangle_{\mathcal{M}_n}} \right], \qquad (4.6.26)$$

where the notation $\langle \cdot \rangle_{\mathcal{M}_n}$ indicates a correlation function on the branched Riemann surface, as detailed in Fig. 4.8.

We make three observations. First, if there are no insertions, *i.e.*, if we compute the asymmetry of the vacuum, then all correlators in (4.6.26) are equal to 1 and thus $\Delta S^{(n)} = \Delta S = 0$, as expected from the general discussion in Sec. 4.4.4. Second, the asymmetries have no explicit dependence on the anomaly, as already anticipated in [32]. Third, in the absence of an anomaly, one could compute the asymmetries using the strongly-symmetric boundary condition, and this would lead to exactly the same formula. In particular, earlier works on asymmetry for groups ignored the entangling surface and used the group algebra instead of the strip algebra; we see here that those less rigorous approaches are in fact validated by our more rigorous approach of using the strip algebra.

Large subsystem limit. In the limit of a large subsystem of size ℓ, the branch cut extends along the whole real axis. Then effectively each sheet gets split into two half-planes, and each lower half-plane is glued to the upper half-plane of the next sheet (*cfr.* with Fig. 4.8). One can perform a conformal block expansion of the $2n$-point functions appearing in (4.6.26), in the channel in which each operator is first contracted with the operator found across the cut after the gluing. When that channel is dominated by exchanges of the identity operator, the $2n$-point function factorizes into the product of n two-point functions. This is always the case for the $2n$-point function at denominator in (4.6.26). When exchanges of the identity operator are not possible in the numerator, the contribution to the sum in (4.6.26) is subdominant — and on the other hand some of the two-point functions vanish. Therefore, in the large subsystem limit we find the formula:

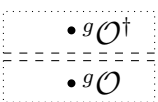
$$\lim_{\ell\to\infty}\lim_{\varepsilon\to 0}\Delta S^{(n)}[\rho]=\frac{1}{1-n}\log\left[\frac{1}{|G|^n}\sum_{g_1,\dots,g_n}\frac{\langle {}^{g_1}\mathcal{O}^\dagger\,{}^{g_2}\mathcal{O}\rangle_{\mathbb{C}}\cdots\langle {}^{g_n}\mathcal{O}^\dagger\,{}^{g_1}\mathcal{O}\rangle_{\mathbb{C}}}{\langle\mathcal{O}^\dagger\mathcal{O}\rangle_{\mathbb{C}}^n}\right]. \tag{4.6.27}$$

We claim that this is the same as the Rényi asymmetry of the full system, *i.e.*, of the state on the real line symmetrized with respect to the fusion algebra $\mathbb{C}[G]$. Indeed, let ρ^{full} be the state on the real line, depicted in Fig. 4.6 left. The symmetrized density matrix for the full system is

$$\rho_{\mathsf{S}}^{\text{full}}=\frac{1}{|G|}\sum\nolimits_{g\in G}\mathcal{L}_g\,\rho^{\text{full}}\,\mathcal{L}_{g^{-1}}\,. \tag{4.6.28}$$

The summand $\mathcal{L}_g\,\rho^{\text{full}}\,\mathcal{L}_{g^{-1}}$ is depicted in Fig. 4.6 right. The Rényi asymmetry is then

$$\Delta S^{(n)}\big[\rho^{\text{full}}\big]=\frac{1}{1-n}\log\left\{\frac{1}{|G|^n}\,\mathrm{Tr}\left[\frac{1}{Z^n}\left(\sum_{g\in G}\right.\right.\right.$$



$$\left.\left.\left.\right)^n\right]\right\}. \tag{4.6.29}$$

We used that ρ^{full} is pure and thus $\mathrm{Tr}\big[(\rho^{\text{full}})^n\big]=1$. The n-th power of the operator appearing inside the trace is obtained by taking n copies of the cut plane and then connecting the lower rim of each cut (which is the "output" of the operator) to the upper rim of the next sheet (which is the "input"). The trace connects them cyclically, in a fashion similar to Fig. 4.8. The partition functions can then be replaced by expectation values, since both at numerator and denominator the required normalization is given by the same partition function with no operator insertions. We conclude that (4.6.29) can be written as in (4.6.27) and therefore

$$\lim_{\ell\to\infty}\lim_{\varepsilon\to 0}\Delta S^{(n)}[\rho]=\Delta S^{(n)}\big[\rho^{\text{full}}\big]\,. \tag{4.6.30}$$

4.6.2 Ising symmetry — circle Hilbert space

The internal symmetry of the two-dimensional Ising CFT is described by a fusion category $\mathscr{C}$ (that we call the Ising fusion category) with 3 simple lines, that we

indicate as $\mathcal{L}_1$, $\mathcal{L}_\eta$, $\mathcal{L}_\mathcal{N}$, satisfying the commutative fusion ring:

$$\mathcal{L}_\eta \times \mathcal{L}_\eta = \mathcal{L}_1 \ , \qquad \mathcal{L}_\eta \times \mathcal{L}_\mathcal{N} = \mathcal{L}_\mathcal{N} \ , \qquad \mathcal{L}_\mathcal{N} \times \mathcal{L}_\mathcal{N} = \mathcal{L}_1 + \mathcal{L}_\eta \ . \tag{4.6.31}$$

Here $\mathcal{L}_1$ is the identity, $\mathcal{L}_\eta$ generates the $\mathbb{Z}_2$ spin-flip symmetry, and $\mathcal{L}_\mathcal{N}$ is the line of Kramers–Wannier duality. The junctions have no multiplicities. The nontrivial F-symbols are:

$$\left[F^{\mathcal{N}}_{\eta\mathcal{N}\eta}\right]_{\mathcal{N}\mathcal{N}} = \left[F^{\eta}_{\mathcal{N}\eta\mathcal{N}}\right]_{\mathcal{N}\mathcal{N}} = -1 \ , \qquad \left[F^{\mathcal{N}}_{\mathcal{N}\mathcal{N}\mathcal{N}}\right]_{ab} = \frac{1}{\sqrt{2}} \begin{pmatrix} 1 & 1 \\ 1 & -1 \end{pmatrix} \ , \tag{4.6.32}$$

where $a, b \in \{1, \eta\}$, while all other F-symbols allowed by fusion are equal to 1. All lines are self-dual. One reads off the Frobenius–Schur (FS) indicators $\varkappa_\eta = \varkappa_\mathcal{N} = 1$ and the quantum dimensions $d_\eta = 1$, $d_\mathcal{N} = \sqrt{2}$. The category $\mathscr{C}$ is the Tambara–Yamagami fusion category $\mathsf{TY}(\mathbb{Z}_2, \chi, +)$ [164] where $\chi(a, b) = e^{i\pi ab}$ is a symmetric $\mathbb{Z}_2$ character that equals -1 only if a, b are both the nontrivial element η, otherwise it equals 1.[35]

Fusion algebra

The fusion algebra has three 1-dimensional representations that we indicate as $\mathbb{1}$, ε, σ. In the Ising CFT these are realized in the Verma module of the identity, the energy, and the spin operator, respectively. The fusion algebra acts on them through (4.3.8), in terms of the unitary and symmetric modular S-matrix:

$$S = \frac{1}{2} \begin{pmatrix} 1 & 1 & \sqrt{2} \\ 1 & 1 & -\sqrt{2} \\ \sqrt{2} & -\sqrt{2} & 0 \end{pmatrix} \ . \tag{4.6.33}$$

The symmetrizer for the fusion algebra is given by the inverse bilinear form:

$$\tilde{K} = \begin{pmatrix} \frac{3}{8} & -\frac{1}{8} & 0 \\ -\frac{1}{8} & \frac{3}{8} & 0 \\ 0 & 0 & \frac{1}{4} \end{pmatrix} \ , \tag{4.6.34}$$

and in particular it takes the form:

$$\rho_{\mathsf{S}} = \frac{1}{8}\Big[3\,\rho + 3\,\mathcal{L}_\eta\,\rho\,\mathcal{L}_\eta - \mathcal{L}_\eta\,\rho - \rho\,\mathcal{L}_\eta + 2\,\mathcal{L}_\mathcal{N}\,\rho\,\mathcal{L}_\mathcal{N}\Big] \ . \tag{4.6.35}$$

[35] The $\mathsf{TY}(\mathbb{Z}_2, \chi, +)$ symmetry appears, for instance, in a system of $\nu = 1, 7, 9, 15 \pmod{16}$ Dirac fermions. A slight generalization is $\mathsf{TY}(\mathbb{Z}_2, \chi, -)$, whose only difference is that $\left[F^{\mathcal{N}}_{\mathcal{N}\mathcal{N}\mathcal{N}}\right]_{ab} = -\chi(a, b)/\sqrt{2}$ and thus $\varkappa_\mathcal{N} = -1$, which appears, for instance, in a system of $\nu = 3, 5, 11, 13 \pmod{16}$ Dirac fermions.

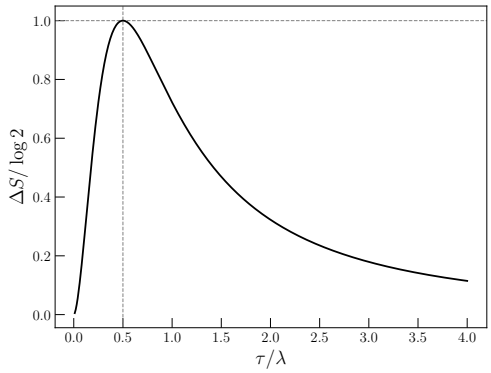


Figure 4.9: Entanglement asymmetry ΔS with respect to the Ising fusion algebra of a state on the real line prepared by inserting $(1+\lambda\,\varepsilon)$ in the path-integral. The asymmetry is plotted as a function of τ/λ, where $-\tau$ is the Euclidean time of the insertion. In the limit $\tau/\lambda \to \infty$ only the identity contributes, so the state becomes symmetric and the asymmetry vanishes. Similarly, in the limit $\tau/\lambda \to 0$ only ε contributes, leading again to a symmetric state with vanishing asymmetry. The asymmetry reaches its maximum at $\tau/\lambda = 1/2$.

Asymmetry of excited states in CFTs. We consider a CFT whose symmetry includes the Ising fusion category. This could be the Ising CFT itself, or a more complicated one (for instance, the tricritical Ising model). The local operators fall into representations of the fusion algebra, that we indicate as $\mathbb{1}$, ε, σ as in (4.6.33). We consider excited states on the line $\mathbb{R}$ produced using a scalar operator $\varepsilon(z)$ of dimension Δ_ε in the Euclidean past, which by definition transforms in the representation ε:

$$|\psi\rangle \;=\; \boxed{\bullet\; 1{+}\lambda\,\varepsilon} \;. \tag{4.6.36}$$

Here λ is a constant of mass dimension $-\Delta_\varepsilon$. Notice that this state is neutral under the $\mathbb{Z}_2$ spin-flip symmetry. To compute its asymmetry with respect to the fusion algebra we can use (4.3.25). Setting the operator insertion at $z = -i\tau$ with $\tau > 0$ (thus $\bar{z} = i\tau$), the relevant two-point function is $\big\langle \varepsilon(\bar{z})\,\varepsilon(z)\big\rangle \equiv \langle \varepsilon^2 \rangle = 1/(2\tau)^{2\Delta_\varepsilon}$. The second Rényi and entanglement asymmetries are then

$$\Delta S^{(2)}\big[|\psi\rangle\langle\psi|\big] = -\log\left[\frac{1+\lambda^4\langle\varepsilon^2\rangle^2}{\big(1+\lambda^2\langle\varepsilon^2\rangle\big)^2}\right], \qquad \Delta S\big[|\psi\rangle\langle\psi|\big] = f\left[\frac{1}{1+\lambda^2\langle\varepsilon^2\rangle}\right] + f\left[\frac{\lambda^2\langle\varepsilon^2\rangle}{1+\lambda^2\langle\varepsilon^2\rangle}\right], \tag{4.6.37}$$

where we used the function $f(x) = -x\log x$.

In the case of the Ising CFT we can take $\varepsilon(x)$ to be the energy conformal primary operator of dimension $\Delta_\varepsilon = 1$. In Fig. 4.9 we plot the entanglement asymmetry as a function of τ/λ.

Spontaneous symmetry breaking. The only indecomposable $\mathscr{C}$-module category of the Ising fusion category is the regular one.[36] This means that in a gapped phase the Ising symmetry is always completely spontaneously broken, and this is due to the presence of an 't Hooft anomaly. In the regular module one could indicate both lines and boundary conditions using the same set of labels. However, in order to adhere to a more commonly used notation, we relabel the boundary conditions as:[37]

$$1 \;\to\; + \,, \qquad\qquad \eta \;\to\; - \,, \qquad\qquad \mathcal{N} \;\to\; f \,. \tag{4.6.38}$$

Correspondingly, we indicate the three normalized vacua (*i.e.*, the three clustering states) as $\big\{|+\rangle\,,\,|-\rangle\,,\,|f\rangle\big\}$. They furnish a NIM-rep of the fusion algebra:

$$\begin{aligned} &\mathcal{L}_\eta\,|+\rangle = |-\rangle\,, \qquad \mathcal{L}_\eta\,|-\rangle = |+\rangle\,, \qquad \mathcal{L}_\eta\,|f\rangle = |f\rangle\,, \\ &\mathcal{L}_\mathcal{N}\,|+\rangle = |f\rangle\,, \qquad \mathcal{L}_\mathcal{N}\,|-\rangle = |f\rangle\,, \qquad \mathcal{L}_\mathcal{N}\,|f\rangle = |+\rangle + |-\rangle\,. \end{aligned} \tag{4.6.39}$$

The gapped phase (some curious properties thereof already noticed in [135]) can be obtained, for instance, from the tricritical Ising model deforming it by the relevant operator ε', as explained in Sec. 7.2.3 of [55].

Consider the pure state $\rho = |f\rangle\langle f|$ for the vacuum $|f\rangle$. Using the symmetrizer (4.6.35) with respect to the fusion algebra, one computes ρ_S. Its diagonalization is $\rho_\mathsf{S} \sim \mathrm{diag}\big(\frac{1}{2},\frac{1}{2},0\big)$ and therefore $\mathrm{Tr}(\rho_\mathsf{S}^n) = 2^{1-n}$. The Rényi and entanglement asymmetries are then

$$\Delta S^{(n)} = \Delta S = \log 2\,. \tag{4.6.40}$$

Notice that this is the same asymmetry as for a spontaneously broken $\mathbb{Z}_2$ symmetry [39].[38] On the other hand, consider the pure state $\rho = |+\rangle\langle +|$ for the vacuum $|+\rangle$ (the vacuum $|-\rangle$ would give the same result). The symmetrized matrix ρ_S has diagonalization $\rho_\mathsf{S} \sim \mathrm{diag}\big(\frac{1}{2},\frac{1}{4},\frac{1}{4}\big)$ and hence $\mathrm{Tr}(\rho_\mathsf{S}^n) = \big(2^{n-1}+1\big)/2^{2n-1}$, from which the Rényi and entanglement asymmetries are

$$\Delta S^{(n)} = \frac{1}{1-n}\log\frac{2^{n-1}+1}{2^{2n-1}}\,, \qquad\qquad \Delta S = \frac{3}{2}\log 2\,. \tag{4.6.41}$$

This time the entanglement asymmetry is larger than for a broken $\mathbb{Z}_2$, but smaller than for a broken $\mathbb{Z}_3$. We conclude that, while for a completely broken invertible symmetry G the entanglement asymmetry of a vacuum is $\Delta S = \log|G|$ [36], for noninvertible symmetries the asymmetry may take more general values. We also observe that different vacua in the same gapped phase can have inequivalent physical properties (as already stressed in [135, 136]) and in particular different asymmetries.

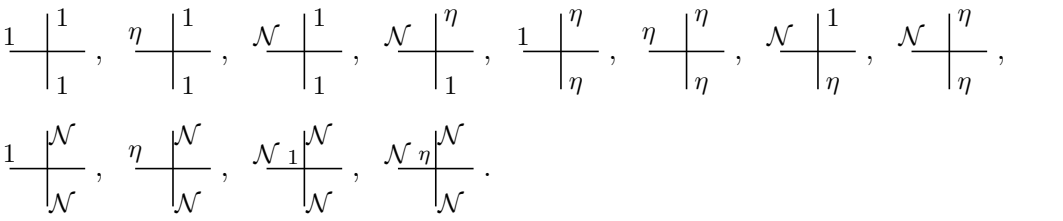
[36] By Th. 6 of [152] (where the Ising category is called $\mathscr{C}_2$ and the module is of type A_3), the Ising fusion category admits only one indecomposable module category. Hence, this must be the regular module, which always exists.

[37] These boundary conditions have a counterpart in a lattice spin model: $\pm$ correspond to up/down fixed boundary conditions for the spins, while f corresponds to the free boundary condition.

[38] This is explained by the fact that the "orbit" of $|f\rangle$ under the noninvertible symmetry is given by two rays, the ones of $|f\rangle$ and $\big(|+\rangle + |-\rangle\big)$, as it happens for a $\mathbb{Z}_2$ symmetry.

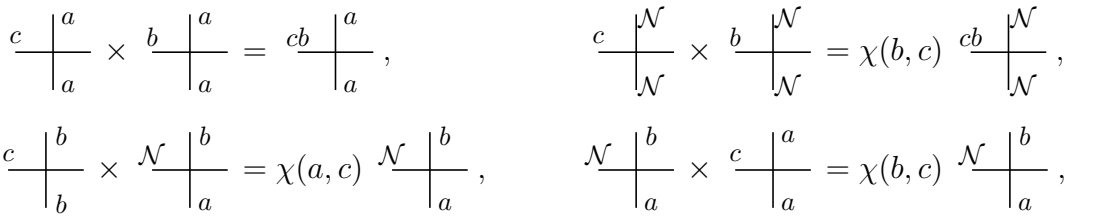
Tube algebra

The tube algebra is generated by the following 12 basis elements (see also [165]):



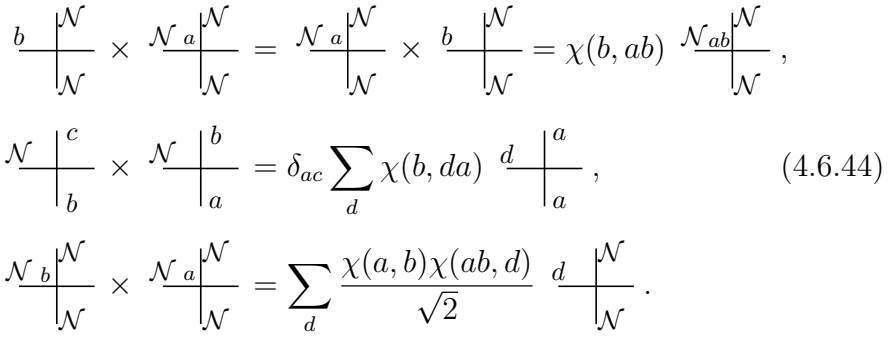
(4.6.42)

By applying the formula (4.3.19) we compute the algebra product. We use the bicharacter $\chi(a,b)$ defined on $\mathbb{Z}_2 = \{1,\eta\}$ above. As in the general discussion, we adopt the convention that the element on the left is stacked on top of the one on the right. We find:



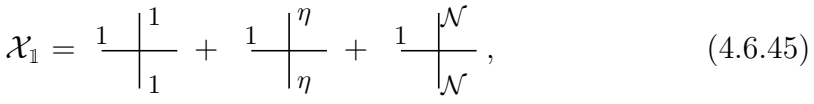
(4.6.43)

as well as



(4.6.44)

The unit of the algebra is



(4.6.45)

which agrees with (4.2.10).

Untwisted and twisted point operators fall into representations of the tube algebra. Such representations are in one-to-one correspondence with simple objects in the Drinfeld center of $\mathscr{C}$. Because $\mathscr{C}$ is modular, its Drinfeld center is isomorphic to the product of two copies of the TY fusion category, therefore it has 9 simple lines, listed in [165].

The total circle Hilbert space (4.3.11) is decomposed as a sum of twisted sectors, each graded by a simple element $a \in \mathrm{Irr}(\mathscr{C})$ of the symmetry category. Similarly,

one can show that (see *e.g.*[166]) any representation of the tube algebra has a grading by elements in $\mathrm{Irr}(\mathscr{C})$: $V = \bigoplus_a V_a$. This grading is such that elements of the tube algebra that have g as the lower vertical line act as zero on those $V_{g'}$ with $g' \neq g$. In other words, the twist of the tube algebra must be compatible with that of the state it is acting on. When listing the irreducible representations of the tube algebra, we thus explicitly report how each vector space decomposes in graded components. In this case one finds:

- Two 1-dimensional irreducible representations $\mathcal{F}_1^{\pm}$ with space $V = \mathbb{C}_1$, and

$$\mathcal{F}_1^{\pm}\left(\begin{array}{c|c} a & 1 \\ \hline & 1 \end{array}\right) = 1\,, \qquad \mathcal{F}_1^{\pm}\left(\begin{array}{c|c} \mathcal{N} & 1 \\ \hline & 1 \end{array}\right) = \pm\sqrt{2}\,, \tag{4.6.46}$$

  while all other ones are mapped to zero. They represent genuine local operators, not charged under $\mathbb{Z}_2$, which could be charged under $\mathcal{N}$ but that remain genuine local operators under its action.

- Two 1-dimensional irreducible representations $\mathcal{F}_\eta$ and $\mathcal{F}_\eta^*$ with space $V = \mathbb{C}_\eta$, and

$$\mathcal{F}_\eta\left(\begin{array}{c|c} a & \eta \\ \hline & \eta \end{array}\right) = \chi(a,\eta)\,, \qquad \mathcal{F}_\eta\left(\begin{array}{c|c} \mathcal{N} & \eta \\ \hline & \eta \end{array}\right) = i\,\sqrt{2}\,, \tag{4.6.47}$$

  while all other ones are mapped to zero. They represent η-twisted operators that are charged under $\mathbb{Z}_2$, and that remain twisted-sector operators under the action of $\mathcal{N}$.

- Four 1-dimensional irreducible representations $\mathcal{F}_{\mathcal{N}}^{\pm}$ and $(\mathcal{F}_{\mathcal{N}}^{\pm})^*$ with space $V = \mathbb{C}_{\mathcal{N}}$, and

$$\begin{aligned} &\mathcal{F}_{\mathcal{N}}^{\pm}\left(\begin{array}{c|c} 1 & \mathcal{N} \\ \hline & \mathcal{N} \end{array}\right) = 1\,, && \mathcal{F}_{\mathcal{N}}^{\pm}\left(\begin{array}{c|c} \eta & \mathcal{N} \\ \hline & \mathcal{N} \end{array}\right) = i\,, \\ &\mathcal{F}_{\mathcal{N}}^{\pm}\left(\begin{array}{c|c} \mathcal{N}\ 1 & \mathcal{N} \\ \hline & \mathcal{N} \end{array}\right) = \pm e^{\frac{i\pi}{8}}\,, && \mathcal{F}_{\mathcal{N}}^{\pm}\left(\begin{array}{c|c} \mathcal{N}\ \eta & \mathcal{N} \\ \hline & \mathcal{N} \end{array}\right) = \pm e^{-\frac{3i\pi}{8}}\,, \end{aligned} \tag{4.6.48}$$

  while all other ones are mapped to zero. They represent $\mathcal{N}$-twisted operators, charged under η and $\mathcal{N}$, that remain $\mathcal{N}$-twisted operators under the action of $\mathcal{N}$.

- One 2-dimensional irreducible representation $\mathcal{F}_2$ with space $V = \mathbb{C}_1 \oplus \mathbb{C}_\eta$,

and

$$\mathcal{F}_2\left(\begin{smallmatrix}1 & \vert^{1}\\ & \vert_{1}\end{smallmatrix}\right)=\begin{pmatrix}1&0\\0&0\end{pmatrix},\quad \mathcal{F}_2\left(\begin{smallmatrix}\eta & \vert^{1}\\ & \vert_{1}\end{smallmatrix}\right)=\begin{pmatrix}-1&0\\0&0\end{pmatrix},\quad \mathcal{F}_2\left(\begin{smallmatrix}\mathcal{N} & \vert^{\eta}\\ & \vert_{1}\end{smallmatrix}\right)=\begin{pmatrix}0&0\\\sqrt{2}&0\end{pmatrix}$$
$$\mathcal{F}_2\left(\begin{smallmatrix}1 & \vert^{\eta}\\ & \vert_{\eta}\end{smallmatrix}\right)=\begin{pmatrix}0&0\\0&1\end{pmatrix},\quad \mathcal{F}_2\left(\begin{smallmatrix}\eta & \vert^{\eta}\\ & \vert_{\eta}\end{smallmatrix}\right)=\begin{pmatrix}0&0\\0&1\end{pmatrix},\quad \mathcal{F}_2\left(\begin{smallmatrix}\mathcal{N} & \vert^{1}\\ & \vert_{\eta}\end{smallmatrix}\right)=\begin{pmatrix}0&\sqrt{2}\\0&0\end{pmatrix} \tag{4.6.49}$$

while all other ones are mapped to zero. It represents a doublet of a genuine local operator $\mathcal{O}_1$ and an η-twisted operator $\mathcal{O}_\eta$ that are exchanged by $\mathcal{N}$. Note that $\mathcal{O}_1$ is charged under $\mathbb{Z}_2$ while $\mathcal{O}_\eta$ is neutral.

Asymmetry of the tube algebra. The inverse bilinear form, in the ordered basis (4.6.42), reads:

$$\tilde{K}=\frac{1}{4}\,\mathrm{diag}\big(1,1,1,0,1,1,0,-1,1,-1,\frac{1}{\sqrt{2}},-\frac{1}{\sqrt{2}}\big)+\frac{1}{4}\,\mathrm{offdiag}_{[4,7]}+\frac{1}{4\sqrt{2}}\,\mathrm{offdiag}_{[11,12]}\,, \tag{4.6.50}$$

where the first term is a diagonal matrix while $\mathrm{offdiag}_{[i,j]}$ is an off-diagonal matrix with a 1 at positions (i,j) and (j,i). The symmetrizer can be computed from $\tilde{K}$.

Let us specialize to a state belonging to the 2d irreducible representation (4.6.49) of the tube algebra. For example, we can choose a pure state $\mathcal{O}_1(z)|0\rangle$ created by the untwisted local operator $\mathcal{O}_1$, which in the Ising model is $\sigma(z)$. In this case the only terms that survive in the symmetrized density matrix are

$$\rho_{\mathsf{S}}=\frac{1}{4}\Big(\rho\;+\;\begin{smallmatrix}\eta & \vert^{1}\\ & \vert_{1}\end{smallmatrix}\;\rho\;\begin{smallmatrix}\eta & \vert^{1}\\ & \vert_{1}\end{smallmatrix}+\begin{smallmatrix}\mathcal{N} & \vert^{\eta}\\ & \vert_{1}\end{smallmatrix}\;\rho\;\begin{smallmatrix}\mathcal{N} & \vert^{1}\\ & \vert_{\eta}\end{smallmatrix}\Big)\,. \tag{4.6.51}$$

One immediately obtains $\Delta S=\log(2)$. More in general, the asymmetry of a pure state that belongs to a single d-dimensional irreducible representation of an algebra is $\Delta S=\log(d)$. Indeed, following the discussion in Fig. 4.1, the symmetrized density matrix is supported on a single block, where it takes the form $\frac{1}{\mathrm{d}}\mathbb{1}_{d\times d}$. Because the entropy of the initial state is zero, one obtains that both the entanglement and Rényi asymmetries are equal to $\log(d)$.

4.6.3 $\mathbb{Z}_2\times\mathbb{Z}_2$ Tambara–Yamagami fusion category

The Ising (or $\mathbb{Z}_2$ TY) fusion category does not admit a fiber functor. This can be seen, for example, from the fact that the noninvertible line has non-integer quantum dimension. Therefore, the symmetry carries an 't Hooft anomaly and does not admit strongly-symmetric boundary conditions (in the language of [106]). Furthermore, it does not admit weakly-symmetric boundary conditions either,

because the only indecomposable module is the regular one, which is not weakly symmetric.

However, one can take the stacking of two decoupled copies of the Ising symmetry and then look at a subsymmetry therein [106, 167]. The full set of simple lines of the stacking is made of objects of the form $a_1 \boxtimes a_2$ with $a_j \in \{1, \eta, \mathcal{N}\}$. We consider the subcategory generated by

$$\mathcal{L}_1 = 1\boxtimes 1\ , \quad \mathcal{L}_\eta = \eta\boxtimes 1\ , \quad \mathcal{L}_{\eta'} = 1\boxtimes\eta\ , \quad \mathcal{L}_{\eta\eta'} = \eta\boxtimes\eta\ , \quad \mathcal{L}_\mathcal{V} = \mathcal{N}\boxtimes\mathcal{N}\ . \tag{4.6.52}$$

Their fusion ring is Abelian and given by:

$$\begin{aligned} &\mathcal{L}_\eta^2 = \mathcal{L}_{\eta'}^2 = \mathcal{L}_{\eta\eta'}^2 = \mathcal{L}_1\ , && \mathcal{L}_\eta \times \mathcal{L}_\mathcal{V} = \mathcal{L}_{\eta'} \times \mathcal{L}_\mathcal{V} = \mathcal{L}_\mathcal{V}\ , \\ &\mathcal{L}_\eta \times \mathcal{L}_{\eta'} = \mathcal{L}_{\eta\eta'}\ , && \mathcal{L}_\mathcal{V} \times \mathcal{L}_\mathcal{V} = \mathcal{L}_1 + \mathcal{L}_\eta + \mathcal{L}_{\eta'} + \mathcal{L}_{\eta\eta'}\ . \end{aligned} \tag{4.6.53}$$

This is in fact the fusion ring of $\mathbb{Z}_2 \times \mathbb{Z}_2$ Tambara–Yamagami fusion categories [164]. In this case, the $\mathbb{Z}_2 \times \mathbb{Z}_2$ symmetric bilinear character is $\gamma\big((s_1, s_2), (s_3, s_4)\big) = e^{i\pi(s_1 s_3 + s_2 s_4)}$ where each $s_j \in \{0, 1\}$, the Frobenius–Schur indicator is $\varkappa_\mathcal{V} = 1$, therefore the nontrivial F-symbols are

$$\big[F^\mathcal{V}_{i\mathcal{V}j}\big]_{\mathcal{V}\mathcal{V}} = \big[F^j_{\mathcal{V}i\mathcal{V}}\big]_{\mathcal{V}\mathcal{V}} = \gamma(i,j)\ , \qquad \big[F^\mathcal{V}_{\mathcal{V}\mathcal{V}\mathcal{V}}\big]_{ij} = \frac{1}{2}\,\gamma(i,j)\ , \tag{4.6.54}$$

where $i, j \in \mathbb{Z}_2^2$. The four invertible lines have quantum dimension 1, while $\mathcal{L}_\mathcal{V}$ has quantum dimension 2. This fusion category is also equivalent to $\mathsf{Rep}(H_8)$, where H_8 is the Kac–Paljutkin Hopf algebra [168]. As all categories of representations of a Hopf algebra, it admits at least one fiber functor given by the forgetful functor that maps a representation to its underlying vector space [153]. In this case one can show that this is the only fiber functor.[39] We conclude that the $\mathsf{Rep}(H_8)$ symmetry admits one (and only one) strongly-symmetric boundary condition. This is our motivation to study this example.

Fusion algebra

The fusion algebra has five 1-dimensional representations that we call $\mathbb{1}$, ε, σ, σ', σ''.[40] The unitary (but not symmetric) S-matrix is

$$S = \frac{1}{2\sqrt{2}} \begin{pmatrix} 1 & 1 & \sqrt{2} & \sqrt{2} & \sqrt{2} \\ 1 & 1 & -\sqrt{2} & \sqrt{2} & -\sqrt{2} \\ 1 & 1 & \sqrt{2} & -\sqrt{2} & -\sqrt{2} \\ 1 & 1 & -\sqrt{2} & -\sqrt{2} & \sqrt{2} \\ 2 & -2 & 0 & 0 & 0 \end{pmatrix}\ . \tag{4.6.55}$$

[39] Indeed, there is a unique maximal haploid algebra object in $\mathsf{Rep}(H_8)$ as shown in [167].

[40] In the case of two decoupled copies of the Ising CFT, the nine conformal primaries split as $1 \supset 1\boxtimes 1, \varepsilon\boxtimes\varepsilon$; $\varepsilon \supset \varepsilon\boxtimes 1, 1\boxtimes\varepsilon$; $\sigma \supset \sigma\boxtimes 1, \sigma\boxtimes\varepsilon$; $\sigma' \supset 1\boxtimes\sigma, \varepsilon\boxtimes\sigma$; $\sigma'' \supset \sigma\boxtimes\sigma$.

The symmetrizer for the fusion algebra is

$$\rho_{\mathsf{S}} = \frac{1}{32}\Big(8\sum_{a\in\mathbb{Z}_2\times\mathbb{Z}_2}\mathcal{L}_a\,\rho\,\mathcal{L}_a - B\,\rho\,B + 4\,\mathcal{L}_{\mathcal{V}}\,\rho\,\mathcal{L}_{\mathcal{V}}\Big) \qquad \text{with} \qquad B = \sum_{a\in\mathbb{Z}_2\times\mathbb{Z}_2}\mathcal{L}_a\ . \tag{4.6.56}$$

Asymmetry of an excited state in CFT. Let us compute the asymmetry of excited states on the line $\mathbb{R}$ produced by Euclidean operator insertions in CFTs. For concreteness, consider the states

$$|\psi\rangle = \Big(1 + \lambda\,\varepsilon(-i\tau)\Big)\,|0\rangle\ , \tag{4.6.57}$$

that are neutral under the invertible part of the symmetry. Using (4.3.25), we obtain exactly the same formula (4.6.37) as before. In the case of two decoupled copies of the Ising CFT, we can take $\varepsilon(z)$ to be the energy operator of one of the two copies of Ising, so that $\Delta_\varepsilon = 1$. We obtain exactly the same function as in Fig. 4.9.

Strip algebra

Strongly-symmetric boundary condition. The left-module category with a single object is described by the fusion coefficients $\tilde{N}_a^{\cdot}{}_{\cdot} = \{1,1,1,1,2\}$. This means that the $\mathbb{Z}_2^2$ lines $\mathcal{L}_{\eta^m\eta'^n}$ have a single junction to the boundary, while the noninvertible line $\mathcal{L}_{\mathcal{V}}$ has two. Writing the $\tilde{F}$-symbols in terms of m-symbols,

$$\big[\tilde{F}_{ab}^{\cdot}{}_{\cdot}\big]_{(c;-\rho)(\cdot\,;\nu\mu)} = \big(m^{c\rho}_{a\mu,b\nu}\big)^*\ , \tag{4.6.58}$$

the nontrivial ones are given by [167]:[41]

$$\begin{aligned} &m^{(ij)}_{i,j} = K_{ij}\ , \qquad m^{\mathcal{V}\rho}_{\eta,\mathcal{V}\mu} = m^{\mathcal{V}\mu}_{\mathcal{V}\rho,\eta} = \sqrt{2}\,m^{\eta}_{\mathcal{V}\mu,\mathcal{V}\rho} = m^{\mathcal{V}\mu}_{\eta',\mathcal{V}\rho} = m^{\mathcal{V}\rho}_{\mathcal{V}\mu,\eta'} = \sqrt{2}\,m^{\eta'}_{\mathcal{V}\rho,\mathcal{V}\mu} = M_{\mu\rho}\ ,\\ &m^{\mathcal{V}\rho}_{1,\mathcal{V}\mu} = m^{\mathcal{V}\rho}_{\mathcal{V}\mu,1} = \sqrt{2}\,m^{1}_{\mathcal{V}\mu,\mathcal{V}\rho} = \delta_{\mu\rho}\ , \qquad m^{\mathcal{V}\rho}_{\eta\eta',\mathcal{V}\mu} = m^{\mathcal{V}\rho}_{\mathcal{V}\mu,\eta\eta'} = \sqrt{2}\,m^{\eta\eta'}_{\mathcal{V}\mu,\mathcal{V}\rho} = (\sigma_z)_{\mu\rho}\ , \end{aligned} \tag{4.6.59}$$

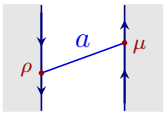
in terms of matrices

$$K_{ij} = \begin{pmatrix} 1 & 1 & 1 & 1\\ 1 & 1 & -i & i\\ 1 & i & 1 & -i\\ 1 & -i & i & 1 \end{pmatrix}\ , \quad M_{\mu\rho} = \begin{pmatrix} 0 & \xi^{-1}\\ \xi & 0 \end{pmatrix}\ , \quad \xi = e^{\frac{3\pi i}{4}}\ , \quad (\sigma_z)_{\mu\rho} = \begin{pmatrix} 1 & 0\\ 0 & -1 \end{pmatrix}\ . \tag{4.6.60}$$

The m-symbols satisfy the associativity condition (4.4.19), while the $\tilde{F}$-symbols satisfy the left-module pentagon equation (4.D.1). We chose a gauge in which the $\tilde{F}$-symbols are unitary.

[41] Which we have adapted to our choice of unitary gauge.

Strip algebra. For the unique strongly-symmetric boundary condition described above, the strip algebra $\mathsf{Strip}_{\mathsf{Rep}(H_8)}(\mathsf{Vec})$ has dimension 8. The fusion coefficients are $\tilde{N}_a^{\cdot}{}_{\cdot} = d_a$ and the basis elements are



(4.6.61)

where $a \in \{1, \eta, \eta', \eta\eta', \mathcal{V}\}$, and for $a = \mathcal{V}$ the junctions are labeled by $\rho, \mu \in \{0, 1\}$. We will use the notation H_i with $i \in \mathbb{Z}_2 \times \mathbb{Z}_2$ and $H_{\mathcal{V}}^{\rho,\mu}$ for the basis elements. Applying (4.4.21) we find the following algebra product:

$$\begin{aligned} H_{\mathcal{V}}^{s,s'} \times H_{\eta^m\eta'^n} &= e^{-\frac{i\pi}{2}(s-s')(m-n+2mn)}\, H_{\mathcal{V}}^{s+m+n,s'+m+n}\,, \qquad H_i \times H_j = H_{(ij)}\,, \\ H_{\eta^m\eta'^n} \times H_{\mathcal{V}}^{s,s'} &= e^{\frac{i\pi}{2}(s-s')(m-n+2mn)}\, H_{\mathcal{V}}^{s+m+n,s'+m+n}\,, \\ H_{\mathcal{V}}^{s_1,s_2} \times H_{\mathcal{V}}^{s_3,s_4} &= \delta_{s_1 s_3}\delta_{s_2 s_4}\Big(H_1 + (-1)^{s_1+s_2} H_{\eta\eta'}\Big) \\ &\quad + \delta_{s_1,1-s_3}\delta_{s_2,1-s_4}\Big(e^{\frac{i\pi}{2}(s_1-s_2)} H_\eta + e^{\frac{i\pi}{2}(s_2-s_1)} H_{\eta'}\Big)\,. \end{aligned} \tag{4.6.62}$$

The symmetrizer, computed with (4.2.11), reads:

$$\rho_{\mathsf{S}} = \frac{1}{8}\left[\sum_{j\,\in\,\mathbb{Z}_2\times\mathbb{Z}_2} H_j\,\rho\,H_j + \sum_{s,\,s'\,\in\,\{0,1\}} H_{\mathcal{V}}^{s,s'}\,\rho\,H_{\mathcal{V}}^{s,s'}\right]. \tag{4.6.63}$$

Strip algebras constructed using strongly-symmetric boundary conditions are Hopf algebras. We review the definition and some properties of Hopf algebras in Appendix 4.B. In this case one obtains an eight-dimensional Hopf algebra which is neither commutative nor cocommutative. It is known that there is only one such Hopf algebra, the Kac–Paljutkin H_8 Hopf algebra [168]. This algebra is not isomorphic to the group algebra of some group, nor to the dual of a group algebra, and it is the smallest-dimensional algebra with such properties [169, 170]. The coproduct is given by

$$\Delta(H_i) = H_i \otimes H_i\,, \qquad \Delta\big(H_{\mathcal{V}}^{s,s'}\big) = \frac{1}{\sqrt{2}}\sum\nolimits_{t\,\in\,\{0,1\}} H_{\mathcal{V}}^{s,t} \otimes H_{\mathcal{V}}^{t,s'}\,. \tag{4.6.64}$$

The counit and the antipode map are

$$\epsilon(H_i) = 1\,, \qquad \epsilon\big(H_{\mathcal{V}}^{s,s'}\big) = \sqrt{2}\,\delta^{s,s'}\,, \qquad S(H_i) = H_i\,, \qquad S\big(H_{\mathcal{V}}^{s,s'}\big) = H_{\mathcal{V}}^{s',s}\,. \tag{4.6.65}$$

In the mathematical literature, the algebra H_8 is usually presented (see, *e.g.*, Sec. 4.2 of [170]) as generated by the elements $1, x, y, z$ where 1 is the identity while

$$x^2 = y^2 = 1\,, \quad z^2 = \tfrac{1}{2}\big(1 + x + y - xy\big)\,, \quad xy = yx\,, \quad xz = zy\,, \quad yz = zx\,. \tag{4.6.66}$$

The basis elements are thus $\{1, x, y, z, xy, xz, yz, xyz\}$. The Hopf algebra structure is

$$\begin{aligned} &\epsilon(x) = 1 \,, && S(x) = x \,, && \Delta(x) = x \otimes x \,, \\ &\epsilon(y) = 1 \,, && S(y) = y \,, && \Delta(y) = y \otimes y \,, \\ &\epsilon(z) = 1 \,, && S(z) = z \,, && \Delta(z) = \tfrac{1}{2}\big(z \otimes z + z \otimes xz + yz \otimes z - yz \otimes xz\big) \,. \end{aligned} \tag{4.6.67}$$

An isomorphism is given by

$$1 = H_1 \,, \quad x = H_\eta \,, \quad y = H_{\eta'} \,, \quad z = \frac{1-i}{\sqrt{8}}\, H_{\mathcal{V}}^{0,0} + \frac{1}{2}\Big(H_{\mathcal{V}}^{1,0} + H_{\mathcal{V}}^{0,1}\Big) + \frac{1+i}{\sqrt{8}}\, H_{\mathcal{V}}^{1,1} \,. \tag{4.6.68}$$

The algebra has four 1-dimensional and one 2-dimensional irreducible representations. The four 1d representations $\mathcal{F}_1^\pm$ and $\mathcal{F}_\eta^\pm$ are

$$\begin{aligned} &\mathcal{F}_1^\pm\colon && H_i \mapsto 1 \,, && H_{\mathcal{V}}^{s,s'} \mapsto \pm\sqrt{2}\, \delta^{s,s'} \,, \\ &\mathcal{F}_\eta^\pm\colon && H_1 \,, H_{\eta\eta'} \mapsto 1 \,, \quad H_\eta \,, H_{\eta'} \mapsto -1 \,, && H_{\mathcal{V}}^{s,s'} \mapsto \pm\sqrt{2}\, \delta^{s,s'}\, e^{i\pi s s'} \,. \end{aligned} \tag{4.6.69}$$

The 2d representation is given by

$$\mathcal{F}_2\colon \qquad H_{\eta^m \eta'^n} \mapsto \begin{pmatrix} (-1)^m & 0 \\ 0 & (-1)^n \end{pmatrix} , \qquad H_{\mathcal{V}}^{s,s'} \mapsto \delta^{s,1-s'}\, \sqrt{2} \begin{pmatrix} 0 & (i)^{s'} \\ (-i)^{s'} & 0 \end{pmatrix} . \tag{4.6.70}$$

The projector, or minimal central idempotent (MCI), to the trivial representation is

$$P_\epsilon = \frac{1}{8}\Big(H_1 + H_\eta + H_{\eta'} + H_{\eta\eta'} + \sqrt{2}\, H_{\mathcal{V}}^{0,0} + \sqrt{2}\, H_{\mathcal{V}}^{1,1}\Big) \,. \tag{4.6.71}$$

This is the only MCI on which the counit ϵ takes value 1. Applying the formula (4.4.37) for the symmetrizer with respect to a Hopf algebra, one reproduces the result (4.6.63) obtained using the general formula.

Example: the (Ising)^2 CFT

Consider the theory given by two decoupled copies of the Ising CFT (which has central charge $c = 1$ and is equivalent to an orbifold of the free compact boson at radius $\sqrt{2}$ times the self-dual radius). We study a subsymmetry of this theory, given by the $\mathbb{Z}_2 \times \mathbb{Z}_2$ Tambara–Yamagami fusion category for the specific choice of bicharacter and Frobenius–Shur indicator already made after (4.6.53), and equivalent to the $\mathsf{Rep}(H_8)$ fusion category. This category admits a strongly-symmetric boundary condition, with which we construct the strip algebra H_8.

Case $\mathbf{1 \boxtimes 1 + \lambda\, \varepsilon \boxtimes 1}$. We study the state on the real line prepared by inserting the operator $\mathcal{O}(z) = 1 \boxtimes 1 + \lambda\, \varepsilon(z) \boxtimes 1$ at position $z = x - i\tau$. Since ε has scaling

dimension $\Delta_\varepsilon = 1$, the coefficient λ has dimensions of a length. The path-integral that prepares the state is done on a half-plane. We study the asymmetry of the reduced density matrix on an interval $A = \left[-\frac{\ell}{2}, \frac{\ell}{2}\right]$, using the setup of Sec. 4.4.2: to prepare the state we cut out two discs of size ε around the entangling surface centered at $\left(\pm\frac{\ell}{2}, 0\right)$ and impose the strongly-symmetric boundary condition $|\mathcal{B}\rangle$ there. We compute the second Rényi asymmetry using the symmetrization formula derived above. This produces

$$\mathrm{Tr}\big(\rho_{\mathsf{S}}^2\big) = \frac{1}{8}\,\mathrm{Tr}\bigg[\sum_{j\,\in\,\mathbb{Z}_2\times\mathbb{Z}_2} \rho\, H_j\, \rho\, H_j + \sum_{s,s'} \rho\, H_{\mathcal{V}}^{s,s'}\, \rho\, H_{\mathcal{V}}^{s,s'}\bigg] = \frac{1}{2}\,\mathrm{Tr}\big(\rho^2 + \rho\rho'\big)\ . \quad (4.6.72)$$

Here ρ' is obtained by swiping a line $\mathcal{L}_{\mathcal{V}}$ across the whole density matrix, transforming the operator $\mathcal{O} = 1\boxtimes 1 + \lambda\,\varepsilon\boxtimes 1$ to $\mathcal{O}' = 1\boxtimes 1 - \lambda\,\varepsilon\boxtimes 1$. We thus get:

$$\Delta S^{(2)}[\rho] = -\log\frac{\mathrm{Tr}\big(\rho_{\mathsf{S}}^2\big)}{\mathrm{Tr}\big(\rho^2\big)} = \log 2 - \log\bigg[1 + \frac{\mathrm{Tr}\big(\rho\rho'\big)}{\mathrm{Tr}\big(\rho^2\big)}\bigg]\ . \quad (4.6.73)$$

We can express $\mathrm{Tr}(\rho\rho')/\,\mathrm{Tr}(\rho^2)$ as a ratio of partition functions on a Riemann surface obtained by gluing two copies of the complex plane with the entangling discs cut out. In the $\varepsilon \to 0$ limit, each entangling disc is replaced by a branch point and the partition functions are multiplied by the g-factor $g_{\mathcal{B}} = \langle\mathcal{B}|0\rangle$ (we already discussed such a procedure in Sec. 4.4.4). The g-factors at numerator and denominator are equal and cancel out. The same procedure is discussed in the paragraph above (4.6.26). In turn, the ratio of partition functions is equal to a ratio of correlation functions on a Riemann surface $\mathcal{M}_2$ with two branch points. We denote a point on $\mathcal{M}_2$ by z_j where $z \in \mathbb{C}$ denotes a point on the complex plane while $j \in \{1, 2\}$ labels the sheet. We get:

$$\frac{\mathrm{Tr}(\rho\rho')}{\mathrm{Tr}(\rho^2)} = \frac{\Big\langle 1 + 2\lambda^2\Big(\varepsilon(z_1)\,\varepsilon(\bar{z}_1) - \varepsilon(z_1)\,\varepsilon(z_2) - \varepsilon(z_1)\,\varepsilon(\bar{z}_2)\Big) + \lambda^4\,\varepsilon(z_1)\,\varepsilon(\bar{z}_1)\,\varepsilon(z_2)\,\varepsilon(\bar{z}_2)\Big\rangle_{\mathcal{M}_2}}{\Big\langle 1 + 2\lambda^2\Big(\varepsilon(z_1)\,\varepsilon(\bar{z}_1) + \varepsilon(z_1)\,\varepsilon(z_2) + \varepsilon(z_1)\,\varepsilon(\bar{z}_2)\Big) + \lambda^4\,\varepsilon(z_1)\,\varepsilon(\bar{z}_1)\,\varepsilon(z_2)\,\varepsilon(\bar{z}_2)\Big\rangle_{\mathcal{M}_2}}\,. \quad (4.6.74)$$

We used the symmetry that cyclically exchanges the sheets, and that the 3-point function of ε vanishes. We can also write

$$\frac{\mathrm{Tr}(\rho_{\mathsf{S}}^2)}{\mathrm{Tr}(\rho^2)} = 1 - \frac{2\lambda^2\,\Big\langle\varepsilon(z_1)\varepsilon(z_2) + \varepsilon(z_1)\varepsilon(\bar{z}_2)\Big\rangle_{\mathcal{M}_2}}{\Big\langle 1 + 2\lambda^2\Big(\varepsilon(z_1)\varepsilon(\bar{z}_1) + \varepsilon(z_1)\varepsilon(z_2) + \varepsilon(z_1)\varepsilon(\bar{z}_2)\Big) + \lambda^4\,\varepsilon(z_1)\varepsilon(\bar{z}_1)\varepsilon(z_2)\varepsilon(\bar{z}_2)\Big\rangle_{\mathcal{M}_2}}\,. \quad (4.6.75)$$

Correlation functions on $\mathcal{M}_2$ are obtained from the ones on the plane by a conformal transformation:

$$z_1 \mapsto \sqrt{\frac{z - \ell/2}{z + \ell/2}} \equiv g(z)\ , \qquad z_2 \mapsto -g(z)\ , \quad (4.6.76)$$

where the square root is taken with its branch cut along the negative real axis. The 2-point functions are then:

$$\big\langle \varepsilon(z_1)\,\varepsilon(\bar{z}_{1,2})\big\rangle_{\mathcal{M}_2} = \frac{\big|g'(z)\big|^{2\Delta_\varepsilon}}{\big|g(z)\mp g(\bar{z})\big|^{2\Delta_\varepsilon}}\,, \qquad \big\langle \varepsilon(z_1)\,\varepsilon(z_2)\big\rangle_{\mathcal{M}_2} = \frac{\big|g'(z)\big|^{2\Delta_\varepsilon}}{\big|2g(z)\big|^{2\Delta_\varepsilon}}\,. \tag{4.6.77}$$

The 4-point function on $\mathcal{M}_2$ is related to the one on the complex plane as

$$\big\langle \varepsilon(z_1)\,\varepsilon(\bar{z}_1)\,\varepsilon(z_2)\,\varepsilon(\bar{z}_2)\big\rangle_{\mathcal{M}_2} = \big|g'(z)\big|^{4\Delta_\varepsilon}\,\big\langle \varepsilon\big(g(z)\big)\,\varepsilon\big(g(\bar{z})\big)\,\varepsilon\big(-g(z)\big)\,\varepsilon\big(-g(\bar{z})\big)\big\rangle_{\mathbb{C}}\,, \tag{4.6.78}$$

and the latter is given by [171]:

$$\big\langle \varepsilon(w_1)\,\varepsilon(w_2)\,\varepsilon(w_3)\,\varepsilon(w_4)\big\rangle_{\mathbb{C}} = \left|\frac{1-\chi+\chi^2}{w_{14}\,w_{23}\,\chi}\right|^2\,, \tag{4.6.79}$$

where $w_{ij}=w_i-w_j$ and $\chi=(w_{12}\,w_{34})/(w_{13}\,w_{24})$ is the conformal cross-ratio.

We report a few plots of the resulting second Rényi asymmetry in Fig. 4.10. Notice that the asymmetry takes values in the interval $[0,\log 2]$. The asymmetry vanishes in both limits $\tau\to\infty$ and $\tau\to 0$: indeed the state is dominated by $1\boxtimes 1\,|0\rangle$ or by $\varepsilon\boxtimes 1\,|0\rangle$, respectively.

Large subsystem limit. When $\ell\to\infty$, the branch cut extends along the real line and correlation functions factorize. The 2-point functions behave as

$$\big\langle \varepsilon(z_1)\,\varepsilon(\bar{z}_1)\big\rangle_{\mathcal{M}_2} \sim \big\langle \varepsilon(z_1)\,\varepsilon(z_2)\big\rangle_{\mathcal{M}_2} \sim \frac{1}{\ell^2}\,, \qquad \big\langle \varepsilon(z_1)\,\varepsilon(\bar{z}_2)\big\rangle_{\mathcal{M}_2} \sim \frac{1}{(2\tau)^2}\,, \tag{4.6.80}$$

while the 4-point function factorizes through the identity channel:

$$\big\langle \varepsilon(z_1)\,\varepsilon(\bar{z}_1)\,\varepsilon(z_2)\,\varepsilon(\bar{z}_2)\big\rangle_{\mathcal{M}_2} \sim \frac{1}{(2\tau)^4}\,. \tag{4.6.81}$$

This gives the asymptotic behavior of the second Rényi asymmetry:

$$\Delta S^{(2)} = \log\frac{\big[1+\big(\frac{\lambda}{2\tau}\big)^2\big]^2}{1+\big(\frac{\lambda}{2\tau}\big)^4} + \mathcal{O}\big(\lambda^2/\ell^2\big)\,. \tag{4.6.82}$$

This expression matches with the Rényi asymmetry (4.6.37) with respect to the fusion algebra of the $\mathbb{Z}_2\times\mathbb{Z}_2$ TY symmetry acting on the circle Hilbert space of the full system.

Non-monotonicity of Rényi asymmetry. It is interesting to notice that Rényi asymmetries, differently from the Von Neumann asymmetry, are not always monotonic in the size of the subsystem. Indeed, when the field is inserted at $z=-i\tau$ and $\tau<\lambda$, the second Rényi asymmetry is not monotonic in ℓ, as shown

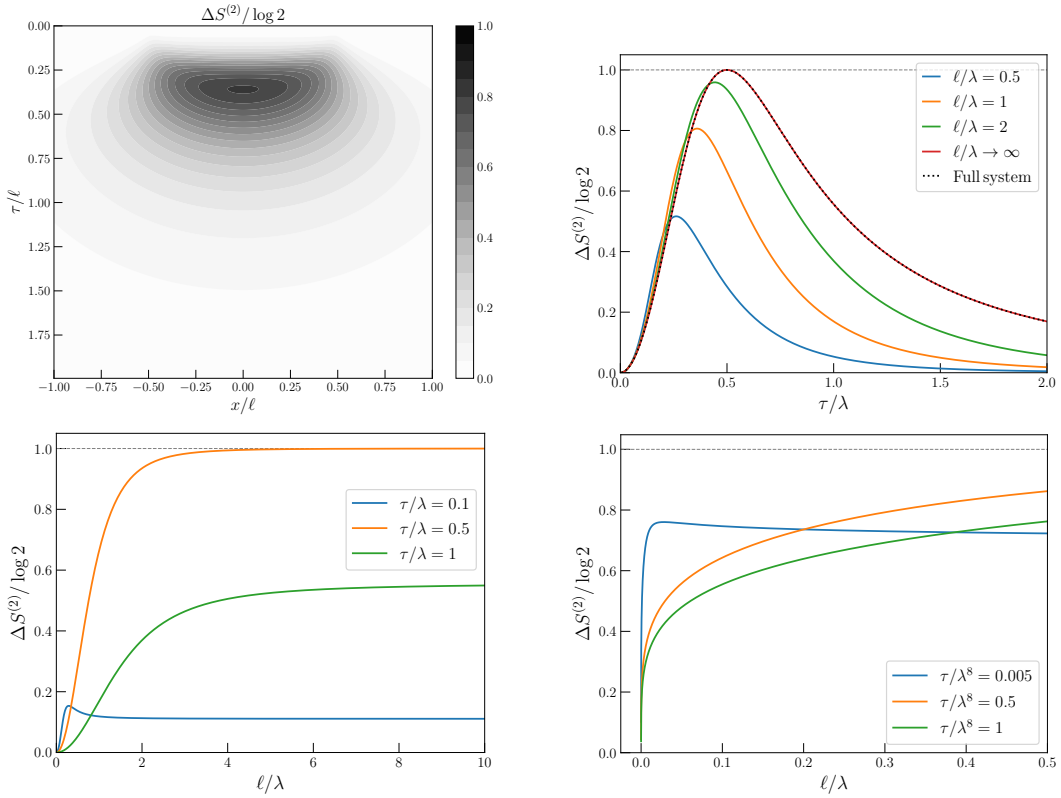


Figure 4.10: Top left: density plot of the second Rényi asymmetry of the state $\big(1 \boxtimes 1 + \lambda\,\varepsilon(z) \boxtimes 1\big)|0\rangle$ for $\lambda = \ell = 1$ and with $z = x - i\tau$. Top right: second Rényi asymmetry when the field is inserted at $z = -i\tau$ as a function of τ, for different values of ℓ (in units of λ). Bottom left: second Rényi asymmetry as a function of ℓ, for different positions of the field insertion at $z = -i\tau$. Bottom right: second Rényi asymmetry of the state $\big(1 + \lambda\,\sigma(-i\tau)\big)|0\rangle$ in the Ising CFT with respect to the ordinary $\mathbb{Z}_2$ spin-flip symmetry (that acts as the strip algebra of the $\mathsf{Vec}_{\mathbb{Z}_2}$ fusion category on the interval Hilbert space with symmetric boundary conditions).

in the bottom left panel of Fig. 4.10. This raises the question of whether such a counterintuitive behavior is a distinctive feature of asymmetries associated with noninvertible symmetries. The answer is negative: a simpler example involving a group-like symmetry also exhibits non-monotonic behavior. Specifically, we consider the state $\big(1 + \lambda\,\sigma(z)\big)|0\rangle$ in the Ising CFT (a single copy) and compute its second Rényi asymmetry with respect to the $\mathbb{Z}_2$ spin-flip symmetry over a subsystem, imposing symmetric conformal boundary conditions at the entangling surface — thus realizing a strip algebra isomorphic to $\mathbb{C}[\mathbb{Z}_2]$. The computation closely parallels the one described above: the second Rényi asymmetry is given by (4.6.73) and (4.6.74), with ε replaced by σ and λ assigned length dimension $\Delta_\sigma = \frac{1}{8}$. The relevant 4-point function of σ is provided in (4.6.84). In the bottom right panel of Fig. 4.10 we plot the second Rényi asymmetry as a function of the subsystem size ℓ, for a field insertion at $z = -i\tau$, showing a non-monotonic behavior for small

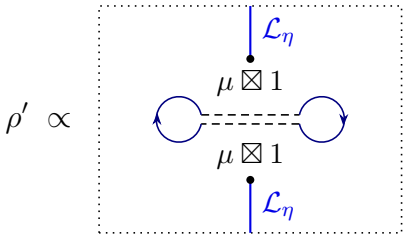


Figure 4.11: Path-integral representation of ρ', described above (4.6.83).

values of τ.

Case $\sigma \boxtimes 1$. Consider now the state created by inserting the operator $\mathcal{O}(z) = \sigma(z)\boxtimes 1$ with dimension $\Delta_\sigma = \frac{1}{8}$ at $z = x - i\tau$. As before, let ρ be the reduced density matrix on $A = \left[-\frac{\ell}{2}, \frac{\ell}{2}\right]$ obtained using the strongly-symmetric boundary condition. The symmetrized matrix ρ_{S} is obtained applying (4.6.63). The invertible lines can freely pass through ρ_{S}, while the noninvertible one changes the untwisted operator σ to the twisted (or disorder) operator μ (with a line $\mathcal{L}_\eta$ attached). Therefore $\rho_{\mathsf{S}} = \frac{1}{2}\big(\rho + \rho'\big)$, where ρ' is the reduced density matrix of the state created by $\mathcal{O}' = \mu \boxtimes 1$. Such a density matrix contains a line $\mathcal{L}_\eta$ that goes through infinity, as depicted in Fig. 4.11.

The second Rényi asymmetry takes the form

$$\Delta S^{(2)}[\rho] = \log 2 - \log\left[1 + \frac{\big\langle \sigma(z_1)\,\sigma(\bar{z}_1)\,\mu(z_2)\,\mu(\bar{z}_2)\big\rangle_{\mathcal{M}_2}}{\big\langle \sigma(z_1)\,\sigma(\bar{z}_1)\,\sigma(z_2)\,\sigma(\bar{z}_2)\big\rangle_{\mathcal{M}_2}}\right], \tag{4.6.83}$$

where we have used the equality of 4-point functions $\langle\sigma^4\rangle = \langle\mu^4\rangle$ as a consequence of Kramers–Wannier duality. On the plane one finds the following 4-point functions [96]:

$$\begin{aligned}
\big\langle \sigma(w_1)\,\sigma(w_2)\,\sigma(w_3)\,\sigma(w_4)\big\rangle_{\mathbb{C}} &= \frac{\big(1 + |\chi| + |1-\chi|\big)^{1/2}}{\sqrt{2}\,\big|w_{14}\,w_{23}\,\chi\big|^{1/4}} = \frac{\big|1+\sqrt{\chi}\big| + \big|1-\sqrt{\chi}\big|}{2\big|w_{14}\,w_{23}\,\chi\big|^{1/4}}\,, \\
\big\langle \sigma(w_1)\,\sigma(w_2)\,\mu(w_3)\,\mu(w_4)\big\rangle_{\mathbb{C}} &= \frac{\big(1 - |\chi| + |1-\chi|\big)^{1/2}}{\sqrt{2}\,\big|w_{14}\,w_{23}\,\chi\big|^{1/4}}\,,
\end{aligned} \tag{4.6.84}$$

where χ is the cross-ratio. The fields σ and μ, because of duality, have the same conformal dimension, therefore the conformal factors in the map between $\mathcal{M}_2$ and $\mathbb{C}$ simplify. This leads to the expression:

$$\Delta S^{(2)} = \log 2 - \log\left[1 + \left(\frac{1 - |\chi| + |1-\chi|}{1 + |\chi| + |1-\chi|}\right)^{1/2}\right], \tag{4.6.85}$$

where $w_1 = g(z)$, $w_2 = g(\bar{z})$, $w_3 = -g(z)$, $w_4 = -g(\bar{z})$. At finite subsystem size ℓ, the asymmetry vanishes in the limit $\tau \to \infty$ in which the field is inserted in the far

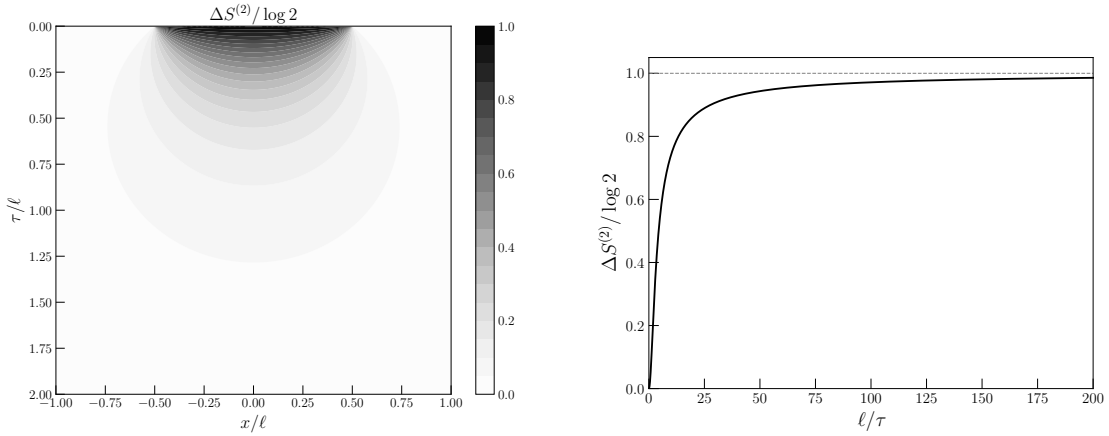


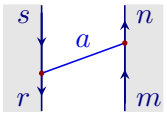
Figure 4.12: Second Rényi asymmetry of the state $\big(\sigma(z)\boxtimes 1\big)|0\rangle$ in two copies of the Ising CFT. Left: density plot of the Rényi asymmetry, as a function of the Euclidean insertion point $z = x - i\tau$. Right: Rényi asymmetry as a function of the subsystem size ℓ (measured in units of τ) for a field insertion at $z = -i\tau$.

Euclidean past. This is because symmetry breaking spreads over $\mathbb{R}$ and thus the subsystem only catches an infinitesimal fraction thereof. On the other hand, in the limit $\tau \to 0$ in which the field is inserted close to the real axis, the asymmetry is equal to $\log(2)$ if $x \in A$ and it vanishes if $x \notin A$. Finally, in the limit $\ell \to \infty$ that the subsystem size goes to infinity, the asymmetry is equal to $\log(2)$ irrespective of the insertion point. Plots of the Rényi asymmetry are in Fig. 4.12.

4.6.4 Ising symmetry — interval Hilbert space

As already mentioned in Sec. 4.6.2, the Ising fusion category admits only one indecomposable module category (that can describe boundary conditions): the regular one. In order to study the asymmetry on a subsystem, then, one has to employ the general procedure of Sec. 4.4.4. In the regular module the $\tilde{F}$-symbols are equal to the F-symbols, and we indicate the boundary conditions as $\{+, -, f\}$. Recall that the Ising symmetry has a multiplicity-free fusion ring, so no junction labels are necessary. Hence, we use the notation

$$H^{s,n}_{r,m}(a) \quad \equiv \quad \tag{4.6.86}$$



for basis elements of the strip algebra, which has dimension 34. The formula (4.4.13) for the strip-algebra product simplifies considerably, given the fact that every F-symbol is a symmetric and involutive matrix, and that every line is self-dual. We will not report it here, though.

The symmetrizer is given by a long expression. Let us write it sector by sector, in terms of the boundary conditions (r, m) for the reduced density matrix ρ.

- For a density matrix in the $(+,+)$ sector we have:

$$\rho_{\mathsf{S}} = \frac{1}{3}\left(H^{++}_{++}(1)\,\rho\,H^{++}_{++}(1) \,+\, H^{--}_{++}(\eta)\,\rho\,H^{++}_{--}(\eta) \,+\, \frac{1}{\sqrt{2}}\,H^{ff}_{++}(\mathcal{N})\,\rho\,H^{++}_{ff}(\mathcal{N})\right). \tag{4.6.87}$$

- In the $(-,-)$ sector:

$$\rho_{\mathsf{S}} = \frac{1}{3}\left(H^{--}_{--}(1)\,\rho\,H^{--}_{--}(1) \,+\, H^{++}_{--}(\eta)\,\rho\,H^{--}_{++}(\eta) \,+\, \frac{1}{\sqrt{2}}\,H^{ff}_{--}(\mathcal{N})\,\rho\,H^{--}_{ff}(\mathcal{N})\right). \tag{4.6.88}$$

- In the $(+,-)$ sector:

$$\rho_{\mathsf{S}} = \frac{1}{3}\left(H^{+-}_{+-}(1)\,\rho\,H^{+-}_{+-}(1) \,+\, H^{-+}_{+-}(\eta)\,\rho\,H^{+-}_{-+}(\eta) \,+\, \frac{1}{\sqrt{2}}\,H^{ff}_{+-}(\mathcal{N})\,\rho\,H^{+-}_{ff}(\mathcal{N})\right). \tag{4.6.89}$$

- In the $(f,+)$ sector:

$$\rho_{\mathsf{S}} = \frac{1}{4}\left(H^{f+}_{f+}(1)\,\rho\,H^{f+}_{f+}(1) \,+\, H^{f-}_{f+}(\eta)\,\rho\,H^{f+}_{f-}(\eta) \,+\, H^{+f}_{f+}(\mathcal{N})\,\rho\,H^{f+}_{+f}(\mathcal{N}) \,+\, H^{-f}_{f+}(\mathcal{N})\,\rho\,H^{f+}_{-f}(\mathcal{N})\right). \tag{4.6.90}$$

- In the $(f,-)$ sector:

$$\rho_{\mathsf{S}} = \frac{1}{4}\left(H^{f-}_{f-}(1)\,\rho\,H^{f-}_{f-}(1) \,+\, H^{f+}_{f-}(\eta)\,\rho\,H^{f-}_{f+}(\eta) \,+\, H^{-f}_{f-}(\mathcal{N})\,\rho\,H^{f-}_{-f}(\mathcal{N}) \,+\, H^{+f}_{f-}(\mathcal{N})\,\rho\,H^{f-}_{+f}(\mathcal{N})\right). \tag{4.6.91}$$

- In the (f,f) sector:

$$\rho_{\mathsf{S}} = \frac{1}{6}\left(H^{ff}_{ff}(1)\,\rho\,H^{ff}_{ff}(1) \,+\, H^{ff}_{ff}(\eta)\,\rho\,H^{ff}_{ff}(\eta)\right) + \frac{1}{3\sqrt{2}}\sum_{s,\,s'\,\in\,\{+,-\}} H^{ss'}_{ff}(\mathcal{N})\,\rho\,H^{ff}_{ss'}(\mathcal{N})\,. \tag{4.6.92}$$

The sectors not reported are easily obtained by exchanging left and right boundary conditions.

We now proceed to compute the entanglement and Rényi asymmetries of the vacuum (*i.e.*, without operator insertions). The procedure is analogous to the group-like case in Sec. 4.6.1.

Consider first a generic density matrix ρ in the $(+,+)$ sector, that we indicate as ρ_{++} (as in Fig. 4.7 left), to which we apply the symmetrizer (4.6.87). Using the strip algebra products $\big[H^{++}_{++}(1)\big]^2 = H^{++}_{--}(\eta)H^{--}_{++}(\eta) = \frac{1}{\sqrt{2}}H^{++}_{ff}(\mathcal{N})H^{ff}_{++}(\mathcal{N}) = H^{++}_{++}(1)$ and orthogonality between different boundary conditions, we find $\mathrm{Tr}\big[(\rho_{++})^n_{\mathsf{S}}\big] = 3^{1-n}\,\mathrm{Tr}(\rho^n_{++})$. Therefore the asymmetry of a state belonging to this sector is always

$$\Delta S^{(n)}[\rho_{++}] = \Delta S[\rho_{++}] = \log(3)\,. \tag{4.6.93}$$

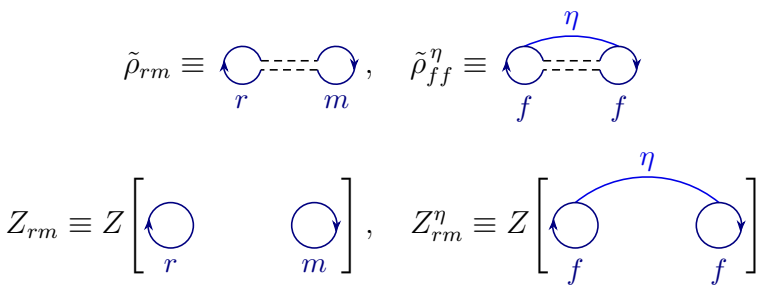


Figure 4.13: Path-integral definitions of various density matrices that enter in the symmetrization with respect to the strip algebra of the Ising fusion category with regular boundary conditions.

Exactly the same result is found for ρ_{--} and ρ_{+-}. This result is valid for any state, and in particular also for the vacuum. By the same argument one finds $\mathrm{Tr}\big[(\rho_{f+})^n_{\mathsf{S}}\big] = 4^{1-n}\,\mathrm{Tr}(\rho^n_{f+})$ and thus, for a generic density matrix ρ_{f+}:

$$\Delta S^{(n)}[\rho_{f+}] = \Delta S[\rho_{f+}] = \log(4)\ . \tag{4.6.94}$$

The same result is found for ρ_{f-}. Consider then the reduced density matrix of the vacuum in the (f,f) sector, that we indicate as ρ_{ff}, and whose symmetrizer is (4.6.92). When computing $\mathrm{Tr}\big[(\rho_{ff})^n_{\mathsf{S}}\big]$, to treat the first term in (4.6.92) one uses the products $H^{ff}_{ff}(a)H^{ff}_{ff}(b) = H^{ff}_{ff}(ab)$ for $a,b \in \{1,\eta\} \cong \mathbb{Z}_2$ and the fact that $H^{ff}_{ff}(a)$ commutes with ρ_{ff}. Since the number of lines $\mathcal{L}_\eta$ is always even, they annihilate among themselves. For the second term one uses $H^{ff}_{ss'}(\mathcal{N})H^{ss'}_{ff}(\mathcal{N}) = \frac{1}{\sqrt{2}}\big(H^{ff}_{ff}(1)+(ss')H^{ff}_{ff}(\eta)\big)$ with $s,s' = \pm 1$. When expanding $\mathrm{Tr}\big[(\rho_{ff})^n_{\mathsf{S}}\big]$, those terms with an odd number of lines $\mathcal{L}_\eta$ cancel out. Eventually $\mathrm{Tr}\big[(\rho_{ff})^n_{\mathsf{S}}\big] = 3^{1-n}\,\mathrm{Tr}(\rho^n_{ff})$ and hence

$$\Delta S^{(n)}[\rho_{ff}] = \Delta S[\rho_{ff}] = \log(3)\ . \tag{4.6.95}$$

In all cases, the asymmetries of the vacuum in a subsystem with fixed simple boundary conditions attain a nonzero value. This is expected since each simple boundary condition breaks the symmetry.

On the other hand, let us apply the averaging procedure of Sec. 4.4.4 to the vacuum state and consider the matrix (recall that $\tilde d_m = d_m$ in the regular module):

$$\rho = \frac{1}{D}\sum\nolimits_{rm} d_r\, d_m\, \rho_{rm}\ . \tag{4.6.96}$$

Here ρ_{rm} is the reduced density matrix of the vacuum with boundary conditions (r,m), as in Fig. 4.7 left but without insertions, the sum is over $r,m \in \{+,-,f\}$, and $D = \big(\sum d_m\big)^2$. It is convenient to write $\rho_{rm} = Z^{-1}_{rm}\,\tilde\rho_{rm}$ where, as in Sec. 4.4.4, $\tilde\rho_{rm}$ is the unnormalized density matrix while Z_{rm} is its trace. They are depicted

in Fig. 4.13. Since $\tilde{\rho}_{rm}$ come from the vacuum, the lines can move through them and the effect of the symmetrizer can be written as [42]

$$\begin{aligned}
(\tilde{\rho}_{++})_{\mathsf{S}} = (\tilde{\rho}_{--})_{\mathsf{S}} &= \frac{1}{3}\Big(\tilde{\rho}_{++} + \tilde{\rho}_{--} + \frac{1}{2}\,\tilde{\rho}_{ff} + \frac{1}{2}\,\tilde{\rho}^{\eta}_{ff}\Big)\,, \\
(\tilde{\rho}_{+-})_{\mathsf{S}} = (\tilde{\rho}_{-+})_{\mathsf{S}} &= \frac{1}{3}\Big(\tilde{\rho}_{+-} + \tilde{\rho}_{-+} + \frac{1}{2}\,\tilde{\rho}_{ff} - \frac{1}{2}\,\tilde{\rho}^{\eta}_{ff}\Big)\,, \\
(\tilde{\rho}_{f+})_{\mathsf{S}} = (\tilde{\rho}_{f-})_{\mathsf{S}} = (\tilde{\rho}_{+f})_{\mathsf{S}} = (\tilde{\rho}_{-f})_{\mathsf{S}} &= \frac{1}{4}\Big(\tilde{\rho}_{f+} + \tilde{\rho}_{f-} + \tilde{\rho}_{+f} + \tilde{\rho}_{-f}\Big)\,, \\
(\tilde{\rho}_{ff})_{\mathsf{S}} &= \frac{1}{3}\Big(\tilde{\rho}_{++} + \tilde{\rho}_{--} + \tilde{\rho}_{+-} + \tilde{\rho}_{-+} + \tilde{\rho}_{ff}\Big)\,.
\end{aligned} \tag{4.6.97}$$

Here $\tilde{\rho}^{\eta}_{ff}$ is a density matrix that contains a line $\mathcal{L}_\eta$ connecting the two boundaries of type f, as described in Fig. 4.13. To proceed, we use that $\lim_{\varepsilon\to 0} Z_{rm} \propto d_r d_m$, proven in Sec. 4.4.4. In the $\varepsilon \to 0$ limit, then, one immediately obtains the weak identity $\rho_{\mathsf{S}} = \rho$, valid when inserted into traces. We thus explicitly confirm that, in the limit, the asymmetries of the reduced vacuum density matrix vanish: $\Delta S^{(n)}[\rho] = \Delta S[\rho] = 0$.

Case $\mathbf{1 + \lambda\,\varepsilon}$. We now wish to compute the asymmetry of an excited state $\mathcal{O}(z)|0\rangle$ obtained by the operator insertion $\mathcal{O}(z) = 1 + \lambda\,\varepsilon(z)$ at $z = -i\tau$, along with its mirror image $\mathcal{O}^\dagger(\bar{z})$. The reduced density matrix is as in (4.6.96), but now ρ_{rm} contain the insertions. When we swipe a line $\mathcal{L}_{\mathcal{N}}$ through them, this time $\mathcal{O} \mapsto \mathcal{O}' = 1 - \lambda\,\varepsilon$ and we call ρ'_{rm} the reduced density matrices with that insertion. The action of the symmetrizer can be written as

$$\begin{aligned}
(\tilde{\rho}_{++})_{\mathsf{S}} = (\tilde{\rho}_{--})_{\mathsf{S}} &= \frac{\tilde{\rho}_{++} + \tilde{\rho}_{--}}{3} + \frac{\tilde{\rho}'_{ff} + \tilde{\rho}^{\eta\prime}_{ff}}{6}, \qquad (\tilde{\rho}_{f+})_{\mathsf{S}} = (\tilde{\rho}_{f-})_{\mathsf{S}} = \frac{\tilde{\rho}_{f+} + \tilde{\rho}_{f-} + \tilde{\rho}'_{+f} + \tilde{\rho}'_{-f}}{4}, \\
(\tilde{\rho}_{+-})_{\mathsf{S}} = (\tilde{\rho}_{-+})_{\mathsf{S}} &= \frac{\tilde{\rho}_{+-} + \tilde{\rho}_{-+}}{3} + \frac{\tilde{\rho}'_{ff} - \tilde{\rho}^{\eta\prime}_{ff}}{6}, \qquad (\tilde{\rho}_{+f})_{\mathsf{S}} = (\tilde{\rho}_{-f})_{\mathsf{S}} = \frac{\tilde{\rho}'_{f+} + \tilde{\rho}'_{f-} + \tilde{\rho}_{+f} + \tilde{\rho}_{-f}}{4}, \\
(\tilde{\rho}_{ff})_{\mathsf{S}} &= \frac{\tilde{\rho}'_{++} + \tilde{\rho}'_{--} + \tilde{\rho}'_{+-} + \tilde{\rho}'_{-+} + \tilde{\rho}_{ff}}{3}.
\end{aligned} \tag{4.6.98}$$

This allows one to compute traces of powers of ρ_{S}. For example, in the $\varepsilon \to 0$ limit, one can write the compact expression

$$\lim_{\varepsilon\to 0} \frac{\mathrm{Tr}(\rho_{\mathsf{S}}^2)}{\mathrm{Tr}(\rho^2)} = \frac{1}{3}\,\frac{\mathrm{Tr}\big[(3-\sqrt{2})\,\tilde{\rho}^{\,2} + \sqrt{2}\,\tilde{\rho}\,\tilde{\rho}'\big]}{\mathrm{Tr}(\tilde{\rho}^{\,2})}\,. \tag{4.6.99}$$

The notation on the r.h.s. should merely be interpreted as an instruction to construct a branched Riemann surface, obtained from the gluing of unnormalized density

[42] Using the tube algebra action (4.5.4) on boundary conditions, one can prove various relations among the vacuum traces, for $n \in \mathbb{Z}_{>0}$: $\mathrm{Tr}(\tilde{\rho}^n_{++}) = \mathrm{Tr}(\tilde{\rho}^n_{--})$, $\mathrm{Tr}(\tilde{\rho}^n_{+-}) = \mathrm{Tr}(\tilde{\rho}^n_{-+})$, $\mathrm{Tr}(\tilde{\rho}^n_{ff}) = \mathrm{Tr}(\tilde{\rho}^n_{++} + \tilde{\rho}^n_{+-})$, $\mathrm{Tr}(\tilde{\rho}^{n-1}_{ff}\tilde{\rho}^{\eta}_{ff}) = \mathrm{Tr}(\tilde{\rho}^n_{++} - \tilde{\rho}^n_{+-})$, as well as $\mathrm{Tr}(\tilde{\rho}^n_{f+}) = \mathrm{Tr}(\tilde{\rho}^n_{f-}) = \mathrm{Tr}(\tilde{\rho}^n_{+f}) = \mathrm{Tr}(\tilde{\rho}^n_{-f})$. Besides, one finds the operator relations $\tilde{\rho}^{\eta}_{ff}\tilde{\rho}^{\eta}_{ff} = \tilde{\rho}_{ff}\tilde{\rho}_{ff}$ and $[\tilde{\rho}_{ff}, \tilde{\rho}^{\eta}_{ff}] = 0$. One can then verify that S is trace-preserving.

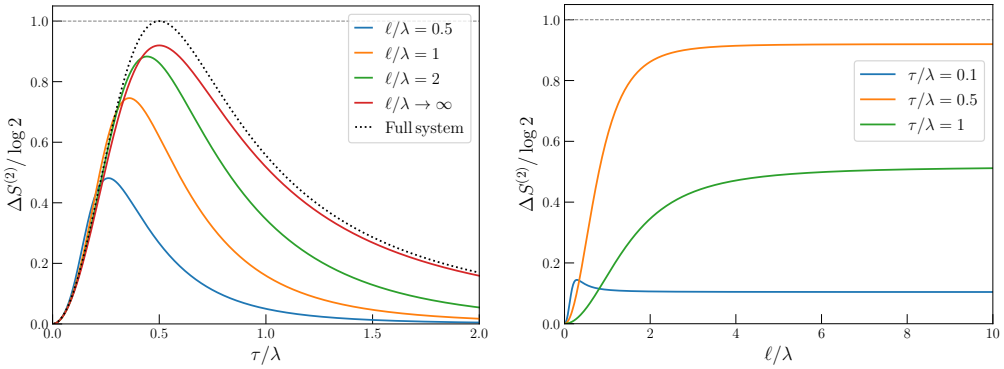


Figure 4.14: Second Rényi asymmetry of the state $\big(1+\lambda\,\varepsilon(z)\big)\,|0\rangle$ in the Ising CFT, with "averaged" boundary conditions at the entangling surface. Left: asymmetry when the field is inserted at $z=-i\tau$, as a function of τ, for different values of ℓ (in units of λ). We compare it with the asymmetry of the full system (dotted line) computed with respect to the fusion algebra. Right: asymmetry as a function of ℓ, for different positions of the field insertion at $z=-i\tau$.

matrices followed by the $\varepsilon\to 0$ limit. The expression can be rewritten in terms of correlation functions on a two-sheeted Riemann surface $\mathcal{M}_2$:

$$\frac{\mathrm{Tr}(\rho_{\mathsf{S}}^2)}{\mathrm{Tr}(\rho^2)} = 1 - \frac{\frac{4\sqrt{2}}{3}\,\lambda^2\left\langle \varepsilon(z_1)\varepsilon(z_2)+\varepsilon(z_1)\varepsilon(\bar z_2)\right\rangle_{\mathcal{M}_2}}{\left\langle 1+2\lambda^2\Big(\varepsilon(z_1)\varepsilon(\bar z_1)+\varepsilon(z_1)\varepsilon(z_2)+\varepsilon(z_1)\varepsilon(\bar z_2)\Big)+\lambda^4\,\varepsilon(z_1)\varepsilon(\bar z_1)\varepsilon(z_2)\varepsilon(\bar z_2)\right\rangle_{\mathcal{M}_2}} \tag{4.6.100}$$

where we used the same notation as in Sec. 4.6.3 and cyclic permutation symmetry of the sheets. This can be used to obtain the second Rényi asymmetry, of which we present some plots in Fig. 4.14 (more generally, the n-th Rényi asymmetry can be written in terms of correlation functions up to $2n$ points). Comparing (4.6.100) with (4.6.75), the two expressions are very similar. Indeed, the second Rényi asymmetry $\Delta S^{(2)}[\rho] = -\log\big[\mathrm{Tr}(\rho_{\mathsf{S}}^2)/\,\mathrm{Tr}(\rho^2)\big]$ of $(1+\lambda\,\varepsilon)|0\rangle$ in the Ising CFT is very similar to (in fact, just slightly smaller than) the one of $(1+\lambda\,\varepsilon\boxtimes 1)|0\rangle$ in two copies of the Ising CFT, plotted in Fig. 4.10.

In the large subsystem limit $\ell\to\infty$, correlation functions factorize as discussed around (4.6.82). For the Ising CFT, where $\Delta_\varepsilon = 1$, we obtain:

$$\lim_{\ell\to\infty}\Delta S^{(2)} = -\log\left[1-\frac{\frac{4\sqrt{2}}{3}\left(\frac{\lambda}{2\tau}\right)^2}{\left(1+\left(\frac{\lambda}{2\tau}\right)^2\right)^2}\right]. \tag{4.6.101}$$

This, as a function of τ/λ, yields a very similar curve to the second Rényi asymmetry of the full system (4.6.37) computed with respect to the fusion algebra, just slightly smaller (the maximum of (4.6.101) is $\log\big(\frac{3}{3-\sqrt{2}}\big)$, smaller than $\log(2)$) . We compare them in Fig. 4.14. So in this case the large subsystem limit of the asymmetry computed with the averaging procedure is not identical to the asymmetry of the full system.

4.6.5 Fibonacci fusion category

The Fibonacci fusion category has 2 simple objects: $\mathcal{L}_1$, $\mathcal{L}_W$. Their fusion rule is [43]

$$\mathcal{L}_W \times \mathcal{L}_W = \mathcal{L}_1 + \mathcal{L}_W \tag{4.6.102}$$

and it is commutative. The quantum dimension of $\mathcal{L}_W$ is

$$d_W = \frac{1+\sqrt{5}}{2} \equiv \varphi \tag{4.6.103}$$

which is the golden ratio (*i.e.*, the positive solution of the equation $\varphi^2 = \varphi + 1$). Both lines are self-dual and $\varkappa_W = 1$. The only nontrivial F-symbol, in terms of $a, b \in \{1, W\}$, is [44]

$$\left[F^W_{WWW}\right]_{ab} = \begin{pmatrix} \varphi^{-1} & \varphi^{-1/2} \\ \varphi^{-1/2} & -\varphi^{-1} \end{pmatrix} , \tag{4.6.104}$$

while all other F-symbols allowed by fusion are equal to 1. The symmetrizer for the fusion algebra is determined by the inverse bilinear form $\tilde{K}$ and takes the form:

$$\rho_{\mathsf{S}} = \frac{1}{5}\left(3\,\rho - \mathcal{L}_W\,\rho - \rho\,\mathcal{L}_W + 2\,\mathcal{L}_W\,\rho\,\mathcal{L}_W\right) . \tag{4.6.105}$$

The fusion algebra has two one-dimensional representations $R_\pm$, where $R_+(\mathcal{L}_W) = \varphi$ while $R_-(\mathcal{L}_W) = -\varphi^{-1}$. The corresponding projectors are given by

$$P_+ = 5^{-\frac{1}{2}}\left(\varphi^{-1}\mathcal{L}_1 + \mathcal{L}_W\right) , \qquad P_- = 5^{-\frac{1}{2}}\left(\varphi\,\mathcal{L}_1 - \mathcal{L}_W\right) . \tag{4.6.106}$$

Spontaneous symmetry breaking. Like in the case of Ising, the only indecomposable module category over the Fibonacci fusion category is the regular one. This means that in a Fibonacci-symmetric gapped phase, the symmetry is always completely spontaneously broken. The clustering vacua form a 2-dimensional NIM-rep spanned by $|1\rangle$ and $|W\rangle$, and

$$\mathcal{L}_W\,|1\rangle = |W\rangle \ , \qquad \mathcal{L}_W\,|W\rangle = |1\rangle + |W\rangle \ , \tag{4.6.107}$$

where $\langle 1|1\rangle = \langle W|W\rangle = 1$. Consider the pure state $\rho = |1\rangle\langle 1|$. Using the symmetrizer (4.6.105), in the basis above we find

$$\rho = |1\rangle\langle 1| \qquad \Rightarrow \qquad \rho_{\mathsf{S}} = \frac{1}{5}\begin{pmatrix} 3 & -1 \\ -1 & 2 \end{pmatrix} . \tag{4.6.108}$$

[43] The Fibonacci fusion category is also a specific instance ($N = 1$) of the Haagerup–Izumi categories, which we will study in Sec. 4.6.6.

[44] There is a unique fusion category whose fusion ring is (4.6.102) and that has unitary F-symbols, see *e.g.*[149, 172]. This category occurs for example as a subsymmetry of the tricritical Ising model [55].

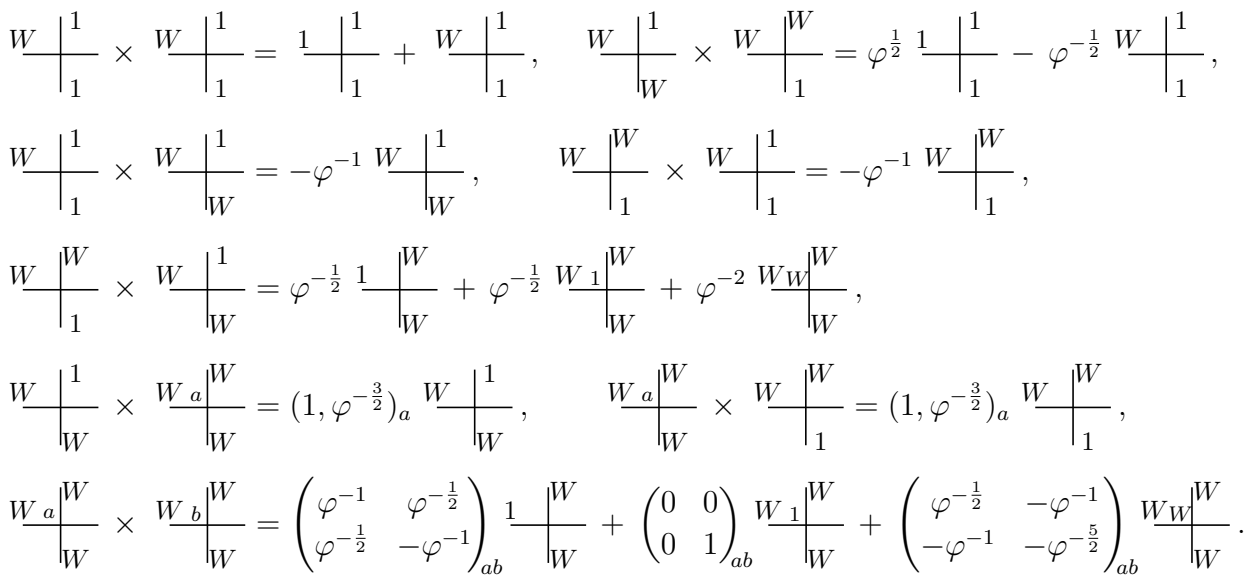


Figure 4.15: Nontrivial products in the tube algebra of the Fibonacci fusion category.

Defining

$$\phi_+ = \frac{\sqrt{5}+1}{2\sqrt{5}} = \frac{\varphi}{\sqrt{5}}\,, \qquad \phi_- = \frac{\sqrt{5}-1}{2\sqrt{5}} = \frac{\varphi^{-1}}{\sqrt{5}}\,, \tag{4.6.109}$$

the eigenvalues of ρ_{S} are $\{\phi_+, \phi_-\}$. Then the Rényi asymmetries are $\Delta S^{(n)} = \frac{1}{1-n}\log\big(\phi_+^n + \phi_-^n\big)$ while the entanglement asymmetry is

$$\Delta S = -\phi_+\log\phi_+ - \phi_-\log\phi_- = \frac{1}{2}\log 5 - \frac{1}{\sqrt{5}}\,\mathrm{arccoth}(\sqrt{5}) \simeq 0.5895\,. \tag{4.6.110}$$

This value is smaller than $\log(2)$, the asymmetry for a spontaneously broken group of order 2. For the other vacuum:

$$\rho = |W\rangle\langle W| \qquad \Rightarrow \qquad \rho_{\mathsf{S}} = \frac{1}{5}\begin{pmatrix} 2 & 1 \\ 1 & 3 \end{pmatrix} \tag{4.6.111}$$

which gives the same asymmetries (because ρ_{S} has the same eigenvalues).

Tube algebra. This has been discussed, *e.g.*, in [149]. It has dimension 7. The elements



(4.6.112)

behave as the identity in the untwisted and twisted sector, respectively. The nonvanishing products are in Fig. 4.15. The algebra has three 1-dimensional and one 2-dimensional irreducible representations, that we now describe.

- A 1-dimensional representation $\mathcal{F}_1$ with space $V = \mathbb{C}_1$:

$$\mathcal{F}_1\left(\begin{smallmatrix} 1 & \vert & 1 \\ \multicolumn{3}{c}{\text{---}\!\!+\!\!\text{---}} \\ & \vert & 1 \end{smallmatrix}\right) = 1\,, \qquad \mathcal{F}_1\left(\begin{smallmatrix} W & \vert & 1 \\ \multicolumn{3}{c}{\text{---}\!\!+\!\!\text{---}} \\ & \vert & 1 \end{smallmatrix}\right) = \varphi\,, \tag{4.6.113}$$

  while all other ones are mapped to zero. It represents genuine local operators invariant under the symmetry (up to multiplication by the quantum dimension of $\mathcal{L}_W$).

- Two 1-dimensional representations $\mathcal{F}_W$ and $\mathcal{F}_W^*$ with space $V = \mathbb{C}_W$, and

$$\mathcal{F}_W\left(\begin{smallmatrix} 1 & \vert & W \\ \multicolumn{3}{c}{\text{---}\!\!+\!\!\text{---}} \\ & \vert & W \end{smallmatrix}\right) = 1\,, \quad \mathcal{F}_W\left(\begin{smallmatrix} W & \vert & W \\ \multicolumn{3}{c}{\text{---}\!\!+\!\!\text{---}} \\ & \vert & W \end{smallmatrix}\right) = e^{\frac{4\pi i}{5}}\,, \quad \mathcal{F}_W\left(\begin{smallmatrix} WW & \vert & W \\ \multicolumn{3}{c}{\text{---}\!\!+\!\!\text{---}} \\ & \vert & W \end{smallmatrix}\right) = e^{-\frac{3\pi i}{5}}\varphi^{\frac{1}{2}}\,, \tag{4.6.114}$$

  while all other ones are zero. It represents W-twisted operators, that remain W-twisted under the action of $\mathcal{L}_W$. Notice that there are two actions of $\mathcal{L}_W$ on these operators.

- One 2-dimensional representation $\mathcal{F}_2$ with space $V = \mathbb{C}_1 \oplus \mathbb{C}_W$ and

$$\mathcal{F}_2\left(\begin{smallmatrix} 1 & \vert & 1 \\ \multicolumn{3}{c}{\text{---}\!\!+\!\!\text{---}} \\ & \vert & 1 \end{smallmatrix}\right) = \begin{pmatrix} 1 & 0 \\ 0 & 0 \end{pmatrix}, \qquad \mathcal{F}_2\left(\begin{smallmatrix} W & \vert & 1 \\ \multicolumn{3}{c}{\text{---}\!\!+\!\!\text{---}} \\ & \vert & 1 \end{smallmatrix}\right) = \begin{pmatrix} -\varphi^{-1} & 0 \\ 0 & 0 \end{pmatrix}, \tag{4.6.115}$$

$$\mathcal{F}_2\left(\begin{smallmatrix} 1 & \vert & W \\ \multicolumn{3}{c}{\text{---}\!\!+\!\!\text{---}} \\ & \vert & W \end{smallmatrix}\right) = \begin{pmatrix} 0 & 0 \\ 0 & 1 \end{pmatrix}, \qquad \mathcal{F}_2\left(\begin{smallmatrix} W & \vert & W \\ \multicolumn{3}{c}{\text{---}\!\!+\!\!\text{---}} \\ & \vert & W \end{smallmatrix}\right) = \begin{pmatrix} 0 & 0 \\ 0 & 1 \end{pmatrix}, \tag{4.6.116}$$

$$\mathcal{F}_2\left(\begin{smallmatrix} W & \vert & W \\ \multicolumn{3}{c}{\text{---}\!\!+\!\!\text{---}} \\ & \vert & 1 \end{smallmatrix}\right) = \begin{pmatrix} 0 & 0 \\ x & 0 \end{pmatrix}, \qquad \mathcal{F}_2\left(\begin{smallmatrix} W & \vert & 1 \\ \multicolumn{3}{c}{\text{---}\!\!+\!\!\text{---}} \\ & \vert & W \end{smallmatrix}\right) = \begin{pmatrix} 0 & x \\ 0 & 0 \end{pmatrix}, \tag{4.6.117}$$

$$\mathcal{F}_2\left(\begin{smallmatrix} WW & \vert & W \\ \multicolumn{3}{c}{\text{---}\!\!+\!\!\text{---}} \\ & \vert & W \end{smallmatrix}\right) = \begin{pmatrix} 0 & 0 \\ 0 & \varphi^{-\frac{3}{2}} \end{pmatrix}, \qquad x = 5^{\frac{1}{4}}\varphi^{-\frac{1}{4}}\,.$$

  It represents a doublet of an untwisted local operator $\mathcal{O}_1$ and a W-twisted operator $\mathcal{O}_W$ that get mixed under the action of $\mathcal{L}_W$.

Full and reduced strip algebras. The only indecomposable module category is the regular one. The corresponding strip algebra has dimension 13, and a basis is given by the elements:



where dashed lines are $\mathcal{L}_1$ while solid lines are $\mathcal{L}_W$. One easily verifies that the boundary $\hat{\mathcal{B}} = \mathcal{L}_W$ provides a weakly-symmetric boundary condition [106], and the

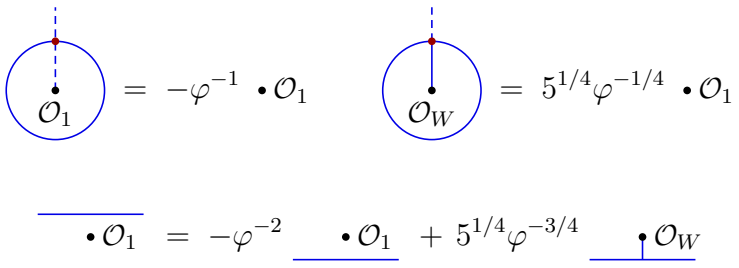


Figure 4.16: Left: lasso action of the Fibonacci tube algebra on the doublet of operators $(\mathcal{O}_1, \mathcal{O}_W)$, extracted from (4.6.115). Right: swiping action of the line $\mathcal{L}_W$ across $\mathcal{O}_1$. The coefficients have been fixed by separately completing the diagram from above and from below to form a circle, and by using the lasso actions on the left.

corresponding reduced strip algebra has dimension 2. In terms of the generators

$$\mathcal{S}_1 \;=\; \left|\text{----}\right| \,, \qquad\qquad \mathcal{S}_W \;=\; \left|\text{——}\right| \,, \tag{4.6.118}$$

the reduced strip algebra is commutative, $\mathcal{S}_1$ is its identity, and the nontrivial product is

$$\mathcal{S}_W \times \mathcal{S}_W = \mathcal{S}_1 + \varphi^{-\frac{3}{2}}\, \mathcal{S}_W \,. \tag{4.6.119}$$

This algebra is very similar to the original fusion algebra (4.6.102), and it is semisimple. The symmetrizer with respect to the reduced strip algebra, computed using (4.2.11), takes the form

$$\rho_{\mathsf{S}} = \frac{1}{2}\left(\rho + \frac{1}{4\varphi^3+1}\left(1-2\varphi^{3/2}\mathcal{S}_W\right)\rho\left(1-2\varphi^{3/2}\mathcal{S}_W\right)\right) . \tag{4.6.120}$$

For the asymmetry of the vacuum, it is clear that the density matrix $\rho = \tilde{\rho}_{WW}/Z_{WW}$ (using the notation of Fig. 4.13) commutes with the action of the reduced strip algebra (4.6.118) (because there is a single boundary condition involved). Hence its asymmetry is zero.

We then compute the asymmetry of an excited state created by the insertion of an untwisted operator. We choose an operator transforming as $\mathcal{O}_1$ in the two-dimensional tube-algebra representation $\mathcal{F}_2$ in (4.6.115) (because the one-dimensional representations are either trivial or contain twisted-sector operators only). As above, we denote by $\mathcal{O}_1$ and $\mathcal{O}_W$ the two operators spanning the 2d irreducible representation, and we let ρ be the reduced density matrix for the state $\mathcal{O}_1(z)|0\rangle$. In order to compute the second Rényi asymmetry, we need to understand the swiping action of the line $\mathcal{L}_W$ across the operator $\mathcal{O}_1$. By looking at (4.6.115), it is clear that this will be a linear combination of $\mathcal{O}_1$ and $\mathcal{O}_W$. The result is reported in Fig. 4.16. When swiping $\mathcal{L}_W$ through ρ, which contains two instances of $\mathcal{O}_1$, it is also useful to perform an F-move described by the F-symbols (4.6.104). Consider

now the limit $\varepsilon \to 0$ of small radius for the discs at the entangling surfaces. The traces of products of density matrices can be written in terms of partition functions on a replicated manifold, with the weakly-symmetric boundary condition at the entangling surfaces, and possibly with a line $\mathcal{L}_W$ connecting the two boundaries or connecting $\mathcal{O}_W$ to one of the boundaries. As discussed around (4.4.31), those partition functions can be analyzed by mapping the geometry to a cylinder and expressing them as amplitudes of Cardy states evolved in the closed channel. If the Cardy states are untwisted, the limit $\varepsilon \to 0$ simply produces two multiplicative g-factors, as in (4.4.29). If the Cardy states are twisted, instead, the ground state in the closed channel necessarily has higher energy than the untwisted vacuum, and the amplitude is suppressed by a positive power of ε. It follows that, in the $\varepsilon \to 0$ limit, partition functions involving a residual line $\mathcal{L}_W$ connected to one or both boundaries do not contribute.

For instance, in the computation of the second moment $\mathrm{Tr}(\rho_S^2)$, we can write

$$\rho\left(1-2\varphi^{3/2}\mathcal{S}_W\right)\rho\left(1-2\varphi^{3/2}\mathcal{S}_W\right) = \left(1+4\varphi^{-1}\right)\rho + 4\cdot 5^{1/2}\varphi\,\rho' + \dots\ , \quad (4.6.121)$$

where ρ' is as ρ but with $\mathcal{O}_W$ in place of $\mathcal{O}_1$ and with a line $\mathcal{L}_W$ connecting the two operators, similarly to Fig. 4.11, while the dots represent terms that are suppressed in the $\varepsilon \to 0$ limit once the trace is taken. In the end, up to an overall normalization which cancels in the ratio, we find:

$$\begin{aligned}\mathrm{Tr}\big(\rho_S^2\big) \ &\propto\ \big(11\sqrt{5}\ -24\big)\,\langle\mathcal{O}_1^\dagger\mathcal{O}_1\mathcal{O}_1^\dagger\mathcal{O}_1\rangle_{\mathcal{M}_2} + \big(25-11\sqrt{5}\big)\,\langle\mathcal{O}_1^\dagger\mathcal{O}_1\mathcal{O}_W^\dagger\mathcal{O}_W\rangle_{\mathcal{M}_2}\ ,\\ \mathrm{Tr}\big(\rho^2\big) \ &\propto\ \langle\mathcal{O}_1^\dagger\mathcal{O}_1\mathcal{O}_1^\dagger\mathcal{O}_1\rangle_{\mathcal{M}_2}\ ,\end{aligned} \quad (4.6.122)$$

where the correlators are computed on the 2-sheeted Riemann surface $\mathcal{M}_2$. Hence:

$$\Delta S^{(2)} = -\log\left[\big(11\sqrt{5}\ -24\big) + \big(25-11\sqrt{5}\big)\,\frac{\langle\mathcal{O}_1^\dagger\mathcal{O}_1\mathcal{O}_W^\dagger\mathcal{O}_W\rangle_{\mathcal{M}_2}}{\langle\mathcal{O}_1^\dagger\mathcal{O}_1\mathcal{O}_1^\dagger\mathcal{O}_1\rangle_{\mathcal{M}_2}}\right]\ . \quad (4.6.123)$$

In the limit of a large subsystem, the correlation four-point functions factorize into two-point functions, see also the discussion around (4.6.27). While the correlator at denominator $\langle\mathcal{O}_1^\dagger\mathcal{O}_1\mathcal{O}_1^\dagger\mathcal{O}_1\rangle_{\mathcal{M}_2}$ has a conformal block decomposition dominated by the identity channel and thus $\langle\mathcal{O}_1^\dagger\mathcal{O}_1\mathcal{O}_1^\dagger\mathcal{O}_1\rangle_{\mathcal{M}_2} \simeq \langle\mathcal{O}_1^\dagger\mathcal{O}_1\rangle_{\mathbb{C}}^2$, in the numerator the OPE $\mathcal{O}_1^\dagger\mathcal{O}_W$ does not contain the identity channel and therefore, keeping into account that $\mathcal{O}_1$ and $\mathcal{O}_W$ have the same conformal dimension, the correlator $\langle\mathcal{O}_1^\dagger\mathcal{O}_1\mathcal{O}_W^\dagger\mathcal{O}_W\rangle_{\mathcal{M}_2}$ is further suppressed. We conclude that, in the large subsystem limit, the second Rényi asymmetry becomes

$$\Delta S^{(2)} = -\log\big(11\sqrt{5}\ -24\big) \simeq 0.516\ . \quad (4.6.124)$$

It is interesting to notice that this value is smaller than the second Rényi asymmetry of the full system computed with respect to the tube algebra. Indeed, by symmetrizing with respect to the tube algebra, one immediately gets $\Delta S^{(n)} = \Delta S = \log(2)$

because $\mathcal{O}_1$ belongs to an irreducible representation of dimension 2, see the discussion after (4.6.51).[45]

4.6.6 Haagerup fusion ring

The simplest fusion category whose product rules are both noninvertible and non-Abelian is the Haagerup fusion category [173–175], that we indicate as $H_{(3)}$. There exists a generalization to Haagerup–Izumi fusion categories [175–178] that we indicate as $H_{(N)}$, with $N > 3$. In this section we will only analyze the fusion algebra, hence we do not report the F-symbols of the category.[46] The fusion ring of $H_{(N)}$ is generated by the objects $\{\mathbb{1}, a, \varrho\}$ subject to the conditions

$$a^N = \mathbb{1} \,, \qquad a \times \varrho = \varrho \times a^{-1} \,, \qquad \varrho^2 = \mathbb{1} + \sum\nolimits_{j=0}^{N-1} a^j \times \varrho \,. \tag{4.6.125}$$

We see that there is a $\mathbb{Z}_N$ subsymmetry and that, for $N \geq 3$, the element ϱ does not commute with a and thus the multiplication is non-Abelian. Conjugation is given by

$$\bar{a} = a^{-1} \,, \qquad \bar{\varrho} = \varrho \,, \qquad \overline{a^j \times \varrho} = a^j \times \varrho \,. \tag{4.6.126}$$

Notice that $H_{(1)}$ coincides with the Fibonacci (commutative) fusion ring that we already discussed in Sec. 4.6.5, while $H_{(2)}$ is the fusion ring of the $SO(3)_6$ WZW model.

The fusion algebra is $2N$-dimensional and a basis is given by the elements

$$\{\mathbb{1}, a, \ldots, a^{N-1}, \varrho, a\varrho, \ldots, a^{N-1}\varrho\} \,. \tag{4.6.127}$$

The symmetrizer with respect to it can be written as:

$$\rho_{\mathsf{S}} = \frac{1}{2N} \sum_{\mathcal{L}} \mathcal{L}\,\rho\,\mathcal{L}^\dagger + \frac{1}{2(N^2+4)} \Big(A\,\rho\,A - B\,\rho\,B \Big) - \frac{1}{N(N^2+4)} \Big(A\,\rho\,B + B\,\rho\,A \Big) \tag{4.6.128}$$

where in the first term we summed over all simple lines, while

$$A = \mathbb{1} + a + \ldots + a^{N-1} = A^\dagger \,, \qquad B = \varrho + a\varrho + \ldots + a^{N-1}\varrho = B^\dagger \,. \tag{4.6.129}$$

[45] On the other hand, the asymmetry with respect to the fusion algebra vanishes: $\Delta S^{(n)} = \Delta S = 0$. To see this, we should restrict the 2d representation $\mathcal{F}_2$ of the tube algebra to its untwisted sector, corresponding to the fusion algebra, and determine how $\mathcal{O}_1$ decomposes in irreducible fusion-algebra representations. From (4.6.115), $\mathcal{O}_1$ lands in the single representation R_-. Since this is one-dimensional, the asymmetry vanishes.

[46] The F-symbols of $H_{(3)}$ can be found in [178, 179]. The F-symbols in [178] are in a particularly convenient gauge, which makes the expressions extremely compact. Numerical evidence for the existence of a CFT with Haagerup symmetry was given in [180]. The F-symbols of $H_{(N)}$ with $3 \leq N \leq 15$ odd can be found in [178].

Let us list the irreducible representations of the fusion algebra. For N odd, there are two 1-dimensional representations R_+, R_- and $\frac{N-1}{2}$ 2-dimensional representations R_j. For N even, there are four 1-dimensional representations R_+, R_-, $R_{\tilde{+}}$, $R_{\tilde{-}}$ and $\frac{N-2}{2}$ 2-dimensional representations R_j. The 1-dimensional representations are:

$$\begin{aligned} R_\pm &: \qquad a = 1 \,, \qquad\qquad \varrho = \tfrac{1}{2}\big(N \pm \sqrt{N^2+4}\big) \,, \\ R_{\tilde{\pm}} &: \qquad a = -1 \,, \qquad\qquad \varrho = \pm 1 \,. \end{aligned} \tag{4.6.130}$$

The 2-dimensional representations R_j with $j = 1, \dots, \frac{N-1}{2}$ (for N odd) or $j = 1, \dots, \frac{N-2}{2}$ (for N even) are:

$$R_j : \qquad a = \begin{pmatrix} \zeta^j & 0 \\ 0 & \zeta^{-j} \end{pmatrix} \,, \qquad \varrho = \begin{pmatrix} 0 & 1 \\ 1 & 0 \end{pmatrix} \,, \qquad \zeta = e^{\frac{2\pi i}{N}} \,. \tag{4.6.131}$$

Spontaneous symmetry breaking. For the Haagerup fusion ring with $N = 3$, let us consider a TQFT describing the full SSB of the symmetry, thus giving 6 vacua. These transform in the regular representation. The inverse bilinear form in the fusion algebra is given by

$$\tilde{K} = \frac{1}{39} \begin{pmatrix} 8 & \frac{3}{2} & \frac{3}{2} & -1 & -1 & -1 \\ \frac{3}{2} & \frac{3}{2} & 8 & -1 & -1 & -1 \\ \frac{3}{2} & 8 & \frac{3}{2} & -1 & -1 & -1 \\ -1 & -1 & -1 & 5 & -\frac{3}{2} & -\frac{3}{2} \\ -1 & -1 & -1 & -\frac{3}{2} & 5 & -\frac{3}{2} \\ -1 & -1 & -1 & -\frac{3}{2} & -\frac{3}{2} & 5 \end{pmatrix} \,. \tag{4.6.132}$$

We take a pure density matrix $\rho = |b\rangle\langle b|$. The symmetrized density matrix ρ_{S} has eigenvalues

$$\lambda_i = \left\{ \frac{\sqrt{13}+3}{6\sqrt{13}}, \frac{1}{6}, \frac{1}{6}, \frac{1}{6}, \frac{1}{6}, \frac{\sqrt{13}-3}{6\sqrt{13}} \right\} \tag{4.6.133}$$

for any of the six vacua. This leads to the entanglement asymmetry $\Delta S \simeq 1.6568$. This value is smaller than $\log(6)$, the asymmetry for a spontaneously broken group of order 6.

4.6.7 The $\frac{1}{2}E_6$ fusion ring

Finally, we briefly discuss the example of the $\frac{1}{2}E_6$ fusion ring, where a multiplicity greater than 1 appears. Since we limit ourselves to the study of the fusion ring, we will not be concerned with its categorifications, which do in fact exist (see [181] and Sec. 6.4 of [55]). One of the corresponding fusion categories appears as a subsymmetry of the non-diagonal $SU(2)_{10}$ WZW model of E_6 type, or of the (A_{10}, E_6) minimal model. Interestingly, the ring does not admit any braiding despite being Abelian.

The ring has three elements $\{\mathcal{L}_{\mathbb{1}}, \mathcal{L}_X, \mathcal{L}_Y\}$ with Abelian product rules

$$\mathcal{L}_X \times \mathcal{L}_X = \mathcal{L}_{\mathbb{1}} \ , \qquad \mathcal{L}_X \times \mathcal{L}_Y = \mathcal{L}_Y \times \mathcal{L}_X = \mathcal{L}_Y \ , \qquad \mathcal{L}_Y \times \mathcal{L}_Y = \mathcal{L}_{\mathbb{1}} + \mathcal{L}_X + 2\mathcal{L}_Y \ . \tag{4.6.134}$$

The non-degenerate inverse bilinear form, that provides the symmetrizer, is

$$\tilde{K} = \frac{1}{12} \begin{pmatrix} 5 & -1 & -1 \\ -1 & 5 & -1 \\ -1 & -1 & 2 \end{pmatrix} \ . \tag{4.6.135}$$

With this, we can compute the asymmetry in the case of fully broken symmetry. We get, for the three vacua, the following eigenvalues of ρ_{S} and the corresponding asymmetries:

$$\begin{aligned} |1\rangle \, , |X\rangle : \qquad & \lambda_i = \left\{ \frac{1}{2}, \ \frac{3+\sqrt{3}}{12}, \ \frac{3-\sqrt{3}}{12} \right\} \qquad && \Delta S \simeq 0.951 \ , \\ |Y\rangle : \qquad & \lambda_i = \left\{ \frac{3+\sqrt{3}}{6}, \ \frac{3-\sqrt{3}}{6}, \ 0 \right\} \qquad && \Delta S \simeq 0.516 \ . \end{aligned} \tag{4.6.136}$$

As in the case of the Ising symmetry, the first two vacua are related by a $\mathbb{Z}_2$ action and thus share the same asymmetry. The third vacuum, instead, has a different asymmetry.

4.A Strongly separable algebras and the symmetrizer

Consider a finite-dimensional unital semisimple associative algebra $\mathcal{X}_a \times \mathcal{X}_b = \sum_c T^c_{ab} \, \mathcal{X}_c$ (often we will omit the product sign $\times$) over $\mathbb{C}$ as in (4.2.5). Here $\{\mathcal{X}_a\}$ is a basis of the algebra, and one defines a trace as $\mathrm{Tr}(\mathcal{X}_a) = \sum_m T^m_{am}$ then extended by linearity. In the finite-dimensional case, such algebras are automatically strongly separable and the symmetric bilinear form K_{ab} defined in (4.2.7) is non-degenerate. We call $\tilde{K} \equiv K^{-1}$ its inverse. Indeed, the Wedderburn–Artin theorem states that every finite-dimensional unital semisimple associative algebra over $\mathbb{C}$ is isomorphic to a sum of matrix algebras,

$$\mathcal{A} \cong \bigoplus\nolimits_{\alpha=1}^{r} \mathrm{Mat}_{N_\alpha \times N_\alpha}(\mathbb{C}) \ , \tag{4.A.1}$$

where r is the number of blocks, N_α are the sizes of the matrices, and those numbers are unique up to permutation. Note that r is also the number of irreducible representations, and N_α are their dimensions. Using the isomorphism (4.A.1), all properties of the algebras can be explicitly checked. Following [182], we construct the dual basis $\{\mathsf{X}^a\}$ with respect to the bilinear form:

$$\mathsf{X}^a = \sum\nolimits_b \tilde{K}^{ab} \mathcal{X}_b \ . \tag{4.A.2}$$

It satisfies $\mathrm{Tr}(\mathcal{X}_a \mathsf{X}^b) = \delta_a^b$. Going to a basis, one proves that for every $x \in \mathcal{A}$:

$$x = \sum\nolimits_a \mathrm{Tr}(x\,\mathcal{X}_a)\,\mathsf{X}^a = \sum\nolimits_a \mathrm{Tr}(x\,\mathsf{X}^a)\,\mathcal{X}_a\ . \tag{4.A.3}$$

The symmetric separability idempotent (SSI) can be written as

$$e = \sum\nolimits_{ab} \tilde{K}^{ab} \mathcal{X}_a \otimes \mathcal{X}_b = \sum\nolimits_a \mathcal{X}_a \otimes \mathsf{X}^a = \sum\nolimits_a \mathsf{X}^a \otimes \mathcal{X}_a\ . \tag{4.A.4}$$

It is clearly symmetric in the exchange of the two factors. One proves that e commutes with every element of $\mathcal{A}$. Using the shorthand notations $\mathcal{X}_b\, e \equiv (\mathcal{X}_b \otimes \mathbb{1})\, e$ and $e\, \mathcal{X}_b \equiv e\, (\mathbb{1} \otimes \mathcal{X}_b)$:

$$\begin{aligned} \mathcal{X}_b\, e &= \sum\nolimits_a \mathcal{X}_b \mathcal{X}_a \otimes \mathsf{X}^a = \sum\nolimits_{ac} \mathrm{Tr}\big(\mathcal{X}_b \mathcal{X}_a \mathsf{X}^c\big) \mathcal{X}_c \otimes \mathsf{X}^a \\ &= \sum\nolimits_{ac} \mathcal{X}_c \otimes \mathrm{Tr}\big(\mathsf{X}^c \mathcal{X}_b \mathcal{X}_a\big) \mathsf{X}^a = \sum\nolimits_c \mathcal{X}_c \otimes \mathsf{X}^c \mathcal{X}_b = e\, \mathcal{X}_b\ . \end{aligned} \tag{4.A.5}$$

We can use K to obtain a pivotal relation. Consider the following element of $\mathcal{A} \otimes \mathcal{A}$:

$$\sum\nolimits_b \mathcal{X}_b \otimes \mathcal{X}_a \mathsf{X}^b = \sum\nolimits_b \mathcal{X}_b \mathcal{X}_a \otimes \mathsf{X}^b = \sum\nolimits_{bc} T^c_{ba} \mathcal{X}_c \otimes \mathsf{X}^b = \sum\nolimits_{bc} \mathcal{X}_b \otimes T^b_{ca} \mathsf{X}^c\ . \tag{4.A.6}$$

In the first equality we used that e commutes with $\mathcal{A}$ also "from the inside", which follows from the fact that e is symmetric. In the last equality we moved the scalars and renamed the indices. Since $\{\mathcal{X}_b\}$ are a basis on the first factor of $\mathcal{A} \otimes \mathcal{A}$, we conclude that

$$\mathcal{X}_a \times \mathsf{X}^b = \sum\nolimits_c T^b_{ca}\, \mathsf{X}^c\ . \tag{4.A.7}$$

This can be rewritten as the pivotal relation (4.2.9). One can also obtain

$$\sum\nolimits_{ab} T^c_{ab}\, \mathsf{X}^b\, \mathsf{X}^a = \mathsf{X}^c\ . \tag{4.A.8}$$

Using the trace relation (4.A.3), the identity element (4.2.10) can be written as

$$\mathcal{X}_{\mathbb{1}} = \sum\nolimits_a \mathrm{Tr}(\mathcal{X}_{\mathbb{1}} \mathcal{X}_a)\, \mathsf{X}^a = \sum\nolimits_{ab} T^b_{ab}\, \mathsf{X}^a = \sum\nolimits_b \mathcal{X}_b\, \mathsf{X}^b = \sum\nolimits_b \mathsf{X}^b\, \mathcal{X}_b\ . \tag{4.A.9}$$

In the third equality we used (4.A.7). Using the notation $xy \equiv \mu(x \otimes y)$ for the product, we can regard the previous relation as the contraction $\mu(e) = \mathcal{X}_{\mathbb{1}}$. Finally, let us show that e is idempotent as an element of $\mathcal{A} \otimes \mathcal{A}^{\mathrm{op}}$ (where $\mathcal{A}^{\mathrm{op}}$ is the same as $\mathcal{A}$ but elements are multiplied in the opposite order). In other words, $e^2 = e$ where e acts on itself from the outside:

$$e^2 = \sum\nolimits_{ab} \mathcal{X}_a \mathcal{X}_b \otimes \mathsf{X}^b \mathsf{X}^a = \sum\nolimits_{abc} T^c_{ab}\, \mathcal{X}_c \otimes \mathsf{X}^b \mathsf{X}^a = \sum\nolimits_c \mathcal{X}_c \otimes \mathsf{X}^c = e\ . \tag{4.A.10}$$

In the third equality we moved the scalars to the other side and used (4.A.8). We have thus shown that e is a *symmetric separability idempotent*, that commutes with the algebra and gives the identity upon contraction.

Relation with special Frobenius algebras. The strong separability condition allows one to make $\mathcal{A}$ into a special Frobenius algebra $(\mathcal{A}, \mu, u, \Delta, \epsilon)$. The product $\mu\colon \mathcal{A}\otimes\mathcal{A}\to\mathcal{A}$ is the one already defined. The unital map $u\colon \mathbb{C}\to\mathcal{A}$ is given by $u(1)=\mathcal{X}_{\mathbb{1}}$ and linearity. They satisfy $\mu\big(x\otimes u(1)\big)=\mu\big(u(1)\otimes x\big)=x$. The coproduct $\Delta\colon \mathcal{A}\to\mathcal{A}\otimes\mathcal{A}$ is defined as

$$\Delta(x) = x\,e = e\,x\ . \tag{4.A.11}$$

It satisfies $\mu\circ\Delta=\mathrm{id}_{\mathcal{A}}$ because $\mu\big(\Delta(x)\big)=\mu(xe)=\mu\big(\sum_a x\mathcal{X}_a\otimes\mathsf{X}^a\big)=\sum_a x\mathcal{X}_a\mathsf{X}^a=x\mathcal{X}_{\mathbb{1}}$. Note that $\Delta\circ\mu\neq\mathrm{id}_{\mathcal{A}\otimes\mathcal{A}}$. The Frobenius relation

$$(\mathrm{id}_{\mathcal{A}}\otimes\mu)\circ(\Delta\otimes\mathrm{id}_{\mathcal{A}}) = (\mu\otimes\mathrm{id}_{\mathcal{A}})\circ(\mathrm{id}_{\mathcal{A}}\otimes\Delta) = \Delta\circ\mu \tag{4.A.12}$$

simply follows from $xey=xye$. One can also define the counital map $\epsilon\colon\mathcal{A}\to\mathbb{C}$ using the trace, $\epsilon(x)=\mathrm{Tr}(x)$. It satisfies $(\mathrm{id}_{\mathcal{A}}\otimes\epsilon)\circ\Delta=\mathrm{id}_{\mathcal{A}}=(\epsilon\otimes\mathrm{id}_{\mathcal{A}})\circ\Delta$. The first equation is

$$(\mathrm{id}_{\mathcal{A}}\otimes\epsilon)\circ\Delta(x) = (\mathrm{id}_{\mathcal{A}}\otimes\epsilon)\left(\textstyle\sum_a x\mathcal{X}_a\otimes\mathsf{X}^a\right) = \displaystyle\sum_a x\,\mathcal{X}_a\ \mathrm{Tr}(\mathsf{X}^a) = x\,\mathcal{X}_{\mathbb{1}} = x\ . \tag{4.A.13}$$

The second equation is similar. One finds $\Delta\big(u(1)\big)=e$ and $\epsilon\big(\mu(e)\big)=\dim\mathcal{A}$.

$*$-structure. A $*$-structure on an algebra $\mathcal{A}$ over the complex field $\mathbb{C}$ is an anti-linear involution $\dagger\colon\mathcal{A}\to\mathcal{A}$ (*i.e.*, such that $X^{\dagger\dagger}=X$ and $(\alpha X+\beta Y)^\dagger=\alpha^* X^\dagger+\beta^* Y^\dagger$ for $\alpha,\beta\in\mathbb{C}$) which is also an anti-homomorphism: $(XY)^\dagger=Y^\dagger X^\dagger$.

If $\mathcal{A}$ is a finite-dimensional C^*-algebra, a version of the Wedderburn–Artin theorem (see [143] Th. 6.3.8) states that the isomorphism to a sum of matrix algebras can be chosen such that the star operation is mapped to the standard matrix adjoint operation. Consider for simplicity the case of a single block of size N: $\mathcal{A}\cong\mathrm{Mat}_{N\times N}(\mathbb{C})$, which means that $\mathcal{A}$ is simple (the following arguments extend to the general case of multiple blocks with minimal modifications). Then we can represent the index a as $a\equiv ij$ with $i,j=1,\dots,N$. Let us work in a special basis in which $\mathcal{X}_a\equiv\mathcal{X}_{ij}$ is mapped by the $*$-algebra isomorphism to the matrix with a single 1 at position (i,j) and all other entries vanishing. In this basis the product is

$$\mathcal{X}_a\times\mathcal{X}_b\equiv\mathcal{X}_{ij}\times\mathcal{X}_{kl}=\delta_{jk}\,\mathcal{X}_{il}\ , \tag{4.A.14}$$

in other words the structure constants are

$$T^c_{ab}\equiv T^{mn}_{ij,kl}=\delta^m_i\delta_{jk}\delta^n_l\ . \tag{4.A.15}$$

The symmetric bilinear form is [47]

$$K_{ab}\equiv K_{ij,kl}=\sum\nolimits_{mnrs}T^{rs}_{ij,mn}\,T^{mn}_{kl,rs}=N\,\delta_{il}\delta_{jk}\ . \tag{4.A.16}$$

[47] In the general case (4.A.1), $\mathcal{A}$ is isomorphic to a sum of matrix algebras. The basis elements can be labeled as $\mathcal{X}_{\alpha ij}$. Then K_{ab} is as in (4.A.16) in each block, namely $K_{\alpha ij,\beta kl}=N_\alpha\,\delta_{\alpha\beta}\,\delta_{il}\delta_{jk}$. All the following formulas apply block by block.

This is indeed invertible, and the inverse is

$$\tilde{K}^{ab} \equiv \tilde{K}^{ij,kl} = N^{-1}\,\delta^{il}\delta^{jk}\ . \tag{4.A.17}$$

In this basis the symmetric separability idempotent takes the simple form

$$e = \sum\nolimits_{ijkl} \tilde{K}^{ij,kl}\,\mathcal{X}_{ij}\otimes\mathcal{X}_{kl} = N^{-1}\sum\nolimits_{ij}\mathcal{X}_{ij}\otimes\mathcal{X}_{ji}\ . \tag{4.A.18}$$

The star operation takes a simple form as well:

$$\mathcal{X}_a^\dagger \equiv \mathcal{X}_{ij}^\dagger = \mathcal{X}_{ji}\ . \tag{4.A.19}$$

We see that e is Hermitian: $e^\dagger = e$. Since Hermiticity does not depend on the basis (it is invariant under isomorphism), we conclude that e is Hermitian in general:

$$e^\dagger = \sum\nolimits_{ab}(\tilde{K}^{ab})^*\,\mathcal{X}_a^\dagger\otimes\mathcal{X}_b^\dagger = e\ . \tag{4.A.20}$$

In the special basis the SSI can also be written as follows:

$$e = N^{-1}\sum\nolimits_{ij}\mathcal{X}_{ij}^\dagger\otimes\mathcal{X}_{ij}\ . \tag{4.A.21}$$

By a rescaling of the basis, $\mathcal{X}_{\underline{a}} \equiv N^{-\frac{1}{2}}\mathcal{X}_{ij}$, it reads $e = \sum_{\underline{a}}\mathcal{X}_{\underline{a}}^\dagger\otimes\mathcal{X}_{\underline{a}}$. This very simple form (which is reached also in the general case of multiple blocks) is not invariant under change of basis, however it is useful that such an expression exists.

Consequences for the symmetrizer. The symmetrizer can be defined in terms of the symmetric separability idempotent e as the linear map $\rho_{\mathsf{S}} = e(\rho) = \sum_{ab}\tilde{K}^{ab}\,\mathcal{X}_a\rho\mathcal{X}_b$. Idempotency of e implies that $(\rho_{\mathsf{S}})_{\mathsf{S}} = \rho_{\mathsf{S}}$ and thus the symmetrizer is a projector. The property $\mu(e) = \mathcal{X}_{\mathbb{1}}$ and symmetry of e imply that $\mathrm{Tr}(\rho_{\mathsf{S}}) = \mathrm{Tr}(\rho)$ and that, if ρ commutes with $\mathcal{A}$, then $\rho_{\mathsf{S}} = \rho$. Since e commutes with $\mathcal{A}$ then ρ_{S} commutes with $\mathcal{A}$. In other words, the image of the projector is precisely given by the matrices that commute with the action of the algebra, and not a subspace thereof.

Since $e = e^\dagger$, when $\rho = \rho^\dagger$ is Hermitian one finds that also ρ_{S} is Hermitian. Finally, assume that the density matrix ρ is nonnegative, namely that $\langle\psi|\rho|\psi\rangle \geq 0$ for every vector $|\psi\rangle$ in the Hilbert space. Then

$$\langle\psi|\rho_{\mathsf{S}}|\psi\rangle = \sum\nolimits_{ab}\tilde{K}^{ab}\langle\psi|\mathcal{X}_a\rho\mathcal{X}_b|\psi\rangle \overset{\text{special basis}}{=} \sum\nolimits_{\underline{a}}\langle\psi|\mathcal{X}_{\underline{a}}^\dagger\rho\mathcal{X}_{\underline{a}}|\psi\rangle \geq 0\ . \tag{4.A.22}$$

In the second equality we used the special basis adapted to the $*$-structure. In that basis we find a sum of nonnegative numbers, which is nonnegative. This proves that also ρ_{S} is nonnegative.

4.A.1 C^*-structure of fusion algebras

A C^*-algebra $\mathcal{A}$ is a Banach algebra[48] over $\mathbb{C}$, with a $*$-structure $\dagger\colon \mathcal{A} \to \mathcal{A}$ and with a norm such that

$$\|x^\dagger x\| = \|x\|^2 \qquad \text{for all } x \in \mathcal{A}\,. \tag{4.A.23}$$

This condition is called the C^* relation and it is very restrictive, indeed, if it exists, such a norm is uniquely fixed by the algebraic structure as

$$\|x\|^2 = \|x^\dagger x\| = \sup\big\{|\lambda| \;\big|\; (x^\dagger x - \lambda \mathbb{1}) \text{ is not invertible}\big\}\,. \tag{4.A.24}$$

One can prove that C^*-algebras are semisimple.

Let us show that finite-dimensional fusion algebras (summarized in Sec. 4.3.1) are C^*-algebras. We show that

$$x^\dagger x = 0 \qquad \Rightarrow \qquad x = 0\,. \tag{4.A.25}$$

For finite-dimensional unital $*$-algebras, this implies that they are C^* (see, *e.g.*, Prop. 2.1 in [183] or Th. 2.4.4 in [184]). Decompose $x = \sum_a x_a \mathcal{L}_a$. Then

$$x^\dagger x = \sum\nolimits_{abcd} x_a^* x_b\, N_{ac}^1\, N_{cb}^d\, \mathcal{L}_d\,. \tag{4.A.26}$$

Assume that $x^\dagger x = 0$, then $\sum_{abc} x_a^* x_b\, N_{ac}^1\, N_{cb}^d = 0$ for all d. Taking $d = 1$ we get $\sum_a |x_a|^2 = 0$, therefore $x = 0$. We conclude that finite-dimensional fusion algebras are C^*-algebras, and thus they are also semisimple.

4.A.2 Explicit form of ρ_S

Let us consider an algebra $\mathcal{A}$, with the same hypotheses as above, which we identify with a matrix algebra by virtue of (4.A.1). We pick a basis of $\mathcal{A}$ given by $\{\mathcal{X}_{\alpha,ij}\}$ as above (4.A.14), where

$$\mathcal{X}_{\alpha,ij} = \left(\begin{array}{c|c|c} 0 & 0 & 0 \\ \hline 0 & e_{ij}^\alpha & 0 \\ \hline 0 & 0 & 0 \end{array}\right) \leftarrow \alpha\text{-th block} \qquad \begin{array}{c} \alpha = 1, \dots, r \\ i, j = 1, \dots, N_\alpha \end{array} \tag{4.A.27}$$

and e_{ij}^α is the $N_\alpha \times N_\alpha$ matrix that has a single 1 in position (i, j) and 0 elsewhere. The β-th representation of $\mathcal{A}$ merely selects the β-th diagonal block from the matrix above. The most generic representation $\mathfrak{R}\colon \mathcal{A} \to \mathrm{End}(V)$ is a direct sum of irreducible representations:

$$V = \bigoplus\nolimits_{\alpha=1}^{r} n_\alpha\, V_\alpha\,, \tag{4.A.28}$$

[48] Meaning that it is associative, it has a norm such that $\|xy\| \le \|x\| \cdot \|y\|$, and it is complete with respect to the metric induced by that norm.

where $\dim(V_\alpha) = N_\alpha$, and thus the matrix that represents $\mathcal{X}_{\alpha,ij}$ is of the form:

$$\mathfrak{R}(\mathcal{X}_{\alpha,ij}) = \left(\begin{array}{c|ccc|c} 0 & & 0 & & 0 \\ \hline & e^\alpha_{ij} & & 0 & \\ 0 & & \ddots & & 0 \\ & 0 & & e^\alpha_{ij} & \\ \hline 0 & & 0 & & 0 \end{array}\right) \leftarrow \alpha\text{-th block} \tag{4.A.29}$$

where e^α_{ij} is repeated n_α times. We now assume that the symmetrizer, which in principle can be any element of $\mathrm{End}\big(\mathrm{End}(V)\big)$, is written in the following form:[49]

$$M_{\mathsf{S}} = \sum\nolimits_{\alpha,i,j,\alpha',i',j'} c_{(\alpha,ij)(\alpha',i'j')}\ \mathfrak{R}(\mathcal{X}_{\alpha,ij})\ M\ \mathfrak{R}(\mathcal{X}_{\alpha',i'j'})\ , \tag{4.A.30}$$

where $M \in \mathrm{End}(V)$ is any matrix, that we also decompose in blocks $M^{\alpha\alpha'}$ according to (4.A.28). Thanks to property 2. and to Schur's lemma,[50] we can conclude that, as a matrix, M_{S} has vanishing off-diagonal blocks, $(M_{\mathsf{S}})^{\alpha\alpha'} = 0$ for $\alpha \neq \alpha'$, while each diagonal block is of the form

$$(M_{\mathsf{S}})^{\alpha\alpha} = \begin{pmatrix} \lambda^{\alpha\alpha}_{11}\mathbb{1}_{N_\alpha} & \cdots & \lambda^{\alpha\alpha}_{1n_\alpha}\mathbb{1}_{N_\alpha} \\ \vdots & \ddots & \vdots \\ \lambda^{\alpha\alpha}_{n_\alpha 1}\mathbb{1}_{N_\alpha} & \cdots & \lambda^{\alpha\alpha}_{n_\alpha n_\alpha}\mathbb{1}_{N_\alpha} \end{pmatrix} . \tag{4.A.31}$$

In principle each coefficient $\lambda^{\alpha\alpha}_{ab}$ is completely generic. However, using the additional assumption (4.A.30), we have

$$M_{\mathsf{S}} = \sum_{\alpha,i,j,i',j'} c_{(\alpha,ij)(\alpha,i'j')} \left(\begin{array}{c|ccc|c} 0 & & 0 & & 0 \\ \hline & e^\alpha_{ij}m^{\alpha\alpha}_{11}e^\alpha_{i'j'} & \cdots & e^\alpha_{ij}m^{\alpha\alpha}_{1n_\alpha}e^\alpha_{i'j'} & \\ 0 & \vdots & \ddots & \vdots & 0 \\ & e^\alpha_{ij}m^{\alpha\alpha}_{n_\alpha 1}e^\alpha_{i'j'} & \cdots & e^\alpha_{ij}m^{\alpha\alpha}_{n_\alpha n_\alpha}e^\alpha_{i'j'} & \\ \hline 0 & & 0 & & 0 \end{array}\right) \leftarrow \alpha\text{-th block} \tag{4.A.32}$$

where $m^{\alpha\alpha}_{ab}$ with $a, b \in \{1, \ldots, n_\alpha\}$ are sub-blocks of $M^{\alpha\alpha}$. The symmetrization in each of the sub-blocks $m^{\alpha\alpha}_{ab}$ depends only on the entries of M of that same sub-block. Let us now focus on such a sub-block. Its symmetrized version is

$$\sum\nolimits_{i,j,i',j'} c_{(\alpha,ij)(\alpha,i'j')}\, e^\alpha_{ij}\, m^{\alpha\alpha}_{ab}\, e^\alpha_{i'j'} = \sum\nolimits_{i,j,i',j'} c_{(\alpha,ij)(\alpha,i'j')}\, (m^{\alpha\alpha}_{ab})_{ji'}\, e^\alpha_{ij'} \ . \tag{4.A.33}$$

[49] This assumption is referred to as "universality" in Sec. 4.2.

[50] Schur's lemma [142] can be stated (under our working hypotheses) as the fact that the module-endomorphisms of an irreducible $\mathcal{A}$-module form a division algebra. But there is only one such algebra over $\mathbb{C}$: the complex numbers themselves. Since the identity is clearly a module-endomorphism, we conclude that all such endomorphisms must be proportional to the identity. In more concrete terms, matrices that commute with all elements of an irreducible representation of $\mathcal{A}$ must be proportional to the identity matrix. This result generalizes the well-known analogous result for groups and group algebras.

This must be proportional to the identity, so it must be $c_{(\alpha,ij)(\alpha,i'j')} = \delta_{ij'}\,\tilde{c}^{\alpha}_{i'j}$. Consider now a matrix M that is nonzero only in the block $m^{\alpha\alpha}_{aa}$. Imposing conservation of the trace gives $\sum_j (m^{\alpha\alpha}_{aa})_{jj} = \mathrm{Tr}(M) \stackrel{!}{=} \mathrm{Tr}(M_{\mathsf{S}}) = N_\alpha \sum_{ji'} \tilde{c}^{\alpha}_{i'j} (m^{\alpha\alpha}_{aa})_{ji'}$. We conclude it must be $\tilde{c}^{\alpha}_{i'j} = \delta_{i'j}/N_\alpha$ and $c_{(\alpha,ij)(\alpha,i'j')} = \delta_{ij'}\delta_{i'j}/N_\alpha$. This means that the sub-block (a,b) of the block (α,α) is

$$\sum\nolimits_{i,j,i',j'} c_{(\alpha,ij)(\alpha,i'j')}\, e^{\alpha}_{ij}\, m^{\alpha\alpha}_{ab}\, e^{\alpha}_{i'j'} = \frac{1}{N_\alpha}\,\mathrm{Tr}(m^{\alpha\alpha}_{ab})\,\mathbb{1}^{\alpha}_{ab}\ . \tag{4.A.34}$$

Notice that conservation of the trace has also fixed those blocks with $a \neq b$.

Said in words, the matrix M_{S} is proportional to the identity in blocks that connect isomorphic irreducible representations, and is zero elsewhere. In each block, the proportionality constant is the trace of that block, divided by its dimension[51] (also see Fig. 4.1).

4.B Hopf algebras, modules, and tensor products

We review here the definition of Hopf algebras, following [138, 159, 160]. An associative algebra $\mathcal{A}$ over $\mathbb{C}$ has an associative product $\mu\colon \mathcal{A}\otimes\mathcal{A}\to\mathcal{A}$ and a unit $u\colon \mathbb{C}\to\mathcal{A}$ such that

$$\mu\circ\big(u(1)\otimes\mathrm{id}\big) = \mathrm{id} = \mu\circ\big(\mathrm{id}\otimes u(1)\big)\ . \tag{4.B.1}$$

We will henceforth denote $u(1)\equiv\mathbb{1}$. Both μ and u are linear, and u is unique when it exists. A coassociative coalgebra $\mathcal{A}$ over $\mathbb{C}$, instead, has a coassociative coproduct $\Delta\colon \mathcal{A}\to\mathcal{A}\otimes\mathcal{A}$, such that $(\Delta\otimes\mathrm{id})\circ\Delta = (\mathrm{id}\otimes\Delta)\circ\Delta \equiv \Delta^2$, and a counit $\epsilon\colon \mathcal{A}\to\mathbb{C}$ such that

$$(\epsilon\otimes\mathrm{id})\circ\Delta = \mathrm{id} = (\mathrm{id}\otimes\epsilon)\circ\Delta\ . \tag{4.B.2}$$

Both Δ and ϵ are linear, and ϵ is unique. It is convenient to use Sweedler's notation: it is always possible to write (in a non-unique way) coproducts as sums: $\Delta(x) = \sum_i x^i_{(1)}\otimes x^i_{(2)}$. This is concisely written as $\Delta(x) = x_{(1)}\otimes x_{(2)}$ with the sum kept implicit.

A weak bialgebra $\mathcal{A}$ has both the algebra and coalgebra structures, which must be compatible in the following sense. The coproduct is an algebra homomorphism: $\Delta(xy) = \Delta(x)\,\Delta(y)$, where on the r.h.s. pairwise multiplication is used. The counit is weakly multiplicative:

$$\epsilon(xyz) = \epsilon\big(x\,y_{(1)}\big)\,\epsilon\big(y_{(2)}\,z\big) = \epsilon\big(x\,y_{(2)}\big)\,\epsilon\big(y_{(1)}\,z\big)\ , \tag{4.B.3}$$

[51] Implicit in this statement is a choice of basis such that all copies of a given representation use the same matrices, as was the case in (4.A.29). This choice implies that also the off-diagonal blocks are proportional to the identity (see footnote 50). Indeed, such blocks are nonzero module-endomorphisms between isomorphic representations and thus, as matrices, commute with all elements of the corresponding irreducible module of $\mathcal{A}$.

where associativity is assumed. The unit is weakly comultiplicative, that can be written as

$$\Delta^2(\mathbb{1}) = \big(\Delta(\mathbb{1}) \otimes \mathbb{1}\big)\big(\mathbb{1} \otimes \Delta(\mathbb{1})\big) = \big(\mathbb{1} \otimes \Delta(\mathbb{1})\big)\big(\Delta(\mathbb{1}) \otimes \mathbb{1}\big) \ , \tag{4.B.4}$$

where coassociativity is assumed in the first expression, while in the second and third expressions pairwise multiplication is used. A *weak Hopf algebra* is a weak bialgebra in which there exists an antipode map $S\colon \mathcal{A} \to \mathcal{A}$ satisfying the following three properties:

$$x_{(1)}\, S\big(x_{(2)}\big) = \epsilon\big(\mathbb{1}_{(1)}\, x\big)\, \mathbb{1}_{(2)} \ , \qquad S\big(x_{(1)}\big)\, x_{(2)} = \mathbb{1}_{(1)}\, \epsilon\big(x\, \mathbb{1}_{(2)}\big) \ , \qquad S\big(x_{(1)}\big)\, x_{(2)}\, S\big(x_{(3)}\big) = S(x) \ . \tag{4.B.5}$$

In the last equation we used Sweedler's notation for $\Delta^2(x)$. It follows [160] that the antipode map is unique, and that it is an algebra anti-homomorphism satisfying:

$$\begin{aligned} S(xy) &= S(y)\, S(x) \ , & S(\mathbb{1}) &= \mathbb{1} \ , \\ S(x)_{(1)} \otimes S(x)_{(2)} &= S\big(x_{(2)}\big) \otimes S\big(x_{(1)}\big) \ , & \epsilon \circ S &= \epsilon \ . \end{aligned} \tag{4.B.6}$$

In finite-dimensional weak Hopf algebras, S is always invertible.

A bialgebra (sometimes called strong bialgebra) is a weak bialgebra in which the counit is multiplicative and the unit is comultiplicative:

$$\epsilon(xy) = \epsilon(x)\, \epsilon(y) \ , \qquad \Delta(\mathbb{1}) = \mathbb{1} \otimes \mathbb{1} \ . \tag{4.B.7}$$

These stronger properties imply the corresponding weaker ones. A *Hopf algebra* (sometimes called a strong Hopf algebra) is a weak Hopf algebra in which one requires, equivalently, multiplicativity of the counit, comultiplicativity of the unit, or the hexagon diagram:

$$x_{(1)}\, S\big(x_{(2)}\big) = S\big(x_{(1)}\big)\, x_{(2)} = \epsilon(x)\, \mathbb{1} \ . \tag{4.B.8}$$

If one of these three properties holds for a weak Hopf algebra, then the other two follow automatically. This means that a Hopf algebra is in particular a bialgebra. Also in this case the antipode S is unique, it satisfies (4.B.6), and it is always invertible in the finite-dimensional case [185]. Besides,[52]

$$S^2 = \mathrm{id} \tag{4.B.9}$$

in finite-dimensional semisimple Hopf algebras over $\mathbb{C}$ [186, 187].

Group algebra. The group algebra $\mathbb{C}[G]$ is a typical example of Hopf algebra, where

$$\mu(g_1 \otimes g_2) = (g_1 g_2) \ , \quad u(1) = \mathbb{1}_G \ , \quad \Delta(g) = g \otimes g \ , \quad \epsilon(g) = 1 \ , \quad S(g) = g^{-1} \ . \tag{4.B.10}$$

One easily verifies that all properties are satisfied.

[52] In finite-dimensional semisimple weak Hopf algebras over $\mathbb{C}$, S is not necessarily involutive.

Integrals. Following [160], in a weak Hopf algebra one introduces the left and right projectors

$$\begin{aligned}\Pi^{\mathrm{L}}(x) &= \epsilon\big(\mathbb{1}_{(1)}\,x\big)\,\mathbb{1}_{(2)} = x_{(1)}\,S\big(x_{(2)}\big)\ ,\\ \Pi^{\mathrm{R}}(x) &= \mathbb{1}_{(1)}\,\epsilon\big(x\,\mathbb{1}_{(2)}\big) = S\big(x_{(1)}\big)\,x_{(2)}\ ,\end{aligned} \tag{4.B.11}$$

acting on $x \in \mathcal{A}$. These are projectors because of (4.B.3), and the second equality is as in (4.B.5). They are related by the antipode map:[53]

$$\Pi^{\mathrm{L}} \circ S = \Pi^{\mathrm{L}} \circ \Pi^{\mathrm{R}} = S \circ \Pi^{\mathrm{R}}\ , \qquad \Pi^{\mathrm{R}} \circ S = \Pi^{\mathrm{R}} \circ \Pi^{\mathrm{L}} = S \circ \Pi^{\mathrm{L}}\ . \tag{4.B.12}$$

Then one defines left and right normalized integrals ℓ and r, respectively, such that:

$$x\,\ell = \Pi^{\mathrm{L}}(x)\,\ell\ , \qquad \Pi^{\mathrm{L}}(\ell) = \mathbb{1}\ , \qquad \text{or} \qquad r\,x = r\,\Pi^{\mathrm{R}}(x)\ , \qquad \Pi^{\mathrm{R}}(r) = \mathbb{1}\ , \tag{4.B.13}$$

for all $x \in \mathcal{A}$. Note that the normalized integrals ℓ, r are themselves projectors. Besides, $S(\ell)$ is a normalized right integral, and $S(r)$ is a normalized left integral (proven by applying S to (4.B.13) and using that S is invertible). An element that is simultaneously a left and right normalized integral is called a Haar integral h. When it exists, the Haar integral is unique. It follows that $S(h) = h$.

(Weak) Hopf algebra modules. A left-module, or representation, consists of a vector space V and a homomorphism $r\colon \mathcal{A} \to \mathrm{End}(V)$ that acts from the left and respects the algebra structure. For a general algebra there is no concept of conjugate representation or of tensor product of representations. Those concepts become available in a (weak) Hopf algebra [188].

Let $\mathcal{M} = (V, r)$ be a left-module for a weak Hopf algebra $\mathcal{A}$ over $\mathbb{C}$. There is a canonical right action on the dual space $V^\vee$, induced by the left action on V simply as $\langle f\,r(x), v\rangle \equiv \langle f, r(x)\,v\rangle$ for all $f \in V^\vee$, $v \in V$ and $x \in \mathcal{A}$. In order to construct a left action, instead, one uses the antipode map S:

$$r^*(x)\,f \equiv f\,r\big(S(x)\big)\ . \tag{4.B.14}$$

The fact that $S(xy) = S(y)\,S(x)$ guarantees that r^* is an algebra homomorphism. Thus $\mathcal{M}^* = (V^\vee, r^*)$ is a left-module that we call the conjugate representation to $\mathcal{M}$.

Let $\mathcal{M}_1$, $\mathcal{M}_2$ be two left-modules. The tensor product representation $\mathcal{M}_1 \otimes \mathcal{M}_2$ on $V_1 \otimes V_2$ is constructed using the coproduct:

$$r_{12} \equiv (r_1 \otimes r_2) \circ \Delta \qquad \text{that is} \qquad r_{12}(x)\,v_1 \otimes v_2 \ \equiv\ \sum\nolimits_i \Big[r_1\big(x^i_{(1)}\big)\,v_1\Big] \otimes \Big[r_2\big(x^i_{(2)}\big)\,v_2\Big]\ . \tag{4.B.15}$$

[53] Let us prove the first relation. First, notice that $\Pi^{\mathrm{L}}(\mathbb{1}) = \Pi^{\mathrm{R}}(\mathbb{1}) = \mathbb{1}$ and $\epsilon \circ \Pi^{\mathrm{L}} = \epsilon \circ \Pi^{\mathrm{R}} = \epsilon$. Then $\Pi^{\mathrm{L}} \circ \Pi^{\mathrm{R}}(x) = \epsilon\big(\mathbb{1}_{(1)} S(x_{(1)}) x_{(2)}\big)\,\mathbb{1}_{(2)} = \epsilon\big(\mathbb{1}_{(1)} S(x_{(1)})_{(2)}\big)\epsilon\big(S(x_{(1)})_{(1)} x_{(2)}\big)\,\mathbb{1}_{(2)} = \epsilon\big(\mathbb{1}_{(1)} S(x_{(1)})\big)\epsilon\big(S(x_{(2)}) x_{(3)}\big)\,\mathbb{1}_{(2)}$. Use $\epsilon\big(S(x_{(2)})x_{(3)}\big) = \epsilon \circ \Pi^{\mathrm{R}}(x_{(2)}) = \epsilon(x_{(2)})$, so that $\Pi^{\mathrm{L}} \circ \Pi^{\mathrm{R}}(x) = \epsilon\big(\mathbb{1}_{(1)} S(x)\big)\,\mathbb{1}_{(2)} = \Pi^{\mathrm{L}} \circ S(x)$.

This defines an algebra homomorphism $r_{12}\colon \mathcal{A} \to \mathrm{End}(V_1 \otimes V_2)$ in the case of Hopf algebras. In strictly weak Hopf algebras, since $\Delta(\mathbb{1}) \neq \mathbb{1} \otimes \mathbb{1}$, there are vectors annihilated by $r_{12}(\mathbb{1})$. To remedy, notice that $\Delta(\mathbb{1})$ is a projector, therefore one constructs the representation on the subspace of $V_1 \otimes V_2$ where $\Delta(\mathbb{1})$ acts as the identity.

In the case of Hopf algebras one can also define the so-called "trivial" one-dimensional representation $r_\epsilon\colon \mathcal{A} \to \mathbb{C}$ using the counit:

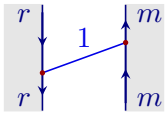
$$r_\epsilon(x) = \epsilon(x)\ . \tag{4.B.16}$$

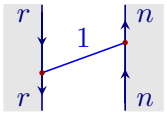
This is an algebra homomorphism thanks to multiplicativity of the counit (4.B.7). The trivial representation multiplies trivially with all other representations (*i.e.*, it is the identity) under tensor product, since $\big((\epsilon \otimes r) \circ \Delta\big)(x) = \big((r \otimes \epsilon) \circ \Delta\big)(x) = r(x)$ using (4.B.2), and besides it is self-conjugate since $\epsilon \circ S = \epsilon$. In strictly weak Hopf algebras, a representation that multiplies trivially with all the other ones exists as well, however it is not one-dimensional.

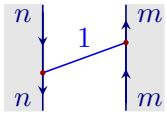
4.B.1 Strip algebras with strongly-symmetric boundaries

It was shown in [137, 138] that strip algebras are weak Hopf algebras. Here we show that a strip algebra constructed using strongly-symmetric boundary conditions is actually a Hopf algebra. We only need to show that $\Delta(\mathbb{1}) = \mathbb{1} \otimes \mathbb{1}$.

A general formula to construct the coproduct Δ in strip algebras was provided in [138] Sec. 2.1. The identity element $\mathbb{1}$ (that we sometimes called $\mathcal{X}_{\mathbb{1}}$) of the strip algebra, and its coproduct computed using that formula, are:

$\mathbb{1} = \sum_{r,m}$ 

, $\Delta(\mathbb{1}) = \sum_{r,n,m}$ 

$\otimes$ 

. (4.B.17)

For strongly-symmetric boundary conditions (and only in that case) the module has only one simple object, $r, m, n = \bullet$, and therefore $\Delta(\mathbb{1}) = \mathbb{1} \otimes \mathbb{1}$.

4.B.2 Symmetrizer in (weak) Hopf algebras

In semisimple Hopf algebras, the symmetrizer is constructed using the object

$$\mathbb{P} = (\mathrm{id} \otimes S) \circ \Delta(P_\epsilon) \ \in \mathcal{A} \otimes \mathcal{A}^{\mathrm{op}}\ , \tag{4.B.18}$$

that we called S in (4.4.37). This is known to provide a separability idempotent with respect to the canonical Frobenius structure of a Hopf algebra, see [159] Remark 3.2.31. This implies that $\mathbb{P}$ satisfies the properties 1. – 3. listed in Sec. 4.2. Let us explicitly check 1., 3. and 4. Idempotency is

$$\begin{aligned}\mathbb{P} \times \mathbb{P} &= P_{\epsilon\,(1)'}\, P_{\epsilon\,(1)} \otimes S\big(P_{\epsilon\,(2)}\big)\, S\big(P_{\epsilon\,(2)'}\big) = P_{\epsilon\,(1)'}\, P_{\epsilon\,(1)} \otimes S\big(P_{\epsilon\,(2)'}\, P_{\epsilon\,(2)}\big) \\ &= (\mathrm{id} \otimes S)\big(\Delta(P_\epsilon)\, \Delta(P_\epsilon)\big) = (\mathrm{id} \otimes S) \circ \Delta\big(P_\epsilon^2\big) = \mathbb{P}\ .\end{aligned} \tag{4.B.19}$$

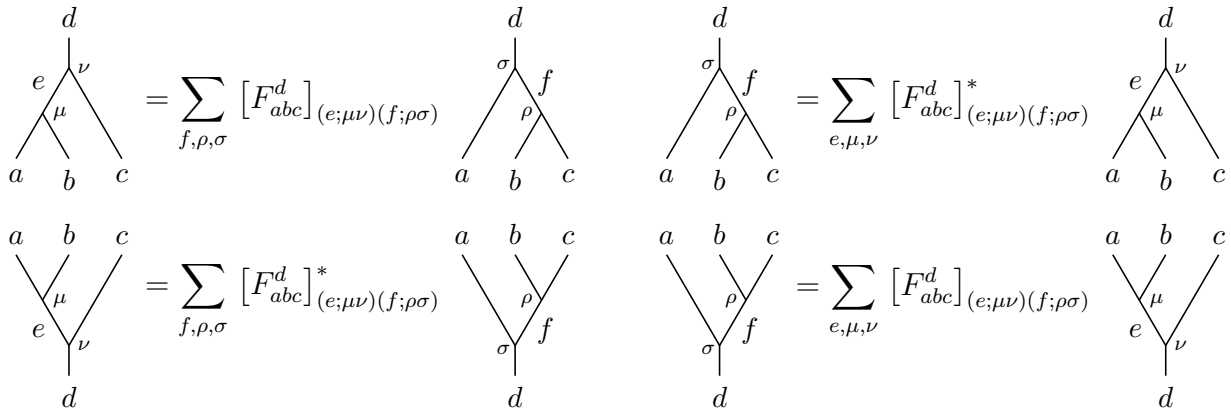


Figure 4.17: Different ways of writing the F-move. All lines are oriented from bottom to top. We take as definition the one in the upper-left corner. The other ones are obtained using that F^d_{abc} is a unitary matrix, as well as manipulating the associator diagrams ◇ and ◇.

The preservation of symmetry-invariant matrices is $\mu(\mathbb{P}) = P_{\epsilon\,(1)}\, S\big(P_{\epsilon\,(2)}\big) = \mathbb{1}$, which immediately follows from (4.B.8) and $\epsilon(P_\epsilon) = 1$. The property of being trace-preserving follows from

$$S\big(P_{\epsilon\,(2)}\big)\, P_{\epsilon\,(1)} = S\Big(S\big(P_{\epsilon\,(1)}\big)\, P_{\epsilon\,(2)}\Big) = S\big(\epsilon(P_\epsilon)\,\mathbb{1}\big) = \mathbb{1}\ , \tag{4.B.20}$$

where we used $S^2 = \mathrm{id}$ repeatedly.

In semisimple weak Hopf algebras where $S^2 = \mathrm{id}$, the symmetrizer is constructed using

$$\mathbb{P} = (\mathrm{id} \otimes S) \circ \Delta(h)\ , \tag{4.B.21}$$

where h is the Haar integral. By Th. 3.13 of [160], the properties 1. – 3. are satisfied. In particular, the preservation of symmetry-invariant matrices follows from

$$\mu(\mathbb{P}) = h_{(1)}\, S\big(h_{(2)}\big) = \Pi^{\mathrm{L}}(h) = \mathbb{1}\ . \tag{4.B.22}$$

The property of being trace-preserving instead follows from

$$S\big(h_{(2)}\big)\, h_{(1)} = S\Big(S\big(h_{(1)}\big)\, h_{(2)}\Big) = S\big(\Pi^{\mathrm{R}}(h)\big) = S(\mathbb{1}) = \mathbb{1}\ , \tag{4.B.23}$$

where we used $S^2 = \mathrm{id}$.

4.C *F*-symbols and the tube algebra

In the definition of the monoidal structure of $\mathscr{C}$ we follow the normalizations of [148]. The F-symbols F^d_{abc} are unitary isomorphisms

$$\bigoplus_e \mathrm{Hom}(\mathcal{L}_a{\otimes}\mathcal{L}_b, \mathcal{L}_e){\otimes}\mathrm{Hom}(\mathcal{L}_e{\otimes}\mathcal{L}_c, \mathcal{L}_d) \xrightarrow{\sim} \bigoplus_f \mathrm{Hom}(\mathcal{L}_a{\otimes}\mathcal{L}_f, \mathcal{L}_d){\otimes}\mathrm{Hom}(\mathcal{L}_b{\otimes}\mathcal{L}_c, \mathcal{L}_f) \tag{4.C.1}$$

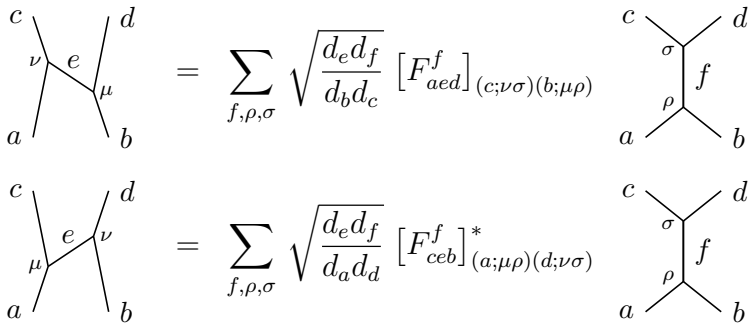


Figure 4.18: Other F-moves, derived from the ones in Fig. 4.17 by manipulating the associator diagrams. All lines run from bottom to top.

represented by a unitary square matrix of size

$$N^d_{abc} = \sum\nolimits_e N^e_{ab}\, N^d_{ec} = \sum\nolimits_f N^d_{af}\, N^f_{bc}\,. \tag{4.C.2}$$

We use the definition in (4.3.13). The vector spaces of morphisms are normalized such that the relations in (4.3.14) hold. Those relations, together with unitarity, allow one to fix various moves that we summarize in Figs. 4.17 and 4.18.

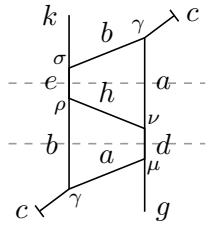
The F-symbols satisfy the pentagon equation:

$$\sum_\delta [F^e_{fcd}]_{(g;\beta\gamma)(l;\nu\delta)}\, [F^e_{abl}]_{(f;\alpha\delta)(k;\mu\lambda)} = \sum_{h,\psi,\sigma,\rho} [F^g_{abc}]_{(f;\alpha\beta)(h;\psi\sigma)}\, [F^e_{ahd}]_{(g;\sigma\gamma)(k;\rho\lambda)}\, [F^k_{bcd}]_{(h;\psi\rho)(l;\nu\mu)}\,. \tag{4.C.3}$$

Unitarity can be used to move the first F-symbol and the sum over $(h;\psi\sigma)$ (or the last F-symbol and the sum over $(h;\psi\rho)$) from the right to the left, obtaining in this way many other equivalent relations.

The basis elements of the tube algebra are defined in (4.3.15), and the structure coefficients M of the algebra are introduced in (4.3.17). To compute them we proceed as follows. First we fuse b with a into c using (4.3.14), then we section the diagram horizontally intro three parts:

$$(4.3.17) = \sum_{c,\gamma} \sqrt{\frac{d_c}{d_a d_b}} \tag{4.C.4}$$



and finally we apply the F-moves in Fig. 4.18. The resulting expression for M is in (4.3.18).

Case of an inverbile symmetry. In the special case of an invertible symmetry group G, possibly with 't Hooft anomaly ω, the fusion category $\mathscr{C}$ is Vec^ω_G. The

anomaly is parametrized by $\omega \in H^3\big(G, U(1)\big)$. The only nonvanishing F-symbols are

$$\big[F^{(abc)}_{abc}\big]_{(ab)(bc)} \equiv F_{abc} = \omega(a,b,c)\ . \tag{4.C.5}$$

On the left we used parenthesis (gh) to indicate the group multiplication, while in the middle we introduced a lighter notation for the F-symbols since they only depend on three group elements. The pentagon equation (4.C.3) is nonvanishing only if $e = (abcd)$, $f = (ab)$, $g = (abc)$, $h = (bc)$, $k = (bcd)$, $l = (cd)$, and it reads $F_{(ab)cd}\, F_{ab(cd)} = F_{abc}\, F_{a(bc)d}\, F_{bcd}$. This is precisely the cocycle condition $d\omega = 1$.

The elements of the tube algebra are specified by two labels: the vertical line incoming from below, and the horizontal line. Referring to (4.3.15), we specify g and a, while $d = ag$ and $h = aga^{-1}$. The nonvanishing structure coefficients of the tube algebra are then specified by three labels:

$$M^{ba,bag}_{g,a,ag,aga^{-1},b,baga^{-1},baga^{-1}b^{-1}} \ \equiv\ M_{g,a,b}\ . \tag{4.C.6}$$

Formula (4.3.19) gives:

$$M_{g,a,b} = \big[F_{baga^{-1}b^{-1},b,a}\big]^*\big[F_{b,aga^{-1},a}\big]\big[F_{b,a,g}\big]^* = \frac{\omega(b,aga^{-1},a)}{\omega(baga^{-1}b^{-1},b,a)\,\omega(b,a,g)}\ . \tag{4.C.7}$$

Associativity of the tube algebra is guaranteed by the following identity:

$$M_{g,a,b}\, M_{g,ba,c} = M_{g,a,cb}\, M_{aga^{-1},b,c}\ . \tag{4.C.8}$$

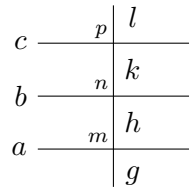
When expanded in terms of ω, this identity becomes equivalent to

$$\frac{d\omega(c,b,a,g)\ d\omega(c,baga^{-1}b^{-1},b,a)}{d\omega(c,b,aga^{-1},a)\ d\omega(cbaga^{-1}b^{-1}c^{-1},c,b,a)} = 1\ , \tag{4.C.9}$$

which is indeed a true equation because ω is a cocycle.

Associativity in the noninvertible case. In the general case, the tube algebra product is given by (4.3.18). Using an argument similar to the previous one, but with lengthier algebra, and in particular applying the pentagon equation (4.C.3) four times, one can show that the product is associative. Let us sketch the proof in the case without multiplicities, *i.e.*, for $N^c_{ab} \in \{0,1\}$. Associativity is the equation

$$\sum_{ds} M^{d,s}_{g,a,m,h,b,n,k}\, M^{f,t}_{g,d,s,k,c,p,l} = \sum_{er} M^{f,t}_{g,a,m,h,e,r,l}\, M^{e,r}_{h,b,n,k,c,p,l} \qquad \text{for} \tag{4.C.10}$$



Substituting the expression for M in (4.3.19), the quantum dimensions are the same on the two sides and can be dropped. One is left with the relation

$$\sum\nolimits_{ds} \big[F^s_{kba}\big]^*_{nd} \big[F^s_{bha}\big]_{nm} \big[F^s_{bag}\big]^*_{dm} \cdot \big[F^t_{lcd}\big]^*_{pf} \big[F^t_{ckd}\big]_{ps} \big[F^t_{cdg}\big]^*_{fs} \\ = \sum\nolimits_{er} \big[F^t_{lea}\big]^*_{rf} \big[F^t_{eha}\big]_{rm} \big[F^t_{eag}\big]^*_{fm} \cdot \big[F^r_{lcb}\big]^*_{pe} \big[F^r_{ckb}\big]_{pn} \big[F^r_{cbh}\big]^*_{en} \,. \quad (4.C.11)$$

This can be proven using the following set of four pentagon equations, obtained from (4.C.3) with various indices and possibly applying unitarity one or twice:

$$\begin{aligned} \big[F^t_{ckd}\big]_{ps} \big[F^s_{kba}\big]^*_{nd} &= \sum\nolimits_r \big[F^t_{pba}\big]^*_{rd} \big[F^r_{ckb}\big]_{pn} \big[F^t_{cna}\big]_{rs} \,, \\ \sum\nolimits_e \big[F^f_{cba}\big]^*_{ed} \big[F^t_{eag}\big]_{fm} \big[F^t_{cbm}\big]_{es} &= \big[F^t_{cdg}\big]_{fs} \big[F^s_{bag}\big]_{dm} \,, \\ \big[F^r_{cbh}\big]^*_{en} \big[F^t_{eha}\big]_{rm} &= \sum\nolimits_s \big[F^t_{cna}\big]_{rs} \big[F^s_{bha}\big]_{nm} \big[F^t_{cbm}\big]^*_{es} \,, \\ \sum\nolimits_d \big[F^t_{pba}\big]_{rd} \big[F^t_{lcd}\big]_{pf} \big[F^f_{cba}\big]^*_{ed} &= \big[F^r_{lcb}\big]_{pe} \big[F^t_{lea}\big]_{rf} \,. \end{aligned} \quad (4.C.12)$$

The first one and the complex conjugate of the second one are used on the l.h.s. of (4.C.11), while the third one and the complex conjugate of the fourth one are used on the r.h.s. On each side one ends up with a quadruple sum $\sum_{dser}$ of the same string, proving associativity.

4.D $\tilde{F}$-symbols and the strip algebra

The $\tilde{F}$-symbols of a left-module category $\mathcal{M}$, as defined in (4.4.6), satisfy a pentagon equation that also involves the F-symbols of the underlying fusion category $\mathscr{C}$:

$$\sum_\rho \big[\tilde{F}^n_{dcm}\big]_{(e;\beta\mu)(p;\nu\rho)} \big[\tilde{F}^n_{abp}\big]_{(d;\alpha\rho)(q;\sigma\tau)} = \sum_{f,\gamma,\delta,\omega} \big[F^e_{abc}\big]_{(d;\alpha\beta)(f;\gamma\delta)} \big[\tilde{F}^n_{afm}\big]_{(e;\delta\mu)(q;\omega\tau)} \big[\tilde{F}^q_{bcm}\big]_{(f;\gamma\omega)(p;\nu\sigma)} \,. \quad (4.D.1)$$

Unitarity of the F and $\tilde{F}$ symbols allows one to move the first or third term on the l.h.s. and the sum to the r.h.s. Similarly, the symbols ${}^R\tilde{F}$ satisfy a right-module pentagon equation:

$$\sum\nolimits_\omega \big[{}^R\tilde{F}^{\bar{m}}_{\bar{q}bc}\big]_{(\bar{p};\sigma\nu)(f;\gamma\omega)} \big[{}^R\tilde{F}^{\bar{m}}_{\bar{n}af}\big]_{(\bar{q};\tau\omega)(e;\delta\mu)} = \\ = \sum\nolimits_{d\alpha\beta\rho} \big[{}^R\tilde{F}^{\bar{p}}_{\bar{n}ab}\big]_{(\bar{q};\tau\sigma)(d;\alpha\rho)} \big[{}^R\tilde{F}^{\bar{m}}_{\bar{n}dc}\big]_{(\bar{p};\rho\nu)(e;\beta\mu)} \big[F^e_{abc}\big]_{(d;\alpha\beta)(f;\gamma\delta)} \,. \quad (4.D.2)$$

Associativity of the strip algebra. The strip algebra product was given in (4.4.13). Let us verify that it gives rise to an associative algebra, working for simplicity in the case that we use the same module on the right and on the left, and that there are no multiplicities. Associativity is the identity:

$$\sum\nolimits_d Q^d_{m,r,a,n,s,b,p,t} \, Q^f_{m,r,d,p,t,c,q,u} = \sum\nolimits_e Q^f_{m,r,a,n,s,e,q,u} \, Q^e_{n,s,b,p,t,c,q,u} \,. \quad (4.D.3)$$

Substituting the expression for Q, the quantum dimensions cancel out and we are left with

$$\sum\nolimits_d \big[\tilde{F}^t_{bar}\big]_{ds} \big[\tilde{F}^p_{bam}\big]^*_{dn} \big[\tilde{F}^u_{cdr}\big]_{ft} \big[\tilde{F}^q_{cdm}\big]^*_{fp} = \sum\nolimits_e \big[\tilde{F}^u_{ear}\big]_{fs} \big[\tilde{F}^q_{eam}\big]^*_{fn} \big[\tilde{F}^u_{cbs}\big]_{et} \big[\tilde{F}^q_{cbn}\big]^*_{ep} . \tag{4.D.4}$$

This identity can be verified using the module pentagon equation (4.D.1) twice, in particular in the following two forms:

$$\begin{aligned} \sum\nolimits_e \big[F^f_{cba}\big]^*_{ed} \big[\tilde{F}^u_{ear}\big]_{fs} \big[\tilde{F}^u_{cbs}\big]_{et} &= \big[\tilde{F}^u_{cdr}\big]_{ft} \big[\tilde{F}^t_{bar}\big]_{ds} , \\ \big[\tilde{F}^q_{eam}\big]_{fn} \big[\tilde{F}^q_{cbn}\big]_{ep} &= \sum\nolimits_d \big[F^f_{cba}\big]_{ed} \big[\tilde{F}^q_{cdm}\big]_{fp} \big[\tilde{F}^p_{bam}\big]_{dn} . \end{aligned} \tag{4.D.5}$$

The second one is used after complex conjugation. On both sides of (4.D.4) we obtain a double sum $\sum_{de}$ with the same string. This proves the identity.

4.E Module categories over $\mathsf{Vec}^{\omega}_{G}$

Consider a symmetry group G. We first consider the case that there is no anomaly, $\omega = 1$, therefore the fusion category is Vec_G. Module categories are labeled by conjugacy classes of subgroups $H \subseteq G$ and cocycles $\psi \in H^2\big(H, U(1)\big)$ (see Example 7.4.10 in [153]). Let us explain how the modules are constructed.

The simple objects $\mathcal{B}_m$ correspond to the right-cosets G/H. We indicate them as $\mu \in G/H$. There is a projection map $[\,\cdot\,]\colon G \to G/H$ so that $[m] = \mu$ if m is a representative of the class μ. The module action is simply

$$a \times [m] = [am] \qquad \text{for } a \in G\,, \quad [m] \in G/H\,. \tag{4.E.1}$$

This product is well defined, in the sense that it does not depend on the representative m chosen, because the coset is a right-coset. We can then write $a \times \mu = a\mu$. Notice that H and kHk^{-1} (where $k \in G$) define equivalent module categories. If we denote $[g]_1 \in G/H$ and $[g]_k \in G/(kHk^{-1})$, the isomorphism is given by $\varphi\big([g]_1\big) = [gk^{-1}]_k$.

In order to construct the $\tilde{F}$-symbols we need a map $h\colon G \times G/H \to H$. First, choose a lift $r\colon G/H \to G$ of $[\,\cdot\,]$, that is a map

$$r(\mu) \qquad \text{such that} \qquad [r(\mu)] = \mu\,. \tag{4.E.2}$$

In general, $a \cdot r(\mu) \neq r(a\mu)$, however $[a \cdot r(\mu)] = a\mu = [r(a\mu)]$, therefore the two terms in the inequality differ by the action of H from the right. This allows us to define

$$h(a,\mu) \qquad \text{such that} \qquad a \cdot r(\mu) = r(a\mu) \cdot h(a,\mu)\,. \tag{4.E.3}$$

By considering $ab \cdot r(\mu)$ one obtains the identity

$$h(ab,\mu) = h(a,b\mu) \cdot h(b,\mu)\,. \tag{4.E.4}$$

Besides, $h(1,\mu)=1$ and so $h(a^{-1},\mu)=h(a,a^{-1}\mu)^{-1}$. We then define the $\tilde{F}$-symbols as

$$\tilde{F}_{ab\mu}=\psi\big(h(a,b\mu),h(b,\mu)\big)\ . \tag{4.E.5}$$

The indices not indicated are fixed. The left-module pentagon equation reads:

$$\tilde{F}_{ab,c,\mu}\ \tilde{F}_{a,b,c\mu}=F_{a,b,c}\ \tilde{F}_{a,bc,\mu}\ \tilde{F}_{b,c,\mu}\ . \tag{4.E.6}$$

As we are assuming that there are no anomalies, $\omega=1$, we have $F_{a,b,c}=1$. The remaining terms organize as

$$\frac{\psi\big[h(b,c\mu),h(c,\mu)\big]\,\psi\big[h(a,bc\mu),h(bc,\mu)\big]}{\psi\big[h(ab,c\mu),h(c,\mu)\big]\,\psi\big[h(a,bc\mu),h(b,c\mu)\big]}=d\psi\big[h(a,bc\mu),h(b,c\mu),h(c,\mu)\big]=1\ . \tag{4.E.7}$$

This equation is satisfied because ψ is a cocycle. Thus the pentagon equation is satisfied.

There are two extreme cases. When $H=\{1\}$ we obtain the regular module, whose simple objects are all the elements of G. Such a module is completely fixed by G. Indeed $r(\mu)=\mu\in G$, $h(a,\mu)=1$, and ψ is trivial so that $\tilde{F}=\omega$ is trivial. When $H=G$, instead, the module has a single simple object (which is then a strongly-symmetric boundary condition) and the inequivalent consistent $\tilde{F}$-symbols parametrize the different SPT phases of G — or equivalently projective representations of G.

Consider now the general case that ω is not necessarily vanishing. This includes the case that ω vanishes in cohomology, but we have chosen a representative that is not identically 1. We will however use normalized cocycles. The fusion category is Vec_G^{ω}. Then module categories are labeled by:

- the conjugacy class of a subgroup $H\subseteq G$ such that $\omega\big|_H$ is trivial in $H^3\big(H,U(1)\big)$;
- a cochain $\psi\in C^2\big(H,U(1)\big)$ such that (using multiplicative notation):

$$d\psi=\omega^{-1}\big|_H\ . \tag{4.E.8}$$

  Such cochains form a torsor over $H^2\big(H,U(1)\big)$.

As before, the simple objects are classes of G/H and fusion is defined in the natural way. Given a lift r of the projection and the map $h(a,\mu)\in H$ defined in (4.E.3), the $\tilde{F}$-symbols are

$$\tilde{F}_{ab\mu}=\psi\big(h(a,b\mu),h(b,\mu)\big)\ \frac{\omega\big(r(ab\mu),h(a,b\mu),h(b,\mu)\big)\,\omega\big(a,b,r(\mu)\big)}{\omega\big(a,r(b\mu),h(b,\mu)\big)}\ . \tag{4.E.9}$$

The only thing to check is that the left-module pentagon equation is satisfied. The condition (4.E.8) on ψ reads:

$$\frac{\psi\big[h(b,c\mu),h(c,\mu)\big]\,\psi\big[h(a,bc\mu),h(bc,\mu)\big]}{\psi\big[h(ab,c\mu),h(c,\mu)\big]\,\psi\big[h(a,bc\mu),h(b,c\mu)\big]} = d\psi = \omega\big[h(a,bc\mu),h(b,c\mu),h(c,\mu)\big]^{-1}\,. \tag{4.E.10}$$

When substituting into the pentagon equation, we obtain

$$\begin{aligned}&\Big\{\omega[a,b,c]\,\omega[a,bc,r(\mu)]\,\omega[a,r(bc\mu),h_{b,c\mu}]\,\omega[b,c,r(\mu)]\,\omega[ab,r(c\mu),h_{c,\mu}]\,\times \qquad (4.E.11)\\ &\omega[r(bc\mu),h_{b,c\mu},h_{c,\mu}]\,\omega[r(abc\mu),h_{a,bc\mu},h_{bc,\mu}]\Big\}\Big/\Big\{\omega[a,b,r(c\mu)]\,\omega[a,r(bc\mu),h_{bc,\mu}]\,\omega[b,r(c\mu),h_{c,\mu}]\,\times\\ &\omega[h_{a,bc\mu},h_{b,c\mu},h_{c,\mu}]\,\omega[ab,c,r(\mu)]\,\omega[r(abc\mu),h_{a,bc\mu},h_{b,c\mu}]\,\omega[r(abc\mu),h_{ab,c\mu},h_{c,\mu}]\Big\}\overset{?}{=}1\,,\end{aligned}$$

where we used a more compact notation for h. The expression on the left is indeed equal to 1, using that $d\omega[a,b,c,r(\mu)]$, $d\omega[a,b,r(c\mu),h_{c,\mu}]$, $d\omega[a,r(bc\mu),h_{b,c\mu},h_{c,\mu}]$, $d\omega[r(abc\mu),h_{a,bc\mu},h_{b,c\mu},h_{c,\mu}]$ are all equal to 1, as well as the multiplication properties of r and h given above.

Chapter 5

Entanglement in non-Hermitian systems

Last years have witnessed a growing interest in non-Hermitian quantum mechanics. This has been particularly motivated by the appearance of non-Hermitian Hamiltonians in the effective description of a wide variety of phenomena [189, 190], as, for example, in the analysis of the PT symmetry [191–193], in the study of optical effects [194, 195], or in the investigation of the non-equilibrium properties of open and dissipative systems [196–198] as well as measurement-induced transitions [199–201], to cite some of them.

One of the most relevant applications of non-Hermitian quantum Hamiltonians nowadays is to measurement-induced phenomena. It has been shown that the unitary time evolution of a quantum state that is subject to a protocol of repeated measurements can be effectively described by a non-Hermitian Hamiltonian in the low-rate regime of measurements. In particular, in [202], the unitary evolution is generated by the Hermitian SSH model while the effective dynamics that takes into account the effect of the measurements introduces a staggered imaginary chemical potential that breaks Hermiticity. An experimental realization of a protocol of repeated measurements has been recently reported in [203] using a superconducting quantum processor.

Entanglement for non-Hermitian systems has been studied with the use of non-unitary CFTs [204–211]. The main difficulty when studying entanglement in non-Hermitian models is the lack of a proper entanglement measure: the reduced density matrix can be non-positive definite and, consequently, the entanglement entropy can actually be negative or even complex. For this reason, several non-Hermitian extensions of it have been proposed in the literature, which include both changing explicitly the definition of the entanglement entropy as in [211], or implicitly by introducing a modified version of the partial trace as in [208]. A common feature of all these approaches is that they are sensitive to criticality and provide information about the non-unitary CFT under study.

Recent experiments with cold atoms and ion traps have shown that some properties of many-body quantum systems can be understood by analyzing the entanglement in the symmetry sectors of the theory [212–216]. The basic tool to investigate how entanglement distributes among symmetry sectors is the *symmetry-resolved entanglement entropy* [82, 83, 217], which provides a finer measure of the entanglement content in extended systems that is not accessible from the total entanglement entropy. This fact has currently triggered an intense research activity on the interplay between symmetries and entanglement in very different systems, including spin chains [82, 83, 141, 218–228], integrable [85, 229–234] and conformal field theories [76, 82, 83, 86, 235–246], and involving diverse contexts such as disorder [247–250], non-equilibrium dynamics [251–255], topological phases [256–258] or holography [259–262].

In the first part of this chapter, we extend the notion of symmetry resolution of entanglement to the non-Hermitian case. To this end, we examine in detail the symmetry resolution of entanglement in the ground state of the non-Hermitian version of the Su-Schrieffer-Heeger (SSH) model at criticality. This is the simplest one-dimensional quadratic fermionic chain that breaks Hermiticity with a global $U(1)$ symmetry associated to particle number conservation, and presents non-trivial features, such as topological phases [263–267]. The critical point is described by the bc-ghost CFT with central charge $c = -2$ [210]. Some properties of the critical ground state entanglement of this model have been already examined in [207, 210, 211]; in particular, it has been found that both the usual entanglement entropy and the generalized version introduced in [211] are proportional to the central charge at leading order in the subsystem size and, therefore, they are negative. Away from criticality, the focus of attention has been the analysis of the entanglement spectrum [210, 268], that is the spectrum of the reduced density matrix, since it offers useful insights on the topology of the model [269].

In Hermitian systems, the entropy of each symmetry sector is usually calculated via the charged moments of the reduced density matrix [82]. Inspired by the generalized entanglement entropy defined in [211], we consider here the charged moments of the absolute value of the reduced density matrix, which we call *absolute charged moments*. We compute them in the ground state of the bc-ghost theory. The analysis of the resulting expression allows us to trace back the origin of the negativeness of the reduced density matrix and, consequently, of the (generalized) Rényi entanglement entropies in the models described by this CFT: the sign of the reduced density matrix eigenvalues depends on the parity of the charge sector to which they belong. With this observation, we can define a positive semi-definite density matrix for each charge sector and, from it, a positive symmetry-resolved Rényi entanglement entropy.

Another remarkable consequence of the charge-dependent signature of the entanglement spectrum in the bc-ghost theory is that the expression of the standard Rényi entanglement entropies depends on the parity of the Rényi index n. As

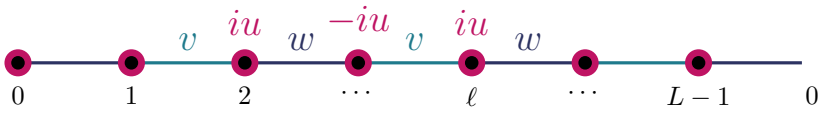


Figure 5.1: Schematic representation of the nH-SSH model, described by (5.1.1). The nearest neighbours hoppings have alternating strengths v and w. The imaginary chemical potential is set to iu on the even sites and $-iu$ on the odd sites.

byproduct of this result, we analytically obtain the distribution of the entanglement spectrum in this CFT, which differs from the unitary case [270], and we check it against the exact numerical entanglement spectrum of the critical non-Hermitian SSH model.

We then conduct an exploratory numerical investigation of the entanglemet Hamiltonian in the non-Hermitian Su-Schrieffer-Heeger model, both in the gapped phase and at criticality. In the gapped phase we observe that the lattice EH has a structure analogous to the one of integrable lattice models. At the critical point, we instead find an additional term not accounted for in the Bisognano-Wichmann theorem, which is responsible for the negativeness of the entanglement entropies.

The chapter is organized as follows. In Sec. 5.1, we introduce the non-Hermitian SSH chain and we diagonalize it. In Sec. 5.2, we review the necessary quantities to generalize the concept of symmetry-resolved entanglement to non-Hermitian systems. In Sec. 5.3, we consider the bc-ghost CFT and we obtain the absolute charged moments of the ground state reduced density matrix. With them, in Sec. 5.4, we calculate the symmetry-resolved entanglement entropy in this system. In Appendix 5.5 we apply the results of the previous section to compute the standard Rényi entanglement entropies, from which, in Appendix 5.6, we determine the distribution of the entanglement spectrum, with some details left to Appendix 5.A. In Appendix 5.8 we repor the numerical lattice EH in the non-Hermitian SSH model: we first consider the topologically trivial gapped phase in Appendix 5.8.1 and we then study the critical point in Appendix 5.8.2. We draw our conclusions in Appendix 5.9.

5.1 PT symmetric non-Hermitian SSH model

In this section we introduce the non-Hermitian model that we study in this work. We consider the non-Hermitian SSH (nH-SSH) chain with PT-symmetry on a discrete circle of $L = 2N$ sites, described by the Hamiltonian

$$H = \sum_{j\in\mathbb{Z}_N} \left(-w\, c_{2j}^\dagger c_{2j+1} - v\, c_{2j-1}^\dagger c_{2j} + \text{h.c.}\right) + iu \sum_{j\in\mathbb{Z}_N} \left(c_{2j}^\dagger c_{2j} - c_{2j+1}^\dagger c_{2j+1}\right), \quad (5.1.1)$$

with $u, v, w > 0$. A schematic representation of this Hamiltonian is depicted in Fig. 5.1. We assume quasi-periodic boundary conditions, i.e., $c_{j+L} = e^{i\delta} c_j$,

with $0 < \delta \ll 1$. The reason for this choice will be explained later. The model is a fermionic chain with nearest neighbours hoppings, which have alternating strength on even-odd links. The staggered imaginary chemical potential breaks the hermiticity of the Hamiltonian. Notice that our conventions match those in [211] after setting $v_1 = 0$ and $v_2 = v$ and identifying their up (down) sites with our even (odd) ones.

Since the Hamiltonian is a linear combination of terms of the form $c_i^\dagger c_j$, it is invariant under the $U(1)$ generated by

$$Q = \sum_{j \in \mathbb{Z}_{2N}} c_j^\dagger c_j \,. \tag{5.1.2}$$

This will be the conserved charge with respect to which we resolve the entanglement in the ground state of the model.

The kernel in the Hamiltonian becomes block diagonal after a Fourier transform of the lattice operators, performed separately on the even and odd sites

$$\tilde{c}_{k,\mathrm{e}} = \frac{1}{\sqrt{N}} \sum_{j \in \mathbb{Z}_N} e^{-ikj} c_{2j} \,, \qquad \tilde{c}_{k,\mathrm{o}} = \frac{1}{\sqrt{N}} \sum_{j \in \mathbb{Z}_N} e^{-ikj} c_{2j+1} \,, \tag{5.1.3}$$

with

$$k \in \frac{2\pi}{N} \left(\mathbb{Z}_N + \frac{\delta}{2\pi} \right), \tag{5.1.4}$$

where the shift in momentum space is due to the δ-twisted boundary conditions. The Hamiltonian then becomes

$$H = \sum_k \begin{pmatrix} \tilde{c}_{k,\mathrm{e}}^\dagger & \tilde{c}_{k,\mathrm{o}}^\dagger \end{pmatrix} \mathcal{H}_k \begin{pmatrix} \tilde{c}_{k,\mathrm{e}} \\ \tilde{c}_{k,\mathrm{o}} \end{pmatrix}, \tag{5.1.5}$$

where

$$\mathcal{H}_k = \begin{pmatrix} iu & \eta_k \\ \eta_k^* & -iu \end{pmatrix}, \qquad \eta_k = -w - ve^{-ik}. \tag{5.1.6}$$

If $u \neq 0$, $\mathcal{H}_k$ is not Hermitian but it is still diagonalizable for almost every k, with an exception that will be discussed later. In fact, there exists an invertible matrix $M(k)$,

$$M(k) = \begin{pmatrix} \frac{\eta_k}{|\eta_k|} \cos(\xi_k) & -\frac{\eta_k}{|\eta_k|} \sin(\xi_k) \\ \sin(\xi_k) & \cos(\xi_k) \end{pmatrix}, \tag{5.1.7}$$

where $2\xi_k = \tan^{-1}(|\eta_k| / (iu))$, such that

$$\mathcal{H}_k = M(k) E(k) M(k)^{-1}, \tag{5.1.8}$$

with $E(k) = \mathrm{diag}(\varepsilon_{+,k}, \varepsilon_{-,k})$ and eigenvalues

$$\varepsilon_{\pm,k} = \pm \sqrt{|\eta_k|^2 - u^2}. \tag{5.1.9}$$



Figure 5.2: Phase diagram of the nH-SSH model, explained in the main text. The orange circle and the green square mark the points in parameter space for which we focus our studies. At the orange circle point, we study the entanglement Hamiltonian; at the green square point, we study the entanglement Hamiltonian and symmetry resolved entanglement.

Therefore, introducing the new creation and annihilation operators $\mathbf{f}_k^\dagger = (f_{+,k}^\dagger, f_{-,k}^\dagger)$ and $\mathbf{d}_k = (d_{+,k}, d_{-,k})^t$,

$$\mathbf{f}_k^\dagger = \begin{pmatrix} \tilde{c}_{k,e}^\dagger & \tilde{c}_{k,o}^\dagger \end{pmatrix} M(k) \qquad \mathbf{d}_k = M(k)^{-1} \begin{pmatrix} \tilde{c}_{k,e} \\ \tilde{c}_{k,o} \end{pmatrix} \tag{5.1.10}$$

the Hamiltonian is diagonal in terms of them,

$$H = \sum_k \mathbf{f}_k^\dagger E(k) \mathbf{d}_k. \tag{5.1.11}$$

Phase diagram Varying the relative strengths of the parameters u, v, w, the model admits three different gapped phases [210]. If $v - w \in (-u, u)$, the PT symmetry is broken so that the energy spectrum is complex and the eigenvalues appear in complex conjugate pairs. In the two phases $v - w > u$ or $v - w < -u$, the PT symmetry is unbroken and the energy spectrum is real. The latter two phases are distinguished by topological properties, as discussed in [265]. The resulting phase diagram is given in Fig. 5.2.

Two critical points occur for $v - w = \pm u$. In these cases, the single-particle spectrum is $\epsilon_{\pm,k} = \pm\sqrt{2vw(1 + \cos k)}$ and the gap closes at $k = \pi$, leading locally to a linear spectrum with speed of sound

$$c_S = \sqrt{vw}. \tag{5.1.12}$$

Moreover, at $k = \pi$ the kernel of the Hamiltonian (5.1.5) is not diagonalisable, as it is made of a 2×2 Jordan block. This is called an exceptional point in momentum space. The exceptional point occurs because, as $k \to \pi$, the two eigenspaces become more and more collinear, and they perfectly coincide at $k = \pi$.

Left and right groundstates The eigenstates of the Hamiltonian can be constructed in the following way. Let us introduce the set of labels of the single particle eigenstates of H, $\Gamma = \{+, -\} \times \{k\}$. The vacuum state $|0\rangle$ is defined as the one annihilated by d_p for every $p \in \Gamma$ and, therefore, $H|0\rangle = 0$. The *right* eigenstates of H are then obtained by applying sequences of $f_p^\dagger$ operators to the vacuum. More precisely, let B be a subset of Γ, then $|B_R\rangle = \prod_{p \in B} f_p^\dagger |0\rangle$ is a right eigenstate

of H with eigenvalue $\sum_{p\in B}\varepsilon_p$. Analogously, *left* eigenstates are constructed by applying sequences of d_p operators to $\langle 0|$ on the right, thus $\langle B_L| = \langle 0|\prod_{p\in B} d_p$ is a left eigenstate of H with eigenvalue $\sum_{p\in B}\varepsilon_p$.

If the spectrum of H is real, then the eigenvalues can be ordered and the notion of ground state is well defined: it is the many-body state in which all the single particle states with negative energy are occupied. We call $|R\rangle$ the right ground state and $\langle L|$ the left ground state, which are explicitly

$$\langle L| = \langle 0|\prod_k d_{k,-} \qquad |R\rangle = \prod_k f^\dagger_{k,-}|0\rangle\,. \tag{5.1.13}$$

In a non-Hermitian setting, the natural way to define the expectation value of an observable $\mathcal{O}$ in the ground state of H is $\langle L|\,\mathcal{O}\,|R\rangle$, see [271]. It follows then that the ground state density matrix is $\rho = |R\rangle\langle L|$. Observe that, if the system is at temperature $1/\beta$, its state may be described by the Gibbs ensemble $\rho_\beta = e^{-\beta H}/\mathrm{Tr}(e^{-\beta H})$, which in the zero-temperature limit leads to $\rho = |R\rangle\langle L|$. As shown in detail in [204, 209], this fact facilitates the study in field theories of the entanglement entropies of ρ since it allows, within the path integral formalism, to straightforwardly identify the moments of the reduced density matrix with partition functions on a replicated Riemann surface or, alternatively, with correlators of twist fields.

One may consider other density matrices, such as $|R\rangle\langle R|$, which is Hermitian, and yields a positive definite reduced density matrix and entanglement entropies. Some entanglement properties of this density matrix in the gapped regions of the Hamiltonian (5.1.1) have been examined in [268]. However, as observed in [209], the Rényi entanglement entropies are harder to compute in field theory since the connection with partition functions on a replicated surface is not as direct as in the case $|R\rangle\langle L|$, it involves a time reversal operation that is in general a difficult problem. Since we are interested in study the universal properties of the symmetry-resolved ground state entanglement of the critical non-Hermitian SSH chain and the corresponding CFT, in the rest of the chapter we take as ground state the density matrix $\rho = |R\rangle\langle L|$. We refer the reader to [209] for a thorough discussion on the possible choices of the total density matrix in non-Hermitian systems.

Correlation matrix A key object in our analysis of the entanglement properties of the left-right ground state is the two-point correlation matrix C with entries [210]

$$C_{2j+a,2l+b} = \langle L|c^\dagger_{2j+a}c_{2l+b}|R\rangle = \frac{1}{N}\sum_k e^{-ik(j-l)}\mathcal{G}(k)_{ab}\,, \quad a,b\in\{0,1\}, \tag{5.1.14}$$

with

$$\mathcal{G}(k) = \frac{1}{2}\begin{pmatrix} 1-\cos(2\xi_k) & -\sqrt{\frac{\eta_k^*}{\eta_k}}\sin(2\xi_k) \\ -\sqrt{\frac{\eta_k}{\eta_k^*}}\sin(2\xi_k) & 1+\cos(2\xi_k)\end{pmatrix}, \tag{5.1.15}$$

where $2\xi_k = \tan^{-1}(|\eta_k|/(iu))$, $\eta_k = -w - ve^{-ik}$. Due to the dimerization of the hopping amplitudes v, w, the correlation matrix C presents a block structure. In the thermodynamic limit $L \to \infty$, C is a block Toeplitz matrix generated by the symbol $\mathcal{G}$.

As we have pointed out in the introduction, in this chapter we are interested in studying the symmetry resolution of the ground state entanglement with respect to the $U(1)$ symmetry associated with particle number conservation at criticality. Therefore, in the following, we will restrict our analysis to the critical line $u = w - v$, which separates the PT-unbroken and topologically trivial phase from the PT-broken phase.

5.2 Symmetry-resolved entanglement

In this section, we introduce all the quantities that we will use to investigate the symmetry-resolved entanglement in the ground state of the critical non-Hermitian SSH model previously discussed.

We consider a spatial bipartition of the system $A \cup \bar{A}$ with A a subset of contiguous sites of length 2ℓ. Then the total Hilbert space factorizes into $\mathscr{H}_A \otimes \mathscr{H}_{\bar{A}}$. As we have seen in the previous section, the ground state density matrix is $\rho = |R\rangle \langle L|$. The reduced density matrix that describes the state of subsystem A is obtained by taking the partial trace to the complementary subsystem $\bar{A}$, $\rho_A = \mathrm{Tr}_{\bar{A}}(\rho)$.

In a non-Hermitian system, we have to take into account that ρ is positive semi-definite, $\rho \geq 0$, but is generally not Hermitian, $\rho^\dagger \neq \rho$ [271]. This fact implies that ρ_A may not be positive semi-definite. Thus the eigenvalues of ρ_A can be negative or even complex. In any case, $\mathrm{Tr}(\rho) = \mathrm{Tr}(\rho_A) = 1$.

Since ρ_A is not positive semi-definite, the entanglement entropy can be complex and ambiguous, depending on which branch of the logarithm we take. In the recent [211] a new quantity dubbed *generalized entanglement entropy* is introduced,

$$S^{\mathrm{g}}(\rho_A) = -\mathrm{Tr}(\rho_A \log |\rho_A|). \tag{5.2.1}$$

Observe that the only difference with the usual entropy is that it takes the logarithm of $|\rho_A|$ instead of ρ_A: if ρ_A is diagonalized by the matrix R such that $\rho_A = R^{-1}\mathrm{diag}(\lambda_j)R$, then $|\rho_A| \coloneqq R^{-1}\mathrm{diag}(|\lambda_j|)R$. This guarantees that S^{g} is real when the eigenvalues of ρ_A are either negative or complex in conjugate pairs. Note that, when $\rho_A \geq 0$, it reduces to the standard entanglement entropy, $S^{\mathrm{g}}(\rho_A) = S(\rho_A)$. Although $S^{\mathrm{g}}(\rho_A)$ can be negative, and its interpretation as an entanglement measure is not clear, it satisfies that $S^{\mathrm{g}}(\rho_A) \neq 0$ only if the subsystems A and $\bar{A}$ are entangled. Moreover, analogously to the standard entanglement entropy, it may be useful to extract information about the (non-unitary) CFTs that describe critical non-Hermitian systems. In fact, in [211], it has been verified for a set

of critical non-Hermitian models, including the non-Hermitian SSH, that $S^{\mathrm{g}}(\rho_A)$ scales as $c/3 \log \ell$, even when the central charge of the associated CFT is negative. In [272], the generalized entanglement entropy (5.2.1) has been employed to study the entanglement of typical eigenstates of non-Hermitian systems and get a non-Hermitian analogue of the Page curve.

Together with the generalized entanglement entropy, one can introduce the *generalized Renyi entropies*

$$S_n^{\mathrm{g}}(\rho_A) = \frac{1}{1-n} \log \mathrm{Tr}\left(\rho_A \left|\rho_A\right|^{n-1}\right) \tag{5.2.2}$$

that satisfy $S^g = \lim_{n\to 1} S_n^{\mathrm{g}}$.

Using the generalized entanglement entropy (5.2.1), we can extend the notion of symmetry-resolved entanglement [82, 83, 217] to non-Hermitian systems. Let us assume that the system has an internal $U(1)$ symmetry generated by a charge operator Q, which in our case will be the particle number operator of (5.1.2). This operator can be decomposed as the sum of the charge in A and $\bar{A}$, $Q = Q_A + Q_{\bar{A}}$. If the left and the right ground states $|R\rangle$ and $\langle L|$ are eigenstates of Q, as occurs in the non-Hermitian SSH model, then $\rho = |R\rangle \langle L|$ commutes with Q. This implies that ρ_A acts separately on each eigenspace of Q_A. Let us denote by Π_q the projector onto the eigenspace of Q_A with eigenvalue $q \in \mathbb{Z}$, also called *charge sector*. We then can construct a density matrix $\rho_{A,q}$ for each charge sector,

$$\rho_{A,q} = \frac{\Pi_q \rho_A \Pi_q}{p(q)}, \tag{5.2.3}$$

where $p(q) = \mathrm{Tr}(\Pi_q \rho_A)$ normalizes it to $\mathrm{Tr}(\rho_{A,q}) = 1$, such that

$$\rho_A = \bigoplus_q p(q) \rho_{A,q}. \tag{5.2.4}$$

In Hermitian systems, $p(q)$ is interpreted as the probability of finding the subsystem A in the sector with charge q. However, now ρ_A is not positive definite, so $p(q)$ may be negative, as well as larger than 1. Hence the interpretation of $p(q)$ as a probability is lost in the non-Hermitian case.

Applying (5.2.4), the generalized entanglement entropy (5.2.1) admits the following decomposition in the charge sectors of Q_A,

$$S^{\mathrm{g}}(\rho_A) = -\sum_q p(q) \log |p(q)| + \sum_q p(q) S^{\mathrm{g}}(\rho_{A,q}). \tag{5.2.5}$$

In the Hermitian case, the first term on the right hand side is commonly referred as the *number entropy* while the second is called *configurational entropy* [212, 222, 273].

The symmetry-resolved Rényi entanglement entropies $S^{\mathrm{g}}(\rho_{A,q})$ can be calculated using the Fourier representation of the projector Π_q. In fact, introducing the *absolute charged moments* of ρ_A

$$Z_n^{\mathrm{g}}(\alpha) = \mathrm{Tr}\left(\rho_A \left|\rho_A\right|^{n-1} e^{i\alpha Q_A}\right) \tag{5.2.6}$$

and their Fourier transform

$$\mathcal{Z}_n^{\rm g}(q) \coloneqq \mathrm{Tr}\left(\Pi_q \rho_A \left|\rho_A\right|^{n-1}\right) = \int_{-\pi}^{\pi} \frac{d\alpha}{2\pi} e^{-i\alpha q} Z_n^{\rm g}(\alpha), \tag{5.2.7}$$

it is possible to express all the ingredients of (5.2.5) in the form $p(q) = \mathcal{Z}_1^{\rm g}(q)$ and

$$S_n^{\rm g}(\rho_{A,q}) = \frac{1}{1-n} \log \frac{\mathcal{Z}_n^{\rm g}(q)}{\mathcal{Z}_1^{\rm g}(q) \left|\mathcal{Z}_1^{\rm g}(q)\right|^{n-1}}. \tag{5.2.8}$$

When ρ_A is positive definite, $Z_n^{\rm g}(\alpha)$ is equal to the usual *charged moments* of ρ_A,

$$Z_n(\alpha) = \mathrm{Tr}\left(\rho_A^n e^{i\alpha Q_A}\right). \tag{5.2.9}$$

In quadratic fermionic chains, the moments $Z_n(\alpha), Z_n^{\rm g}(\alpha)$ as well the whole reduced density matrix ρ_A are accessible through the two-point correlation matrix of (5.1.14) restricted to the subsystem A. This result was initially derived for Hermitian systems [102] but it also holds in the non-Hermitian case [268]. Since the Hamiltonian is quadratic, then the ground state reduced density matrix satisfies the Wick theorem and, therefore, it is in general a Gaussian operator of the form

$$\rho_A = \frac{e^{-K_A}}{Z_A}, \tag{5.2.10}$$

with

$$K_A = \sum_{ij \in A} c_i^\dagger k_{ij}^A c_j. \tag{5.2.11}$$

The relation with the two-point correlation matrix is set by

$$k^A = \log\left[C_A^{-1} - \mathbb{I}\right]^T, \tag{5.2.12}$$

and $Z_A^{-1} = \det(I - C_A)$, where C_A is the restriction of C to subsystem A, and the superscript t indicates transposition. The entanglement Hamiltonian K_A will be studied in detail in Appendix 5.8. Denoting by ν_j the eigenvalues of C_A, it follows that

$$\log Z_n^{\rm g}(\alpha) = \sum_{j=1}^{2\ell} \log\left[\nu_j |\nu_j|^{n-1} e^{i\alpha} + (1-\nu_j)|1-\nu_j|^{n-1}\right] \tag{5.2.13}$$

and

$$S^{\rm g}(\rho_A) = -\sum_{j=1}^{2\ell} \left[\nu_j \log|\nu_j| + (1-\nu_j)\log|1-\nu_j|\right]. \tag{5.2.14}$$

The standard quantities $Z_n(\alpha)$ and $S(\rho_A)$ follow analogue formulae without the absolute values. In particular,

$$\log Z_n(\alpha) = \sum_{j=1}^{2\ell} \log\left[\nu_j^n e^{i\alpha} + (1-\nu_j)^n\right]. \tag{5.2.15}$$

5.3 Absolute charged moments in the *bc*-ghost CFT

In this section, we obtain the absolute charged moments $Z_n^{\mathrm{g}}(\alpha)$, defined in (5.2.6), in the ground state of the non-Hermitian SSH model along the critical line $u = w - v$. To this end, we study them both numerically using (5.2.13) and analytically by considering the non-unitary CFT that describes the model at criticality.

On the critical line $u = w - v$, the low-energy physics of the non-Hermitian SSH model of (5.1.1) is captured by the *bc*-ghost CFT with central charge $c = -2$, see [210]. The action of this theory reads [96, 274]

$$S_{bc} = \int d^2z (\psi_b \bar{\partial} \psi_c + \bar{\psi}_b \partial \bar{\psi}_c), \tag{5.3.1}$$

where $\psi_b(z)$ and $\psi_c(z)$ are anti-commuting holomorphic primary fields with conformal weights $h_b = 1$ and $h_c = 0$ respectively, while $\bar{\psi}_b(\bar{z})$ and $\bar{\psi}_c(\bar{z})$ denote their anti-holomorphic counterparts.

The *bc*-ghost CFT has a global $U(1)$ symmetry associated to *ghost number* conservation, which on the lattice corresponds to the particle number of (5.1.2). The holomorphic Noether current is

$$j(z) = - : \psi_b(z)\psi_c(z) : . \tag{5.3.2}$$

To determine the universal terms of the different moments of ρ_A introduced in Sec. 5.2, we consider the orbifold theory $\mathrm{CFT}^{\otimes n}/\mathbb{Z}_n$, obtained by taking n copies on the complex plane of the CFT under study and then quotient the resulting tensor product by the $\mathbb{Z}_n$ symmetry related to the the cyclic permutation of the replicas.

Before proceeding, it is important to remark that we are assuming that the CFT is defined in the complex plane, which corresponds to taking an infinite system, i.e. $L \to \infty$, while the numerical calculations are done for a finite chain with periodic boundary conditions. In CFT, a finite periodic system is obtained by conformally mapping the complex plane to a cylinder. Since the moments of ρ_A are given by correlators of primary fields, the effect of this map in the expression for the moments of ρ_A is simply to replace the subsystem length ℓ by the chord length

$$\ell_{\mathrm{e}} = \frac{L}{\pi} \sin\left(\frac{\pi \ell}{L}\right). \tag{5.3.3}$$

In unitary CFTs, the ground state neutral moments $Z_n(0) = \mathrm{Tr}(\rho_A^n)$ are given by the two-point correlation function of the orbifold [11, 275]

$$Z_n(0) = \langle 0 | \, \tau_n(0) \tilde{\tau}_n(\ell) \, | 0 \rangle \, . \tag{5.3.4}$$

Here $|0\rangle$ denotes the conformal vacuum, i.e. the state of the CFT invariant under global conformal transformations, and the fields τ_n, $\tilde{\tau}_n$ are called twist and anti-twist

fields. The winding around the point where τ_n ($\tilde{\tau}_n$) is inserted takes a field $\mathcal{O}_k$ living in the copy k of the orbifold into the copy $k+1$ ($k-1$), for example

$$\mathcal{O}_k(e^{2\pi i}z)\tau_n(0) = \tau_n(0)\mathcal{O}_{k+1}(z). \tag{5.3.5}$$

The twist and anti-twist fields are spinless primaries with conformal dimension

$$h_n^\tau = \frac{c}{24}\left(n - \frac{1}{n}\right). \tag{5.3.6}$$

In non-unitary CFTs, the previous discussion is more subtle because the physical ground state is not the conformal vacuum $|0\rangle$. In general, the physical ground state corresponds to the lowest eigenstate of the Virasoro operator L_0. In unitary CFTs, such eigenstate is the conformal vacuum since all the non-trivial primary fields have positive conformal dimension. On the contrary, in non-unitary CFTs, we can find primary fields with negative dimension. This implies that the ground state is the state $|\phi\rangle = \phi(0)\,|0\rangle$ associated to the primary ϕ with the lowest dimension $h_\phi \leq 0$. In [204, 205], it was proposed that in such case the ground state neutral moments are given by the orbifold two-point correlations

$$Z_n(0) = \frac{\langle 0|\, \tau_n^\phi(0)\tilde{\tau}_n^\phi(\ell)\,|0\rangle}{\langle 0|\, \phi(0)\phi(\ell)\,|0\rangle^n}, \tag{5.3.7}$$

involving the composite field $\tau_n^\phi \equiv \tau_n \cdot \phi$, which is a spinless primary field of the orbifold with dimension

$$h_n^{\tau^\phi} = h_n^\tau + \frac{h_\phi}{n}. \tag{5.3.8}$$

Therefore, (5.3.7) implies the following behaviour for $Z_n(0)$ in terms of ℓ

$$Z_n(0) \sim \ell^{-\frac{c_{\text{eff}}}{6}\left(n-\frac{1}{n}\right)}, \tag{5.3.9}$$

where $c_{\text{eff}} = c - 24h_\phi$. In the case of the bc-ghost theory, the lowest dimension field ϕ is ψ_c, which has dimension $h_c = 0$, and then one may conclude that, in this case, $c_{\text{eff}} = c = -2$.

However, the numerical analysis of the moments $Z_n(0)$ in the ground state of the non-Hermitian SSH model reveals that they do not behave as expected from (5.3.9) for any integer n but as

$$\log Z_n(0) = \begin{cases} \frac{1}{3}\left(n - \frac{1}{n}\right)\log \ell + O(\ell^0) & n \text{ odd}, \\ \left(\frac{n}{3} + \frac{1}{6n}\right)\log \ell + O(\ell^0) & n \text{ even}. \end{cases} \tag{5.3.10}$$

In fact, in the upper panel of Fig. 5.3, we numerically study $\log Z_n(0)$ as a function of the subsystem length, taking $\ell = L/2$ and varying the total system size for several values of n. The points are the exact numerical value of $\log Z_n(0)$ for the non- Hermitian SSH model obtained by diagonalizing the correlation matrix (5.1.14) and applying (5.2.15). The continuous lines correspond to (5.3.10).

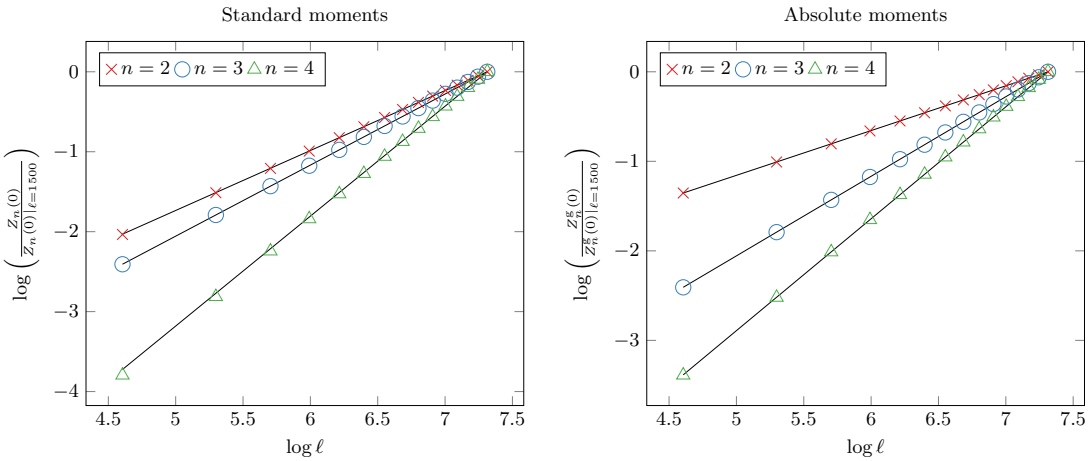


Figure 5.3: Standard moments $Z_n(0)$ (upper panel) and absolute moments $Z_n^{\mathrm{g}}(0)$ (lower panel) of ρ_A as a function of the subsystem size ℓ and different values of the exponent n. We plot the ratio with the corresponding value for $\ell = 1500$, taken as an arbitrary reference point. The symbols are their exact numerical value for the non-Hermitian SSH chain of length $L = \ell/2$ and parameters $w = 3/2$, $v = 1$ and $u = 1/2$, computed through the two-point correlation matrix (5.1.14) using (5.2.15) for $Z_n(0)$ and (5.2.13) for $Z_n^{\mathrm{g}}(0)$. The solid lines correspond to the analytic expressions (5.3.10) in the upper panel and (5.3.11) in the lower one, upon replacing ℓ by the chord length ℓ_{e}.

On the other hand, as the lower panel of Fig. 5.3 shows, we find that the absolute moments $Z_n^{\mathrm{g}}(0) = \mathrm{Tr}(\rho_A|\rho_A|^{n-1})$ do follow the behaviour of (5.3.9) for any n,

$$\log Z_n^{\mathrm{g}}(0) = \frac{1}{3}\left(n - \frac{1}{n}\right)\log \ell + O(\ell^0), \tag{5.3.11}$$

as also has been numerically checked in [211]. In Fig. 5.3, the points are the exact numerical value of $\log Z_n^{\mathrm{g}}(0)$ taking as subsystem length $2\ell = L/2$ and varying L for several Rényi indices n. They have been calculated using the two-point correlation matrix (5.1.14) through (5.2.13). The continuous lines correspond to (5.3.11).

The previous analysis leads to conclude that, in the case of the bc-ghost theory, the ground state absolute moments of ρ_A are given by the orbifold correlation function

$$Z_n^{\mathrm{g}}(0) = \langle 0|\, \tau_n(0)\tilde{\tau}_n(\ell)\, |0\rangle\,. \tag{5.3.12}$$

In Sec. 5.5, we will see that the alternating behavior in n of the standard moments in (5.3.10) originates from the property that the eigenvalues of ρ_A have constant sign in each charge sector and this sign depends on the parity of the charge. Combining this property and (5.3.12), we will determine the twist field correlation function that gives the correct result for n even in (5.3.10).

The absolute charged moments $Z_n^{\mathrm{g}}(\alpha)$ of (5.2.6) can also be calculated using the orbifold $\mathrm{CFT}^{\otimes n}/\mathbb{Z}_n$. In the orbifold, the operator $e^{i\alpha Q_A}$ has the effect of adding a phase $e^{i\alpha}$ when a charged particle moves along a closed path that crossed all the

copies. This phase shift can be incorporated in the correlators by inserting a local $U(1)$ operator $\mathcal{V}_\alpha(z)$ that gives rise to a term $e^{i\alpha}$ when going around it. Similarly to unitary CFTs with a $U(1)$ symmetry, see [82], we can construct the composite twist field $\tau_{n,\alpha} \equiv \tau_n \cdot \mathcal{V}_\alpha$ such that, when winding around the point where it is inserted, a field $\mathcal{O}_k$ living in the copy k is mapped to the copy $k+1$ with an extra phase $e^{i\alpha/n}$,

$$\mathcal{O}_k(e^{2\pi i}z)\tau_{n,\alpha}(0) = e^{i\alpha/n}\tau_{n,\alpha}(0)\mathcal{O}_{k+1}(z). \tag{5.3.13}$$

If $\mathcal{V}_\alpha$ is a spinless primary field with conformal dimension $h^{\mathcal{V}}_\alpha$, then the composite twist field $\tau_{n,\alpha}$ is also a spinless primary of dimension [82]

$$h_{n,\alpha} = h^\tau_n + \frac{h^{\mathcal{V}}_\alpha}{n}. \tag{5.3.14}$$

Thus we propose that, in the bc-ghost theory, the absolute charged moments are given by the orbifold two-point correlation function

$$Z^{\mathrm{g}}_n(\alpha) = \langle 0|\, \tau_{n,\alpha}(0)\tilde{\tau}_{n,-\alpha}(\ell)\, |0\rangle\,. \tag{5.3.15}$$

Observe that this expression simplifies to (5.3.12) when $\alpha = 0$.

The field $\mathcal{V}_\alpha$ can be determined by applying the fact that the bc-ghost model is equivalent via bosonization to a Gaussian theory coupled to a background charge [274]. The bosonization prescription works as follows. Let us consider a free bosonic field theory and we introduce a background charge $\mathcal{Q}$,

$$S_{\mathcal{Q}} = \frac{1}{2\pi}\int d^2z \left(\partial\varphi\bar{\partial}\varphi + \frac{i\mathcal{Q}}{4}\varphi\right). \tag{5.3.16}$$

The scalar field $\varphi(z)$ is compactified on a circle of radius one, i.e. $\varphi \sim \varphi + 2\pi m$ with $m \in \mathbb{Z}$. The inclusion of a background charge in the action (5.3.16) modifies the central charge of the theory to $c = 1 - 3\mathcal{Q}^2$ as well as the conformal dimension of the vertex operators $V_\alpha(z) = e^{i\sqrt{2}\alpha\varphi(z)}$, which is now $h^V_\alpha = \alpha^2 - \alpha\mathcal{Q}/\sqrt{2}$. On the other hand, in presence of a background charge, $\partial\varphi$ is not a primary. If we take $\mathcal{Q} = 1$, this theory has central charge $c = -2$, the fields ψ_b and ψ_c are identified with the vertex operators

$$\psi_b(z) \sim V_{-\frac{1}{\sqrt{2}}}(z), \quad \psi_c(z) \sim V_{\frac{1}{\sqrt{2}}}(z), \tag{5.3.17}$$

and the $U(1)$ current

$$j(z) = -\partial\varphi(z) \tag{5.3.18}$$

is equivalent to the ghost current of (5.3.2).

Therefore, using these bosonization relations, the charge operator in the interval A is

$$Q_A = -\frac{1}{2\pi}\int_A dx\partial_x\varphi = \frac{1}{2\pi}\left(\varphi(0) - \varphi(\ell)\right), \tag{5.3.19}$$

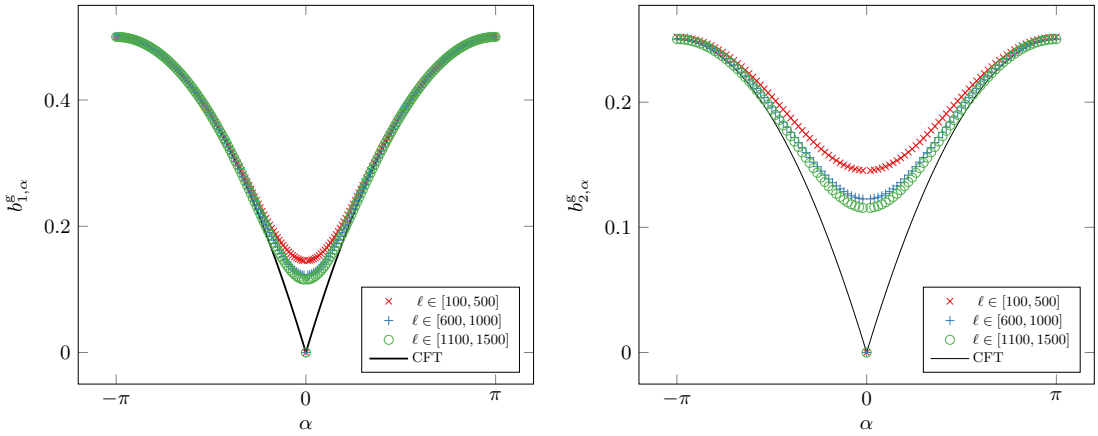


Figure 5.4: Numerical check of the CFT prediction (5.3.22) for the absolute charged moments $Z^{\mathrm{g}}_n(\alpha)$ when $n = 1$ (upper panel) and $n = 2$ (lower panel). As explained in the main text, the points are the value of the coefficient $b^{\mathrm{g}}_{n,\alpha}$ in (5.3.24) obtained by computing numerically Δ^{g} in the non-Hermitian SSH model for several lengths ℓ with $L = 2\ell$ at fixed α and then fit (5.3.24) to them. The different symbols correspond to the three sets of subsystem lengths taken to perform the fits: $\ell \in [100, 500]$, $\ell \in [600, 1000]$, $\ell \in [1100, 1500]$, in steps of 100. The parameters of the Hamiltonian are $w = 3/2$, $v = 1$, $u = 1/2$. The solid line is the CFT prediction (5.3.25) for $b^{\mathrm{g}}_{n,\alpha}$.

and the local $U(1)$ operator $\mathcal{V}_\alpha$ can be identified as the vertex operator

$$\mathcal{V}_\alpha(z) = e^{i\frac{\alpha}{2\pi}\varphi(z)} \tag{5.3.20}$$

with conformal dimension

$$h^{\mathcal{V}}_\alpha = \frac{|\alpha|}{4\pi}\left(\frac{|\alpha|}{2\pi} - 1\right). \tag{5.3.21}$$

Notice that such dimension is different from the standard one in the Hermitian CFT which is proportional to α^2.

Finally, applying (5.3.21) in (5.3.15), we conclude that the ground state absolute charged moments of the non-Hermitian SSH model along the critical line are of the form

$$Z^{\mathrm{g}}_n(\alpha) = c_{n,\alpha} e^{i\alpha\langle Q_A\rangle} \ell^{\frac{1}{3}\left(n-\frac{1}{n}\right)-\frac{|\alpha|}{\pi n}\left(\frac{|\alpha|}{2\pi}-1\right)}. \tag{5.3.22}$$

Observe that in this expression we have included a phase $e^{i\alpha\langle Q_A\rangle}$, which depends on the average charge $\langle Q_A\rangle$ in the subsystem A. This term is not captured by the previous CFT calculations since it depends on the particular microscopical model under consideration. In the critical non-Hermitian SSH chain, the ground state is half-filled, see (5.1.13), and $\langle Q_A\rangle = \ell$.

We check numerically the result (5.3.22) in the following way. Let us define

$$\Delta^{\mathrm{g}} := \log \frac{Z^{\mathrm{g}}_n(\alpha)}{Z^{\mathrm{g}}_n(0)} - i\alpha\langle Q_A\rangle. \tag{5.3.23}$$

According to (5.5.3), we expect

$$\Delta^{\mathrm{g}} \sim b^{\mathrm{g}}_{n,\alpha} \log \ell \tag{5.3.24}$$

for large ℓ, with

$$b^{\mathrm{g}}_{n,\alpha} = -\frac{|\alpha|}{\pi n}\left(\frac{|\alpha|}{2\pi} - 1\right). \tag{5.3.25}$$

The quantity Δ^{g} can be exactly computed numerically for the ground state of the critical non-Hermitian SSH model using (5.2.13). Hence to verify that the coefficient $b^{\mathrm{g}}_{n,\alpha}$ has the form of (5.3.25), we fit the curve $b^{\mathrm{g}}_{n,\alpha} \log \ell_{\mathrm{e}}$ to a set of numerical values of Δ^{g} corresponding to different subsystem sizes $2\ell = L/2$ with α and n fixed. In Fig. 5.4, we plot the values obtained in the fit for the coefficient $b^{\mathrm{g}}_{n,\alpha}$ in terms of α, and compare it with the CFT prediction (5.3.25). To perform the fits, we consider three different sets of subsystem lengths, $\ell \in [100, 500]$, $\ell \in [600, 1000]$ and $\ell \in [1100, 1500]$ in steps of 100. For α large enough, there is an excellent agreement between the CFT prediction and the result of the fit. This agreement is worse as α decreases, while at $\alpha = 0$ there is again a very good matching. Repeating the fitting procedure with each set of points, we find that the larger ℓ the better the agreement with the analytic result. This behaviour suggests that the convergence to (5.3.22) for large ℓ is not uniform in α.

Unfortunately, the non-universal factor $c_{n,\alpha}$ cannot be determined from the CFT or applying the usual lattice techniques employed in the case of the Hermitian SSH model, i.e. corner transfer matrix, block Toeplitz determinants. Nevertheless, the numerical analysis of $c_{n,\alpha}$ reveals that the dominant term is due to the momentum shift κ, which has a simple form

$$c_{n,\alpha} \sim \begin{cases} \kappa^{1-n} & \alpha = 0, \\ \kappa^{-n} & \alpha \neq 0. \end{cases} \tag{5.3.26}$$

5.4 Symmetry-resolved entanglement entropy of the *bc*-ghost CFT

In this section, we use the results obtained in (5.3.22) for the absolute charged moments $Z^{\mathrm{g}}_n(\alpha)$ to calculate the symmetry-resolved entanglement entropy $S^{\mathrm{g}}_n(\rho_{A,q})$.

To this end, according to (5.2.8), we need to determine the Fourier transform of $Z^{\mathrm{g}}_n(\alpha)$. If we insert the CFT prediction of (5.3.22) for the absolute charged moments in (5.2.7), dropping the unknown non-universal term $c_{n,\alpha}$, then we obtain

$$\mathcal{Z}^{\mathrm{g}}_n(q) = (-1)^{\Delta q} Z_n(0) \sqrt{\frac{n\pi \ell^{\frac{1}{n}}}{2\log \ell}} e^{-\frac{n\pi^2 \Delta q^2}{2\log \ell}} \times \mathrm{Re}\,\mathrm{Erf}\left(\frac{\log \ell + i\pi n \Delta q}{\sqrt{2n \log \ell}}\right), \tag{5.4.1}$$

with $Z_n(0) = \ell^{1/3(n-1/n)}$ and $\Delta q = q - \langle Q_A \rangle$.

For large $\log \ell$, the error function has the asymptotic form $\mathrm{Erf}(x) \sim 1 - e^{-x^2}/(\sqrt{\pi}x)$ and, therefore, (5.4.1) can be expanded as

$$\mathcal{Z}_n^{\mathrm{g}}(q) \sim Z_n(0) \left[(-1)^{\Delta q} \sqrt{\frac{n\pi \ell^{\frac{1}{n}}}{2\log \ell}} e^{-\frac{n\pi^2 \Delta q^2}{2\log \ell}} - \frac{n \log \ell}{(\log \ell)^2 + (n\pi \Delta q)^2} \right]. \tag{5.4.2}$$

Observe the leading term in ℓ is a Gaussian with an alternating sign $(-1)^{\Delta q}$, while the subleading one has Lorentzian form. It is important to not neglect this term, because it is a correction only for fixed $|\Delta q| \ll \log \ell$, while it becomes leading in the regime $|\Delta q| \gtrsim \log \ell$. To understand this crossover, let us focus on the case $n = 1$ which gives the normalization term $p(q) = \mathcal{Z}_1^{\mathrm{g}}(q)$ in the charge sector decomposition (5.2.4) of ρ_A,

$$p(q) \sim (-1)^{\Delta q} \sqrt{\frac{\pi \ell}{2\log(\ell)}} e^{-\frac{\pi^2 \Delta q^2}{2\log \ell}} - \frac{\log \ell}{(\log \ell)^2 + (\pi q)^2}. \tag{5.4.3}$$

Since $p(q) = \mathrm{Tr}\,(\Pi_q \rho_A)$, this quantity must satisfy $\sum_q p(q) = 1$. To get this, we have actually to take into account the two terms of (5.4.3). One can check that

$$\sum_{q \in \mathbb{Z}} p(q) = \sqrt{\frac{\pi \ell}{2\log \ell}} \vartheta_4(e^{-\pi^2/(2\log \ell)}) - \frac{\ell^2 + 1}{\ell^2 - 1}, \tag{5.4.4}$$

where the first term comes from the Gaussian in (5.4.3) and the second one from the Lorentzian. Expanding for large ℓ, which is the only regime where the above equation makes sense (using $\vartheta_4(e^{-x}) \sim 2\sqrt{\pi} e^{-\pi^2/(4x)}/\sqrt{x}$ for $x \sim 0$), we find that (5.4.4) tends to one in the large ℓ limit, but the Gaussian alone would provide 2 and -1 comes from the Lorentzian. It is then clear that both terms should be always taken into account.

Another interesting property of (5.4.2) is that, for large ℓ, the sign of $\mathcal{Z}_n^{\mathrm{g}}(q)$ is $(-1)^{\Delta q}$. In particular, in the case $n = 1$, this means that the sum of the eigenvalues of ρ_A in each charge sector of the bc-ghost theory has sign $(-1)^{\Delta q}$ (as long as $|\Delta q| \lesssim \log \ell$). The presence of this alternating sign can be understood by the relation

$$\rho_A = (-1)^{Q_A - \langle Q_A \rangle} |\rho_A|. \tag{5.4.5}$$

This identity can be derived in the lattice for any subsystem of arbitrary length ℓ. In fact, along the critical line $u = w - v$, half of the eigenvalues ν_j of two-point correlation matrix C_A of (5.1.14) are $\nu_j < 0$ and the other half $\nu_j > 1$. Given the relation (5.2.12) between the two-point correlation matrix and single particle entanglement Hamiltonian H^{E}, the eigenvalues ε_j of the latter are complex

$$\varepsilon_j = \log \left| \frac{1 - \nu_j}{\nu_j} \right| + i\pi. \tag{5.4.6}$$

We can construct the eigenvalues of ρ_A from those of H^{E}. If we label them with the occupation numbers relative to the single particle entanglement Hamiltonian, then

$$\lambda_{\{n_j\}} = Z_A^{-1} e^{-\sum_j \varepsilon_j n_j}. \tag{5.4.7}$$

Since $Z_A = \prod_{j=1}^{2\ell}(1-\nu_j)$ and half of the eigenvalues ν_j are $\nu_j < 0$ and the other half $\nu_j > 1$, then $Z_A = (-1)^{\ell}|Z_A|$. Combining this with (5.4.6) and identifying $\sum_j n_j = q$ and $\langle Q_A \rangle = \ell$, we obtain

$$\lambda_{\{n_j\}} = (-1)^{q-\langle Q_A\rangle} |\lambda_{\{n_j\}}|. \tag{5.4.8}$$

from which (5.4.5) follows.

This result indicates that the non-positiveness of ρ_A is due to the global sign $(-1)^{q-\langle Q_A\rangle}$ on each charge sector q. Observe that in the decomposition of (5.2.4), this factor is absorbed in the normalization $p(q)$ and, therefore, the density matrices $\rho_{A,q}$ are positive definite. This implies that the generalized entanglement entropy and the standard entanglement entropy of $\rho_{A,q}$ are equal, $S_n^{\mathrm{g}}(\rho_{A,q}) = S_n(\rho_{A,q})$.

Plugging (5.4.2) into (5.2.8), we obtain that the symmetry-resolved Rényi entanglement entropy in each charge sector behaves when $\log \ell \gg 1$ as

$$S_n^{\mathrm{g}}(\rho_{A,q}) = \frac{n+1}{6n} \log \ell - \frac{1}{2} \log\log \ell + O(\ell^0). \tag{5.4.9}$$

and, in the limit $n \to 1$,

$$S^{\mathrm{g}}(\rho_{A,q}) = \frac{1}{3} \log \ell - \frac{1}{2} \log\log \ell + O(\ell^0). \tag{5.4.10}$$

Note that, contrary to the generalized entanglement entropy of the full reduced density matrix ρ_A, the symmetry-resolved entanglement entropies are positive. Moreover, the expansions of Eqs. (5.4.9) and (5.4.10) coincide with the symmetry-resolved entanglement entropies of the $1+1$ free massless Dirac fermion [82, 85]. An important property of Eqs. (5.4.9) and (5.4.10) is that they do not depend on the charge q: at leading order in ℓ, the symmetry-resolved entropy is equally distributed among all the charge sectors. This feature is known as entanglement equipartition [83]. As usually happens in Hermitian systems, one should further analyze the subleading $O(\ell^0)$ terms of (5.4.9) in order to find corrections that explicitly depend on q. Unfortunately, we lack the proper tools to determine the first term that breaks the equipartition.

An interesting consistency test consists in recovering the total generalized entanglement entropy plugging in the decomposition (5.2.5) in charge sectors the result of (5.4.2) for $\mathcal{Z}_n^{\mathrm{g}}(q)$. Unfortunately, performing the sum analytically is complicated due to the the alternating sign $(-1)^{\Delta q}$ and to the interplay of the Gaussian and Lorentzian terms. Anyhow, we have checked numerically that the sum (5.2.5) behaves as

$$S^{\mathrm{g}}(\rho_A) \sim -\frac{2}{3} \log \ell, \tag{5.4.11}$$

which is the correct result for the generalized entanglement entropy (obtained also by plugging $Z_n^{\rm g}(0)$ of (5.3.11) in (5.2.2) and taking the limit $n \to 1^+$).

5.5 Charged moments and standard Rényi entropies

In the previous section, we obtained that along the critical line $u = w - v$, the matrices ρ_A and $|\rho_A|$ are related by (5.4.5). Here we apply this identity to understand the dependence (5.3.10) on the parity of $n \in \mathbb{Z}$ of the standard moments of ρ_A, that we numerically observed in Fig. 5.3.

We proceed as follows. First, in the definition (5.2.9) of the standard charged moments $Z_n(\alpha)$, we split $\rho_A^n = \rho_A \rho_A^{n-1}$. Then we use (5.4.5) in the ρ_A^{n-1} factor to relate $Z_n(\alpha)$ to the absolute charged moments $Z_n^{\rm g}(\alpha)$ (cf. (5.2.6)), obtaining

$$Z_n(\alpha) = e^{-i\pi(n-1)\langle Q_A\rangle} Z_n^{\rm g}(\alpha + \pi(n-1)). \tag{5.5.1}$$

This equality implies that

$$Z_n(\alpha) = \begin{cases} Z_n^{\rm g}(\alpha) & n \text{ odd}, \\ (-1)^{\langle Q_A\rangle} Z_n^{\rm g}(\alpha+\pi) & n \text{ even}. \end{cases} \tag{5.5.2}$$

Employing the analytic expression obtained in (5.3.22) for $Z_n^{\rm g}(\alpha)$, we find that, for large ℓ,

$$Z_n(\alpha) = \begin{cases} c_{n,\alpha} e^{i\alpha\langle Q_A\rangle} \ell^{\frac{1}{3}\left(n-\frac{1}{n}\right) - \frac{|\alpha|}{\pi n}\left(\frac{|\alpha|}{2\pi}-1\right)} & n \text{ odd}, \\ c_{n,\alpha+\pi} e^{i\alpha\langle Q_A\rangle} \ell^{\frac{n}{3}+\frac{1}{6n}-\frac{\alpha^2}{2n\pi^2}} & n \text{ even}. \end{cases} \tag{5.5.3}$$

Note that, for $\alpha = 0$, this result leads to the expressions conjectured in (5.3.10) for the neutral moments of ρ_A. In (5.3.15), we write the absolute charged moments of ρ_A in the bc-ghost CFT as a correlation function of the composite twist fields $\tau_{n,\alpha}$ and $\tilde\tau_{n,-\alpha}$. In the light of (5.5.3), the standard charged moments are also given for n odd by the same correlator, while for n even we have to perform a shift in the phase $\alpha \mapsto \alpha + \pi$,

$$Z_n(\alpha) = \begin{cases} \langle 0|\, \tau_{n,\alpha}(0)\tilde\tau_{n,-\alpha}(\ell)\, |0\rangle & n \text{ odd}, \\ \langle 0|\, \tau_{n,\alpha+\pi}(0)\tilde\tau_{n,-\alpha-\pi}(\ell)\, |0\rangle & n \text{ even}. \end{cases} \tag{5.5.4}$$

It is interesting to comment that the sensitivity of $Z_n(\alpha)$ to the parity of the exponent n resembles the result for the entanglement negativity in Hermitian systems. The negativity is an entanglement measure for mixed states that can be obtained from the moments of the partial transpose of a given reduced density matrix [276]. As for our density matrix ρ_A, the partial transpose in Hermitian systems is in general non-positive definite and, in unitary CFTs, its moments also

display a dependence on the parity of n, similar to (5.5.3), although with a different power law in ℓ [276, 277].

The results of (5.5.3) for the standard charged moments can be checked with exact numerical calculations in the critical non-Hermitian SSH model by following the same strategy as for the absolute charged moments presented in Sec. 5.3. In fact, we consider the quantity

$$\Delta \coloneqq \log \frac{Z_n(\alpha)}{Z_n(0)} - i\alpha\langle Q_A\rangle, \tag{5.5.5}$$

which according to (5.5.3), should behave as

$$\Delta \sim b_{n,\alpha} \log \ell \tag{5.5.6}$$

with

$$b_{n,\alpha} = \begin{cases} -\frac{|\alpha|}{\pi n}\left(\frac{|\alpha|}{2\pi} - 1\right) & n \text{ odd}, \\ -\frac{\alpha^2}{2\pi n^2} & n \text{ even}. \end{cases} \tag{5.5.7}$$

We can exactly calculate Δ in the non-Hermitian SSH model using (5.2.15). We therefore obtain numerically its value for several subsystem lengths, with α and n fixed, and we fit the function $b_{n,\alpha}\log \ell_{\mathrm{e}}$ to them. In Fig. 5.5, we show the outcome for the coefficient $b_{n,\alpha}$ in the fit as a function of α and two particular values of n, $n = 1$ (upper panel) and $n = 2$ (lower panel). The different symbols in the plot correspond to different sets of subsystem lengths chosen to perform the fit. The continuous black curves are the analytic prediction of (5.5.7) for large ℓ. Observe that, as we have found in (5.5.1), there is relative phase shift $\alpha \leftrightarrow \alpha + \pi$ between n even and odd, consequence of the form (5.4.5) of the reduced density matrix. Similarly to the absolute charged moments, cf. Fig. 5.4, the figure shows that the convergence to the asymptotic expression is not uniform in α and worsens when approaching the cusp.

The oscillation in n of the moments of ρ_A implies that the standard Rényi entanglement entropies also present such behaviour. From (5.5.3), we straightforwardly get

$$S_n(\rho_A) = \begin{cases} -\frac{1}{3}\left(1 + \frac{1}{n}\right)\log \ell + O(\ell^0) & n \text{ odd}, \\ \frac{1}{1-n}\left(\frac{n}{3} + \frac{1}{6n}\right)\log \ell + O(\ell^0) & n \text{ even}. \end{cases} \tag{5.5.8}$$

Finally, note that if we apply in the definition of the standard von Neumann entanglement entropy the relation (5.4.5) between ρ_A and $|\rho_A|$, and we take into account that $\langle Q_A\rangle = \mathrm{Tr}(\rho_A Q_A)$, we find that it coincides in this case with the generalized one,

$$S(\rho_A) = S^{\mathrm{g}}(\rho_A) \sim -\frac{2}{3}\log \ell. \tag{5.5.9}$$

This asymptotic behaviour can be also extracted by taking the limit $n \to 1^+$ in the expression (5.5.8) of the standard Rényi entropies for n odd. This result agrees

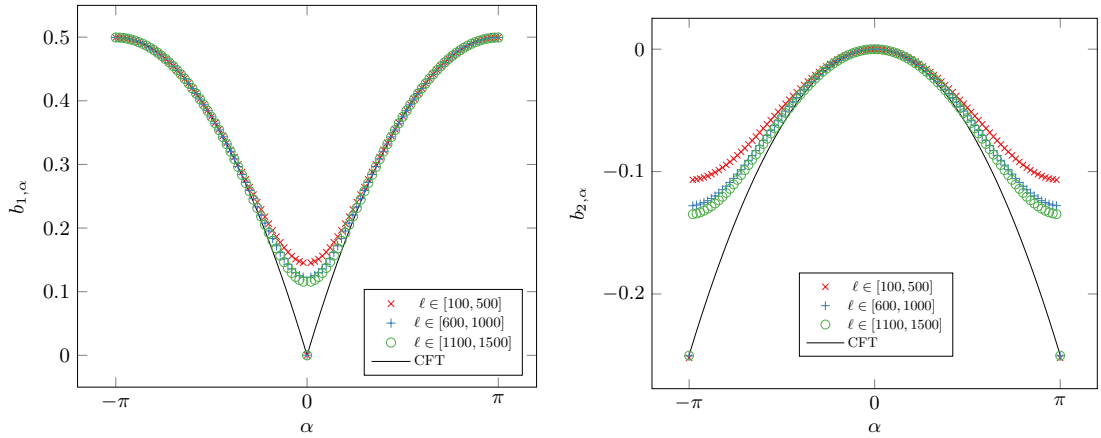


Figure 5.5: Numerical check of the analytic expression of (5.5.3) for the standard charged moments $Z_n(\alpha)$, with $n = 1$ (upper panel) and $n = 2$ (lower panel). As explained in the main text, the symbols are the results obtained for the coefficient $b_{n,\alpha}$ in a fit of (5.5.5) to a set of values of Δ computed numerically in the non-Hermitian SSH model and corresponding to different subsystem lengths ($\ell \in [100, 500]$, $\ell \in [600, 1000]$ and $\ell \in [1100, 1500]$ in steps of 100) for a given α. The parameters of the Hamiltonian are $w = 3/2$, $v = 1$, $u = 1/2$. The solid curves are the analytic prediction of (5.5.7) for $b_{n,\alpha}$ and large subsystem size.

with the one obtained in [207, 210] for this quantity. However, to our knowledge, the alternating behaviour in n given by (5.5.8) of the standard Rényi entropies has not been reported in previous works.

5.6 Entanglement spectrum

Using the results obtained in the previous section for the moments of the reduced density matrix ρ_A, we can investigate the distribution $P(\lambda)$ of the its eigenvalues, that is of the entanglement spectrum. This is defined as

$$P(\lambda) = \sum_j \delta(\lambda - \lambda_j), \tag{5.6.1}$$

where λ_j are the eigenvalues of ρ_A. In [270], the distribution $P(\lambda)$ was determined for unitary CFTs from the knowledge of the moments $Z_n(0)$. That approach was extended to analyze the negativity spectrum, i.e. the eigenvalues of the partial transpose of a density matrix, in unitary CFTs [278] and free fermions [279]. As we already pointed out, the moments of ρ_A in our non-Hermitian system present the same qualitative dependence on the parity of the exponent n as the moments of the partial transpose in unitary CFTs. We can therefore easily apply here the techniques of [278] to obtain $P(\lambda)$ in the ground state of the non-Hermitian SSH model at criticality, which is the entanglement spectrum of the bc-ghost CFT.

The main idea of [270], and also [278], is that the distribution $P(\lambda)$ is univocally determined by its moments

$$Z_n(0) = \sum_j \lambda_j^n = \int d\lambda P(\lambda)\lambda^n. \tag{5.6.2}$$

In fact, the Stieltjes transform $f(s)$ of $\lambda P(\lambda)$,

$$f(s) = \frac{1}{\pi}\sum_{n=1}^{\infty} Z_n(0)s^{-n} = \frac{1}{\pi}\int d\lambda \frac{\lambda P(\lambda)}{s-\lambda}, \tag{5.6.3}$$

is an analytic function in the complex plane except along the support of $\lambda P(\lambda)$ on the real line, where it has a branch cut. The discontinuity of $\lambda P(\lambda)$ at the branch cut gives $P(\lambda)$ through the formula [280]

$$P(\lambda) = \frac{1}{\lambda}\lim_{\epsilon\to 0^+} f(\lambda - i\epsilon). \tag{5.6.4}$$

This result implies that there is a one-to-one correspondence between the Stieltjes transform $f(s)$ and the distribution $P(\lambda)$. Therefore, given that we know the form of the moments $Z_n(\alpha)$, the strategy is to compute the function $f(s)$ as the Laurent series of (5.6.3) and then determine $P(\lambda)$ by applying (5.6.4).

Before proceeding, it is important two emphasize two points. When checking numerically the analytic expressions that we obtain in the following, it is crucial to take into account the shift κ in the momenta that we have to perform to regularize the two-point correlation matrix (5.1.14) of the lattice system. We recall that this shift enters in the expression (5.5.3) of the moments $Z_n(0)$ through the non-universal constant $c_{n,\alpha}$, whose dependence on κ was determined in (5.3.26). The second relevant aspect is to multiply the expressions (5.5.3) of the moments $Z_n(0)$ by a global factor g^{1-n}, both for n even and odd, that accounts for a possible global degeneracy of the entanglement spectrum in the non-Hermitian SSH model, as it is explained in detailed in [281] for unitary CFTs.

Including those two extra ingredients, in Appendix 5.A, we show in detail the calculation of the Stieljes transform $f(s)$, whose final expression reads

$$f(s) = \frac{g\kappa}{2\pi}\sum_{k=0}^{\infty}\frac{(-\log\ell)^k}{3^k k!}\left[\mathrm{Li}_k\left(\frac{\lambda_M}{s}\right) - \mathrm{Li}_k\left(-\frac{\lambda_M}{s}\right)\right] + \frac{g}{\pi}\sum_{k=0}^{\infty}\frac{1}{k!}\left(\frac{\log\ell}{12}\right)^k \mathrm{Li}_k\left(\frac{\lambda_M^2}{s^2}\right), \tag{5.6.5}$$

where $\mathrm{Li}_k(z)$ stands for the polylogarithm function and

$$\lambda_M = \frac{\ell^{\frac{1}{3}}}{g\kappa} \tag{5.6.6}$$

is the largest eigenvalue of ρ_A for large subsystem size ℓ. In fact, the limit $n \to \infty$ of the standard moments $Z_n(0)$ gives the largest eigenvalue λ_M of ρ_A such that $\lim_{n\to\infty} Z_n(0)^{1/n} = \lambda_M$. If we take $n \to \infty$ in (5.5.3), then we obtain that in our case λ_M is precisely (5.6.6). Note that this limit does not depend on the parity on n of the Rényi entanglement entropy in (5.5.3) and, therefore, it is well-defined.

If we plug now (5.6.5) in the inversion formula (5.6.4), we can obtain the distribution $P(\lambda)$. This requires to apply some properties of the polylogarithm $\mathrm{Li}_k(z)$. The reader can find a thorough description of this calculation in Appendix 5.A. The final expression for $P(\lambda)$ is

$$\begin{aligned} P(\lambda) &= g\frac{1+\kappa}{2}\delta(\lambda-\lambda_M) + g\frac{1-\kappa}{2}\delta(\lambda+\lambda_M) \\ &+ g\frac{\Theta(\lambda_M-|\lambda|)}{2\lambda\sqrt{\log(\lambda_M/|\lambda|)}}\left[-\kappa\sqrt{\frac{\log\ell}{3}}J_1\left(2\xi_\ell(\lambda)\right) + \mathrm{sgn}(\lambda)\sqrt{\frac{\log\ell}{6}}I_1\left(\sqrt{2}\xi_\ell(\lambda)\right)\right], \end{aligned} \tag{5.6.7}$$

where $J_\nu(z)$ and $I_\nu(z)$ are the Bessel and modified Bessel functions of the first kind and

$$\xi_\ell(\lambda) = \sqrt{\frac{\log(\ell)\log(\lambda_M/|\lambda|)}{3}}. \tag{5.6.8}$$

The entanglement spectrum distribution (5.6.7) presents some remarkable properties. It is reminiscent of the negativity spectrum of two intervals [278] rather than the one-interval entanglement spectrum[270] of unitary CFTs. Its support is the interval $[-\lambda_M, \lambda_M]$. The delta peaks at $\lambda = \pm\lambda_M$ indicate that there is a finite contribution from these two eigenvalues to the (generalized) entanglement entropies. As the momentum shift $\kappa \to 0$, the contribution of the function J_1 vanishes and $P(\lambda)$ becomes an even function in λ. Observe that the constant g is still undetermined, we will fix it by comparing with the numerical data of the lattice model.

A non-trivial numerical check of the correctness of (5.6.7) is to study the tail or number distribution function $n_\ell(\lambda)$, that is the mean number of eigenvalues larger than a given λ,

$$n_\ell(\lambda) = \int_\lambda^{\lambda_M} d\lambda' P(\lambda'). \tag{5.6.9}$$

Inserting (5.6.7) in this expression, we find for $\lambda > 0$

$$n_\ell(\lambda) = \frac{g\kappa}{2}J_0(2\xi_\ell(\lambda)) + \frac{g}{2}I_0(\sqrt{2}\xi_\ell(\lambda)). \tag{5.6.10}$$

The main feature of this result is that the number distribution admits a particular form in which the joint dependence on λ and ℓ is combined through the scaling variable $\xi_\ell(\lambda)$ such that

$$n_\ell(\lambda) = n(\xi_\ell(\lambda)), \tag{5.6.11}$$

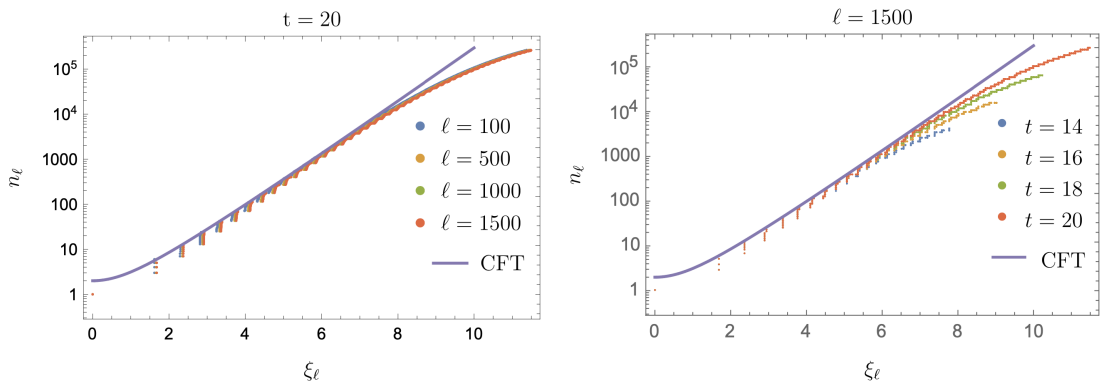


Figure 5.6: Number distribution of the entanglement spectrum n_ℓ as a function of the scaling variable ξ_ℓ of (5.6.8). The points have been obtained numerically as explained in the main text for the critical non-Hermitian SSH model and correspond to plot parametrically the number of eigenvalues of ρ_A in the interval $[\lambda, \infty)$ in terms of $\xi_\ell(\lambda)$. In the upper panel, we consider different subsystem sizes ℓ, truncating the spectrum of the correlation matrix to the $t = 20$ largest eigenvalues. In the lower panel, we fix the subsystem size to $\ell = 1500$ sites and we change the truncation to analyze its effect on the numerical results. In both panels, the solid line represents the CFT prediction for $n(\xi)$ obtained in (5.6.10) and (5.6.11) with $g = 4$. The parameters of the Hamiltonian are $w = 3/2$, $v = 1$, $u = 1/2$.

with $n(x)$ a universal function that does not depend on the subsystem size. A similar property is found in the entanglement and negativity spectrum of unitary CFTs [270, 278].

The structure of (5.6.11) is particularly useful when we want to make a comparison with the numerical data of the non-Hermitian SSH model. We can compute numerically the spectrum of ρ_A for the non-Hermitian SSH model for a given subsystem length ℓ and plot, as we do in Fig. 5.6, the number of eigenvalues λ_j that lie in the interval $[\lambda, \infty)$ in terms of the scaling variable $\xi_\ell(\lambda)$ of (5.6.8), taking as λ_M the highest eigenvalue of the numerical spectrum and replacing ℓ by the chord length ℓ_e.

If we repeat this procedure for different subsystem lengths, the numerical points should converge to the CFT prediction for the number distribution of (5.6.10). In that expression, the only free term is the global factor g, which is still undetermined. We numerically find that the spectrum of ρ_A for the non-Hermitian SSH model presents a global two-fold degeneracy. This forces, in particular, that the prefactor of the delta peaks in $\lambda = \pm\lambda_M$ of the distribution (5.6.7) must be 2 when $\kappa \to 0$. Thus we have to take $g = 4$. In Fig. 5.6, the solid line corresponds to (5.6.10) choosing this value for g. We obtain a very good agreement up to a certain value of $\xi_\ell(\lambda)$. In fact, for $\xi_\ell \to \infty$ ($\lambda \to 0$), the CFT prediction for $n_\ell(\lambda)$ in (5.6.10) diverges since the number of eigenvalues in the continuum is infinite. The deviation of the numerical data for large ξ_ℓ is due to the finiteness of the entanglement

spectrum on the lattice and the truncation method used to obtain it numerically.

The spectrum of ρ_A for the non-Hermitian SSH model can be determined numerically by means of the eigenvalues ν_j of the two-point correlation matrix, which is a $2\ell \times 2\ell$ matrix. Using (5.2.12) and (5.4.6), the 2^ℓ eigenvalues λ_j of the reduced density matrix are given by

$$\lambda_{\{n_j\}} = \prod_{j=1}^{2l} \nu_j^{n_j} (1-\nu_j)^{1-n_j}, \tag{5.6.12}$$

where they are labelled by a set $\{n_j\}$ of occupation numbers, cf. (5.4.8). Since for large ℓ the storage of the 2^ℓ eigenvalues $\lambda_{\{n_j\}}$ exhausts the memory capabilities, we restrict to the eigenvalues with largest absolute value and compute them with the following approximation. We truncate the spectrum of the correlation matrix to the first t eigenvalues ν_j that maximize the distance with respect to 0 and 1 and we compute $\lambda_{\{n_j\}}$ according to (5.6.12), with $j = 1, \ldots, t$. The eigenvalues ν_j around 0 or 1 would produce a multiplicative factor that is near to either 0 or to 1. As long as we focus on the largest eigenvalues of ρ_A, like in Fig. 5.6, the multiplicative factor we are missing should be close to 1 [270]. In the upper panel of Fig. 5.6, we take a fixed truncation $t = 20$ and consider different subsystem sizes. In the lower panel, we study the effect of the truncation for a given subsystem size; as clear from the plot, the distribution of the largest eigenvalues ($\xi_\ell \to 0$) is not affected when t is increased.

5.7 Entanglement Hamiltonians

In this section, we review a few important results about the entanglement Hamiltonian

The entanglement (or modular) Hamiltonian is defined as the logarithm of the (normalised) reduced density matrix [282–284]

$$\rho_A = \frac{e^{-K_A}}{Z_A}. \tag{5.7.1}$$

This operator contains much more information than the entanglement entropies, since, unlike the latter, its specific form depends not only on the eigenvalues but also on the eigenvectors of ρ_A.

Although calculating the EH is considerably more challenging than determining the entanglement entropies, a rich theoretical framework has been developed during the last decades. The most remarkable result is the Bisognano-Wichmann theorem [282–286]. Considering the vacuum state of a unitary relativistic quantum field theory (QFT) on $\mathbb{R}^{d+1}$ and taking as subsystem the half-space $x^1 > 0$, the Bisognano-Wichmann theorem asserts that the EH in the half-space is the generator

of Lorentz boosts

$$K_A = 2\pi \int_{x^1>0} \mathrm{d}^d x \, x^1 \, T_{00}(x) \,, \tag{5.7.2}$$

where $T_{00}(x)$ is the energy density. This result is remarkable for several reasons. First, it is extremely general, holding for all unitary Lorentz invariant QFTs, independently of the dimension of space-time and of the mass spectrum. Another significant property is the fact that the EH in (5.7.2) has a local structure, given by the integral of local operator with a linearly increasing local entanglement temperature $\beta(x) = x^1$. Finally, the Bisognano-Wichmann theorem provides a mathematical proof of the Unruh effect [287–289], as discussed in [282–284].

For generic massive QFTs, the Bisognano-Wichmann theorem in (5.7.2) is the only known analytic result. For conformal field theories (CFT), instead, the extended symmetry makes it possible to obtain more general results. In particular, the Hislop-Longo theorem [282, 290] (see also [124, 291, 292]) provides the EH of the ground state of a CFT in any ball shaped region. Even more general results can be obtained in $1+1$-dimensional unitary CFTs, where the infinite dimensional Virasoro symmetry allows one to map the Bisognano-Wichmann result in (5.7.2) in several different geometries [124, 292]. In particular, for the conformal vacuum state, if the subsystem is a single interval ($A = [0, \ell]$) the EH takes the form [124, 290–292]

$$K_A = 2\pi \int_0^\ell \mathrm{d}x \, \beta(x) \, T_{00}(x) \,, \qquad \text{with } \beta(x) = \frac{x\,(\ell - x)}{\ell} \,, \tag{5.7.3}$$

a formula that inherits the local structure of the Bisognano-Wichmann result, with a parabolic local entanglement temperature $\beta(x)$. We remark that this local structure is very peculiar and it fails to hold as soon as we consider minor modifications such as for the lowest excited states [293] and when considering multiple intervals [294, 295]. This property is not only of theoretical interest, but recently in [296–300] it has been leveraged to efficiently construct in synthetic quantum systems the ground state of lattice models using a variational approach.

A separate line of research, yielding numerous results, concerns the study of the EH in unitary $1+1$-dimensional integrable lattice models [301–316]. In these systems, the EH of the ground state in the half-space $x > 0$ is intimately related to Baxter's corner transfer matrix (CTM) $\widehat{A}$ [317–319]. Considering, for example, isotropic square lattices, the effect of the CTM is to add a full angular segment to a piece of lattice, mapping a horizontal row to a vertical one and vice versa. Using this property it is possible to show that the lattice reduced density matrix in the half-line can be expressed as the product of four CTMs [11, 304, 320]

$$\rho_A = \frac{\widehat{A}^4}{\operatorname{Tr} \widehat{A}^4}, \tag{5.7.4}$$

where $Z = \operatorname{Tr} \widehat{A}^4$ is the partition function. Recalling the definition (5.7.1) of the EH, (5.7.4) implies that it is proportional to the logarithm of fourth power of the

CTM [304]

$$K_A = -\log \widehat{A}^4. \tag{5.7.5}$$

This correspondence between EHs and CTMs has made it possible to obtain the EHs in several integrable models. It has been observed that in certain integrable models, the logarithm of the CTM and the EH can be written in terms of the density of the lattice Hamiltonian h_j with a linearly increasing local temperature

$$K_A \propto \sum_{j=0}^{\infty} j\, h_j\,, \tag{5.7.6}$$

with a non-trivial proportionality constant. This behaviour has been identified in various spin systems such as the Ising model [302–304], the XXZ [305, 306, 317], the XYZ chains [307–309], the anisotropic XX chain [312], and in bosonic models such as the harmonic chain [310–312]. Comparing (5.7.6) with the Bisognano-Wichmann theorem in (5.7.2), it is evident that the two EHs share the same structure. In fact, the connection between the two results runs deeper than a superficial similarity. Tetel'man [307] and Itoyama and Thacker [308, 321–323] independently showed that in these integrable models the logarithm of the CTM is the generator of a continuous group of lattice Lorentz transformations, akin to the role played by the generator of Lorentz boosts in the Bisognano-Wichmann theorem.

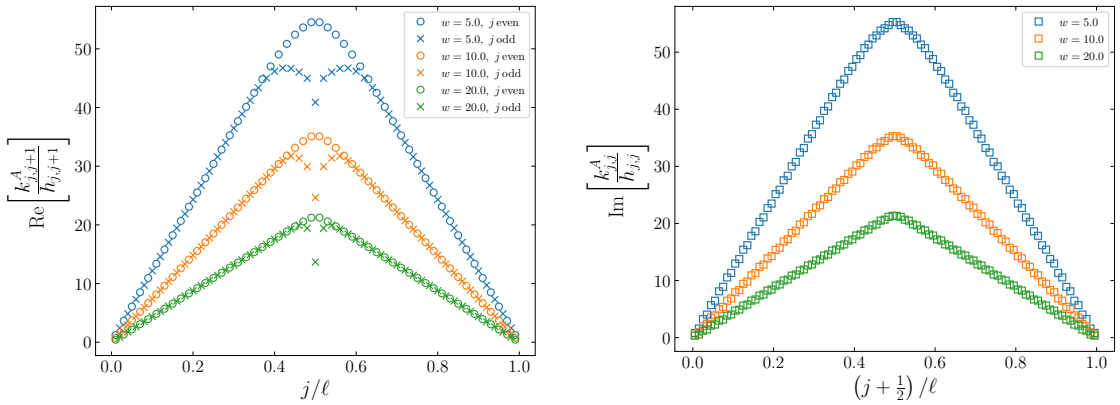
Despite the wealth of results for unitary models, nothing is known for non-Hermitian theories. In particular, since one of the hypothesis of the Bisognano-Wichmann theorem (5.7.2) is that the Hilbert space carries a unitary representation of the Poincaré group [282, 285, 286], it is not obvious how to adapt to non-unitary CFTs this theorem and its corollary (5.7.3).

In the following sections, we will conduct exploratory numerical investigation of the EH in the non-Hermitian Su-Schrieffer-Heeger model, both in the gapped phase and at criticality. In the gapped phase we observe that the lattice EH has a structure analogous to the one of integrable lattice models reported in (5.7.6). At the critical point, we instead find an additional term not accounted for in the Bisognano-Wichmann corollary in (5.7.3), which is responsible for the negativeness of the entanglement entropies.

5.8 Lattice entanglement Hamiltonians of the non-Hermitian SSH model

This section contains the main results of this chapter, the numerical lattice EH in the non-Hermitian SSH model and an analytic conjecture for its behaviour.

The kernel of the entanglement Hamiltonian k^A can be obtained from the two-point function restricted on A (5.2.12). We remark that the numerical computation of the formula (5.2.12) suffers from numerical instabilities and must be conducted



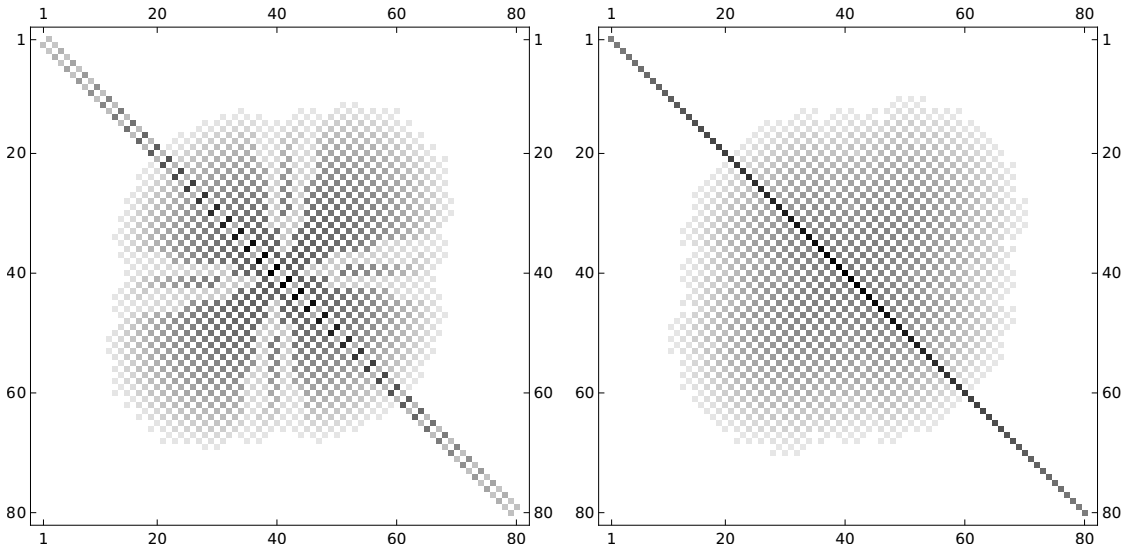
(a) Real part of the nearest-neighbour coupling $k^A_{j,j+1}$.

(b) Imaginary part of the chemical potential $k^A_{j,j}$.

Figure 5.7: Entanglement temperature in the gapped phase $w - v > u$. In both plots we fix $v = u = 1$ and we consider different values of $w = 5, 10$ and 20 and we take a subsystem of length $\ell = 100$ in a full system of total length $L = 2000$. In the left plot we report, as a function of j/ℓ, the real part of the ratio of the nearest-neighbour EH coupling $k^A_{j,j+1}$ with the coupling $(h_{j,j+1})$, i.e. $-w$ for even j (circles) and $-v$ for odd j (crosses). The purpose of this ratio is to isolate the entanglement temperature. Apart from a small region in the center of the interval, the ratio follows the expected triangular shape (see discussion below (5.8.1)). In the right plot we report the imaginary part of the ratio between the staggered imaginary chemical potential $k^A_{j,j}$ with $+u$ $(-u)$ for even (odd) site j. Again, up to a small finite size oscillation, the ratio follows the predicted triangular shape.

at high precision. The reason for this instability is that many eigenvalues of the correlation matrix C_A are arbitrarily close to 0 and 1, and as a consequence the matrix inside of the logarithm in (5.2.12) has eigenvalues which are very close to 0 or very large. In our study we used the `python` library `mpmath` [324] and the software `Mathematica`, keeping up to 500 digits.

In rest of this section, we present the results for the EH of an interval $A = [0, \ell]$ in the left-right ground state. We first study the topologically trivial gapped phase $w - v > u$ with periodic boundary conditions and we compare with the known results in unitary integrable lattice models [312]. We then consider the critical point $w - v = u$ with a small twisting of the boundary conditions $\delta = 10^{-7}$, which as we explained before is described by the $c = -2$ bc-ghost CFT. We compare the results with the continuum prediction from unitary CFTs and we use our observations to formulate a conjecture for the EH of an interval in the ground state of the bc-ghost theory.



(a) Real part of the EH kernel k^A. **(b)** Imaginary part of the EH kernel k^A.

Figure 5.8: Matrix plot of the EH kernel k^A in the gapped phase $w - v > u$ with $w = 20$, $v = 2$ and $u = 2$, for an interval of length $\ell = 80$ in a system of length $L = 2000$. Left (Right): Absolute value of the real (imaginary) part of k^A. Consistently with the Tetel'man-Thacker behaviour (5.8.1), near the two endpoints the only non-vanishing elements of the EH are the imaginary chemical potential (main diagonal in the right plot) and the coupling between nearest-neighbours (first sub-diagonals in the left plots). The latter couplings (left) display the alternating value between the odd and even sites (see (5.8.1)). In the middle of the interval, the EH deviates from (5.8.1) and also couplings at higher distances are non-zero.

5.8.1 Entanglement Hamiltonian in the trivial gapped phase

Before studying the non-Hermitian model, it is instructive to first recall the known results in unitary gapped lattice models, in order to compare them with ours. As we reported in (5.7.6), in certain integrable models the EH in the half-space follows the structure recognised by Tetel'man, Itoyama and Thacker, i.e., the EH is proportional to the Hamiltonian density with a local temperature equal to the lattice site, analogous to a lattice Bisognano-Wichmann behaviour [284, 307, 308, 318, 319, 321]. If we instead consider a finite interval, in the general case there are very few known analytic results. If the gap is sufficiently large, however, in [312] it was observed via numerical computations that near the two endpoints of the interval the EH follows the half-space result of (5.7.6), only deviating from this behaviour in the middle of the interval, which give rise to a characteristic triangular entanglement temperature.

This triangular behaviour has been observed in several Hermitian models, such as the Hermitian Su-Schrieffer-Heeger model (or dimerised hopping chain) and the harmonic chain [312]. Its physical interpretation is that, for short-range correlated

systems, the EH density is affected only by the closest boundary, as the contribution from the furthest one is exponentially suppressed. Then the EH density behaves as the one of a semi-infinite subsystem (see (5.7.6)) and the RDM effectively factorises [325]. This argument is independent of unitarity and holds also for the non-hermitian model under consideration. It is therefore natural to wonder if this factorisation holds also for the non-Hermitian model under study.

Another important consequence of (5.7.6) is that in unitary lattice integrable modes, the half-space lattice EH does not couple fermions at distances larger than those in the corresponding lattice Hamiltonian. Correspondingly, within an interval, it was noted that near the endpoints, the EH does not exhibit higher couplings, only manifesting them in the crossover region at the center [312].

Let us now consider the non-Hermitian SSH model. Assuming that the structure of the EH in (5.7.6) holds also for this theory, from the Hamiltonian in (5.1.1) we can conjecture that the half-space lattice EH takes the form

$$K_A \propto \sum_{j=0}^{+\infty} \Bigg[(2j)\, w \left(c^\dagger_{2j} c_{2j+1} + c^\dagger_{2j+1} c_{2j} \right) + (2j+1)\, v \left(c^\dagger_{2j-1} c_{2j} + c^\dagger_{2j} c_{2j-1} \right) + \\ + i \left(2j + \frac{1}{2} \right) u\, c^\dagger_{2j} c_{2j} - i \left(2j + \frac{3}{2} \right) u\, c^\dagger_{2j+1} c_{2j+1} \Bigg], \quad (5.8.1)$$

with some unknown proportionality constant. Since we cannot access numerically the full EH of the half-space, in order to test the conjecture in (5.8.1) we study the EH of an interval $[0, \ell]$ in a finite system of length $L \gg \ell$. In analogy with the unitary case, we expect that for a sufficiently large gap, near the endpoints the EH will follow the half-space result in (5.8.1), with a crossover in the middle of the interval, giving rise to the typical triangular shape.

In Fig. 5.7 we report the results of the numerical calculation of the lattice EH in the gapped phase, for an interval of length $\ell = 100$ in a system of total length $L = 2000$ with periodic boundary conditions. We fix the parameters $v = u = 1$ and we study different gaps by varying the value of w, in particular we take $w = 5, 10$ and 20. The plots report the ratio between the kernel of the EH, k^A, obtained from (5.2.12) and the one of the Hamiltonian h in (5.1.1) as a function of the lattice site. On the left, in Fig. 5.7b we report the real part of the nearest-neighbour coupling $k^A_{j,j+1}$, divided by $(-w)$ for j even (circles) and by $(-v)$ for j odd (crosses). Dividing by these coupling constants, we isolate the entanglement temperature, which is expected to follow the triangular shape (see (5.8.1) and discussion below). Indeed we see that, apart from a small crossover region in the center of the interval, the nearest-neighbour coupling follows the expected behaviour for all values of w that we considered. This behaviour is completely analogous to what observed in [312] for the dimerised hopping chain. The novel result is reported in the right plot, in Fig. 5.7b, where we show the staggered imaginary chemical potential $k^A_{j,j}$, divided by u for j even and by $(-u)$ for j odd. Again, the role of this division is to

isolate the entanglement temperature, which should agree with the one obtained from the nearest-neighbour coupling. Indeed we observe that, apart from a small oscillation due to finite size effects, the imaginary chemical potential follows the same triangular shape as the nearest-neighbour coupling, as expected from our conjecture in (5.8.1).

As a further check, in Fig. 5.8 we report the matrix plots of the real (left plot) and of the imaginary parts (right plot) of the single-particle EH k^A. According to our conjecture in (5.8.1), the half-space EH does not couple fermions at distances higher than one, similarly to what happens for unitary integrable models in (5.7.6). In the left plot in Fig. 5.8a, we see that near the endpoints the only non-zero elements of the real part of the EH kernel are the nearest-neighbour couplings $k^A_{j,j+1}$ and $k^A_{j,j-1}$. The higher couplings are non-zero only in a crossover region in the middle of the interval, as expected. This behaviour is again completely analogous to what was observed in [312] for the dimerised hopping chain. The new results are given by the imaginary part, shown in the right plot in Fig. 5.8b. We see that also the imaginary part follows the expected behaviour, with only the main diagonal k^A being significantly different from zero near the endpoints. This confirms the validity of our local conjecture in (5.8.1) for the half space EH in the non-Hermitian SSH model. We remark that this is the first observation of a Bisognano-Wichmann like behaviour in a non-Hermitian model.

Before concluding this section, we wish to comment on the proportionality constant in (5.8.1), i.e., the slope of the triangles in Fig. 5.7. This constant is actually related to the velocity of the excitations in the gapped model. In [312], the analogous proportionality constant in the dimerised hopping chain was computed analytically using the knowledge of the exact CTM. It would be interesting to obtain analytically the CTM in the non-Hermitian SSH model, which would refine our conjecture (5.8.1) for the half-space EH. This computation would not only allow us to predict the slope of the linearly increasing entanglement temperature, but it could also provide a quantitative understanding of the finite size oscillations of the chemical potential in Fig. 5.7b which are not captured by (5.8.1). This is however a rather involved calculation which goes beyond the scope of this work.

5.8.2 Entanglement Hamiltonian at the critical point

In this section we study the EH at the critical point $w - v = u$ (green square in Fig. 5.2). As discussed in Appendix 5.1, at the critical point and for periodic boundary conditions, the lattice Hamiltonian (5.1.1) presents a Jordan block. Then, to treat the system numerically we need to introduce a small twisting of the boundary conditions δ [210]. In all the following discussion we fix $\delta = 10^{-7}$. In full analogy to the study we performed for the gapped phase in Appendix 5.8.1, we compute numerically the lattice EH kernel k^A using (5.2.12), performing all calculations at high precision. However, at the critical point there is an additional

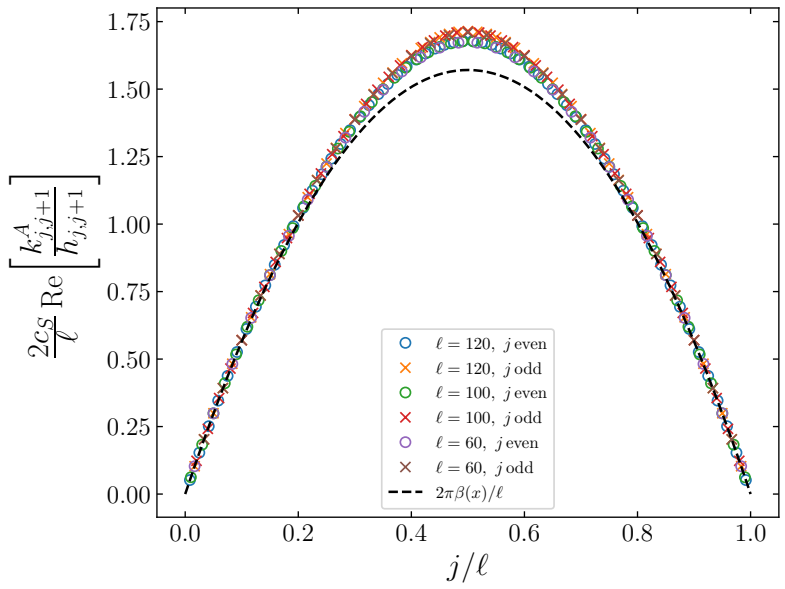


Figure 5.9: Real part of the ratio of the EH nearest-neighbour coupling $k^A_{j,j+1}$ with the coupling w (v) for j even (odd), rescaled by $2c_S/\ell$, where ℓ is the length of the interval and c_S is the speed of sound (5.1.12). The circles represent even sites and the crosses are odd sites. For all lengths considered we observe a perfect collapse. The black dashed parabola is the field theory prediction for the local temperature $2\pi\beta(x)$ in (5.7.3), divided by ℓ. Near the endpoints of the interval we find a very good agreement between the lattice result and the field theory. The deviation in the middle of the interval is due to the contribution of higher couplings, analogously to what happens in Hermitian lattice models.

subtlety. In [210] it was shown that at criticality all eigenvalues ν_j of the correlation matrix are real and lie outside of the interval $[0, 1]$. As a consequence, the matrix appearing inside the logarithm in (5.2.12) has all negative eigenvalues. This is susceptible to numerical instabilities, giving an imaginary part of the logarithm which (unphysically) oscillates wildly between $+i\pi$ and $-i\pi$. In this work we always fix it to be equal to $+i\pi$.

Before presenting our numerical results for the critical non-Hermitian SSH model, we would like to reiterate what occurs in the case of unitary gapless models. According to (5.7.3), in the vacuum of the CFT describing the continuum limit of a critical model, the EH of an interval is proportional to the energy density with a parabolic entanglement temperature $\beta(x)$ [124, 290–292]. One could be tempted to conclude that the EH of an interval in a critical model should be proportional to the critical Hamiltonian density with the parabolic temperature in (5.7.3). This behaviour would in particular imply that all terms of the lattice EH that couple fermions at distances higher than those in the Hamiltonian must be negligible. However, as recognised first in [326], this is not the case, and the EH contains couplings at arbitrary distances (see also [313–315]). Moreover, when expanding

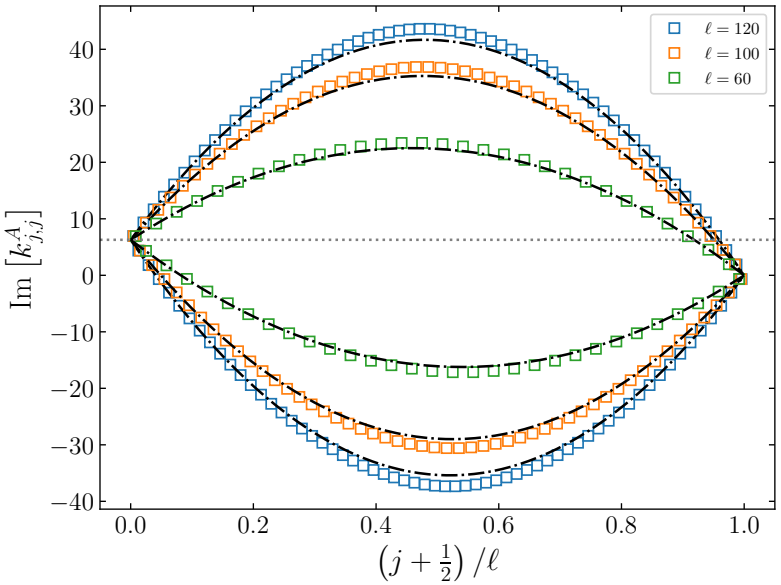


Figure 5.10: Imaginary chemical potential $k^A_{j,j}$ at criticality $w - v = u$ for different lengths of the interval $\ell = 60, 100$ and 120. The black dash-dotted curves are reported in (5.8.3) and are obtained as the sum of the naive field theory prediction for the entanglement temperature in (5.7.3) and of the conjectured form of the novel term in (5.8.2). Close to the endpoints we observe a perfect agreement which becomes slightly worse in the middle of the interval.

the lattice fermions in the lattice spacing, all these higher couplings contribute to the continuum energy density T_{00} [327, 328]. In [327–329] it was shown that in order to recover the CFT entanglement temperature $\beta(x)$ in (5.7.3), it is necessary to perform a careful continuum limit which takes into account all of these higher contributions. This limiting procedure has allowed to reconstruct the CFT EH in many systems at criticality, both at finite temperature and in the ground state [327–329] and also in the presence of boundaries [328–330], in inhomogeneous and out-of-equilibrium systems [331, 332] and in higher dimensions [333]. In [330, 334] it has also been extended to the recently introduced negativity Hamiltonian [335], i.e., the logarithm of the partial transposed density matrix. On the other hand, this limit is highly dependent on the lattice model and, to date, it is only understood in the case of free massless lattice fermions and the harmonic chain.

Considering now the non-Hermitian SSH model, in Figs. 5.9 and 5.10, we report the numerical lattice EH, obtained from (5.2.12) with a choice of parameters $w = 1.5$, $v = 1$ and $u = w - v = 0.5$ and different interval lengths $\ell = 60, 100$ and 120 in a total system of length $L = 2000$. In Fig. 5.9 we plot the real part of the nearest-neighbour coupling $k^A_{j,j+1}$, divided by $(-w)$ for j even and by $(-v)$ for j odd, analogously to what we have done in the massive case. We further make the quantity dimensionless by multiplying it by $2c_S/\ell$, where c_S is the speed of sound (5.1.12) in the critical lattice model. Indeed, notice that if we reintroduce

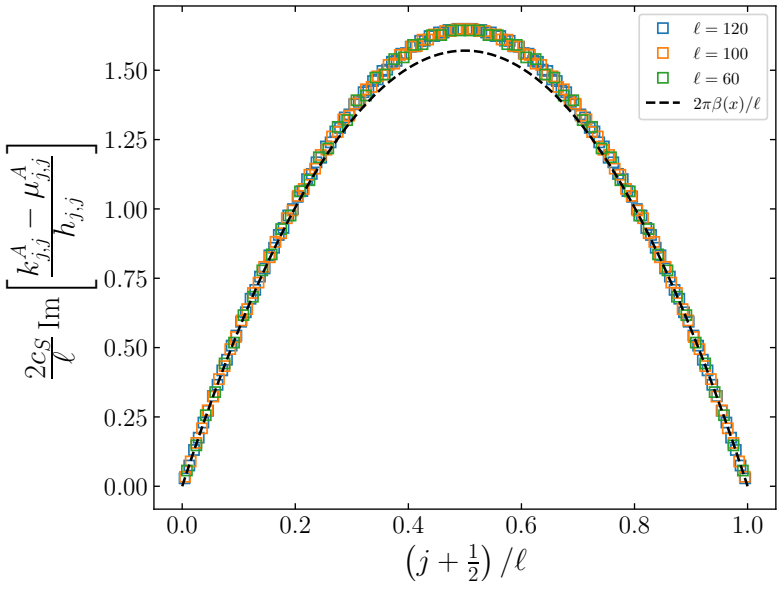


Figure 5.11: Imaginary part of $(k^A_{j,j} - \mu^A_{j,j})/h_{j,j}$ (i.e. the difference between the EH chemical potential and $\mu^A_{j,j}$ in (5.8.2), all in units of $h_{j,j}$), rescaled with $2c_S/\ell$, where c_S is the speed of sound in (5.1.12). We consider intervals of length $\ell = 60, 100$ and 120 in a system of total length $L = 2000$, with parameters $w = 1.5$, $v = 1$ and $u = w - v = 0.5$. For all ℓ, we observe a perfect collapse, suggesting that we have successfully isolated the scaling part. The black dashed curve is the CFT prediction for the entanglement temperature $2\pi\beta$ in (5.7.3) divided by ℓ. Analogously to the nearest-neighbour coupling in Fig. 5.9, the agreement is perfect at the endpoints and is slightly worse in the middle of the interval, due to the contribution of higher order couplings.

the dimensions, k^A is dimensionless, while w and v have the dimensions of an inverse time. We observe a perfect collapse for all the lengths considered. The black dashed line in Fig. 5.9 is the parabolic entanglement temperature $2\pi\beta(x)$ for unitary CFTs reported in (5.7.3), divided by the length of the interval ℓ. While near the endpoints we find a good agreement, we see a deviation in the middle of the interval. Similarly to what happens for unitary lattice models, the origin of this discrepancy is the presence of higher couplings which in the continuum limit give contributions to the continuum energy density. We expect that a proper continuum limit should exactly reproduce the parabola in (5.7.3) (as for Hermitian free fermions [327]), but this is beyond our goals.

In Fig. 5.10 we instead report the staggered imaginary chemical potential (the alternating sign with respect to Fig. 5.7b is due to not having divided by either u or $(-u)$). This quantity displays the most significant difference with respect to the Hermitian case. For all the lengths ℓ of the interval, at the left endpoint $j/\ell = 0$ the chemical potential takes the value $2\pi i$ (grey dotted line), while at the right one $j/\ell = 1$ it vanishes. Based on this observation, we conjecture that besides the approximate parabolic result, at the critical point appears an additional term of

the form

$$\sum_{j=0}^{\ell} \mu^A_{j,j}\, c^\dagger_j c_j = 2\pi i \sum_{j=0}^{\ell} \left(1 - \frac{\left(j+\frac{1}{2}\right)}{\ell}\right) c^\dagger_j c_j, \tag{5.8.2}$$

i.e., a chemical potential term which interpolates linearly between $2\pi i$ and 0. We remark that, differently from the parabolic entanglement temperature $\beta(x)$ in (5.7.3), this novel term does not scale with the system size. In order to check (5.8.2), in Fig. 5.10 we compare the two curves (dash-dotted black lines)

$$\frac{\pi\,(\pm u)}{c_S}\left(\frac{(\ell-x)x}{\ell}\right) + 2\pi\left(1-\frac{x}{\ell}\right), \tag{5.8.3}$$

with the imaginary part of the EH chemical potential term for $\ell = 60, 100$ and 120. Near the endpoints we find a perfect match for all the lengths considered, while the agreement gets slightly worse in the middle of the interval, but still acceptable.

To facilitate the comparison, we extract the part of the EH chemical potential that scales with the length of the interval by subtracting the conjectured form $\mu^A_{j,j}$ in (5.8.2) from the numerical result for $k^A_{j,j}$. We then divide by u for j even and by $(-u)$ for j odd to isolate the entanglement temperature and we rescale with $2c_S/\ell$ to make the quantity dimensionless. The result of this procedure is reported in Fig. 5.11. For all the values of the length considered we observe a perfect collapse, which suggests that the novel non-scaling term $\mu^A_{j,j}$ takes indeed the conjectured form (5.8.2). The black dashed curve is again the parabolic CFT prediction for the entanglement temperature in (5.7.3) divided by ℓ. Once again, we have a perfect agreement near the endpoints of the interval, while we observe a deviation in the middle. This deviation is always due to the presence of contributions from higher couplings.

Summing up our findings, recalling from Appendix 5.1 that the critical point is described by the $c = -2$ bc-ghost CFT, we propose that the continuum limit of the difference $(k^A - \mu^A)$ must reproduce the continuum CFT EH in (5.7.3). Meanwhile, the continuum limit associated with the new chemical potential term μ^A in (5.8.2) will yield

$$\sum_{j=0}^{\ell} \mu^A_{j,j}\, c^\dagger_j c_j \sim 2\pi i \int_0^\ell \mathrm{d}x \left(1-\frac{x}{\ell}\right) J(x) + \text{irrelevant operators}, \tag{5.8.4}$$

where $J(x) =: cb : (x)$ is the ghost number operator. Putting all together, we conjecture that the EH of the $c = -2$ bc-ghost CFT would take the form

$$K_A = \int_0^\ell \mathrm{d}x\, \frac{x\,(\ell-x)}{\ell}\, T_{00}(x) + 2\pi i \int_0^\ell \mathrm{d}x \left(1-\frac{x}{\ell}\right) J(x)\,, \tag{5.8.5}$$

which is one of the main results of this chapter. Comparing the proposed EH with the result for unitary CFTs in (5.7.3), the main difference is the presence of the

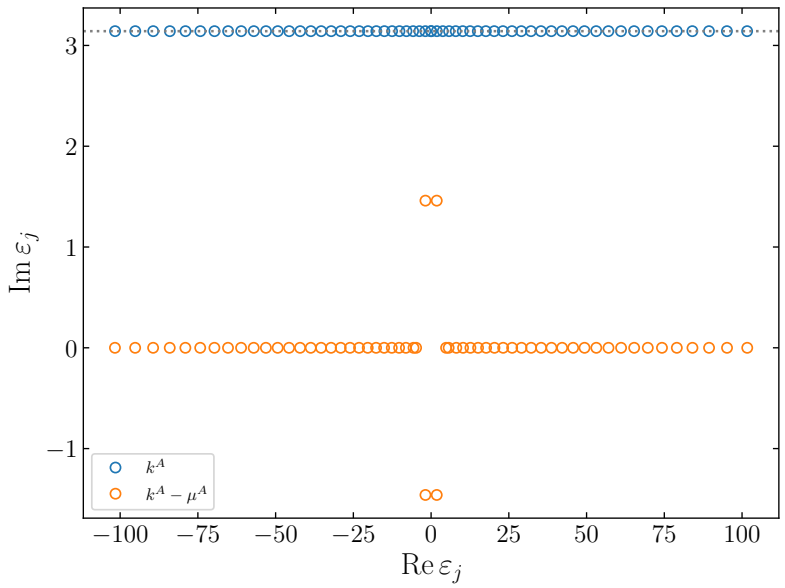


Figure 5.12: Spectra of the single-particle EH k^A (blue) and of the difference $(k^A - \mu^A)$ (orange), where μ^A is given by (5.8.2). The data are for an interval of length $\ell = 120$, in a system of size $L = 2000$, and couplings $w = 1.5$, $v = 1$ and $u = w - v = 0.5$. All eigenvalues of the EH have imaginary part equal to π (gray dotted line). Subtracting μ^A has the net effect of making almost all the eigenvalues real.

imaginary term proportional to the ghost number $J(x)$. Nevertheless, since this term is again the integral of a local operator, our conjecture (5.8.5) retains a local structure. Notice that, since the conformal dimension of the ghost number operator $J(x)$ is $\Delta_J = 1$, the local weight $(1 - x/\ell)$ is dimensionless and it does not scale with the system size, as we observed on the lattice.

In order to understand the role played by the term μ^A in (5.8.2), in Fig. 5.12 we compare the single-particle entanglement spectrum, i.e., the eigenvalues of k^A, with the eigenvalues of the matrix $(k^A - \mu^A)$. All the eigenvalues ε_j of the single-particle EH (blue circles) possess an imaginary part equal to π. As already mentioned, this imaginary part is due to the fact that the eigenvalues ν_j of the correlation matrix all belong to $(-\infty, 0) \cup (1, +\infty)$, which, using (5.2.12), leads to (5.4.6). As discussed before, the impact of the imaginary part in (5.4.6) on the many-body spectrum of the reduced density matrix is to impart an alternating sign to the eigenvalues of ρ_A depending on the charge sector, i.e., the number of ghosts, according to (5.4.5), which in turn is responsible for the negative sign of the entanglement entropy. On the other hand, in Fig. 5.12 we see that the eigenvalues of $(k^A - \mu^A)$ (orange circles) are almost all real. We can therefore argue that the novel operator μ^A in (5.8.2) (and its continuum limit (5.8.4) in the *bc*-ghost CFT) is the one responsible for the alternating sign of the entanglement spectrum. Without the operator μ^A, the reduced density matrix ρ_A would be positive defined and, as a consequence, the entanglement entropy would be positive too.

5.9 Concluding remarks

In this work, we have studied the symmetry resolved entanglement for the critical point of the non-Hermitian SSH model described by the $c = -2$ bc-ghost CFT. We have then studed numerically the entanglement Hamiltonian, both at that critical point and in the trival gapped phase.

Symmetry resolved entanglement

Regarding symmetry resolved entanglement, we have considered the generalization of the Rényi entanglement entropy based on the modulus $|\rho_A|$ of the reduced density matrix ρ_A recently introduced in [211], which circumvents the problems that arise in the standard entanglement entropy due to the non-positiviness of ρ_A. We have then focused on the ground state of the bc-ghost theory with central charge $c = -2$. This non-unitary CFT is the scaling limit of the non-Hermitian SSH model at criticality and has a global $U(1)$ symmetry. From a technical side, the main advantage of the non-Hermitian SSH model is that it is a quadratic fermionic chain, a fact that allows us to perform exact numerical calculations for large subsystem sizes thanks to Wick theorem. By applying bosonization techniques in the field theory, and with the support of exact lattice numerical calculations, we have derived the analytic expression of the absolute charged moments in the bc-ghost theory. They boil down to a two-point correlator of composite twist fields that properly includes the phase shift associated to the inserted charge.

From the result obtained for the absolute charged moments, we have found that the sign of the eigenvalues of ρ_A in the bc-ghost CFT is determined by the charge sector to which they belong. This property is also true in the lattice system for any subsystem size. Hence, since the eigenvalues of each charge sector have equal sign, we can define a positive-definite reduced density matrix in each sector and from it a positive symmetry-resolved entanglement entropy. Interestingly, we have obtained that the symmetry-resolved entanglement entropy of the bc-ghost is the same as the one of the massless Dirac fermion.

We have also analytically determined the standard charged moments of ρ_A. They present different expressions when the Rényi index n is either odd or even, a behaviour that stems from the dependence of the sign of the entanglement spectrum on the charge sector. This property is inherited by the standard Rényi entanglement entropies and resembles the case of the negativity in unitary CFTs [277]. To our knowledge, this feature has not been reported in the literature, but it is expected to occur if the signs of the spectrum of ρ_A have the same charge-resolved structure as in our case. We have seen that the standard charged moments of the bc-ghost theory are also given by a correlator of composite twist fields with a different phase shift for n even or odd.

Finally, using the results for the standard moments of ρ_A, we have analytically

derived the distribution of the entanglement spectrum in the *bc*-ghost theory, which is different from that of unitary CFTs [270], although its number distribution turns out to be also a function of a scaling variable with no free parameters.

Our work leaves many open questions for future research. Here we have restricted to a particular non-unitary CFT. It would be interesting to study how our results extend to other theories or non-Hermitian systems and, in particular, to see how universal are the expressions for the symmetry-resolved entanglement entropy and the entanglement spectrum distribution that we obtain for the *bc*-ghost theory with central charge -2. In this respect, it would be needed a careful analysis using a path integral approach of the twist field correlators that give the (absolute) charged moments of ρ_A. Another relevant line would be to explore theories in which the spectrum of ρ_A has other forms, e.g. it is complex, and wonder if the symmetry-resolved entropy is positive-definite as well. Moreover, here we have considered as ground state density matrix $|\psi_R\rangle \langle\psi_L|$, but this is not the only possible choice; for example $|\psi_R\rangle \langle\psi_R|$, whose reduced density matrix is positive definite, is another reasonable alternative. It would be nice to study the symmetry-resolved entanglement entropies in such state and compare with our results. Of course, the entanglement entropy is not the only entanglement measure that can be resolved in symmetry sectors, for example the negativity, which can be employed to study entanglement in disjoint subsystems [236, 242], or the operator entanglement [216]. One can also consider to carry out a similar analysis for them.

Entanglement Hamiltonian

Regarding the entanglement Hamiltonian, in the gapped phase, the EH assumes the typical triangular shape (see (5.8.1) and discussion) that was already observed in [312] for unitary integrable gapped models. Near the endpoints of the interval, the entanglement temperature grows linearly with the lattice site, according to the half-space prediction in (5.8.1). Remarkably, we observe that the same behaviour is true for the imaginary part of the EH. This is the first example of a lattice Bisognano-Wichmann like behaviour in a non-Hermitian model.

At the critical point, described by the *bc*-ghost CFT, we find a departure from the parabolic EH in (5.7.3) predicted by the Bisognano-Wichmann theorem for unitary CFTs. In addition to a term proportional to the energy density with a parabolic entanglement temperature, we observe a term proportional to the number operator $c_i^\dagger c_i$ with an imaginary chemical potential interpolating between $2\pi i$ and 0, cf. (5.8.2). This operator has a profound effect on the entanglement spectrum. As depicted in Fig. 5.12, removing the operator in (5.8.2) ensures that almost all the eigenvalues are real. As discussed previously, the imaginary part of the single-particle entanglement spectrum in (5.4.6) is responsible for the negativeness of the entanglement entropy. If the operator in (5.8.2) were not present, the entanglement entropy would be positive. Based on these results, we formulate a conjecture given

by (5.8.5) for the EH in the bc-ghost CFT. Such a conjecture consists of a term analogous to the Bisognano-Wichmann EH in (5.7.3) and of an imaginary chemical potential term proportional to the ghost number $J(x)$.

Three open problems emerges very naturally. Firstly, in the gapped phase, it would be interesting to derive analytically the CTM. As discussed in Appendix 5.8.1, this would determine the slope of the triangular entanglement temperature in Fig. 5.7 and could validate the lattice Bisognano-Wichmann behaviour. Secondly, it is desirable to analytically derive the EH at the critical point, akin to the work done for free massless fermions in [294]. Thirdly, the robustness of our findings remains uncertain, such as whether the conjectured form of the EH withstands the presence of relevant interactions. Other unexplored research directions include understanding the EH for non-Hermitian systems that lack a real Hamiltonian spectrum.

5.A Details of the computation of $P(\lambda)$

In this appendix, we discuss in detail how to obtain the entanglement spectrum distribution $P(\lambda)$ of ρ_A from its moments $Z_n(0)$ through the Stieljes transform $f(s)$.

In order to lighten the notation, let us rewrite the moments (5.5.3) of ρ_A in the form

$$Z_n(0) = \begin{cases} g\kappa e^{-bn+b'/n}, & n \text{ odd}, \\ g e^{-bn+b'/(2n)}, & n \text{ even}, \end{cases} \tag{5.A.1}$$

where

$$e^{-b} = \frac{\ell^{1/3}}{g\kappa}, \quad e^{b'} = \ell^{1/3}. \tag{5.A.2}$$

As explained in the main text, we have assumed in (5.A.1) that the non-universal term $c_{n,\alpha}$ is of the form of (5.3.26) and we have multiplied the expressions both for n even and odd by a global factor g^{n-1} to take into account a possible global degeneracy of the entanglement spectrum.

According to (5.6.3), the moments of ρ_A are the coefficients of the Laurent series expansion of $f(s)$. Taking int account the dependence of $Z_n(0)$ on the parity of n, we split the series in the form

$$f(s) = \frac{1}{\pi}\left[\sum_{n=0}^{\infty} Z_{2n+1}(0) s^{-(2n+1)} + \sum_{n=1}^{\infty} Z_{2n}(0) s^{-2n}\right]. \tag{5.A.3}$$

Inserting (5.A.1) in this expression, and taking the Taylor series of $e^{b'/n}$ and $e^{b'/(2n)}$

in the odd and even terms respectively,

$$f(s) = \frac{g}{\pi}\left[\kappa\sum_{n=0}^{\infty} e^{-b(2n+1)-\frac{b'}{2n+1}} s^{-(2n+1)} + \sum_{n=1}^{\infty} e^{-b2n+\frac{b'}{4n}} s^{-2n}\right]$$
$$= \frac{g}{\pi}\left[\frac{\kappa e^{-b}}{s}\sum_{k=0}^{\infty}\frac{(-b')^k}{k!}\sum_{n=0}^{\infty}\frac{(e^{-2b}/s^2)^n}{(2n+1)^k} + \sum_{k=0}^{\infty}\frac{1}{k!}\left(\frac{b'}{4}\right)^k\sum_{n=1}^{\infty}\frac{(e^{-2b}/s^2)^n}{n^k}\right], \tag{5.A.4}$$

we can then identify the Lerch trascendent $\phi(z,\nu,\alpha) = \sum_{n=0}^{\infty}\frac{z^n}{(n+\alpha)^\nu}$ in the odd term and the polylogarithm function $\mathrm{Li}_\nu(z) = \sum_{k=1}^{\infty} z^k/k^\nu$ in the even term,

$$f(s) = \frac{g}{\pi}\left[\frac{\kappa e^{-b}}{s}\sum_{k=0}^{\infty}\frac{(-b')^k}{2^k k!}\phi(e^{-2b}/s^2,k,1/2) + \sum_{k=0}^{\infty}\frac{1}{k!}\left(\frac{b'}{4}\right)^k \mathrm{Li}_k\left(\frac{e^{-2b}}{s^2}\right)\right]. \tag{5.A.5}$$

Finally, making use of the identity

$$2^{-k} z\phi(z^2,k,1/2) = \frac{1}{2}\left(\mathrm{Li}_k(z) - \mathrm{Li}_k(-z)\right), \tag{5.A.6}$$

we arrive at (5.6.5)

$$f(s) = \frac{g\kappa}{2\pi}\sum_{k=0}^{\infty}\frac{(-b')^k}{k!}\left[\mathrm{Li}_k\left(\frac{e^{-b}}{s}\right) - \mathrm{Li}_k\left(-\frac{e^{-b}}{s}\right)\right] + \frac{g}{\pi}\sum_{k=0}^{\infty}\frac{1}{k!}\left(\frac{b'}{4}\right)^k \mathrm{Li}_k\left(\frac{e^{-2b}}{s^2}\right). \tag{5.A.7}$$

Once the Stieljes transform $f(s)$ is determined, we can obtain the distribution $P(\lambda)$ using the inversion formula (5.6.4). The technical crucial point when applying (5.6.4) is that the polylogarith function $\mathrm{Li}_k(z)$ for $k \geq 1$ is a multivalued function with a branch point at $z = 1$. If we take as branch cut the real interval $[1,\infty)$, the discontinuity across the cut is

$$\lim_{\epsilon\to 0^+} \mathrm{Im}\,\mathrm{Li}_k(y \pm i\epsilon) = \begin{cases} \pm\pi(\log y)^{k-1}/\Gamma(k) & y \geq 1 \\ 0 & y < 1. \end{cases} \tag{5.A.8}$$

Using this property, we can easily obtain $P(\lambda)$ with (5.6.4) and (5.A.7). To this end, let us consider separately the two terms of (5.A.7). We define the function

$$f^{>}_{\mathrm{odd}}(s) = \frac{g\kappa}{2\pi}\sum_{k=1}^{\infty}\frac{(-b')^k}{k!}\left(\mathrm{Li}_k(e^{-b}/s) - \mathrm{Li}_k(-e^{-b}/s)\right), \tag{5.A.9}$$

which corresponds to the first term of (5.A.7), but removing the mode $k = 0$. If we apply (5.A.8), then we find

$$\lim_{\epsilon\to 0^+} \mathrm{Im}\, f^{>}_{\mathrm{odd}}(\lambda - i\epsilon) = \frac{g\kappa\Theta(e^{-b}-\lambda)}{2\log(e^{-b}/|\lambda|)}\sum_{k=1}^{\infty}\frac{1}{k!\Gamma(k)}\left(-b'\log\frac{e^{-b}}{|\lambda|}\right)^k$$
$$= -\frac{g\kappa\Theta(e^{-b}-\lambda)}{2\log(e^{-b}/|\lambda|)}\sqrt{b'\log\frac{e^{-b}}{|\lambda|}}\, J_1\left(2\sqrt{b'\log\frac{e^{-b}}{|\lambda|}}\right) \tag{5.A.10}$$

where Θ is the Heaviside step function and J_1 is the Bessel function of the first kind. Note that for the last equality we have used that $b' > 0$

Analogously, we define

$$f^{>}_{\text{even}}(s) = \frac{g}{\pi}\sum_{k=1}^{\infty}\frac{1}{k!}\left(\frac{a}{2}\right)^k \text{Li}_k\left(\frac{e^{-2b}}{s^2}\right), \tag{5.A.11}$$

which is the second term of $f(s)$ in (5.A.7) without the mode $k = 0$. If we again apply here (5.A.8), we have to take into account that for small ϵ, the argument of the polylogarithm in (5.A.11) behaves as

$$\frac{e^{-2b}}{(\lambda - i\epsilon)^2} = \frac{e^{-2b}}{\lambda^2} + i\epsilon 2\frac{e^{-2b}}{\lambda^3} + o(\epsilon^2) \tag{5.A.12}$$

and, therefore, it approaches the branch cut from above or from below depending on the sign of λ. It then follows that

$$\begin{aligned}\lim_{\epsilon\to 0^+}\text{Im} f^{>}_{\text{even}}(\lambda - i\epsilon) &= \text{sgn}(\lambda)\frac{g\Theta(e^{-b} - |\lambda|)}{2\log(e^{-b}/|\lambda|)}\sum_{k=1}^{\infty}\frac{1}{k!\Gamma(k)}\left(\frac{b'}{2}\log\frac{e^{-b}}{|\lambda|}\right)^k \\ &= g\Theta(e^{-b} - |\lambda|)\frac{\text{sgn}(\lambda)}{2\log\frac{e^{-b}}{|\lambda|}}\sqrt{\frac{b'}{2}\log\frac{e^{-b}}{|\lambda|}}\, I_1\left(2\sqrt{\frac{b'}{2}\log\frac{e^{-b}}{|\lambda|}}\right)\end{aligned} \tag{5.A.13}$$

where I_1 is the modified Bessel function of the first kind and in the last equality we have used $b' > 0$.

We still have to study the modes $k = 0$ of $f(s)$ in (5.A.7),

$$f_0(s) = \frac{g}{\pi}\,\text{Im}\left[\frac{\kappa}{2}\,\text{Li}_0\left(\frac{e^{-b}}{s}\right) - \frac{\kappa}{2}\,\text{Li}_0\left(\frac{-e^{-b}}{s}\right) + \text{Li}_0\left(\frac{e^{-2b}}{s^2}\right)\right]. \tag{5.A.14}$$

Taking into account that $\text{Li}_0(z) = z/(1-z)$, they can be rewritten as

$$f_0(s) = \frac{g}{\pi}\left[\frac{\kappa}{2}\frac{1}{s/e^{-b} - 1} + \frac{\kappa}{2}\frac{1}{s/e^{-b} + 1} + \frac{1}{s^2/e^{-2b} - 1}\right]. \tag{5.A.15}$$

Applying the Sokhotski–Plemelj formula

$$\lim_{\epsilon\to 0^+}\frac{1}{x \pm i\epsilon} = \mp i\pi\delta(x) + \text{PV}\left(\frac{1}{x}\right), \tag{5.A.16}$$

where PV stands for the Cauchy principal value, we get

$$\lim_{\epsilon\to 0^+}\text{Im}\, f_0(\lambda - i\epsilon) = g\lambda\frac{1+\kappa}{2}\delta(\lambda - e^{-b}) + g\lambda\frac{1-\kappa}{2}\delta(\lambda + e^{-b}). \tag{5.A.17}$$

Finally, putting (5.A.10), (5.A.13), and (5.A.17) together in the inversion formula (5.6.4), we get (5.6.7)

$$P(\lambda) = g\frac{1+\kappa}{2}\delta(\lambda-\lambda_M) + g\frac{1-\kappa}{2}\delta(\lambda+\lambda_M)+ \\ +g\frac{\Theta(\lambda_M-|\lambda|)}{2\lambda\sqrt{\log(\lambda_M/|\lambda|)}}\left[-\kappa\sqrt{b'}J_1\left(2\sqrt{b'\log\left(\lambda_M/|\lambda|\right)}\right) + \mathrm{sgn}(\lambda)\sqrt{b'/2}I_1\left(2\sqrt{b'/2\log\left(\lambda_M/|\lambda|\right)}\right)\right] \tag{5.A.18}$$

where we have used that $e^{-b} = \lambda_M$.

Outlook

Let us discuss some possible developments of the work presented in this thesis.

First, it would be interesting to clarify the relation between the entropic order parameters of [21, 22] and the entanglement asymmetry, to determine whether the two quantities strictly coincide or are merely closely related. Those works study scenarios that have not yet been treated in the entanglement-asymmetry literature, such as spontaneous symmetry breaking of a continuous group symmetry. Indeed, while SSB of a finite group symmetry produces a finite number of vacua — and thus the asymmetry of the full system equals the logarithm of the number of vacua — SSB of a continuous symmetry yields not only a continuous family of vacua but also Nambu–Goldstone bosons. Hence, even in the deep infrared the dynamics is not restricted to the set of vacua, requiring different approaches than those discussed in Secs. 4.5 and 4.6.1.

Regarding non-invertible symmetries, we found that in the presence of SSB, different vacua can have different asymmetries — a further indication that, in this case, vacua are physically inequivalent. The asymmetry with respect to the fusion algebra of a fusion category $\mathscr{C}$ can be readily computed in the TQFT describing the vacua, but this must be done on a case-by-case basis. Whether the value of the asymmetry in a given vacuum depends on specific properties of the module category over $\mathscr{C}$, and if so, which ones, remains to be understood.

It would also be interesting to study entanglement asymmetry in lattice models. The symmetrizer we introduced in (4.2.11) applies to a generic symmetry and would hold in this case as well. Studying lattice models would allow for numerical simulations, providing access to more complex states, such as out-of-equilibrium states arising during quantum quenches. Quantum quenches could also be studied analytically in (1+1)-dimensional CFTs, both for ordinary and non-invertible symmetries.

Bibliography

[1] J. D. Bekenstein, *Black holes and entropy*, *Phys. Rev. D* **7** (1973) 2333–2346.

[2] S. W. Hawking, *Particle Creation by Black Holes*, *Commun. Math. Phys.* **43** (1975) 199–220. [Erratum: Commun.Math.Phys. 46, 206 (1976)].

[3] L. Bombelli, R. K. Koul, J. Lee, and R. D. Sorkin, *A Quantum Source of Entropy for Black Holes*, *Phys. Rev. D* **34** (1986) 373–383.

[4] M. Srednicki, *Entropy and area*, *Phys. Rev. Lett.* **71** (1993) 666–669, arXiv:hep-th/9303048.

[5] C. Holzhey, F. Larsen, and F. Wilczek, *Geometric and renormalized entropy in conformal field theory*, *Nucl. Phys. B* **424** (1994) 443, arXiv:hep-th/9403108.

[6] T. J. Osborne and M. A. Nielsen, *Entanglement in a simple quantum phase transition*, *Phys. Rev. A* **66** (2002) 032110, arXiv:quant-ph/0202162.

[7] A. Osterloh, L. Amico, G. Falci, and R. Fazio, *Scaling of entanglement close to a quantum phase transition*, *Nature* **416** (2002) 608–610, arXiv:quant-ph/0202029.

[8] G. Vidal, J. I. Latorre, E. Rico, and A. Kitaev, *Entanglement in quantum critical phenomena*, *Phys. Rev. Lett.* **90** (2003) 227902, arXiv:quant-ph/0211074.

[9] G. Vidal, *Efficient Classical Simulation of Slightly Entangled Quantum Computations*, *Phys. Rev. Lett.* **91** (2003) 147902, arXiv:quant-ph/0301063.

[10] G. Vidal, *Efficient simulation of one-dimensional quantum many-body systems*, *Phys. Rev. Lett.* **93** (2004) 040502, arXiv:quant-ph/0310089.

[11] P. Calabrese and J. L. Cardy, *Entanglement entropy and quantum field theory*, *J. Stat. Mech.* (2004) P06002, arXiv:hep-th/0405152.

[12] S. Ryu and T. Takayanagi, *Holographic derivation of entanglement entropy from AdS/CFT*, *Phys. Rev. Lett.* **96** (2006) 181602, arXiv:hep-th/0603001.

[13] K. Ohmori and Y. Tachikawa, *Physics at the entangling surface*, *J. Stat. Mech.* (2015) P04010, arXiv:1406.4167.

[14] S. Ryu and T. Takayanagi, *Aspects of Holographic Entanglement Entropy*, *JHEP* **08** (2006) 045, arXiv:hep-th/0605073.

[15] T. Nishioka, S. Ryu, and T. Takayanagi, *Holographic Entanglement Entropy: An Overview*, *J. Phys. A* **42** (2009) 504008, arXiv:0905.0932.

[16] H. Casini, E. Testé, and G. Torroba, *Markov Property of the Conformal Field Theory Vacuum and the a Theorem*, *Phys. Rev. Lett.* **118** (2017) 261602, arXiv:1704.01870.

[17] A. Kitaev and J. Preskill, *Topological entanglement entropy*, *Phys. Rev. Lett.* **96** (2006) 110404, arXiv:hep-th/0510092.

[18] M. Levin and X.-G. Wen, *Detecting Topological Order in a Ground State Wave Function*, *Phys. Rev. Lett.* **96** (2006) 110405, arXiv:cond-mat/0510613.

[19] J. A. Vaccaro, F. Anselmi, H. M. Wiseman, and K. Jacobs, *Tradeoff between extractable mechanical work, accessible entanglement, and ability to act as a reference system, under arbitrary superselection rules*, *Phys. Rev. A* **77** (2008) 032114, arXiv:quant-ph/0501121.

[20] F. Ares, S. Murciano, and P. Calabrese, *Entanglement asymmetry as a probe of symmetry breaking*, *Nature Commun.* **14** (2023) 2036, arXiv:2207.14693.

[21] H. Casini, M. Huerta, J. M. Magán, and D. Pontello, *Entanglement entropy and superselection sectors. Part I. Global symmetries*, *JHEP* **02** (2020) 014, arXiv:1905.10487.

[22] H. Casini, M. Huerta, J. M. Magán, and D. Pontello, *Entropic order parameters for the phases of QFT*, *JHEP* **04** (2021) 277, arXiv:2008.11748.

[23] F. Benini, P. Calabrese, M. Fossati, A. H. Singh, and M. Venuti, *Entanglement Asymmetry for Higher and Noninvertible Symmetries*, arXiv:2509.16311.

[24] S. D. Bartlett and H. M. Wiseman, *Entanglement constrained by superselection rules*, *Phys. Rev. Lett.* **91** (2003) 097903, arXiv:quant-ph/0303140.

[25] M. A. Nielsen and I. L. Chuang, *Quantum Computation and Quantum Information*. Cambridge University Press, Cambridge, 6, 2012.

[26] G. Gour, I. Marvian, and R. W. Spekkens, *Measuring the quality of a quantum reference frame: The relative entropy of frameness*, *Phys. Rev. A* **80** (2009) 012307, arXiv:0901.0943.

[27] M. Mazzoni, L. Capizzi, and L. Piroli, *Breaking global symmetries with locality-preserving operations*, arXiv:2508.15892.

[28] C. Rylands, K. Klobas, F. Ares, P. Calabrese, S. Murciano, and B. Bertini, *Microscopic Origin of the Quantum Mpemba Effect in Integrable Systems*, *Phys. Rev. Lett.* **133** (10, 2024) 010401, arXiv:2310.04419.

[29] S. Murciano, F. Ares, I. Klich, and P. Calabrese, *Entanglement asymmetry and quantum Mpemba effect in the XY spin chain*, *J. Stat. Mech.* (2024) 013103, arXiv:2310.07513.

[30] K. Klobas, *Non-equilibrium dynamics of symmetry-resolved entanglement and entanglement asymmetry: exact asymptotics in Rule 54**, *J. Phys. A* **57** (7, 2024) 505001, arXiv:2407.21793.

[31] F. Ares, S. Murciano, E. Vernier, and P. Calabrese, *Lack of symmetry restoration after a quantum quench: An entanglement asymmetry study*, *SciPost Phys.* **15** (2023) 089, arXiv:2302.03330.

[32] F. Benini, V. Godet, and A. H. Singh, *Entanglement asymmetry in conformal field theory and holography*, *PTEP* **2025** (7, 2024) 063B05, arXiv:2407.07969.

[33] X. Turkeshi, P. Calabrese, and A. De Luca, *Quantum Mpemba Effect in Random Circuits*, *Phys. Rev. Lett.* **135** (5, 2024) 040403, arXiv:2405.14514.

[34] S. Liu, H.-K. Zhang, S. Yin, and S.-X. Zhang, *Symmetry restoration and quantum Mpemba effect in symmetric random circuits*, *Phys. Rev. Lett.* **133** (2024) 140405, arXiv:2403.08459.

[35] F. Ares, P. Calabrese, and S. Murciano, *The quantum Mpemba effects*, *Nature Reviews Physics* **7** (2025) 451–460, arXiv:2502.08087.

[36] L. Capizzi and V. Vitale, *A universal formula for the entanglement asymmetry of matrix product states*, *J. Phys. A: Math. Theor.* **57** (2024) 45LT01, arXiv:2310.01962.

[37] F. Ferro, F. Ares, and P. Calabrese, *Non-equilibrium entanglement asymmetry for discrete groups: the example of the XY spin chain*, *J. Stat. Mech.* (2024) 023101, arXiv:2307.06902.

[38] M. Lastres, S. Murciano, F. Ares, and P. Calabrese, *Entanglement asymmetry in the critical XXZ spin chain*, *J. Stat. Mech.* (7, 2025) 013107, arXiv:2407.06427.

[39] L. Capizzi and M. Mazzoni, *Entanglement asymmetry in the ordered phase of many-body systems: the Ising field theory*, *JHEP* **12** (2023) 144, arXiv:2307.12127.

[40] M. Fossati, F. Ares, J. Dubail, and P. Calabrese, *Entanglement asymmetry in CFT and its relation to non-topological defects*, *JHEP* **05** (2024) 059, arXiv:2402.03446.

[41] M. Fossati, C. Rylands, and P. Calabrese, *Entanglement asymmetry in CFT with boundary symmetry breaking*, *JHEP* **06** (2025) 089, arXiv:2411.10244.

[42] M. Chen and H.-H. Chen, *Rényi entanglement asymmetry in (1+1)-dimensional conformal field theories*, *Phys. Rev. D* **109** (2024) 065009, arXiv:2310.15480.

[43] F. Ares, S. Murciano, L. Piroli, and P. Calabrese, *Entanglement asymmetry study of black hole radiation*, *Phys. Rev. D* **110** (2024) L061901, arXiv:2311.12683.

[44] H.-H. Chen and Z.-J. Tang, *Entanglement asymmetry in the Hayden-Preskill protocol*, *Phys. Rev. D* **111** (2025) 066003, arXiv:2411.17695.

[45] A. Russotto, F. Ares, and P. Calabrese, *Non-Abelian entanglement asymmetry in random states*, *JHEP* **06** (2025) 149, arXiv:2411.13337.

[46] A. Russotto, F. Ares, and P. Calabrese, *Symmetry breaking in chaotic many-body quantum systems at finite temperature*, arXiv:2504.06146.

[47] D. Gaiotto, A. Kapustin, N. Seiberg, and B. Willett, *Generalized Global Symmetries*, *JHEP* **02** (2015) 172, arXiv:1412.5148.

[48] E. P. Verlinde, *Fusion Rules and Modular Transformations in 2D Conformal Field Theory*, *Nucl. Phys. B* **300** (1988) 360–376.

[49] J. Fuchs, I. Runkel, and C. Schweigert, *TFT construction of RCFT correlators 1. Partition functions*, *Nucl. Phys. B* **646** (2002) 353–497, arXiv:hep-th/0204148.

[50] J. Frohlich, J. Fuchs, I. Runkel, and C. Schweigert, *Kramers-Wannier duality from conformal defects*, *Phys. Rev. Lett.* **93** (2004) 070601, arXiv:cond-mat/0404051.

[51] D. Aasen, R. S. K. Mong, and P. Fendley, *Topological Defects on the Lattice I: The Ising model*, *J. Phys. A* **49** (2016) 354001, arXiv:1601.07185.

[52] D. Aasen, P. Fendley, and R. S. K. Mong, *Topological Defects on the Lattice: Dualities and Degeneracies*, arXiv:2008.08598.

[53] A. Kitaev, *Anyons in an exactly solved model and beyond*, *Annals Phys.* **321** (2006) 2–111, arXiv:cond-mat/0506438.

[54] L. Bhardwaj and Y. Tachikawa, *On finite symmetries and their gauging in two dimensions*, *JHEP* **03** (2018) 189, arXiv:1704.02330.

[55] C.-M. Chang, Y.-H. Lin, S.-H. Shao, Y. Wang, and X. Yin, *Topological defect lines and renormalization group flows in two dimensions*, *JHEP* **01** (2019) 026, arXiv:1802.04445.

[56] R. Thorngren and Y. Wang, *Fusion category symmetry. Part I. Anomaly in-flow and gapped phases*, *JHEP* **04** (2024) 132, arXiv:1912.02817.

[57] M. Henkel and A. Patkos, *Conformal invariance and line defects in the two-dimensional ising model*, *Journal of Physics A: Mathematical and General* **21** (Feb, 1988) L231.

[58] M. Henkel, A. Patkos, and M. Schlottmann, *The Ising Quantum Chain With Defects. 1. The Exact Solution*, *Nucl. Phys. B* **314** (1989) 609–624.

[59] L. Turban, *Conformal invariance and linear defects in the two-dimensional ising model*, *Journal of Physics A: Mathematical and General* **18** (1985) L325.

[60] F. Iglói, I. Peschel, and L. Turban, *Inhomogeneous systems with unusual critical behaviour*, *Adv. Phys.* **42** (1993) 683–740.

[61] M. Oshikawa and I. Affleck, *Defect lines in the Ising model and boundary states on orbifolds*, *Phys. Rev. Lett.* **77** (1996) 2604–2607, arXiv:hep-th/9606177.

[62] M. Oshikawa and I. Affleck, *Boundary conformal field theory approach to the critical two-dimensional Ising model with a defect line*, *Nucl. Phys. B* **495** (1997) 533–582, arXiv:cond-mat/9612187.

[63] V. B. Petkova and J. B. Zuber, *Generalized twisted partition functions*, *Phys. Lett. B* **504** (2001) 157, arXiv:hep-th/0011021.

[64] T. Quella, I. Runkel, and G. M. T. Watts, *Reflection and transmission for conformal defects*, *JHEP* **04** (2007) 095, arXiv:hep-th/0611296.

[65] P. Fendley, M. P. A. Fisher, and C. Nayak, *Boundary Conformal Field Theory and Tunneling of Edge Quasiparticles in non-Abelian Topological States*, *Annals Phys.* **324** (2009) 1547–1572, arXiv:0902.0998.

[66] C. Bachas, I. Brunner, and D. Roggenkamp, *Fusion of Critical Defect Lines in the 2D Ising Model*, *J. Stat. Mech.* (2013) P08008, arXiv:1303.3616.

[67] S. Murciano, P. Sala, Y. Liu, R. S. K. Mong, and J. Alicea, *Measurement-Altered Ising Quantum Criticality*, *Phys. Rev. X* **13** (2023) 041042, arXiv:2302.04325.

[68] K. Sakai and Y. Satoh, *Entanglement through conformal interfaces*, *JHEP* **12** (2008) 001, arXiv:0809.4548.

[69] V. Eisler and I. Peschel, *Solution of the fermionic entanglement problem with interface defects*, *Ann. Phys. (Berlin)* **522** (2010) 679, arXiv:1005.2144.

[70] P. Calabrese, M. Mintchev, and E. Vicari, *Entanglement Entropy of Quantum Wire Junctions*, *J. Phys. A* **45** (2012) 105206, arXiv:1110.5713.

[71] V. Eisler and I. Peschel, *Exact results for the entanglement across defects in critical chains*, *J. Phys. A* **45** (2012) 155301.

[72] E. M. Brehm and I. Brunner, *Entanglement entropy through conformal interfaces in the 2D Ising model*, *JHEP* **09** (2015) 080, arXiv:1505.02647.

[73] M. Gutperle and J. D. Miller, *Entanglement entropy at CFT junctions*, *Phys. Rev. D* **95** (2017) 106008, arXiv:1701.08856.

[74] M. Mintchev and E. Tonni, *Modular Hamiltonians for the massless Dirac field in the presence of a defect*, *JHEP* **03** (2021) 205, arXiv:2012.01366.

[75] L. Capizzi, S. Murciano, and P. Calabrese, *Rényi entropy and negativity for massless Dirac fermions at conformal interfaces and junctions*, *JHEP* **08** (2022) 171, arXiv:2205.04722.

[76] L. Capizzi, S. Murciano, and P. Calabrese, *Full counting statistics and symmetry resolved entanglement for free conformal theories with interface defects*, *J. Stat. Mech.* (2023) 073102, arXiv:2302.08209.

[77] Z. Yang, D. Mao, and C.-M. Jian, *Entanglement in a one-dimensional critical state after measurements*, *Phys. Rev. B* **108** (2023) 165120, arXiv:2301.08255.

[78] Z. Weinstein, R. Sajith, E. Altman, and S. J. Garratt, *Nonlocality and entanglement in measured critical quantum Ising chains*, *Phys. Rev. B* **107** (2023) 245132, arXiv:2301.08268.

[79] J. Y. Lee, C.-M. Jian, and C. Xu, *Quantum Criticality Under Decoherence or Weak Measurement*, *PRX Quantum* **4** (2023) 030317, arXiv:2301.05238.

[80] Y. Ashida, S. Furukawa, and M. Oshikawa, *System-environment entanglement phase transitions*, *Phys. Rev. B* **110** (2024) 094404, arXiv:2311.16343.

[81] P. Ruggiero, P. Calabrese, T. Giamarchi, and L. Foini, *Electrostatic solution of massless quenches in Luttinger liquids*, *SciPost Phys.* **13** (2022) 111, arXiv:2203.06740.

[82] M. Goldstein and E. Sela, *Symmetry-resolved entanglement in many-body systems*, *Phys. Rev. Lett.* **120** (2018) 200602, arXiv:1711.09418.

[83] J. C. Xavier, F. C. Alcaraz, and G. Sierra, *Equipartition of the entanglement entropy*, *Phys. Rev. B* **98** (2018) 041106, arXiv:1804.06357.

[84] E. Cornfeld, M. Goldstein, and E. Sela, *Imbalance entanglement: Symmetry decomposition of negativity*, *Phys. Rev. A* **98** (2018) 032302, arXiv:1804.00632.

[85] S. Murciano, G. Di Giulio, and P. Calabrese, *Entanglement and symmetry resolution in two dimensional free quantum field theories*, *JHEP* **08** (2020) 073, arXiv:2006.09069.

[86] H.-H. Chen, *Symmetry decomposition of relative entropies in conformal field theory*, *JHEP* **07** (2021) 084, arXiv:2104.03102.

[87] Y. Kusuki, S. Murciano, H. Ooguri, and S. Pal, *Symmetry-resolved entanglement entropy, spectra & boundary conformal field theory*, *JHEP* **11** (2023) 216, arXiv:2309.03287.

[88] L. Bhardwaj, L. E. Bottini, L. Fraser-Taliente, L. Gladden, D. S. W. Gould, A. Platschorre, and H. Tillim, *Lectures on generalized symmetries*, *Phys. Rept.* **1051** (2024) 1–87, arXiv:2307.07547.

[89] J. L. Cardy and I. Peschel, *Finite Size Dependence of the Free Energy in Two-dimensional Critical Systems*, *Nucl. Phys. B* **300** (1988) 377.

[90] B. Bertini, K. Klobas, M. Collura, P. Calabrese, and C. Rylands, *Dynamics of charge fluctuations from asymmetric initial states*, *Phys. Rev. B* **109** (2024) 184312, arXiv:2306.12404.

[91] L. Capizzi and V. Vitale, *A universal formula for the entanglement asymmetry of matrix product states*, *J. Phys. A* **57** (10, 2023) 45LT01, arXiv:2310.01962.

[92] J.-M. Stéphan and J. Dubail, *Logarithmic corrections to the free energy from sharp corners with angle 2π*, *J. Stat. Mech.* (2013) P09002, arXiv:1303.3633.

[93] J.-M. Stéphan, *Emptiness formation probability, Toeplitz determinants, and conformal field theory*, *J. Stat. Mech.* (2014) P05010, arXiv:1303.5499.

[94] A. Lamacraft and P. Fendley, *Order parameter statistics in the critical quantum Ising chain*, *Phys. Rev. Lett.* **100** (2008) 165706, arXiv:0802.1246.

[95] P. Calabrese and J. Cardy, *Entanglement entropy and conformal field theory*, *J. Phys. A* **42** (2009) 504005, arXiv:0905.4013.

[96] P. Di Francesco, P. Mathieu, and D. Senechal, *Conformal Field Theory*. Graduate Texts in Contemporary Physics. Springer-Verlag, New York, 1997.

[97] R. W. Cherng and E. Demler, *Quantum noise analysis of spin systems realized with cold atoms*, *New Journal of Physics* **9** (Jan, 2007) 7, arXiv:cond-mat/0609748.

[98] S. Groha, F. H. L. Essler, and P. Calabrese, *Full counting statistics in the transverse field Ising chain*, *SciPost Phys.* **4** (2018) 043, arXiv:1803.09755.

[99] D. A. Ivanov and A. G. Abanov, *Characterizing correlations with full counting statistics: classical Ising and quantum XY spin chains*, *Phys. Rev. E* **87** (2013) 022114, arXiv:1203.6325.

[100] F. Ares, M. A. Rajabpour, and J. Viti, *Exact full counting statistics for the staggered magnetization and the domain walls in the XY spin chain*, *Phys. Rev. E* **103** (2021) 042107, arXiv:2012.14012.

[101] E. H. Lieb, T. Schultz, and D. Mattis, *Two soluble models of an antiferromagnetic chain*, *Annals Phys.* **16** (1961) 407–466.

[102] I. Peschel, *Calculation of reduced density matrices from correlation functions*, *J. Phys. A* **36** (2003) L205, arXiv:cond-mat/0212631.

[103] T. Kennedy and H. Tasaki, *Hidden Z2×Z2 symmetry breaking in Haldane-gap antiferromagnets*, *Phys. Rev. B* **45** (1992) 304.

[104] T. Kennedy and H. Tasaki, *Hidden symmetry breaking and the Haldane phase inS=1 quantum spin chains*, *Communications in Mathematical Physics* **147** (1992) 431.

[105] R. Bonsignori, L. Capizzi, and P. Panopoulos, *Boundary Symmetry Breaking in CFT and the string order parameter*, *JHEP* **05** (2023) 027, arXiv:2301.08676.

[106] Y. Choi, B. C. Rayhaun, Y. Sanghavi, and S.-H. Shao, *Comments on Boundaries, Anomalies, and Non-Invertible Symmetries*, *Phys. Rev. D* **108** (5, 2023) 125005, arXiv:2305.09713.

[107] J. L. Cardy, *Conformal Invariance and Surface Critical Behavior*, *Nucl. Phys. B* **240** (1984) 514.

[108] G. M. T. Watts, *On the boundary Ising model with disorder operators*, *Nucl. Phys. B* **596** (2001) 513, arXiv:hep-th/0002218.

[109] J. L. Cardy, O. A. Castro-Alvaredo, and B. Doyon, *Form factors of branch-point twist fields in quantum integrable models and entanglement entropy*, *J. Statist. Phys.* **130** (2008) 129–168, arXiv:0706.3384.

[110] O. A. Castro-Alvaredo and B. Doyon, *Permutation operators, entanglement entropy, and the XXZ spin chain in the limit \Delta -> -1*, *J. Stat. Mech.* (2011) P02001, arXiv:1011.4706.

[111] D. X. Horváth and P. Calabrese, *Symmetry resolved entanglement in integrable field theories via form factor bootstrap*, *JHEP* **11** (2020) 131, arXiv:2008.08553.

[112] P. Calabrese, J. Cardy, and E. Tonni, *Entanglement entropy of two disjoint intervals in conformal field theory II*, *J. Stat. Mech.* (2011) P01021, arXiv:1011.5482.

[113] J. Hauschild and F. Pollmann, *Efficient numerical simulations with Tensor Networks: Tensor Network Python (TeNPy)*, *SciPost Phys. Lect. Notes* **5** (2018) 1, arXiv:1805.00055.

[114] J. L. Cardy, *Boundary Conditions, Fusion Rules and the Verlinde Formula*, *Nucl. Phys. B* **324** (1989) 581.

[115] J. L. Cardy, *Operator Content of Two-Dimensional Conformally Invariant Theories*, *Nucl. Phys. B* **270** (1986) 186.

[116] S.-H. Shao, *What's Done Cannot Be Undone: TASI Lectures on Non-Invertible Symmetries*, in *Theoretical Advanced Study Institute in Elementary Particle Physics 2023: Aspects of Symmetry*. 8, 2023. arXiv:2308.00747.

[117] L. K. Joshi *et al.*, *Observing the Quantum Mpemba Effect in Quantum Simulations*, *Phys. Rev. Lett.* **133** (1, 2024) 010402, arXiv:2401.04270.

[118] I. Affleck, M. Oshikawa, and H. Saleur, *Boundary critical phenomena in the three state Potts model*, *J. Phys. A* **31** (1998) 5827, arXiv:cond-mat/9804117.

[119] J. Fuchs and C. Schweigert, *Completeness of boundary conditions for the critical three state Potts model*, *Phys. Lett. B* **441** (1998) 141, arXiv:hep-th/9806121.

[120] P. Calabrese and J. L. Cardy, *Time-dependence of correlation functions following a quantum quench*, *Phys. Rev. Lett.* **96** (2006) 136801, arXiv:cond-mat/0601225.

[121] T. W. Burkhardt and T. Xue, *Conformal invariance and critical systems with mixed boundary conditions*, *Nucl. Phys. B* **354** (1991) 653.

[122] I. Runkel, *Boundary structure constants for the A series Virasoro minimal models*, *Nucl. Phys. B* **549** (1999) 563–578, arXiv:hep-th/9811178.

[123] I. Runkel, *Structure constants for the D series Virasoro minimal models*, *Nucl. Phys. B* **579** (2000) 561–589, arXiv:hep-th/9908046.

[124] J. Cardy and E. Tonni, *Entanglement hamiltonians in two-dimensional conformal field theory*, *J. Stat. Mech.* (2016) 123103, arXiv:1608.01283.

[125] J. L. Cardy, *Effect of Boundary Conditions on the Operator Content of Two-Dimensional Conformally Invariant Theories*, *Nucl. Phys. B* **275** (1986) 200.

[126] I. Affleck and A. W. W. Ludwig, *Universal noninteger 'ground state degeneracy' in critical quantum systems*, *Phys. Rev. Lett.* **67** (1991) 161–164.

[127] J. Hauschild and F. Pollmann, *Efficient numerical simulations with Tensor Networks: Tensor Network Python (TeNPy)*, *SciPost Phys. Lect. Notes* (2018) 5, arXiv:1805.00055. Code available from https://github.com/tenpy/tenpy.

[128] F. Benini, E. Garcia-Valdecasas, and S. Vitouladitis. Work in progress.

[129] L. Bhardwaj, L. E. Bottini, D. Pajer, and S. Schafer-Nameki, *Categorical Landau Paradigm for Gapped Phases*, *Phys. Rev. Lett.* **133** (2024) 161601, arXiv:2310.03786.

[130] C. L. Douglas and D. J. Reutter, *Fusion 2-categories and a state-sum invariant for 4-manifolds*, arXiv:1812.11933.

[131] D. Gaiotto and T. Johnson-Freyd, *Condensations in higher categories*, arXiv:1905.09566.

[132] T. Johnson-Freyd, *On the classification of topological orders*, *Commun. Math. Phys.* **393** (2022) 989–1033, arXiv:2003.06663.

[133] L. Bhardwaj, L. E. Bottini, S. Schafer-Nameki, and A. Tiwari, *Non-invertible higher-categorical symmetries*, *SciPost Phys.* **14** (2023) 007, arXiv:2204.06564.

[134] A. Ocneanu, *Chirality for operator algebras*, in *Subfactors: Proceedings of the Taniguchi Symposium on operator algebras*, H. Araki and others, eds., pp. 39–63. World Scientific, Singapore, 1994.

[135] D. A. Huse, *Exact exponents for infinitely many new multicritical points*, *Phys. Rev. B* **30** (1984) 3908–3915.

[136] J. A. Damia, R. Argurio, F. Benini, S. Benvenuti, C. Copetti, and L. Tizzano, *Non-invertible symmetries along 4d RG flows*, *JHEP* **02** (2024) 084, arXiv:2305.17084.

[137] A. Kitaev and L. Kong, *Models for gapped boundaries and domain walls*, *Commun. Math. Phys.* **313** (2012) 351–373, arXiv:1104.5047.

[138] C. Córdova, N. Holfester, and K. Ohmori, *Representation theory of solitons*, *JHEP* **06** (2024) 001, arXiv:2408.11045.

[139] R. Thorngren and Y. Wang, *Anomalous symmetries end at the boundary*, *JHEP* **09** (2021) 017, arXiv:2012.15861.

[140] Z. Ma, C. Han, Y. Meir, and E. Sela, *Symmetric inseparability and number entanglement in charge-conserving mixed states*, *Phys. Rev. A* **105** (2022) 042416, arXiv:2110.09388.

[141] C. Han, Y. Meir, and E. Sela, *Realistic Protocol to Measure Entanglement at Finite Temperatures*, *Phys. Rev. Lett.* **130** (2023) 136201, arXiv:2210.10713.

[142] S. Lang, *Algebra*, vol. 211 of *Graduate Texts in Mathematics*. Springer, New York, NY, 2002.

[143] G. J. Murphy, *C^*-algebras and operator theory*. Academic Press, Inc., 1990.

[144] S. Hellerman, A. Henriques, T. Pantev, E. Sharpe, and M. Ando, *Cluster decomposition, T-duality, and gerby CFT's*, *Adv. Theor. Math. Phys.* **11** (2007) 751–818, arXiv:hep-th/0606034.

[145] E. Sharpe, *An introduction to decomposition*, in *2021-2022 MATRIX Annals*, D. R. Wood, J. de Gier, and C. E. Praeger, eds., vol. 5 of *MATRIX Book Series*, pp. 145–168. Springer, 2024. arXiv:2204.09117.

[146] Y.-H. Lin, M. Okada, S. Seifnashri, and Y. Tachikawa, *Asymptotic density of states in 2d CFTs with non-invertible symmetries*, *JHEP* **03** (2023) 094, arXiv:2208.05495.

[147] J. Fuchs, *Fusion rules in conformal field theory*, *Fortsch. Phys.* **42** (1994) 1–48, arXiv:hep-th/9306162.

[148] M. Barkeshli, P. Bonderson, M. Cheng, and Z. Wang, *Symmetry Fractionalization, Defects, and Gauging of Topological Phases*, *Phys. Rev. B* **100** (2019) 115147, arXiv:1410.4540.

[149] T. Bartsch, *Unitary Categorical Symmetries*, arXiv:2502.04440.

[150] H. Fujimura and S. Shimamori, *Entanglement Asymmetry and Quantum Mpemba Effect for Non-Abelian Global Symmetry*, arXiv:2509.05597.

[151] Y. Kusuki, S. Murciano, H. Ooguri, and S. Pal, *Entanglement asymmetry and symmetry defects in boundary conformal field theory*, *JHEP* **01** (2025) 057, arXiv:2411.09792.

[152] V. Ostrik, *Module categories, weak Hopf algebras and modular invariants*, *Transform. Groups* **8** (2003) 177–206, arXiv:math/0111139.

[153] P. Etingof, S. Gelaki, D. Nikshych, and V. Ostrik, *Tensor categories*, vol. 205 of *Mathematical Surveys and Monographs*. American Math. Soc., 2015. https://math.mit.edu/~etingof/tenscat.pdf.

[154] T.-C. Huang, Y.-H. Lin, and S. Seifnashri, *Construction of two-dimensional topological field theories with non-invertible symmetries*, *JHEP* **12** (2021) 028, arXiv:2110.02958.

[155] J. Fuchs, I. Runkel, and C. Schweigert, *TFT construction of RCFT correlators. 3. Simple currents*, *Nucl. Phys. B* **694** (2004) 277–353, arXiv:hep-th/0403157.

[156] A. Recknagel and V. Schomerus, *Boundary Conformal Field Theory and the Worldsheet Approach to D-Branes*. Cambridge Monographs on Mathematical Physics. Cambridge University Press, 2013.

[157] J. Fuchs and C. Schweigert, *Category theory for conformal boundary conditions*, *Fields Inst. Commun.* **39** (2003) 25, arXiv:math/0106050.

[158] B. Day, *On closed categories of functors*, in *Reports of the Midwest Category Seminar IV*, vol. 137 of *Lecture Notes in Mathematics*, pp. 1–38. Springer, Berlin, 1970.

[159] C. Schweigert, *Hopf Algebras, Quantum Groups and Topological Field Theory*, 2023. https://www.math.uni-hamburg.de/home/schweigert/skripten/hskript.pdf.

[160] G. Böhm, F. Nill, and K. Szlachányi, *Weak Hopf algebras: I. Integral theory and C^*-structure*, *J. Algebra* **221** (1999) 385–438, arXiv:math/9805116.

[161] L. Bhardwaj, L. E. Bottini, D. Pajer, and S. Schäfer-Nameki, *Gapped phases with non-invertible symmetries: (1+1)d*, *SciPost Phys.* **18** (2025) 032, arXiv:2310.03784.

[162] Y. Hu, Y. Wan, and Y.-S. Wu, *Twisted quantum double model of topological phases in two dimensions*, *Phys. Rev. B* **87** (2013) 125114, arXiv:1211.3695.

[163] F. Benini, C. Córdova, and P.-S. Hsin, *On 2-group global symmetries and their anomalies*, *JHEP* **03** (2019) 118, arXiv:1803.09336.

[164] D. Tambara and S. Yamagami, *Tensor categories with fusion rules of self-duality for finite Abelian groups*, *J. Algebra* **209** (1998) 692–707.

[165] T. Bartsch, M. Bullimore, and A. Grigoletto, *Representation theory for categorical symmetries*, arXiv:2305.17165.

[166] K. Kawagoe, C. Jones, S. Sanford, D. Green, and D. Penneys, *Levin-Wen is a Gauge Theory: Entanglement from Topology*, *Commun. Math. Phys.* **405** (2024) 266, arXiv:2401.13838.

[167] O. Diatlyk, C. Luo, Y. Wang, and Q. Weller, *Gauging non-invertible symmetries: topological interfaces and generalized orbifold groupoid in 2d QFT*, *JHEP* **03** (2024) 127, arXiv:2311.17044.

[168] G. I. Kats and V. Palyutkin, *Finite ring groups*, *Trudy Moskovskogo Matematicheskogo Obshchestva* **15** (1966) 224–261.

[169] A. Masuoka, *Semisimple Hopf algebras of dimension 6, 8*, *Israel J. Math.* **92** (1995) 361–373.

[170] D. S. Sage and M. D. Vega, *Twisted Frobenius–Schur indicators for Hopf algebras*, *J. Algebra* **354** (2012) 136–147, arXiv:1107.0742.

[171] M. P. Mattis, *Correlations in Two-dimensional Critical Theories*, *Nucl. Phys. B* **285** (1987) 671–686.

[172] D. Penneys, "Fusion Categories." Lecture notes, 2021. https://people.math.osu.edu/penneys.2/8110/Notes/FusionCat.pdf.

[173] U. Haagerup, *Principal graphs of subfactors in the index range* $4 < [M : N] < 3 + \sqrt{2}$, in *Subfactors: Proceedings of the Taniguchi Symposium on operator algebras*, H. Araki and others, eds., pp. 1–38. World Scientific, Singapore, 1994.

[174] M. Asaeda and U. Haagerup, *Exotic subfactors of finite depth with Jones indices* $(5+\sqrt{13})/2$ *and* $(5+\sqrt{17})/2$, *Commun. Math. Phys.* **202** (1999) 1–63, math/9803044.

[175] P. Grossman and N. Snyder, *Quantum subgroups of the Haagerup fusion categories*, *Commun. Math. Phys.* **311** (2012) 617–643, arXiv:1102.2631.

[176] M. Izumi, *The structure of sectors associated with Longo–Rehren inclusions. II: Examples*, *Rev. Math. Phys.* **13** (2001) 603–674.

[177] P. Grossman and M. Izumi, *Drinfeld centers of fusion categories arising from generalized Haagerup subfactors*, *Quantum Topol.* **13** (2023) 593–668, arXiv:1501.07679.

[178] T.-C. Huang and Y.-H. Lin, *The F-Symbols for Transparent Haagerup–Izumi Categories with $G = \mathbb{Z}_{2n+1}$*, arXiv:2007.00670.

[179] T. J. Osborne, D. E. Stiegemann, and R. Wolf, *The F-symbols for the $\mathcal{H}_3$ fusion category*, arXiv:1906.01322.

[180] T.-C. Huang, Y.-H. Lin, K. Ohmori, Y. Tachikawa, and M. Tezuka, *Numerical Evidence for a Haagerup Conformal Field Theory*, *Phys. Rev. Lett.* **128** (2022) 231603, arXiv:2110.03008.

[181] T. J. Hagge and S.-M. Hong, *Some non-braided fusion categories of rank 3*, *Commun. Contemp. Math.* **11** (2009) 615–637.

[182] M. Aguiar, *A note on strongly separable algebras*, *Boletín de la Academia Nacional de Ciencias* **65** (2000) 51–60. Journal page.

[183] M. Müger, *Galois Theory for Braided Tensor Categories and the Modular Closure*, *Adv. Math.* **150** (2000) 151–201, arXiv:math/9812040.

[184] D. Penneys, "Operator algebras and their modules." Notes on Unitary quantum symmetries (Chapter 2), 2018. https://people.math.osu.edu/penneys.2/UQSL/PartI/UQSLPartIChapter2.pdf.

[185] R. G. Larson and M. E. Sweedler, *An associative orthogonal bilinear form for Hopf algebras*, *Amer. J. Math.* **91** (1969) 75–94.

[186] R. G. Larson and D. E. Radford, *Semisimple cosemisimple Hopf algebras*, *Amer. J. Math.* **110** (1988) 187–195.

[187] R. G. Larson and D. E. Radford, *Finite dimensional cosemisimple Hopf algebras in characteristic 0 are semisimple*, *J. Alg.* **117** (1988) 267–289.

[188] G. Böhm and K. Szlachányi, *Weak Hopf algebras: II. Representation theory, dimensions, and the Markov trace*, *J. Algebra* **233** (2000) 156–212, arXiv:math/9906045.

[189] N. Moiseyev, *Non-Hermitian Quantum Mechanics*. Cambridge University Press, 2011.

[190] Y. Ashida, Z. Gong, and M. Ueda, *Non-Hermitian physics*, *Adv. Phys.* **69** (2021) 249, arXiv:2006.01837.

[191] C. M. Bender and S. Boettcher, *Real spectra in nonHermitian Hamiltonians having PT symmetry*, *Phys. Rev. Lett.* **80** (1998) 5243, arXiv:physics/9712001.

[192] C. M. Bender, *PT-symmetric quantum theory*, *J. Phys. Conf. Ser.* **631** (2015) 012002.

[193] R. El-Ganainy, K. G. Makris, M. Khajavikhan, Z. H. Musslimani, S. Rotter, and D. N. Christodoulides, *Non-Hermitian physics and PT symmetry*, *Nature Phys.* **14** (2018) 11.

[194] L. Feng, R. El-Ganainy, and L. Ge, *Non-Hermitian photonics based on parity–time symmetry*, *Nature Photon.* **11** (2017) 752.

[195] M.-A. Miri and A. Alù, *Exceptional points in optics and photonics*, *Science* **363** (2019) aar7709.

[196] E. M. Graefe, H. J. Korsch, and A. E. Niederle, *Mean-Field Dynamics of a Non-Hermitian Bose-Hubbard Dimer*, *Phys. Rev. Lett.* **101** (2008) 150408, arXiv:0807.1777.

[197] I. Rotter, *A non-Hermitian Hamilton operator and the physics of open quantum systems*, *J. Phys. A* **42** (2009) 153001, arXiv:0711.2926.

[198] M. Müller, S. Diehl, G. Pupillo, and P. Zoller, *Engineered Open Systems and Quantum Simulations with Atoms and Ions*, *Advances in Atomic, Molecular and Optical Physics* **61** (2012) 1, arXiv:1203.6595.

[199] S. Gopalakrishnan and M. J. Gullans, *Entanglement and Purification Transitions in Non-Hermitian Quantum Mechanics*, *Phys. Rev. Lett.* **126** (2021) 170503, arXiv:2012.01435.

[200] A. Biella and M. Schiró, *Many-Body Quantum Zeno effect and measurement-induced subradiance transition*, *Quantum* **5** (2021) , arXiv:2011.11620.

[201] T. Müller, S. Diehl, and M. Buchhold, *Measurement-Induced Dark State Phase Transitions in Long-Ranged Fermion Systems*, *Phys. Rev. Lett.* **128** (2022) 010605, arXiv:2105.08076.

[202] Y. Le Gal, X. Turkeshi, and M. Schirò, *Volume-to-area law entanglement transition in a non-Hermitian free fermionic chain*, *SciPost Phys.* **14** (2023) 138, arXiv:2210.11937.

[203] J. M. Koh, S.-N. Sun, M. Motta, and A. J. Minnich, *Measurement-induced entanglement phase transition on a superconducting quantum processor with mid-circuit readout*, *Nature Phys.* **19** (2023) 1314–1319, arXiv:2203.04338.

[204] D. Bianchini, O. A. Castro-Alvaredo, B. Doyon, E. Levi, and F. Ravanini, *Entanglement Entropy of Non Unitary Conformal Field Theory*, *J. Phys. A* **48** (2015) 04FT01, arXiv:1405.2804.

[205] D. Bianchini, O. A. Castro-Alvaredo, and B. Doyon, *Entanglement Entropy of Non-Unitary Integrable Quantum Field Theory*, *Nucl. Phys. B* **896** (2015) 835–880, arXiv:1502.03275.

[206] D. Bianchini and F. Ravanini, *Entanglement Entropy from Corner Transfer Matrix in Forrester Baxter non-unitary RSOS models*, arXiv:1509.04601.

[207] K. Narayan, *On dS_4 extremal surfaces and entanglement entropy in some ghost CFTs*, *Phys. Rev. D* **94** (2016) 046001, arXiv:1602.06505.

[208] R. Couvreur, J. L. Jacobsen, and H. Saleur, *Entanglement in nonunitary quantum critical spin chains*, *Phys. Rev. Lett.* **119** (2017) 040601, arXiv:1611.08506.

[209] T. Dupic, B. Estienne, and Y. Ikhlef, *Entanglement entropies of minimal models from null-vectors*, *SciPost Phys.* **4** (2018) 031, arXiv:1709.09270.

[210] P.-Y. Chang, J.-S. You, X. Wen, and S. Ryu, *Entanglement spectrum and entropy in topological non-Hermitian systems and nonunitary conformal field theory*, *Phys. Rev. Res.* **2** (2020) 033069, arXiv:1909.01346.

[211] Y.-T. Tu, Y.-C. Tzeng, and P.-Y. Chang, *Rényi entropies and negative central charges in non-Hermitian quantum systems*, *SciPost Phys.* **12** (2022) 194, arXiv:2107.13006.

[212] A. Lukin, M. Rispoli, R. Schittko, M. E. Tai, A. M. Kaufman, S. Choi, V. Khemani, J. Léonard, and M. Greiner, *Probing entanglement in a many-body–localized system*, *Science* **364** (2019) aau0818.

[213] D. Azses, R. Haenel, Y. Naveh, R. Raussendorf, E. Sela, and E. G. Dalla Torre, *Identification of Symmetry-Protected Topological States on Noisy Quantum Computers*, *Phys. Rev. Lett.* **125** (2020) 120502, arXiv:2002.04620.

[214] A. V. Andreev, A. G. Balanov, T. M. Fromhold, M. T. Greenaway, A. E. Hramov, W. Li, V. V. Makarov, and A. M. Zagoskin, *Emergence and control of complex behaviors in driven systems of interacting qubits with dissipation*, *npj Quantum Inf.* **7** (2021) 1, arXiv:1907.03602.

[215] V. Vitale, A. Elben, R. Kueng, A. Neven, J. Carrasco, B. Kraus, P. Zoller, P. Calabrese, B. Vermersch, and M. Dalmonte, *Symmetry-resolved dynamical purification in synthetic quantum matter*, *SciPost Phys.* **12** (2022) 106, arXiv:2101.07814.

[216] A. Rath, V. Vitale, S. Murciano, M. Votto, J. Dubail, R. Kueng, C. Branciard, P. Calabrese, and B. Vermersch, *Entanglement Barrier and its Symmetry Resolution: Theory and Experimental Observation*, *PRX Quantum* **4** (2023) 010318, arXiv:2209.04393.

[217] N. Laflorencie and S. Rachel, *Spin-resolved entanglement spectroscopy of critical spin chains and Luttinger liquids*, *J. Phys. A* **2014** (2014) P11013, arXiv:1407.3779.

[218] R. Bonsignori, P. Ruggiero, and P. Calabrese, *Symmetry resolved entanglement in free fermionic systems*, *J. Phys. A* **52** (2019) 475302, arXiv:1907.02084.

[219] S. Murciano, G. Di Giulio, and P. Calabrese, *Symmetry resolved entanglement in gapped integrable systems: a corner transfer matrix approach*, *SciPost Phys.* **8** (2020) 046, arXiv:1911.09588.

[220] P. Calabrese, M. Collura, G. Di Giulio, and S. Murciano, *Full counting statistics in the gapped XXZ spin chain*, *EPL* **129** (2020) 60007, arXiv:2002.04367.

[221] H. M. Wiseman and J. A. Vaccaro, *Entanglement of Indistinguishable Particles Shared between Two Parties*, *Phys. Rev. Lett.* **91** (2003) 097902, arXiv:quant-ph/0210002.

[222] H. Barghathi, E. Casiano-Diaz, and A. Del Maestro, *Operationally accessible entanglement of one-dimensional spinless fermions*, *Phys. Rev. A* **100** (2019) 022324, arXiv:1905.03312.

[223] H. Barghathi, J. Yu, and A. Del Maestro, *Theory of noninteracting fermions and bosons in the canonical ensemble*, *Phys. Rev. Res.* **2** (2020) 043206, arXiv:2007.15661.

[224] M. T. Tan and S. Ryu, *Particle number fluctuations, Rényi entropy, and symmetry-resolved entanglement entropy in a two-dimensional Fermi gas from multidimensional bosonization*, *Phys. Rev. B* **101** (2020) 235169, arXiv:1911.01451.

[225] F. Ares, S. Murciano, and P. Calabrese, *Symmetry-resolved entanglement in a long-range free-fermion chain*, *J. Stat. Mech.* (2022) 063104, arXiv:2202.05874.

[226] N. G. Jones, *Symmetry-Resolved Entanglement Entropy in Critical Free-Fermion Chains*, *J. Statist. Phys.* **188** (2022) 28, arXiv:2202.11728.

[227] L. Piroli, E. Vernier, M. Collura, and P. Calabrese, *Thermodynamic symmetry resolved entanglement entropies in integrable systems*, arXiv:2203.09158.

[228] S. Murciano, P. Calabrese, and L. Piroli, *Symmetry-resolved Page curves*, *Phys. Rev. D* **106** (2022) 046015, arXiv:2206.05083.

[229] D. X. Horvath, L. Capizzi, and P. Calabrese, *U(1) symmetry resolved entanglement in free 1+1 dimensional field theories via form factor bootstrap*, *JHEP* **05** (2021) 197, arXiv:2103.03197.

[230] D. X. Horvath, P. Calabrese, and O. A. Castro-Alvaredo, *Branch Point Twist Field Form Factors in the sine-Gordon Model II: Composite Twist Fields and Symmetry Resolved Entanglement*, *SciPost Phys.* **12** (2022) 088, arXiv:2105.13982.

[231] L. Capizzi, D. X. Horváth, P. Calabrese, and O. A. Castro-Alvaredo, *Entanglement of the 3-state Potts model via form factor bootstrap: total and symmetry resolved entropies*, *JHEP* **05** (2022) 113, arXiv:2108.10935.

[232] L. Capizzi, O. A. Castro-Alvaredo, C. De Fazio, M. Mazzoni, and L. Santamaría-Sanz, *Symmetry resolved entanglement of excited states in quantum field theory. Part I. Free theories, twist fields and qubits*, *JHEP* **12** (2022) 127, arXiv:2203.12556.

[233] L. Capizzi, C. De Fazio, M. Mazzoni, L. Santamaría-Sanz, and O. A. Castro-Alvaredo, *Symmetry resolved entanglement of excited states in quantum field theory. Part II. Numerics, interacting theories and higher dimensions*, *JHEP* **12** (2022) 128, arXiv:2206.12223.

[234] O. A. Castro-Alvaredo and M. Mazzoni, *Two-point functions of composite twist fields in the Ising field theory*, *J. Phys. A* **56** (2023) 124001, arXiv:2301.01745.

[235] L. Capizzi, P. Ruggiero, and P. Calabrese, *Symmetry resolved entanglement entropy of excited states in a CFT*, *J. Stat. Mech.* (2020) 073101, arXiv:2003.04670.

[236] S. Murciano, R. Bonsignori, and P. Calabrese, *Symmetry decomposition of negativity of massless free fermions*, *SciPost Phys.* **10** (2021) 111, arXiv:2102.10054.

[237] L. Capizzi and P. Calabrese, *Symmetry resolved relative entropies and distances in conformal field theory*, *JHEP* **10** (2021) 195, arXiv:2105.08596.

[238] L. Y. Hung and G. Wong, *Entanglement branes and factorization in conformal field theory*, *Phys. Rev. D* **104** (2021) 026012, arXiv:1912.11201.

[239] P. Calabrese, J. Dubail, and S. Murciano, *Symmetry-resolved entanglement entropy in Wess-Zumino-Witten models*, *JHEP* **10** (2021) 067, arXiv:2106.15946.

[240] R. Bonsignori and P. Calabrese, *Boundary effects on symmetry resolved entanglement*, *J. Phys. A* **54** (2021) 015005, arXiv:2009.08508.

[241] B. Estienne, Y. Ikhlef, and A. Morin-Duchesne, *Finite-size corrections in critical symmetry-resolved entanglement*, *SciPost Phys.* **10** (2021) 054, arXiv:2010.10515.

[242] H.-H. Chen, *Charged Rényi negativity of massless free bosons*, *JHEP* **02** (2022) 117, arXiv:2111.11028.

[243] A. Milekhin and A. Tajdini, *Charge fluctuation entropy of Hawking radiation: A replica-free way to find large entropy*, *SciPost Phys.* **14** (2023) 172, arXiv:2109.03841.

[244] M. Ghasemi, *Universal thermal corrections to symmetry-resolved entanglement entropy and full counting statistics*, *JHEP* **05** (2023) 209, arXiv:2203.06708.

[245] F. Ares, P. Calabrese, G. Di Giulio, and S. Murciano, *Multi-charged moments of two intervals in conformal field theory*, *JHEP* **09** (2022) 051, arXiv:2206.01534.

[246] G. Di Giulio, R. Meyer, C. Northe, H. Scheppach, and S. Zhao, *On the boundary conformal field theory approach to symmetry-resolved entanglement*, *SciPost Phys. Core* **6** (2023) 049, arXiv:2212.09767.

[247] X. Turkeshi, P. Ruggiero, V. Alba, and P. Calabrese, *Entanglement equipartition in critical random spin chains*, *Phys. Rev. B* **102** (2020) 014455, arXiv:2005.03331.

[248] M. Kiefer-Emmanouilidis, R. Unanyan, M. Fleischhauer, and J. Sirker, *Evidence for Unbounded Growth of the Number Entropy in Many-Body Localized Phases*, *Phys. Rev. Lett.* **124** (2020) 243601, arXiv:2003.04849.

[249] M. Kiefer-Emmanouilidis, R. Unanyan, M. Fleischhauer, and J. Sirker, *Slow delocalization of particles in many-body localized phases*, *Phys. Rev. B* **103** (2021) 024203.

[250] N. Feldman and M. Goldstein, *Dynamics of Charge-Resolved Entanglement after a Local Quench*, *Phys. Rev. B* **100** (2019) 235146, arXiv:1905.10749.

[251] S. Fraenkel and M. Goldstein, *Entanglement measures in a nonequilibrium steady state: Exact results in one dimension*, *SciPost Phys.* **11** (2021) 085, arXiv:2105.00740.

[252] G. Parez, R. Bonsignori, and P. Calabrese, *Dynamics of charge-imbalance-resolved entanglement negativity after a quench in a free-fermion model*, *J. Stat. Mech.* (2022) 053103, arXiv:2202.05309. [Erratum: J.Stat.Mech. 2308, 089902 (2023)].

[253] S. Scopa and D. X. Horváth, *Exact hydrodynamic description of symmetry-resolved Rényi entropies after a quantum quench*, *J. Stat. Mech.* (2022) 083104, arXiv:2205.02924.

[254] H.-H. Chen, *Dynamics of charge imbalance resolved negativity after a global quench in free scalar field theory*, *JHEP* **08** (2022) 146, arXiv:2205.09532. [Erratum: JHEP 10, 157 (2022)].

[255] B. Bertini, P. Calabrese, M. Collura, K. Klobas, and C. Rylands, *Nonequilibrium Full Counting Statistics and Symmetry-Resolved Entanglement from Space-Time Duality*, *Phys. Rev. Lett.* **131** (2023) 140401, arXiv:2212.06188.

[256] K. Monkman and J. Sirker, *Operational entanglement of symmetry-protected topological edge states*, *Phys. Rev. Res.* **2** (2020) 043191, arXiv:2005.13026.

[257] D. Azses and E. Sela, *Symmetry-resolved entanglement in symmetry-protected topological phases*, *Phys. Rev. B* **102** (2020) 235157, arXiv:2008.09332.

[258] B. Oblak, N. Regnault, and B. Estienne, *Equipartition of entanglement in quantum Hall states*, *Phys. Rev. B* **105** (2022) 115131, arXiv:2112.13854.

[259] S. Zhao, C. Northe, and R. Meyer, *Symmetry-resolved entanglement in AdS_3/CFT_2 coupled to U(1) Chern-Simons theory*, *JHEP* **07** (2021) 030, arXiv:2012.11274.

[260] K. Weisenberger, S. Zhao, C. Northe, and R. Meyer, *Symmetry-resolved entanglement for excited states and two entangling intervals in AdS_3/CFT_2*, *JHEP* **12** (2021) 104, arXiv:2108.09210.

[261] S. Zhao, C. Northe, K. Weisenberger, and R. Meyer, *Charged moments in W_3 higher spin holography*, *JHEP* **05** (2022) 166, arXiv:2202.11111.

[262] S. Baiguera, L. Bianchi, S. Chapman, and D. A. Galante, *Shape deformations of charged Rényi entropies from holography*, *JHEP* **06** (2022) 068, arXiv:2203.15028.

[263] M. S. Rudner and L. S. Levitov, *Topological Transition in a Non-Hermitian Quantum Walk*, *Phys. Rev. Lett.* **102** (2009) 065703.

[264] S.-D. Liang and G.-Y. Huang, *Topological invariance and global Berry phase in non-Hermitian systems*, arXiv:1502.00443.

[265] S. Lieu, *Topological phases in the non-Hermitian Su-Schrieffer-Heeger model*, *Phys. Rev. B* **97** (2018) 045106.

[266] S. Yao and Z. Wang, *Edge States and Topological Invariants of Non-Hermitian Systems*, *Phys. Rev. Lett.* **121** (2018) 086803.

[267] C. H. Lee, *Exceptional Bound States and Negative Entanglement Entropy*, *Phys. Rev. Lett.* **128** (2022) 010402, arXiv:2011.09505.

[268] L. Herviou, N. Regnault, and J. H. Bardarson, *Entanglement spectrum and symmetries in non-Hermitian fermionic non-interacting models*, *SciPost Phys.* **7** (2019) 069, arXiv:1908.09852.

[269] H. Li and F. Haldane, *Entanglement Spectrum as a Generalization of Entanglement Entropy: Identification of Topological Order in Non-Abelian Fractional Quantum Hall Effect States*, *Phys. Rev. Lett.* **101** (2008) 010504, arXiv:0805.0332.

[270] P. Calabrese and A. Lefevre, *Entanglement spectrum in one-dimensional systems*, *Phys. Rev. A* **78** (2008) 032329, arXiv:0806.3059.

[271] D. C. Brody, *Biorthogonal quantum mechanics*, *J. Phys. A* **47** (2013) 035305, arXiv:1308.2609.

[272] G. Cipolloni and J. Kudler-Flam, *Entanglement Entropy of Non-Hermitian Eigenstates and the Ginibre Ensemble*, *Phys. Rev. Lett.* **130** (2023) 010401, arXiv:2206.12438.

[273] H. Barghathi, C. . Herdman, and A. D. Maestro, *Rényi Generalization of the Accessible Entanglement Entropy*, *Phys. Rev. Lett.* **121** (2018) 150501, arXiv:1804.01114.

[274] D. Friedan, E. J. Martinec, and S. H. Shenker, *Conformal invariance, supersymmetry and string theory*, *Nucl. Phys. B* **271** (1986) 93–165.

[275] P. Calabrese, J. Cardy, and B. Doyon, *Entanglement entropy in extended quantum systems*, *J. Phys. A* **42** (2009) 500301.

[276] P. Calabrese, J. Cardy, and E. Tonni, *Entanglement negativity in extended systems: A field theoretical approach*, *J. Stat. Mech.* (2013) P02008, arXiv:1210.5359.

[277] P. Calabrese, J. Cardy, and E. Tonni, *Entanglement negativity in quantum field theory*, *Phys. Rev. Lett.* **109** (2012) 130502, arXiv:1206.3092.

[278] P. Ruggiero, V. Alba, and P. Calabrese, *Negativity spectrum of one-dimensional conformal field theories*, *Phys. Rev. B* **94** (2016) 195121, arXiv:1607.02992.

[279] H. Shapourian, P. Ruggiero, S. Ryu, and P. Calabrese, *Twisted and untwisted negativity spectrum of free fermions*, *SciPost Phys.* **7** (2019) 037, arXiv:1906.04211.

[280] L. A. Pastur and V. A. Marčenko, *Distribution of Eigenvalues for Some Sets of Random Matrices*, *Math. USSR Sb.* **1** (1967) 457.

[281] V. Alba, P. Calabrese, and E. Tonni, *Entanglement spectrum degeneracy and the Cardy formula in 1+1 dimensional conformal field theories*, *J. Phys. A* **51** (2018) 024001, arXiv:1707.07532.

[282] R. Haag, *Local Quantum Physics*. Theoretical and Mathematical Physics. Springer, Berlin, 1996.

[283] E. Witten, *APS Medal for Exceptional Achievement in Research: Invited article on entanglement properties of quantum field theory*, *Rev. Mod. Phys.* **90** (2018) 045003, arXiv:1803.04993.

[284] M. Dalmonte, V. Eisler, M. Falconi, and B. Vermersch, *Entanglement Hamiltonians: From Field Theory to Lattice Models and Experiments*, *Annalen Phys.* **534** (2022) 2200064, arXiv:2202.05045.

[285] J. J. Bisognano and E. H. Wichmann, *On the Duality Condition for a Hermitian Scalar Field*, *J. Math. Phys.* **16** (1975) 985.

[286] J. J. Bisognano and E. H. Wichmann, *On the Duality Condition for Quantum Fields*, *J. Math. Phys.* **17** (1976) 303.

[287] S. A. Fulling, *Nonuniqueness of canonical field quantization in Riemannian space-time*, *Phys. Rev. D* **7** (1973) 2850.

[288] P. C. W. Davies, *Scalar particle production in Schwarzschild and Rindler metrics*, *J. Phys. A* **8** (1975) 609.

[289] W. G. Unruh, *Notes on black hole evaporation*, *Phys. Rev. D* **14** (1976) 870.

[290] P. D. Hislop and R. Longo, *Modular Structure of the Local Algebras Associated With the Free Massless Scalar Field Theory*, *Commun. Math. Phys.* **84** (1982) 71.

[291] H. Casini, M. Huerta, and R. C. Myers, *Towards a derivation of holographic entanglement entropy*, *JHEP* **05** (2011) 036, arXiv:1102.0440.

[292] G. Wong, I. Klich, L. A. Pando Zayas, and D. Vaman, *Entanglement Temperature and Entanglement Entropy of Excited States*, *JHEP* **12** (2013) 020, arXiv:1305.3291.

[293] G. Sárosi and T. Ugajin, *Modular Hamiltonians of excited states, OPE blocks and emergent bulk fields*, *JHEP* **01** (2018) 012, arXiv:1705.01486.

[294] H. Casini and M. Huerta, *Reduced density matrix and internal dynamics for multicomponent regions*, *Class. Quant. Grav.* **26** (2009) 185005, arXiv:0903.5284.

[295] R. E. Arias, H. Casini, M. Huerta, and D. Pontello, *Entropy and modular Hamiltonian for a free chiral scalar in two intervals*, *Phys. Rev. D* **98** (2018) 125008, arXiv:1809.00026.

[296] M. Dalmonte, B. Vermersch, and P. Zoller, *Quantum Simulation and Spectroscopy of Entanglement Hamiltonians*, *Nature Phys.* **14** (2018) 827, arXiv:1707.04455.

[297] C. Kokail, R. van Bijnen, A. Elben, B. Vermersch, and P. Zoller, *Entanglement Hamiltonian tomography in quantum simulation*, *Nature Phys.* **17** (2021) 936, arXiv:2009.09000.

[298] C. Kokail, B. Sundar, T. V. Zache, A. Elben, B. Vermersch, M. Dalmonte, R. van Bijnen, and P. Zoller, *Quantum Variational Learning of the Entanglement Hamiltonian*, *Phys. Rev. Lett.* **127** (2021) 170501, arXiv:2105.04317.

[299] T. V. Zache, C. Kokail, B. Sundar, and P. Zoller, *Entanglement Spectroscopy and probing the Li-Haldane Conjecture in Topological Quantum Matter*, *Quantum* **6** (2022) 702, arXiv:2110.03913.

[300] M. K. Joshi, C. Kokail, R. van Bijnen, F. Kranzl, T. V. Zache, R. Blatt, C. F. Roos, and P. Zoller, *Exploring large-scale entanglement in quantum simulation*, *Nature* **624** (2023) 539, arXiv:2306.00057.

[301] I. Peschel and T. T. Truong, *Corner transfer matrices and conformal invariance*, *Z. Phys. B* **69** (1987) 385.

[302] B. Davies, *Corner transfer matrices for the Ising model*, *Physica A* **154** (1988) 1.

[303] T. T. Truong and I. Peschel, *Diagonalisation of finite-size corner transfer matrices and related spin chains*, *Z. Phys. B* **75** (1989) 119.

[304] I. Peschel, M. Kaulke, and Ö. Legeza, *Density-matrix spectra for integrable models*, *Ann. Physik (Leipzig)* **8** (1999) 153.

[305] B. Davies, *On the spectrum of six-vertex corner transfer matrices*, *Physica A* **159** (1989) 171.

[306] H. Frahm and H. B. Thacker, *Corner transfer matrix eigenstates for the six vertex model*, *J. Phys. A* **24** (1991) 5587.

[307] M. G. Tetel'man, *Lorentz group for two-dimensional integrable lattice systems*, *Sov. Phys. JETP* **55** (1982) 306.

[308] H. B. Thacker, *Corner Transfer Matrices and Lorentz Invariance on a Lattice*, *Physica D* **18** (1986) 348.

[309] E. Ercolessi, S. Evangelisti, and F. Ravanini, *Exact entanglement entropy of the XYZ model and its sine-Gordon limit*, *Phys. Lett. A* **374** (2010) 2101, arXiv:0905.4000.

[310] I. Peschel and T. T. Truong, *Corner Transfer Matrices for the Gaussian Model*, *Ann. Physik (Leipzig)* **48** (1991) 185.

[311] I. Peschel and M.-C. Chung, *Density matrices for a chain of oscillators*, *J. Phys. A* **32** (1999) 8419, arXiv:cond-mat/9906224.

[312] V. Eisler, G. Di Giulio, E. Tonni, and I. Peschel, *Entanglement Hamiltonians for non-critical quantum chains*, *J. Stat. Mech.* (2020) 103102, arXiv:2007.01804.

[313] G. Giudici, T. Mendes-Santos, P. Calabrese, and M. Dalmonte, *Entanglement Hamiltonians of lattice models via the Bisognano-Wichmann theorem*, *Phys. Rev. B* **98** (2018) 134403, arXiv:1807.01322.

[314] T. Mendes-Santos, G. Giudici, M. Dalmonte, and M. A. Rajabpour, *Entanglement Hamiltonian of quantum critical chains and conformal field theories*, *Phys. Rev. B* **100** (2019) 155122, arXiv:1906.00471.

[315] J. Zhang, P. Calabrese, M. Dalmonte, and M. A. Rajabpour, *Lattice Bisognano-Wichmann modular Hamiltonian in critical quantum spin chains*, *SciPost Phys. Core* **2** (2020) 007, arXiv:2003.00315.

[316] V. Eisler, *Entanglement Hamiltonian of a nonrelativistic Fermi gas*, arXiv:2311.16348.

[317] R. J. Baxter, *Exactly solved models in statistical mechanics*. Academic Press, London, 1982.

[318] R. J. Baxter, *Corner transfer matrices of the eight-vertex model. 1. Low-temperature expansions and conjectured properties*, *J. Statist. Phys.* **15** (1976) 485.

[319] R. J. Baxter, *Corner transfer matrices of the eight-vertex model. 2. The Ising model case*, *J. Statist. Phys.* **17** (1977) 1.

[320] T. Nishino and K. Okunishi, *Corner transfer matrix algorithm for classical renormalization group*, *J. Phys. Soc. Japan* **66** (1997) 3040, arXiv:cond-mat/9705072.

[321] H. Itoyama and H. B. Thacker, *Lattice Virasoro Algebra and Corner Transfer Matrices in the Baxter Eight Vertex Model*, *Phys. Rev. Lett.* **58** (1987) 1395.

[322] H. B. Thacker and H. Itoyama, *Integrability, Conformal Symmetry, and Noncritical Virasoro Algebras*, *Nucl. Phys. B Proc. Suppl.* **5** (1988) 9.

[323] H. Itoyama and H. B. Thacker, *Integrability and Virasoro Symmetry of the Noncritical Baxter-Ising Model*, *Nucl. Phys. B* **320** (1989) 541.

[324] The `mpmath` development team, `mpmath`*: a Python library for arbitrary-precision floating-point arithmetic (version 1.3.0)*, 2023. http://mpmath.org/.

[325] V. Alba, M. Haque, and A. M. Läuchli, *Boundary-locality and perturbative structure of entanglement spectra in gapped systems*, *Phys. Rev. Lett.* **108** (2012) 227201, arXiv:1107.1726.

[326] R. Arias, D. Blanco, H. Casini, and M. Huerta, *Local temperatures and local terms in modular Hamiltonians*, *Phys. Rev. D* **95** (2017) 065005, arXiv:1611.08517.

[327] V. Eisler, E. Tonni, and I. Peschel, *On the continuum limit of the entanglement Hamiltonian*, *J. Stat. Mech.* (2019) 073101, arXiv:1902.04474.

[328] V. Eisler, E. Tonni, and I. Peschel, *Local and non-local properties of the entanglement Hamiltonian for two disjoint intervals*, *J. Stat. Mech.* (2022) 083101, arXiv:2204.03966.

[329] G. Di Giulio and E. Tonni, *On entanglement hamiltonians of an interval in massless harmonic chains*, *J. Stat. Mech.* (2020) 033102, arXiv:1911.07188.

[330] F. Rottoli, S. Murciano, E. Tonni, and P. Calabrese, *Entanglement and negativity Hamiltonians for the massless Dirac field on the half line*, *J. Stat. Mech.* (2023) 013103, arXiv:2210.12109.

[331] F. Rottoli, S. Scopa, and P. Calabrese, *Entanglement Hamiltonian during a domain wall melting in the free Fermi chain*, *J. Stat. Mech.* (2022) 063103, arXiv:2202.04380.

[332] R. Bonsignori and V. Eisler, *Entanglement Hamiltonian for inhomogeneous free fermions*, arXiv:2403.14766.

[333] N. Javerzat and E. Tonni, *On the continuum limit of the entanglement Hamiltonian of a sphere for the free massless scalar field*, *JHEP* **02** (2022) 086, arXiv:2111.05154.

[334] F. Rottoli, S. Murciano, and P. Calabrese, *Finite temperature negativity Hamiltonians of the massless Dirac fermion*, *JHEP* **06** (2023) 139, arXiv:2304.09906.

[335] S. Murciano, V. Vitale, M. Dalmonte, and P. Calabrese, *Negativity Hamiltonian: An Operator Characterization of Mixed-State Entanglement*, *Phys. Rev. Lett.* **128** (2022) 140502, arXiv:2201.03989.